

Title	Respiratory control in the mdx mouse model of Duchenne muscular dystrophy
Authors	Burns, David P.
Publication date	2018
Original Citation	Burns, D. P. 2018. Respiratory control in the mdx mouse model of Duchenne muscular dystrophy. PhD Thesis, University College Cork.
Type of publication	Doctoral thesis
Rights	© 2018, David P. Burns. - http://creativecommons.org/licenses/by-nc-nd/3.0/
Download date	2024-09-22 04:49:02
Item downloaded from	https://hdl.handle.net/10468/6821



UCC

University College Cork, Ireland
 Coláiste na hOllscoile Corcaigh



Respiratory Control in the *mdx* Mouse Model of Duchenne Muscular Dystrophy

David P. Burns, BSc (Hons)

Department of Physiology

*Thesis submitted to National University of Ireland, Cork
for the award of Doctor of Philosophy*

Under the supervision of:

**Professor Ken D. O'Halloran,
Head of Department and Chair**

April 2018

Table of contents	
Declaration	x
Acknowledgements	xi
Abstract	xiii
Chapter 1. The control of breathing in Duchenne muscular dystrophy	1
Abbreviations	2
1.1 Control of breathing in neuromuscular disease	3
1.1.1 The control of breathing	3
1.1.1.1 The neural control of breathing	3
1.1.1.2 Respiratory plasticity	5
1.1.1.3 Compensatory plasticity in breathing	7
1.1.2 Duchenne muscular dystrophy (DMD)	8
1.1.3 Pulmonary function in DMD	9
1.1.4 Respiratory muscle weakness in DMD	10
1.1.5 Respiratory disturbances in DMD	12
1.1.6 Blood-gas homeostasis in DMD	14
1.1.7 Non-ventilatory behaviours in DMD	15
1.1.8 Assisted ventilation in DMD	16
1.1.9 Cardiovascular function in DMD	17
1.2 Dystrophin-deficient <i>mdx</i> mouse	18
1.2.1 Dystrophin and the striated muscles of breathing	18
1.2.2 Respiratory function in the <i>mdx</i> mouse	20
1.2.3 Dystrophin and the upper airway	21
1.2.4 Dystrophin and the airways	22
1.2.5 Dystrophin and the nervous system	23
1.2.6 Dystrophin and chemoreception	25
1.2.7 Dystrophin and neuromechanical control of breathing	26
1.2.8 Other animal models of DMD	27
1.3 Role of inflammation in DMD pathophysiology	29
1.3.1 Inflammation in <i>mdx</i> mice	29
1.3.2 Inflammation and oxidative stress	30
1.3.3 Targeting inflammation as a therapy in DMD	30
1.3.4 Cytokines	31
1.3.5 Interleukin-6	32
1.3.6 Anabolic signalling in muscle	33
1.3.7 Knowledge gaps addressed in this thesis	35
1.4 Thesis structure and specific aims	36
1.5 References	38

Chapter 2. Sensorimotor control of breathing in the <i>mdx</i> mouse model of Duchenne muscular dystrophy	64
Cover art	65
Key points	66
Abbreviations	67
Abstract	68
2.1 Introduction	69
2.2 Methods	71
2.2.1 Ethical approval	71
2.2.2 Experimental animals	71
2.2.3 Respiratory recordings	71
2.2.4 Metabolism measurements	73
2.2.5 Blood gas analysis	73
2.2.6 Arterially perfused <i>ex vivo</i> carotid-body-carotid sinus nerve preparation	74
2.2.7 <i>Ex vivo</i> muscle function tests	75
2.2.8 Muscle immunohistochemistry	77
2.2.9 Diaphragm EMG activity and responsiveness	78
2.2.10 Statistical analysis	80
2.3 Results	81
2.3.1 Baseline ventilation and metabolism	82
2.3.2 Blood gas analysis	84
2.3.3 Carotid sinus nerve discharge	85
2.3.4 Ventilatory responsiveness to hypoxia and hypercapnia	88
2.3.5 Diaphragm muscle function	94
2.3.6 Diaphragm muscle fibre size and distribution	96
2.3.7 Diaphragm EMG responsiveness	98
2.4 Discussion	101
2.5 Translational perspective	109
2.6 Additional information	110
2.7 References	111
Chapter 3. Breathing with neuromuscular disease: Does compensatory plasticity in the motor drive to breathe offer a potential therapeutic target in muscular dystrophy?	115
Highlights and abbreviations	116
Abstract	117
3.1 Duchenne muscular dystrophy (DMD): Respiratory morbidity and mortality	118
3.2 The dystrophin-deficient <i>mdx</i> mouse: Diaphragm dysfunction recapitulating human DMD	119

3.3 Control of breathing in the <i>mdx</i> mouse: Neural adaptation or maladaptation?	119
3.4 Control of breathing in the <i>mdx</i> mouse: Deficits and dysfunction	120
3.5 Control of breathing in the <i>mdx</i> mouse: Compensation and limitations	121
3.6 Control of breathing in the <i>mdx</i> mouse: Knowledge gaps	124
3.7 Control of breathing in the <i>mdx</i> mouse: Therapeutic intermittent hypoxia to boost respiratory drive?	124
3.8 Conclusion	125
3.9 References	127
Chapter 4. Neuromechanical control of breathing in the dystrophin-deficient <i>mdx</i> mouse	131
Cover art	132
Key points and abbreviations	133
Abstract	135
4.1 Introduction	136
4.2 Methods	139
4.2.1 Ethical approval	139
4.2.2 Experimental animals	139
4.2.3 Whole-body plethysmography	139
4.2.3.1 Respiratory stability	140
4.2.3.2 Ventilatory responsiveness to chemostimulation	140
4.2.4 Diaphragm EMG and oesophageal pressure recordings	141
4.2.5 <i>Ex vivo</i> diaphragm muscle function	142
4.2.6 Tissue collection	143
4.2.7 Spinal cord immunostaining	144
4.2.8 Terminal deoxynucleotidyl Transferase (TdT) dUTP Nick-End Labelling assay (TUNEL assay)	145
4.2.9 High performance liquid chromatography (HPLC)	146
4.2.10 RNA extraction and real-time polymerase chain reaction (RT-PCR)	147
4.2.11 Statistical analysis	148
4.3 Results	149
4.3.1 Breathing variability	149
4.3.2 Ventilatory responsiveness to hypercapnic hypoxia	151
4.3.3 Oesophageal pressure and diaphragm EMG activity <i>in vivo</i>	153
4.3.4 Diaphragm muscle contractile function <i>ex vivo</i>	156
4.3.5 Cervical spinal cord immune cell density	158
4.3.6 Cervical spinal cord monoamine concentration	161
4.3.7 Cervical spinal cord gene expression	162

4.4 Discussion	163
4.5 Additional information	169
4.6 References	170
Chapter 5. Restoration of pharyngeal dilator muscle force in dystrophin-deficient (<i>mdx</i>) mice following co-treatment with neutralising interleukin-6 receptor antibodies and urocortin 2	176
Cover art	177
Key points and abbreviations	178
Abstract	179
5.1 Introduction	180
5.2 Methods	183
5.2.1 Ethical approval	183
5.2.2 Animals	183
5.2.3 Muscle physiology	183
5.2.3.1 <i>Ex vivo</i> muscle preparation	183
5.2.3.2 Isometric protocol	184
5.2.3.3 Isotonic protocol	184
5.2.4 Muscle immunohistochemistry and histology	185
5.2.4.1 Tissue preparation	185
5.2.4.2 Myosin heavy chain fluorescence immunohistochemistry	185
5.2.4.3 Histological analysis	186
5.2.5 Molecular studies	187
5.2.5.1 Tissue preparation	187
5.2.5.2 Chemokines	187
5.2.6 Data and image analysis	188
5.2.7 Statistical analysis	189
5.3 Results	190
5.3.1 Body mass	190
5.3.2 Isometric force and twitch contractile kinetics	190
5.3.3 Isotonic contractile parameters and kinetics	192
5.3.4 Isotonic load relationships	194
5.3.5 Myosin heavy chain fibre type distribution	196
5.3.6 Fibre cross-sectional area	196
5.3.7 Central nucleation and putative inflammatory cell infiltration	199
5.3.8 Collagen content	201
5.3.9 Chemokines	201
5.4 Discussion	204
5.5 Additional information	213
5.6 References	214

Chapter 6. Recovery of respiratory function in <i>mdx</i> mice co-treated with neutralizing interleukin-6 receptor antibodies and urocortin 2	219
Key points	220
Abbreviations	221
Abstract	222
6.1 Introduction	223
6.2 Methods	225
6.2.1 Ethical approval	225
6.2.2 Animals	225
6.2.3 Respiratory measurements	226
6.2.4 Metabolism measurements	227
6.2.5 Tissue collection	227
6.2.6 Muscle physiology	227
6.2.6.1 <i>Ex vivo</i> muscle preparation	227
6.2.6.2 Isometric protocol	228
6.2.6.3 Isotonic protocol	228
6.2.7 Muscle immunohistochemistry and histology	229
6.2.7.1 Tissue preparation	229
6.2.7.2 Myosin heavy chain fluorescence immuno-histochemistry	229
6.2.7.3 Histological analysis	231
6.2.7.4 Fluorescently labelled collagen binding protein	232
6.2.8 Molecular studies	232
6.2.8.1 Tissue preparation	232
6.2.8.2 Cytokines	233
6.2.9 Statistical analysis	233
6.3 Results	234
6.3.1 Body mass and organ measurement	234
6.3.2 Baseline ventilation and metabolism	236
6.3.3 Ventilatory responsiveness to hypoxia	239
6.3.4 Isometric force and twitch contractile kinetics	241
6.3.5 Isotonic contractile parameters and kinetics	241
6.3.6 Isotonic load relationships	243
6.3.7 Myosin heavy chain fibre-type distribution	245
6.3.8 Fibre cross-sectional area	245
6.3.9 Central nucleation and putative inflammatory cell infiltration	248
6.3.10 Collagen content	248
6.3.11 Inflammatory mediators	248
6.4 Discussion	253
6.5 Additional information	261

6.6 References	262
Chapter 7. Combinational pharmacotherapy in the treatment of respiratory deficits in dystrophin-deficient <i>mdx</i> mice	267
Abstract and abbreviations	268
7.1 Respiratory dysfunction in Duchenne muscular dystrophy (DMD)	269
7.2 Respiratory muscle remodelling in the dystrophin-deficient <i>mdx</i> Mouse	270
7.3 Respiratory muscle weakness in the <i>mdx</i> mouse	272
7.4 Ventilatory deficits in <i>mdx</i> mice	273
7.5 Combinational pharmacotherapy in DMD	274
7.6 Combination pharmacotherapy in <i>mdx</i> mice: Ventilation	276
7.7 Combinational pharmacotherapy in <i>mdx</i> mice: Respiratory muscle function	276
7.8 Combinational pharmacotherapy in <i>mdx</i> mice: Respiratory muscle form	277
7.9 Combinational pharmacotherapy in <i>mdx</i> mice: Knowledge gaps	278
7.10 Towards combinational pharmacotherapy for the treatment of respiratory dysfunction in DMD	279
7.11 References	281
Chapter 8. Summary and conclusion	287
8.1 Summary of major findings	288
8.2 Future studies	292
8.3 Conclusion	295
Publications	296
Presentations	298
Conference proceedings	299

List of figures

Chapter 2.

Figure 2.1 Baseline ventilation in conscious mice	82
Figure 2.2 <i>Ex vivo</i> carotid sinus nerve discharge	86
Figure 2.3 Ventilatory and metabolic responsiveness to graded hypoxia	89
Figure 2.4 Ventilatory and metabolic responsiveness to sustained hypoxia	91
Figure 2.5 Ventilatory responsiveness to hypercapnia	93
Figure 2.6 <i>Ex vivo</i> diaphragm muscle contractile function	95
Figure 2.7 Diaphragm muscle structure	97
Figure 2.8 Diaphragm EMG	99

Chapter 3.

Figure 3.1 Diaphragm muscle weakness in dystrophin-deficient <i>mdx</i> mice	123
Figure 3.2 Summary of the effects of dystrophin-deficiency on respiratory control in young <i>mdx</i> mice	126

Chapter 4.

Figure 4.1 Respiratory measurements in conscious mice	150
Figure 4.2 Ventilation in response to chemostimulation in conscious mice	152
Figure 4.3 Oesophageal pressure and diaphragm muscle EMG activity in anaesthetised mice	154
Figure 4.4 <i>Ex vivo</i> diaphragm muscle contractile function	157
Figure 4.5 Cervical spinal cord immunohistochemistry	159
Figure 4.6 Cervical spinal cord TUNEL assay	160
Figure 4.7 Cervical spinal cord monoamine concentrations	161
Figure 4.8 Cervical spinal cord gene expression analysis	162

Chapter 5.

Figure 5.1 Peak isometric tetanic force	191
Figure 5.2 Sternohyoid muscle isotonic contractile properties	195
Figure 5.3 Sternohyoid muscle fibre distribution and cross-sectional area	197
Figure 5.4 Central nucleation and inflammatory cell infiltration of sternohyoid muscle	200
Figure 5.5 Collagen deposition in sternohyoid muscle	202
Figure 5.6 Chemokine expression in sternohyoid muscle	203

Chapter 6.

Figure 6.1 Ventilation in conscious mice	237
Figure 6.2 Ventilatory responsiveness to hypoxia	240
Figure 6.3 Diaphragm muscle function	244

Figure 6.4 Diaphragm muscle fibre distribution and cross-sectional area	246
Figure 6.5 Diaphragm muscle histology	250
Figure 6.6 Cytokine concentrations in diaphragm muscle	252

List of tables

Chapter 2.

Table 2.1 Baseline ventilation and metabolic measurements	83
Table 2.2 Intra-cardiac blood gas analysis	84
Table 2.3 Carotid sinus nerve afferent discharge in normoxia and hypoxia	87
Table 2.4 Diaphragm muscle twitch force and contractile kinetics	94

Chapter 4.

Table 4.1 Real-time ready catalog and custom assays used for cDNA Amplification	147
Table 4.2 Baseline respiratory parameters in anaesthetised mice	155
Table 4.3 <i>Ex vivo</i> diaphragm muscle contractile kinetics	156

Chapter 5.

Table 5.1 Sternohyoid muscle contractile properties	193
---	-----

Chapter 6.

Table 6.1 Body mass, somatic growth, organ and muscle mass	235
Table 6.2 Baseline ventilation and metabolic measurements	238
Table 6.3 Diaphragm muscle contractile properties	242

Declaration

I hereby declare that this thesis is my own, original work. It has not been submitted to another institution for an award. The contribution of others through collaborations has been acknowledged.

David Burns

April 2018

Acknowledgements

Professor Ken O'Halloran, I am eternally grateful for your mentorship, supervision and friendship during the course of my training. From the swamp to Lake Louise, Namche to the Gas Lamp District, Manly to Boston Commons; it's been one hell of an adventure! I am truly thankful for the rich intellectual and collaborative environment you have provided me with and for your instrumental role in training me as a physiologist. Thank you for encouraging and supporting my training overseas and attendance at international meetings and symposia. I look forward to continuing our collaborations and working closely together into the future. And who knows, maybe I'll make it to Kala Patthar next time!

Dr. Deirdre Edge, thank you for your collegiality and collaboration. I truly appreciate your support, enthusiasm and close friendship while in Cork and afar! I wish you the very best into the future.

Thank you to Dr. Arijit Roy, Dr. Fiona McDonald and Prof. Richard Wilson (University of Calgary) for your collaboration and for graciously hosting me at your institution. Go Flames!

To Prof. David Fuller (University of Florida), thank you for affording me the opportunity to develop my skillset and broaden my network. Special thanks to *WERKERZ* for introducing me to Happy Hour, Queso and last but not least, Ramen. I very much look forward to crossing paths again in our future careers. Go Gators!

To the academic, technical and administrative staff at the Department of Physiology, University College Cork. Thank you for your support over the last number of years. Thank you to my collaborators at the department, particularly Dr. Eric Lucking. Thank you to the staff of the Biological Services Unit, University College Cork. Thank you to my thesis examiners, Professor Aideen Sullivan and Professor Gordon Mitchell.

To my friends and family, at home and abroad, thank you for your well wishes. To my fellow postgraduates, thank for your friendship, peer support and for the many trips to Tom Barry's – "*sure we'll havta!*".

To Aoife, you make each day a new exciting adventure. Thank you for your love, affection and guidance throughout. I look forward to the next chapter.

To my parents, Damien and Catherine, and siblings, Adam, Eoin and Kate. I am so grateful for all you have done over the years in support of my education. For your dear love, kindness and unwavering support for each of my endeavours, I dedicate this thesis to you.

Abstract

Duchenne muscular dystrophy (DMD) is a genetic disease that occurs in males due to the absence of the dystrophin (427 kDa) protein. Patients have severe skeletal muscle weakness that extends to the striated muscles of breathing. Maximal inspiratory pressures are low in DMD and the diaphragm is severely compromised. Respiratory disturbances occur in patients, particularly during sleep, such as apnoea and hypoventilation. Comprehensive studies on the control of breathing in DMD and animal models of the dystrophinopathies are lacking. We examined the integrated respiratory control system in a pre-clinical model of DMD – the *mdx* mouse. Since inflammation is a major pathological feature of DMD, we assessed the potential of a combined anti-inflammatory and anti-stress interventional strategy in ameliorating respiratory deficits in *mdx* mice.

Young (8-week-old) wild-type and *mdx* mice were studied. We assessed ventilation and metabolism during normoxia and in response to physiological gas challenges. Respiratory stability and ventilatory capacity were determined. Diaphragm EMG activity and inspiratory pressure generating capacity was examined in anaesthetised spontaneously breathing mice *in vivo*. Diaphragm muscle structure and force-generating capacity were assessed. Carotid body afferent activity was determined *ex vivo*. Monoamine concentrations, density of activated astrocytes and microglia, and pro-inflammatory gene expression was determined in the spinal cord (C3-C5), containing the phrenic motor nucleus. Interventional studies consisted of a combinational treatment of a neutralizing interleukin-6-receptor (xIL-6R) antibody and urocortin 2 (Ucn2, corticotrophin releasing factor receptor 2 agonist), or saline for 2 weeks. Following treatment, ventilation and metabolism, as well as diaphragm and upper airway (sternohyoid) muscle form and function, and inflammatory status were determined.

During normoxia, *mdx* mice hypoventilated (decreased ventilatory equivalent for carbon dioxide), due to decreased tidal volume with no evidence of perturbed respiratory rhythm. Carotid sinus nerve responses to hyperoxia were blunted in *mdx*, suggesting hypoactivity (sensory deficit). *Mdx* mice retained a remarkable

capacity to increase ventilation during hypercapnic hypoxic breathing despite profound diaphragm muscle weakness and major structural remodelling. Peak inspiratory oesophageal pressure generation was preserved during basal breathing and was greater during augmented breaths in *mdx* compared to wild-type mice, probably due to recruitment of accessory muscles of breathing. EMG recordings assessing neural drive to the diaphragm in anaesthetised vagotomised mice, revealed enhanced neural drive to the diaphragm in *mdx* mice during chemoactivation (near maximal drive) compared with wild-type. Monoamine concentrations were elevated in the C3-C5 spinal cord of *mdx* mice, and the density of activated immune cells and pro-inflammatory gene expression was unchanged, indicating no evidence of neuroinflammation. xIL-6R and Ucn2 co-treatment in *mdx* mice completely restored ventilation during normoxia and significantly improved diaphragm and sternohyoid muscle force- and power-generating capacity. Combinational therapy restored myosin heavy chain complement in diaphragm and sternohyoid muscles.

We conclude that respiratory control is altered in young *mdx* mice, such that considerable deficits arising from dystrophin lack are adequately compensated, limiting ventilatory deficits. We reason that compensatory neuroplasticity in accessory motor pathways preserves ventilatory capacity in *mdx* mice despite profound diaphragm muscle weakness. Interventional studies indicate that strategies aimed at preserving muscle fibre complement and promoting muscle fibre quality in *mdx* respiratory muscles can alleviate breathing and muscle functional deficits. These data may have relevance to the development of interventional strategies designed to alleviate respiratory dysfunction in the human dystrophinopathies.

Chapter 1. The control of breathing in Duchenne muscular dystrophy

Abbreviations: AHI, apnoea-hypopnoea index; ATP, adenosine triphosphate; BDNF, brain-derived neurotrophic factor; CIAP, cellular inhibitor of apoptosis; CNS, central nervous system; CRF, corticotrophin-releasing factor; CRFR, CRF-receptor; CO₂, carbon dioxide; DAPC, dystrophin associated protein complex; DGC, dystrophin-glycoprotein complex; DMD, Duchenne muscular dystrophy; FEV₁, forced expired volume in one second; FVC, forced vital capacity; GRMD, golden retriever model of muscular dystrophy; gp130, glycoprotein 130; IL, interleukin; IL-6R, IL-6-receptor; xIL-6R, neutralising IL-6R; MyHC, myosin heavy chain; MRI, magnetic resonance imaging; NIV, non-invasive ventilation; NIPPV, non-invasive positive pressure ventilation; NSAID, non-steroidal anti-inflammatory drug; NTS, nucleus tractus solitarius; OSA, obstructive sleep apnoea; PaCO₂, partial pressure of arterial CO₂; Pdi, trans-diaphragmatic pressure; PEEP, positive end expiratory pressure; Pgas, gastric pressure; PO₂, partial pressure of oxygen; Poes, oesophageal pressure; REM, rapid eye movement; SDB, sleep-disordered breathing; TALENS, transcript activator-like effector nuclease; TNF- α , tumour necrosis factor-alpha.

1.1 Control of breathing in neuromuscular disease

1.1.1 The control of breathing

Breathing is an active neuro-mechanical process essential for life. Adequate ventilation is required to maintain blood oxygenation levels to facilitate the metabolic demands of the body. The respiratory system is an integrated system involving a number of components including the central nervous system (CNS), motor nerves, skeletal musculature and the lungs and conducting airways. The function of the respiratory control network is to maintain respiratory homeostasis in response to physiological perturbations, which occur in health and disease. Respiratory insufficiency or failure can result from inadequate gas exchange by the respiratory system due to major deficits at one or more sites of the respiratory control network.

1.1.1.1 The neural control of breathing

Breathing is a state-dependent process consisting of an inspiratory phase which involves active contraction of the respiratory pump muscles (diaphragm and external intercostal muscles) followed by a passive expiratory phase. A third phase, termed post-inspiration, is also evident, characterised by lengthening contraction of the diaphragm and adduction of the laryngeal muscles, which slows expiratory airflow (Del Negro *et al.*, 2018). Expiration can have an active component (active expiration) under certain conditions (e.g. during exercise), in which the abdominal and internal intercostal muscles are recruited to facilitate ventilation. The central drive to breathe originates from distinct sites within the brainstem where central pattern is generated by a complex diffuse neural network, originating from the rhythm-generating sites of the pre-Bötzinger complex and the parafacial respiratory group (Feldman & Del Negro, 2006; Smith *et al.*, 2009; Feldman *et al.*, 2013). Neurons found in the pre- Bötzing complex display activity in phase with inspiration. Neuronal axons from this complex project to motor neurons which innervate respiratory pump and airway resistance

muscles, in addition to other ponto-medullary and supra-pontine sites (Del Negro *et al.*, 2018).

The end effectors of breathing are the respiratory pump muscles. The phrenic motor nucleus is located in the ventral horn of the cervical spinal cord and contains a heterogeneous group of motor neurons which provide efferent motor input to the diaphragm muscle. Phrenic motor neurons receive excitatory input from medullary bulbospinal neurons. The intercostal muscles are controlled by motor neurons located in the thoracic spinal cord. Neuromotor control of the diaphragm is achieved by phrenic motor units, which consist of a phrenic motor neuron and the corresponding diaphragm muscle fibres it innervates. Axon terminals of the phrenic nerve terminate at the neuromuscular junction, where motor outflow is transduced into mechanical contraction of diaphragm myofibres. This is facilitated by release of the excitatory neurotransmitter acetylcholine at the motor end plate.

Although neural drive to the respiratory muscles is an automatic process, motor output is influenced by sensory information relayed to the respiratory centres of the brainstem. Chemoreceptors relay sensory information regarding the gaseous composition and acid-base status of blood. Peripheral chemoreceptors located at the aortic arch and carotid body detect the partial pressure of oxygen (PO_2) in arterial blood (Prabhakar & Peng, 2004; Teppema & Dahan, 2010; Kumar & Prabhakar, 2012; Prabhakar & Peng, 2017). The carotid body is the principal oxygen sensor in the body located at the bifurcation of the common carotid artery, relaying chemoafferent information to the brainstem. The carotid body has a key role in eliciting the initial ventilatory and arterial blood pressure response to hypoxaemia (decreased PO_2 of arterial blood). The carotid body receives sensory innervation from a branch of the glossopharyngeal nerve, the carotid sinus nerve. Peripheral chemoreceptor tissue is composed of type I (glomus) cells, which are of neural origin, and type II sustentacular (glia-like) cells. Sensory discharge from the carotid body is modest during normoxia

(~100 mmHg PO₂), but increases rapidly with even a slight decrease in arterial PO₂. Central chemoreceptors are located throughout the CNS and are sensitive to changes in the hydrogen ion concentration (pH) of brain extracellular fluid. In addition to the sensory chemoreceptor control of breathing, sensory information is also received from the respiratory muscles (muscle spindles), the lungs (pulmonary stretch receptors) and receptors located in the upper airway (temperature, irritant and mechanical receptors).

1.1.1.2 Respiratory plasticity

Neuroplasticity is a term which describes nervous system changes that occur in response to natural stimuli (e.g. learning or aging/ development) and as a result of the development of pathological conditions (Fuller & Mitchell, 2017). Plasticity is now recognised as a fundamental property of the integrated system controlling breathing (Feldman *et al.*, 2003). Respiratory neuroplasticity can be defined as a persistent change in a neural control system (morphology and/or function) based on a prior experience (Johnson & Mitchell, 2002; Mitchell & Johnson, 2003). Environmental and physiological stressors can challenge the respiratory control system's ability to maintain homeostasis, such as during exercise, swallowing, speech and at altitude (among other challenges). Modifications within the neural network controlling breathing as a result of such challenges can be considered adaptive plastic changes which are necessary to maintain adequate blood oxygenation and pH regulation. Respiratory plasticity can occur a result of (but is not limited to) changes in physiological gases such as oxygen and carbon dioxide or due to experiences during sensitive stages of development *in utero* or during the post-natal period, which can have long-lasting effects on ventilatory control into adulthood (Mitchell & Johnson, 2003).

The first evidence of plasticity within the respiratory control system was demonstrated by Elridge, Millhorn and colleagues during studies of electrical stimulation of the

carotid sinus nerve resulting in long-lasting elevations in phrenic nerve activity (Eldridge & Millhorn, 1986). This was later termed phrenic long-term facilitation and is now a well-described exemplar of respiratory motor plasticity (Fuller *et al.*, 2000; Devinney *et al.*, 2013). In addition to motor facilitation of the diaphragm, sensory facilitation of the carotid body has also been documented (Peng *et al.*, 2003; Prabhakar, 2011; Roy *et al.*, 2017), as well as plasticity within the complex circuitry of the brainstem in response to, for example, chronic hypoxia (Dwinell *et al.*, 2000; Powell *et al.*, 2000; Wilkinson *et al.*, 2010) and chronic intermittent hypoxia (Almado *et al.*, 2012; Moraes *et al.*, 2012).

Respiratory plasticity induced as a result of hypoxia (oxygen deficiency) has been well studied in recent years. Hypoxia can modulate multiple sites of the respiratory control network and evoke increased sensory (Peng *et al.*, 2003) and motor nerve output (Bach & Mitchell, 1996). Hypoxia, such as that experienced at high altitude, can evoke robust plasticity in carotid chemoafferent neurons (Vizek *et al.*, 1987; Nielsen *et al.*, 1988). Ventilatory acclimatisation to chronic hypoxia consists of a progressive increase in ventilation beyond the acute response during prolonged periods of low oxygen (Powell *et al.*, 1998). In addition to increased chemoafferent discharge, brainstem plasticity can occur in the nucleus tractus solitaries (NTS), where projections from chemoafferent neurons of the carotid body terminate, resulting in a change in the central neural integration of chemoafferent inputs (Dwinell & Powell, 1999). Such changes can result in a progressive increase in ventilation for sustained periods (hours to days) following removal of the initial hypoxic stimulus (Powell *et al.*, 1998).

Sensory long-term facilitation of the carotid chemoreceptors has been well studied by Prabhakar and colleagues (Kumar & Prabhakar, 2012). Carotid chemoafferent neuron activity is increased following intermittent hypoxia and the sensitivity of these neurons to an additional hypoxic stimulus is potentiated (Peng *et al.*, 2003; Kumar & Prabhakar, 2012). In addition to the carotid chemoreceptors, plasticity is observed following

intermittent hypoxia at chemoafferent integration sites in the NTS (Kline *et al.*, 2007; Kline, 2010). These alterations in sensory function have been shown to be dependent on reactive oxygen species formation by NADPH oxidase (Peng *et al.*, 2009), transcriptional regulation of hypoxia-inducible factors (Peng *et al.*, 2006b) and serotonergic signalling (Peng *et al.*, 2006a) at the level of the carotid body.

Studies by Mitchell and colleagues have demonstrated that hypoxia-induced spinal plasticity can evoke phrenic long-term facilitation, in the absence of sensory long-term facilitation (Fuller *et al.*, 2000; Devinney *et al.*, 2013). Plasticity within spinal pathways to phrenic motor neurons accounts for elements of this facilitation (Devinney *et al.*, 2013; Fields & Mitchell, 2015). In addition to the motor pathway to the diaphragm, studies support a capacity for motor facilitation of pathways to the inspiratory intercostal (Fregosi & Mitchell, 1994), hypoglossal (ElMallah *et al.*, 2016; Wilkerson *et al.*, 2017) and laryngeal (Bautista *et al.*, 2012) nerves. Studies examining mechanisms of phrenic long-term facilitation have identified a number of essential mediators, some of which include: spinal serotonin release and spinal serotonin receptor (type 2) activation (Baker-Herman & Mitchell, 2002); synthesis of brain derived neurotrophic factor (BDNF) and activation of TrkB receptor (Baker-Herman *et al.*, 2004); ERK MAPK activity (Wilkerson & Mitchell, 2009); and reactive oxygen species formation from the NADPH oxidase complex (MacFarlane *et al.*, 2009; MacFarlane *et al.*, 2014).

1.1.1.3 Compensatory plasticity in breathing

The neural network controlling breathing must adapt adequately to maintain breathing during a broad range of environmental and physiological challenges that occur during health and disease, throughout life. Disorders affecting any component of the respiratory system have the potential to disrupt breathing. Central nervous system disorders including myelin disorders, motor neuron loss (such as in amyotrophic lateral sclerosis) and cervical spinal cord lesions in spinal cord injury, are known to disrupt neural pathways important for breathing. Interestingly, some patients can maintain

ventilatory capacity despite severe nervous system pathology (such as motor neuron loss in amyotrophic lateral sclerosis). Rodent models of motor neuron loss indicate a remarkable capacity for respiratory plasticity within the respiratory control system, which can compensate for such deficits (Nichols *et al.*, 2013; Nichols *et al.*, 2014; Seven *et al.*, 2018). Similarly, recovery of inspiratory muscle activity has been reported in models of cervical spinal cord injury (Fuller *et al.*, 2008; Sandhu *et al.*, 2009; Dougherty *et al.*, 2012).

A number of mechanisms have been proposed which can operate at sites within the system to maintain ventilatory capacity, these include: 1) an alteration in central respiratory drive; 2) plasticity at motor neuronal pools such as the phrenic motor nucleus; 3) plasticity at the neuromuscular junction; 4) respiratory muscle plasticity and altered contribution of respiratory muscles to breathing (e.g recruitment of accessory muscles of breathing) (Johnson & Mitchell, 2013).

1.1.2 Duchenne muscular dystrophy (DMD)

Respiratory failure is a common feature of many neuromuscular diseases and is one of the leading causes of death in boys with Duchenne muscular dystrophy (DMD) (Bye *et al.*, 1990; Shneerson, 1996; Syabbalo, 1998b; Yiu & Kornberg, 2008). DMD is a devastating genetic disease where patients lack the structural protein dystrophin (Muntoni *et al.*, 2003; Nowak & Davies, 2004; Yiu & Kornberg, 2008). Dystrophin is the protein product of the gene defective in DMD (Hoffman *et al.*, 1987) and is the largest described human gene (Muntoni *et al.*, 2003). Full-length dystrophin is rod-shaped (427 kDa) and contains four major domains: amino-terminal domain (connects to actin), flexible rod domain, cysteine-rich domain (connects cytoskeleton to extracellular matrix) and a carboxy-terminal domain (Hoffman *et al.*, 1987; Koenig *et al.*, 1988). The protein is expressed in skeletal, cardiac and smooth muscle and the CNS (Hoffman *et al.*, 1987; Lidov, 1996; Muntoni *et al.*, 2003).

Dystrophin interacts with a group of proteins which collectively form the dystrophin-glycoprotein complex (DGC), or commonly termed the dystrophin associated protein complex (DAPC) (Blake *et al.*, 2002; Ehmsen *et al.*, 2002; Kanagawa & Toda, 2006; Ervasti, 2007). Dystrophin has a structural role in muscle where it provides mechanical support by linking cytoskeletal actin to the sub-sarcolemmal face functioning to prevent stretch-induced damage during muscle contraction (Koenig *et al.*, 1988; Ervasti & Campbell, 1991; Ozawa *et al.*, 1999; Allen & Whitehead, 2011). In the absence of dystrophin, muscle fibres are at risk of contraction-induced injury due to intracellular mechanical destabilisation. Serum creatine kinase is markedly increased in patients, suggesting poor muscle integrity (Petrof *et al.*, 1993a; Petrof, 1998; Ozawa *et al.*, 1999; Yiu & Kornberg, 2008, 2015).

Skeletal muscle weakness is progressive in DMD and initially affects the distal limb musculature, eventually resulting in loss of ambulation when boys are in their teens (Yiu & Kornberg, 2008). Pathological features of dystrophic muscles include muscle fibre degeneration and necrosis with mononuclear cell infiltration, increased variability of muscle fibre size and an increased number of muscle fibres in the regenerative phase (Yiu & Kornberg, 2015). Branched muscle fibres are often observed in dystrophic muscle and lipid accumulation and fibrosis are prominent in muscles where functional fibres are lost (Chan & Head, 2011). Magnetic resonance imaging (MRI) in DMD patients indicates a loss of muscle contractile content and an increase in the lipid content of DMD muscle, which is dependent on disease progression (Forbes *et al.*, 2014; Lott *et al.*, 2014; Willcocks *et al.*, 2014; Vohra *et al.*, 2015).

1.1.3 Pulmonary function in DMD

Since the respiratory system is implicated in DMD, clinicians have examined pulmonary function in patients in order to predict survival and mortality and inform when assisted ventilation is required to sustain gas exchange. Pulmonary function tests examining lung function and volumes in DMD boys have consistently reported that forced vital

capacity (FVC) is significantly lower than predicted values (Baydur *et al.*, 1990; Mohr & Hill, 1990; Kirk *et al.*, 2000; De Bruin *et al.*, 2001; Bersanini *et al.*, 2012; Canapari *et al.*, 2015). Once FVC peaks in the early-to-mid teens in DMD, there is a progressive decline in FVC with increasing age at a rate of approximately 5% of predicted values per year (Baydur *et al.*, 1990; Phillips *et al.*, 2001; Roberto *et al.*, 2011; Khirani *et al.*, 2014; Mayer *et al.*, 2015; Meier *et al.*, 2017). Given the progressive nature of the disease, when vital capacity falls below one litre in DMD boys, it is believed to be a strong predictor of subsequent mortality (Phillips *et al.*, 2001). Truncal fat mass, as measured by dual X-ray absorptimetry, was shown to have a significant inverse relationship with FVC in DMD subjects (Canapari *et al.*, 2015). Recent data from MRI studies in ambulatory DMD boys indicates that DMD patients breathe at lower lung volumes than healthy subjects, although FVC may be within the normal range (Mankodi *et al.*, 2017). Curvature of the spine can impact on lung capacity and scoliosis is known to occur in DMD boys, which further impacts on lung volumes and ventilatory capacity (Rodillo *et al.*, 1988; LoMauro *et al.*, 2014; Yiu & Kornberg, 2015). Pulmonary function testing is a useful tool for monitoring disease progression and clinical outcome measures in patients.

1.1.4 Respiratory muscle weakness in DMD

The thoracic diaphragm is the principal inspiratory pump muscle, phasically active throughout life. The diaphragm is a dome-shaped skeletal muscle that separates the thoracic cavity from the abdomen, receiving neural innervation from the phrenic nerve, originating at the cervical spinal cord. Rhythmic diaphragm muscle contraction increases the volume of the thoracic cavity, in turn decreasing intra-thoracic pressure facilitating inflation of the lungs and thus allowing gas exchange to occur. Trans-diaphragmatic pressure (Pdi) is a surrogate measure for contractile strength of the diaphragm muscle *in vivo*. Pdi is the difference between gastric pressure (Pgas) (reflects abdominal muscle strength) and oesophageal pressure (Poes) (reflects intrapleural pressure, dynamically generated by inspiratory muscles) (Syabballo,

1998a). Khirani *et al.* (2014) measured Pdi during maximal sniff behaviours in DMD patients and reported that values for Pdi were low compared with predicted values of normal subjects (Khirani *et al.*, 2014). Pdi declined steadily after 10 years of age at an average rate of ~ 4 cmH₂O per year (Khirani *et al.*, 2014), revealing a progressive impairment of diaphragm mechanical function. These data describe progressive inspiratory muscle weakness in DMD boys, which undoubtedly has implications for the control of breathing in DMD and adequate ventilatory performance. In addition to inspiratory muscle weakness, expiratory muscle strength is also compromised in DMD. Pgas during cough was measured in DMD boys and reported to be low compared with predicted values and found to decline at a rate of ~ 6 cmH₂O per year (Khirani *et al.*, 2014). The authors describe this expiratory muscle weakness to present, perhaps even prior to inspiratory muscle weakness during the first decade of life. Consistent with these data, a similar study found that reductions in expiratory muscle strength were found to precede inspiratory muscle dysfunction in DMD boys (Hahn *et al.*, 1997), further suggesting an early involvement of expiratory muscles in DMD. Chest wall motion during spontaneous breathing in wakefulness and supine position is an important indicator of the degree of respiratory muscle impairment in DMD (Lo Mauro *et al.*, 2010).

MRI studies of the diaphragm muscle in young DMD boys reported that diaphragm length, contractility and motion were not significantly different from healthy subjects (Mankodi *et al.*, 2017). In contrast, chest wall motion was reduced in patients compared with healthy subjects (Mankodi *et al.*, 2017), with likely consequences for ventilatory reserve capacity. These findings are surprising in the context of the current literature which describes altered diaphragm muscle mechanics in DMD boys (Beck *et al.*, 2006; Khirani *et al.*, 2014). Perhaps overt diaphragm muscle pathology had not yet manifested in these DMD boys given their relatively young age (~ 8 years of age). Thickening of the diaphragm muscle has been described in DMD, along with reduced diaphragm muscle strength (De Bruin *et al.*, 1997; Beck *et al.*, 2006). In addition to the

contribution of the inspiratory muscles to eupnoeic (basal) breathing in DMD boys, the abdominal muscles have been shown to contribute to tidal volume generation, which may be a compensatory mechanism to sustain ventilation (LoMauro *et al.*, 2014). Rapid shallow breathing is observed in some patients and may also be considered an adaptive mechanism aimed at reducing the work of breathing, thus delaying diaphragm muscle fatigue (Lo Mauro *et al.*, 2010). Strength training of the inspiratory muscles in DMD patients has been shown to improve respiratory muscle functional parameters such as Poes and Pdi during the early stages of DMD (Wanke *et al.*, 1994).

1.1.5 Respiratory disturbances in DMD

Sleep can provide a significant challenge for the respiratory control system, particularly in conditions where respiratory function may already be compromised, such as in neuromuscular diseases (Cerveri *et al.*, 1993). Sleep can naturally result in reductions in resting ventilation and responsiveness to chemoreceptor challenges such as hypoxia and hypercapnia (Douglas *et al.*, 1982a; Douglas *et al.*, 1982b; Douglas *et al.*, 1982c; Worsnop *et al.*, 1998). During sleep there is an absence of the excitatory drive to breathe present during wakefulness, and breathing in turn becomes reliant on chemoreceptor input (Fink, 1961; Skatrud & Dempsey, 1983; Meza *et al.*, 1998). During wakefulness, upper airway muscle hypotonia and negative (sub-atmospheric) pressure generated during diaphragmatic contraction increases upper airway resistance, in turn increasing the mechanical load placed on the upper airway musculature and activation of airway mechanoreceptors occurs, resulting in a reflex increase in pharyngeal dilator muscle activity to offset the negative pressure and prevent airway collapse (Fogel *et al.*, 2001). This reflex physiological response is dampened during sleep and as such individuals are at risk of sleep-related breathing disturbances such as airway collapse.

Sleep-disordered breathing (SDB) is a general term describing breathing difficulties during sleep and can include respiratory pause (apnoea), inadequate ventilation (hypopnoea) or respiratory depression (hypoventilation). Apnoeas can be obstructive

or central in nature. Obstructive apnoeas are a result of collapse of the upper airway, whereas central apnoeas are due to diminished neural drive to the upper airway (White, 2005). Children with neuromuscular disease appear to be at a greater risk of developing SDB compared with healthy subjects. Indeed, SDB is a well-recognised feature of DMD (Yiu & Kornberg, 2015; LoMauro *et al.*, 2017).

Obstructive sleep apnoea (OSA) is a common form of SDB characterised by recurrent collapse of the upper airway, resulting in a pathological cycle of oxygen desaturation (hypoxaemia) and re-oxygenation events (Ryan & Bradley, 2005; Eckert & Malhotra, 2008; Sankri-Tarbichi, 2012; White & Younes, 2012). OSA is common in DMD boys as young as seven years of age (Hill *et al.*, 1992; Khan & Heckmatt, 1994; Mellies *et al.*, 2003c; Suresh *et al.*, 2005; Sawnani *et al.*, 2015). It is unclear why patients with DMD are at such risk of developing OSA. Some risk factors for the occurrence of OSA in the general population include age, sex, airway anatomy and obesity (Schwab *et al.*, 1995; Wellman *et al.*, 2004). Obesity is reported in DMD boys (Zanardi *et al.*, 2003), with body mass index increased compared with healthy subjects. Since dystrophin is expressed in skeletal muscle, is it plausible to speculate that the skeletal musculature of the upper airway is weakened in DMD, rendering the upper airway to a greater risk of collapse during sleep. This may be one explanation for the increased incidence of OSA in DMD, notwithstanding the other complex mechanisms influencing airway control including central respiratory gain (Dempsey *et al.*, 2010) and factors affecting motor drive to the upper airway (Castele *et al.*, 1985; Mifflin, 1990; Badr, 1996; Funk *et al.*, 1997; Jordan, 2001).

The severity of sleep apnoea is scored clinically by the apnoea-hypopnea index (AHI); the number of apnoeas and hypopnoeas per hour of sleep, as a result of upper airway collapse. Smith *et al.* (1989) reported the AHI of DMD patients to be 12.6 events/hr (Smith *et al.*, 1989a). Later, Bersanini *et al.* (2012) reported the average AHI of 11 DMD patients during sleep to be 18 events/hr (Bersanini *et al.*, 2012). Based on the AHI

scale, both studies suggest DMD boys suffer from moderate sleep apnoea. Central apnoeas have also been recorded in DMD boys during sleep (Manni *et al.*, 1989). Sawnani *et al.* (2015) observed a reduced FVC (80% of predicted values) in DMD patients and reported 64% of patients to be suffering from OSA, 37% had central sleep apnoea and 17% had hypoventilation (Sawnani *et al.*, 2015). Co-morbidities can manifest as a result of OSA including daytime hypersomnolence and headache, both of which are observed in DMD boys with SDB (Barbé *et al.*, 1994). In addition, hypertension, neurocognitive impairment and cardiac dysfunction often present as a result of OSA.

Despite diaphragm muscle weakness in DMD, minute ventilation can be normal in boys during wakefulness, with irregular ventilation prominent during sleep (Smith *et al.*, 1989b). As patients reach the second decade of life, hypoventilation during sleep presents (Smith *et al.*, 1989b, a; Hukins & Hillman, 2000; Kirk *et al.*, 2000; Suresh *et al.*, 2005; Sawnani *et al.*, 2015). Hypoventilation has been shown to occur during all sleep stages in DMD boys (Smith *et al.*, 1989b). During non-rapid eye movement sleep (non-REM), the diaphragmatic contribution to breathing was found to be lower in DMD compared with predicted values and this was correlated with the magnitude of oxygen desaturation during REM sleep (Smith *et al.*, 1989b), suggesting impaired force-generating capacity of the diaphragm muscle with resultant hypoventilation and blood-gas disturbance. Protriptyline is an anti-cholinergic drug which can suppress REM sleep. The effects of protriptyline on oxygen desaturation and disordered breathing were assessed in DMD patients and found to effectively reduce sleep hypoxaemia and disordered breathing (reduced AHI) (Smith *et al.*, 1989a).

1.1.6 Blood-gas homeostasis in DMD

Disrupted blood-gas homeostasis can occur in DMD due to apnoeic events and hypoventilation. Arterial oxygen desaturations appear to be common, with DMD boys experiencing bouts of hypoxaemia during sleep (Smith *et al.*, 1988; Manni *et al.*, 1989;

Smith *et al.*, 1989b, a; Hill *et al.*, 1992; Barbé *et al.*, 1994; Khan & Heckmatt, 1994; Melacini *et al.*, 1996; Hukins & Hillman, 2000; Bersanini *et al.*, 2012). Khan *et al.* (1994) report that oxygen desaturations were more frequent with increasing age in DMD (Khan & Heckmatt, 1994), consistent with the highly progressive nature of the disease. Simultaneously, nocturnal hypercapnia occurs due to the retention of CO₂ as a result of sleep-related hypoventilation (Baydur *et al.*, 1990; Mohr & Hill, 1990; Melacini *et al.*, 1996; Kirk *et al.*, 2000; Bersanini *et al.*, 2012). Elevations in PaCO₂ were associated with decreased maximum inspiratory pressure in patients (Hahn *et al.*, 1997). Although vital capacity levels can be low in DMD, patients can remain normocapnic once vital capacity remains > 1,820ml (Toussaint *et al.*, 2007).

The causes and consequences of OSA and nocturnal hypoventilation in DMD remain to be elucidated. OSA and hypoventilation can be multifactorial and can occur due to decreased ventilatory drive from the CNS, poor chemical control of breathing during sleep or altered respiratory mechanics. Since prominent weakness of the inspiratory and expiratory muscles is observed in DMD, worsened respiratory mechanics is likely a major contributor. However, whether chemoreceptor control of breathing or ventilatory drive is altered in DMD remains to be determined. Nocturnal hypoventilation and OSA results in hypoxaemia and hypercapnia during sleep and in some cases diurnal hypercapnia presents. Studies in animal models have clearly demonstrated the adaptive and maladaptive consequences of hypoxia on the integrated respiratory control system, in addition to its effects on autonomic control and metabolic and cardiovascular function (O'Halloran *et al.*, 2002; Peng *et al.*, 2003; Prabhakar *et al.*, 2005; Dick *et al.*, 2007; Edge *et al.*, 2010; Terada & Mitchell, 2011; Edge *et al.*, 2012; Lucking *et al.*, 2014; Souza *et al.*, 2015, 2016). In the light of these data, the potential consequences of hypoxaemia in DMD, a disease where the respiratory system is already compromised, could prove catastrophic for the control of breathing.

1.1.7 Non-ventilatory behaviours in DMD

The respiratory system contributes to many non-ventilatory functions including coughing, sneezing and airway clearance manoeuvres. Patients with DMD can have inefficient cough due to reduced lung volumes and chest wall compliance and muscle weakness of the expiratory and inspiratory musculature (Kravitz, 2009; LoMauro *et al.*, 2014). Poor cough efficiency in DMD is associated with reduced operating lung and chest wall volume as a result of inspiratory muscle weakness (LoMauro *et al.*, 2014). Such inefficiencies make patients at risk of respiratory infections and aspiration (Aloysius *et al.*, 2008; Toussaint *et al.*, 2016).

1.1.8 Assisted ventilation in DMD

Current respiratory management strategies for DMD include non-invasive ventilation (NIV) (Arens & Muzumdar, 2010; Yiu & Kornberg, 2015; Birnkrant *et al.*, 2016), lung volume recruitment and systemic steroids (Katz *et al.*, 2004). Non-invasive positive pressure ventilation (NIPPV) has been shown to have the most beneficial effects on ventilation in patients with neuromuscular disease compared with negative pressure ventilation, which can contribute to upper airway obstruction, reduced chest wall movements and oxygen desaturation (Ellis *et al.*, 1987; Hill *et al.*, 1992). Suresh *et al.* (2015) reported a significant improvement in the AHI of DMD boys following non-invasive ventilation (Suresh *et al.*, 2005). Long-term NIV in DMD patients has the capacity to normalise nocturnal gas exchange and improve diurnal gas exchange and sleep quality (Mellies *et al.*, 2003b), along with improving side-effects of SDB such as morning headaches, mood, concentration and daytime sleepiness (Mellies *et al.*, 2003a). In comparison, a randomised trial of NIPPV in DMD patients found that NIPPV did not improve respiratory function, suggesting that the use of NIPPV should be avoided in DMD patients with FVC values between 20 and 50% of predicted values (Raphael *et al.*, 1994).

Currently no cure exists for DMD; steroidal treatment with glucocorticoids is the current strategy adopted to treat patients (Yiu & Kornberg, 2015). Steroid therapy in boys with DMD has the capacity to stabilise or delay loss of lung function, independent of ambulatory state (Machado *et al.*, 2012). Similarly, chronic glucocorticoid use can partially preserve respiratory muscle strength and lung volumes in DMD (Buyse *et al.*, 2013).

Due to the progressive decline in respiratory function in DMD and chronic disruption to blood gas homeostasis, in some severe cases, patients require invasive procedures such as tracheostomy to facilitate adequate ventilation (Mohr & Hill, 1990; Baydur *et al.*, 2000). Since the use of NIV strategies for DMD patients in combination with corticosteroid therapy, there has been a concomitant increase in life expectancy. Lung inflation training using a positive end-expiratory pressure (PEEP) valve in tracheotomised DMD patients for four months significantly increased maximum PEEP lung inflation capacity (Matsumura *et al.*, 2012). A holistic approach to improving pulmonary function in DMD boys via yoga breathing exercises has been demonstrated to significantly increase FVC and forced expiratory volume (FEV₁) (Rodrigues *et al.*, 2014).

1.1.9 Cardiovascular function in DMD

Cardiac function has now become the major determinant of survival in patients using assisted ventilation (Melacini *et al.*, 1996; Birnkrant *et al.*, 2016). Patients with advanced DMD show abnormal electrocardiograms, left ventricular wall abnormalities, left ventricular dilation with decreased ejection fraction and pulmonary hypertension (Melacini *et al.*, 1996). Dilated cardiomyopathy and left ventricular dysfunction are the most common features of cardiac dysfunction in DMD patients (Faysoil *et al.*, 2017).

1.2 Dystrophin-deficient *mdx* mouse

The *mdx* mouse is a mutant model of DMD which arose from an inbred C57BL10 colony of mice (Bulfield *et al.*, 1984). The *mdx* mouse has a premature stop codon which terminates on exon 23 of the dystrophin gene and the *mdx* mouse subsequently lacks the largest dystrophin isoform (427kDa). The model has been extensively studied and has greatly contributed to understanding of the pathophysiology of DMD (Manning & O'Malley, 2015). Dystrophin is absent from skeletal, cardiac and smooth muscle and the CNS of *mdx* mice. A relatively mild phenotype in terms of limb pathology is observed in *mdx* mice compared with human DMD (Lynch *et al.*, 2001). Dystrophic limb muscle initially undergoes fibre degeneration and weakness in the first few weeks of life (3-8 weeks of age). Thereafter, the limb muscles can recover and compensate for the lack of dystrophin by upregulating a protein of similar homology called utrophin. In comparison, dystrophic diaphragm muscle from *mdx* mice exhibits severe mechanical dysfunction and muscle weakness during life (Stedman *et al.*, 1991; Petrof *et al.*, 1993b; Coirault *et al.*, 1999; Coirault *et al.*, 2003).

1.2.1 Dystrophin and the striated muscles of breathing

Diaphragm muscle weakness presents as early as six weeks of age in the *mdx* mouse (Coirault *et al.*, 2003) and persists throughout life (Stedman *et al.*, 1991; Stevens & Faulkner, 2000; Whitehead *et al.*, 2016). The absence of dystrophin in *mdx* diaphragm exposes the sarcolemma to a greater risk of mechanical instability, contraction induced injury (Petrof *et al.*, 1993a) and reduced muscle elasticity and fibre length (Stedman *et al.*, 1991). Diaphragm muscle fibre degeneration and repair occurs due to muscle fibre damage. Centralised myonuclei (indicative of muscle fibre damage and repair) are present in *mdx* diaphragm together with progressive fibrosis (Stedman *et al.*, 1991; Gosselin & McCormick, 2004; Gosselin *et al.*, 2007; Ishizaki *et al.*, 2008; Barros Maranhão *et al.*, 2015; Gutpell *et al.*, 2015; Smith *et al.*, 2016). *Mdx* diaphragm undergoes inflammation, with an increase in mononuclear cell infiltration. Over time, necrotic muscle fibres are replaced by connective tissue and lipid deposits.

Structural alterations in myosin heavy chain (MyHC) isoform composition are sometimes observed in dystrophic skeletal muscle. Skeletal muscle fibres are categorised based on their MyHC isoform composition, which ultimately determines the muscle fibres intrinsic contractile properties, resistance to fatigue and metabolic enzyme activity. The diaphragm muscle is a mixed muscle comprising all four types of MyHC: type I (slow oxidative fibres), type IIa (fast-twitch oxidative-glycolytic) and type IIx and IIb (fast-twitch glycolytic fibres). Type II fibres display a progressive increase in force production from IIa to IIb, with IIb producing the greatest forces and maintaining the least resistance to fatigue (Polla *et al.*, 2004; Schiaffino & Reggiani, 2011).

Dystrophic diaphragm muscle from *mdx* mice expresses a reduced number of MyHC IIx fibres and increased MyHC IIa fibres compared with wild-type (Coirault *et al.*, 1999), probably as a result of a lack of maturation of muscle fibres due to ongoing muscle damage and repair processes. In addition to diaphragm muscle weakness and altered MyHC complement in *mdx* mice, the total number of cross-bridges per mm², the elementary force per cross-bridge and the peak mechanical efficiency are decreased compared with age-matched wild-type mice (Coirault *et al.*, 1999). Bates *et al.* (2013) demonstrated muscle weakness in the diaphragm muscle at the level of intact muscle strips, however molecular myosin function and the mechanics of single permeabilized muscle cells were not affected (Bates *et al.*, 2013). The number of regenerating muscle fibres in *mdx* diaphragm increase with age, while fibre cross-sectional area, sarcomere length and the number of branched fibres are decreased (Henry *et al.*, 2017).

Respiratory muscle training in *mdx* mice with CO₂ breathing increases diaphragm muscle force and the expression of the DAPC protein, α -dystrobrevin (Matecki *et al.*, 2005). Interestingly, there is a paucity of information in relation to the accessory muscles of breathing in the *mdx* mouse model of DMD, namely the intercostal and abdominal muscles. Studies indicate the intercostal muscles may present with less severe histological changes compared with *mdx* diaphragm (Stedman *et al.*, 1991;

Ishizaki *et al.*, 2008). Studies of the structural and functional consequences of dystrophin-deficiency on the accessory muscles of breathing in *mdx* mice are lacking.

1.2.2 Respiratory function in the *mdx* mouse

Although diaphragm muscle weakness is well described in the *mdx* mouse and is observed from a young age, few studies have thoroughly examined the functional consequences of dystrophin deficiency on respiratory behaviour and ventilatory capacity in *mdx* mice. Moreover, studies have not tracked ventilatory capacity as a function of ageing in *mdx* mice, despite the fact that the diaphragm muscle undergoes a progressive pathology.

Impaired normoxic ventilation was reported in 2- and 6-month-old *mdx* mice (Mosqueira *et al.*, 2013; Burns *et al.*, 2015). At 2 months of age, *mdx* mice appear to have significantly reduced minute ventilation compared with age-matched wild-type mice during normoxia (Burns *et al.*, 2015). Mosqueira *et al.* (2013) reported significantly reduced respiratory frequency, tidal volume and minute ventilation during normoxic breathing in 6-7 month old *mdx* mice compared with age-matched wild-type mice (Mosqueira *et al.*, 2013). Ishizaki *et al.* (2008) demonstrated significant reductions in respiratory frequency in 2- and 4-month-old *mdx* mice. Further, Huang *et al.* (2011) concluded that *mdx* mice have significant reductions in respiratory frequency and tidal volume at 3 and 6 months of age (Huang *et al.*, 2011). Markham *et al.* (2015) report that *mdx* mice at 7 months of age have significantly reduced respiratory frequency and minute ventilation compared with wild-type (Markham *et al.*, 2015).

Surprisingly, no study to date has examined indices of respiratory stability in *mdx* mice such as breath-to-breath variability and apnoeic events. Ventilatory capacity in *mdx* mice has been briefly studied by stimulating central chemoreceptors with CO₂, enhancing neural drive to the diaphragm muscle, thereby driving ventilation. A significant blunting of the hypercapnic ventilatory response was observed in 7-month-

old *mdx* mice (Gosselin *et al.*, 2003). In comparison, Gayraud *et al.* (2007) observed no differences in ventilation between wild-type and *mdx* mice during normoxia and preservation of hypercapnic breathing at 5 months of age. In older mice (16 months old), *mdx* had higher respiratory frequency and a blunted response to CO₂ challenge compared with wild-type mice (Gayraud *et al.*, 2007). Some discrepancies are apparent in this body of literature. Studies of peripheral chemoreceptor function and examination of hypoxic sensitivity in *mdx* mice are lacking.

1.2.3 Dystrophin and the upper airway

In addition to diaphragm muscle weakness, the skeletal musculature of the upper airway is also compromised by dystrophin deficiency in the *mdx* mouse (Attal *et al.*, 2000; Burns & O'Halloran, 2016). Upper airway muscles have a physiological role in maintaining upper airway patency during wakefulness and vulnerable periods such as sleep. Pharyngeal dilator muscles of the upper airway, such as the genioglossus and sternohyoid muscles, are phasically active during respiration and contribute to control of upper airway resistance. Attal *et al.* (2000) hypothesised that the sternohyoid muscle from *mdx* mice would have intrinsic muscle weakness. At six months of age, peak tetanic tension was 50% lower for *mdx* sternohyoid compared with wild-type muscle (Attal *et al.*, 2000).

The upper airway muscles are primarily composed of MyHC type II fibres, allowing these pharyngeal dilator muscles to generate large forces and produce faster contraction times, while concomitantly demonstrating reduced fatigue resistance compared with the diaphragm muscle (Dick & van Lunteren, 1990; Van Lunteren & Vafaie, 1993; Cantillon & Bradford, 1998, 2000; McGuire *et al.*, 2002; Skelly *et al.*, 2012). This profound weakness in *mdx* sternohyoid muscle is associated with a shift in the MyHC isoform composition from MyHc IIb to IIx. Mechanical dysfunction has also been described in sternohyoid muscle from young *mdx* mice (eight weeks of age) (Burns & O'Halloran, 2016). Alterations in the MyHC composition of dystrophic

sternomastoid muscle from *mdx* mice also occurs with a significant reduction in MyHC IIb and an increase in centralised myonuclei (Guido *et al.*, 2010). These data have relevance to the control of upper airway patency in DMD. Since obstructive apnoeas occur in DMD boys, these data support the hypothesis that weakening of the upper airway musculature due to dystrophin-deficiency may contribute to upper airway collapse in DMD, and potentially lead to alternating periods of hypoxia and re-oxygenation due to airway obstruction. Studies of upper airway muscle function are lacking in DMD and *mdx* mice. Adequate upper airway muscle performance is key for the homeostatic regulation of breathing. Despite the pronounced muscle weakness observed in *mdx* sternohyoid muscle, studies have not examined the neural control of the upper airway in DMD and *mdx* mice, and it is unclear if motor control of the upper airway is compromised by dystrophin deficiency. Indeed, there is a general paucity of knowledge in respect of the neural control of breathing in the human dystrophinopathies.

1.2.4 Dystrophin and the airways

In addition to skeletal muscle, dystrophin is expressed in smooth muscle, and of relevance to the current review, the smooth muscle of the airways express dystrophin. Surprisingly, little work has examined the physiological implications of dystrophin deficiency on airway smooth muscle function. Sharma *et al.* (2014) described the consequences of dystrophin lack for airway smooth muscle contraction. Peak airway resistance in response to maximal stimulation with methacholine was significantly reduced in *mdx* mice compared with wild-type (Sharma *et al.*, 2014). These data indicate that dystrophin's absence and thus inadequate mechanical linkage between the actin cytoskeleton and the DAPC have implications for airway smooth muscle function in *mdx* mice.

1.2.5 Dystrophin and the nervous system

In addition to muscle, dystrophin is expressed in the CNS. The largest isoform of dystrophin (Dp427) is absent from the CNS of *mdx* mice (Nichols *et al.*, 2015; Aranmolate *et al.*, 2017). In DMD, cognitive impairment is observed in patients owing to a lack of dystrophin expression in the brain (Anderson *et al.*, 2002; Cyrulnik & Hinton, 2008). In a similar manner, learning and memory deficits are seen in *mdx* mice (Chaussonot *et al.*, 2015; Rae & O'Malley, 2016).

Some consequences of dystrophin absence from the CNS of *mdx* mice include delayed myelination in the cerebral cortex (Aranmolate *et al.*, 2017), decreased neurons in the trigeminal sensory nuclear complex (Pinto *et al.*, 2007), increased size of the lateral ventricles (Xu *et al.*, 2015), damaged motor pathways (Carretta *et al.*, 2001), decreased neuronal projections (Pinto *et al.*, 2008) and a leaky blood-brain-barrier (Goodnough *et al.*, 2014). The number of neurons containing the calcium-binding proteins parvalbumin and calbindin are increased in the motor and somatosensory cortices of *mdx* mice (Carretta *et al.*, 2001) and an increase in the number of anterior horn neurons of the spinal cord has been noted (Papapetropoulos & Bradley, 1972).

Deficits within the peripheral nervous system of dystrophic mice include reduced number of axons in the tibial nerve, despite normal fibre diameter and axon packing (Harris *et al.*, 1972). Jaros *et al.* (1983) examined the common peroneal nerve and the tibial nerve of dystrophic mice and reported an increase in the number of Schwann cell nuclei associated with myelinated axons, decreased inter-nodal length and a reduction in the number of myelinated axons (Jaros & Jenkison, 1983).

There is no evidence of utrophin upregulation and compensation in the *mdx* brain, similar to that seen in the limb muscles (Knuesel *et al.*, 2000; Perronnet *et al.*, 2012). Biochemically, there is an increase in choline containing compounds in *mdx* cerebellum and hippocampus, and altered glucose metabolism (Rae *et al.*, 2002; Xu *et al.*, 2015).

One function of dystrophin in the CNS is the stabilization of neurotransmitter receptors such as GABA and acetylcholine receptors (Knuesel *et al.*, 1999; Brünig *et al.*, 2002; Pilgram *et al.*, 2010; Parames *et al.*, 2014). Dysfunction of the GABAergic system occurs in the brains of *mdx* mice (Sekiguchi *et al.*, 2009; Vaillend & Chaussonot, 2017), with disrupted GABA neurotransmission (Xu *et al.*, 2015), suggesting a removal of central inhibition in dystrophic brains. Alterations in antioxidant enzymes are reported in dystrophic brains from *mdx* mice. Superoxide dismutase is increased in the cerebellum, prefrontal cortex, hippocampus and striatum, while catalase is reduced in the striatum (Comim *et al.*, 2009a). Glutathione is increased in the hippocampus and taurine is increased in the pre-frontal cortex (Xu *et al.*, 2015). These data suggest an alteration in redox status within the CNS of *mdx* mice. Neurotrophins are a family of proteins that support the survival, development and function of neurons. Studies of neurotrophic factors in *mdx* mice are lacking. Comim *et al.* (2009) examined BDNF in the pre-frontal cortex, cerebellum, hippocampus and striatum of *mdx* mice. No change in BDNF was found in the cerebellum, hippocampus, and cortex, whereas BDNF was reduced in *mdx* striatum and pre-frontal cortex (Comim *et al.*, 2009b).

Of particular relevance to the control of breathing, dystrophin is expressed in the brainstem of mice. The effects of dystrophin deficiency on the key cardio-respiratory integrating sites and rhythm and pattern generating sites of the brainstem are unknown. The brainstem contains the hypoglossal (XII) motor nucleus which provides motor control of the upper airway via the hypoglossal nerve; it has not been determined if the major motor pathway of the upper airway shows pathological features resulting from dystrophin deficiency in *mdx* mice. Studies examining peripheral nerve morphometry in respiratory motor pathways are lacking, despite pathological changes reported in the tibial nerve of dystrophic mice.

Dystrophin is expressed at the neuromuscular junction (Huard *et al.*, 1991; Pilgram *et al.*, 2010; Pratt *et al.*, 2015a), where it has a scaffolding function for neuronal receptors

(Xu & Salpeter, 1997). Remodelling of the neuromuscular junction is observed in dystrophic muscle, evidenced by decreased neuromuscular junction occupancy, increased nerve branching and increased nerve discontinuity in *mdx* quadriceps muscle (Pratt *et al.*, 2015b). There is an increase in neural transmission variability at the neuromuscular junction of *mdx* diaphragm and disrupted post-synaptic acetylcholine receptor clustering (Xu & Salpeter, 1997; Personius & Sawyer, 2006; van der Pijl *et al.*, 2016). Van der Pijl *et al.* (2016) reported an increase in the number of acetylcholine quanta released per nerve impulse, suggesting a homeostatic increase in the neurotransmitter release at the neuromuscular junction in *mdx* muscle (van der Pijl *et al.*, 2016). Increased nerve branching or sprouting could serve to compensate for degenerating neuromuscular junctions and fibres in dystrophic muscle.

1.2.6 Dystrophin and chemoreception

Dystrophin is expressed in the carotid body of wild-type mice and absent from the carotid bodies of *mdx* mice (Mosqueira *et al.*, 2013). The carotid body is the most vascularised tissue in the body and is composed of two types of cells called glomus type I (neural crest) and glomus type II (glial cells) cells. Type I cells are electrically excitable and become depolarized when there is a decrease in the PO₂ of arterial blood, an increase in arterial PCO₂ or a decrease in the pH of arterial blood. Depolarization opens voltage gated calcium channels, increasing intracellular calcium concentration, stimulating exocytosis of vesicles which contain a wide variety of neurotransmitters. Release of the neurotransmitters ATP, noradrenaline, acetylcholine and adenosine (among others), facilitates action potential generation on afferent nerve fibres. Type II cells act as supporting cells. The carotid body signals along the carotid sinus nerve, which is a branch of the glossopharyngeal nerve, and relays sensory afferent information to the NTS of the brainstem.

In muscle, dystrophin is known to have a structural and mechanical function and a cell signalling role as part of the DAPC. At this juncture, it is unclear if there is a pivotal role

for dystrophin in carotid body function. Dystrophin in the CNS is important for receptor localisation and arrangement, particularly for GABA and acetylcholine receptors. Perhaps dystrophin has a similar function in the peripheral oxygen sensor, where there are abundant neurochemicals. Dystrophin may also have a stabilisation role in the cytoskeleton of the peripheral oxygen sensor, affecting synaptic vesicle arrangement and trafficking during exocytosis. The consequences of dystrophin deficiency within the carotid body are unclear. Investigations are necessary to examine any potential deficits within the carotid body of *mdx* mice, which may have implications for the control of breathing and adequate chemoreception during physiological perturbations in arterial blood gases. Similarly, the consequences of dystrophin deficiency on central chemoreception is unclear. Central chemoreceptors are sensitive to changes in CO₂ and pH. It is now clear that hypoxaemia and hypercapnia are common features of DMD, particularly during sleep, when ventilation is heavily dependent on chemoreceptor input. If chemoreception is affected by dystrophin deficiency in *mdx* mice (and DMD), then this would have major implications for the control of breathing.

1.2.7 Dystrophin and neuromechanical control of breathing

There is a paucity of information pertaining to the neural control of breathing in DMD and indeed animal models of DMD, despite respiratory morbidity and mortality being dominant features of the disease. Studies are required to understand the extent of respiratory system deficits and compensation in DMD and animal models, and to characterise temporal changes within the respiratory control network over the course of disease progression. Knowledge of fundamental aspects of respiratory control is essential in the consideration of respiratory management of patients with DMD. Studies should examine the capacity for plasticity within the motor pathway of the diaphragm, to potentially compensate for diaphragm functional deficits. A better appreciation of the intrinsic compensatory processes (if any) at play in DMD could help inform therapeutic strategies. Examination of the motor neuron pools involved in breathing and motor unit activity across ventilatory and non-ventilatory behaviours will

be important in determining if respiratory muscle activation is altered due to dystrophin deficiency. It is clear that neurotransmission in the CNS can be augmented in the absence of dystrophin. The neuro-modulators of relevance to breathing should be assessed to determine if the neurochemical control of breathing is intact in *mdx* mice.

1.2.8 Other animal models of DMD

Since the *mdx* mouse experiences a mild limb muscle phenotype compared with that observed in DMD boys, researchers have tried to develop more severe murine models by removing utrophin, a protein that purportedly compensates for the lack of dystrophin in the limb, thus responsible for the relative sparing of limb muscles in *mdx* mice. The dystrophin/utrophin double knockout mouse (*mdx/utrn*^{+/-}), which exhibits a severe limb muscle pathology and a shortened lifespan, has been widely studied in recent years (McDonald *et al.*, 2015). The *mdx/utrn*^{+/-} mouse experiences cardiac damage similar to that of DMD patients (Delfín *et al.*, 2012) and has greater skeletal muscle fibrosis compared with *mdx* mice, with the diaphragm muscle undergoing the greatest degree of fibrosis (Gutpell *et al.*, 2015).

A dystrophin deficient rat model of DMD was recently developed using transcript activator-like effector nucleases (TALENs) targeting exon 23. This model presents with limb and diaphragm muscle necrosis and regeneration, severe fibrosis and adipose tissue infiltration, reduced muscle strength and decreased spontaneous motor activity. A cardiac phenotype was evident that resembled dilated cardiomyopathy and altered diastolic function (Larcher *et al.*, 2014).

A common canine model of DMD is also used by researchers to study DMD and potential therapeutics (Howell *et al.*, 1997; Nakamura & Takeda, 2011). Golden retriever muscular dystrophy (GRMD) is characterised by progressive skeletal muscle weakness and atrophy and cardiac dysfunction. Diaphragm muscle from the GRMD

model shows anatomical changes such as increased muscle thickness (Thibaud *et al.*, 2017). Mead *et al.* (2014) examined respiratory mechanics in the GRMD model and demonstrated a rapid progressive loss of ventilatory capacity in concert with major remodelling of the diaphragm muscle (Mead *et al.*, 2014). The mechanics of breathing were extensively altered in the GRMD, with the main role of the diaphragm muscle becoming the passive elastic storage of energy transferred from the abdominal wall muscles, thus allowing the expiratory musculature to participate in the process of inspiration (Mead *et al.*, 2014). These data are of major significance and are consistent with studies in DMD boys, and indicate accessory muscle compensation by the abdominal muscles. Additional research is required to examine the abdominal muscles in DMD and their potential role in facilitating breathing in DMD boys and models of DMD. Other models of DMD include a porcine model (Klymiuk *et al.*, 2013), feline model (Kohn *et al.*, 1993), and further genetic manipulations of *mdx* mice (Gosselin *et al.*, 2003; Willmann *et al.*, 2009; Nitahara-Kasahara *et al.*, 2014; Pelosi *et al.*, 2015b).

1.3 Role of inflammation in DMD pathophysiology

Inflammation is a prominent feature of DMD, secondary to muscle fibre damage. Absence of dystrophin in DMD renders the skeletal muscle plasma membrane to a greater risk of contraction induced injury during muscle contraction. This mechanical damage can result in sarcolemmal tears and fibre damage, which triggers the recruitment of inflammatory mediators to the damaged muscle leading to immune cell infiltration (Deconinck & Dan, 2007). There is elevated expression of chemokines in serum and muscle samples from DMD patients (Pescatori *et al.*, 2007; Abdel-Salam *et al.*, 2010; De Paepe *et al.*, 2012) and *mdx* mice (Porter *et al.*, 2003; Demoule *et al.*, 2005). Inflammatory chemokines are formed in pathological conditions and have a role as chemoattractant molecules, which function to attract monocytes and lymphocytes to sites of inflammation.

Similarly, there is heightened expression of pro-inflammatory cytokines in plasma and muscle biopsies from DMD boys. As such, systemic and muscle inflammation are pathological features of DMD and are major contributing factors in promoting disease progression. Cytokine expression studies in DMD report that interleukin-6 (IL-6) is significantly increased in DMD serum (Rufo *et al.*, 2011; Cruz-Guzmán *et al.*, 2015), along with increased levels of IL-1 β and tumour necrosis factor- α (TNF- α) (Cruz-Guzmán *et al.*, 2015). There is increased mRNA and protein expression of TNF- α and IL-6 in DMD muscle biopsies (Messina *et al.*, 2011) and increased expression of IL-17 mRNA (De Pasquale *et al.*, 2012).

1.3.1 Inflammation in *mdx* mice

Histological and immuno-histochemical studies of diaphragm muscle from *mdx* mice demonstrate extensive muscle inflammation throughout life. Cytokine concentrations are elevated in *mdx* diaphragm muscle homogenates compared with wild-type diaphragm. Such findings indicate that dystrophin deficiency in the diaphragm can activate immune cell signalling. In stark contrast, limb muscle from *mdx* mice exhibits

extensive muscle inflammation at an early age (3 to 8 weeks of age), which subsides as mice age.

1.3.2 Inflammation and oxidative stress

There is increasing evidence in support of the link between inflammation and oxidative stress in dystrophic muscle. Inflammatory cells such as neutrophils can promote muscle damage following injury, while macrophages can also mediate muscle damage through the release of free radicals (Tidball, 2005). Elevated levels of free radicals can shift the redox balance and cause overt tissue damage and disruption to signalling cascades in muscle and other tissues (Tidball & Wehling-Henricks, 2007; Kozakowska *et al.*, 2015). Diaphragm muscle weakness in *mdx* mice is associated with altered redox balance (Lawler, 2011; Kim *et al.*, 2013). There is an increase in protein thiol oxidation and protein carbonyl content in *mdx* diaphragm (El-Shafey *et al.*, 2011). The reactive oxygen species generating complex, NADPH oxidase, is upregulated in *mdx* diaphragm and is implicated in promoting muscle dysfunction (Loehr *et al.*, 2018). Reactive oxygen species production is increased in *mdx* muscle (Dudley *et al.*, 2006a; Dudley *et al.*, 2006b; Whitehead *et al.*, 2006; Allen *et al.*, 2010; Kim & Lawler, 2012; Kim *et al.*, 2013). Lipofuscin granules, a marker of oxidative stress, are elevated in *mdx* diaphragm (Nakae & Stoward, 2016) and glutathione peroxidase mRNA and protein expression are increased in DMD muscle (Messina *et al.*, 2011). Dystrophic diaphragm has significant reductions in Nrf2 protein and SIRT1 gene expression, increased dihydroethidium (DHE) staining, indicating a pro-oxidant environment, with a concomitant increase in pro-inflammatory gene expression (Pelosi *et al.*, 2017). Antioxidant interventions in *mdx* mice have shown improvements in skeletal muscle form and function (Ismail *et al.*, 2014; Capogrosso *et al.*, 2016; Burns *et al.*, 2017; Mâncio *et al.*, 2017).

1.3.3 Targeting inflammation as a therapy in DMD

Curcumin, a potent NF- κ B inhibitor, has been examined as a potential therapeutic agent in *mdx* mice. This anti-inflammatory agent was found to improve sarcolemmal

integrity, improve grip strength and alleviate structural deficits observed in dystrophic muscle (Pan *et al.*, 2008). Moreover, the concentrations of the pro-inflammatory cytokines IL-1 β and TNF- α were significantly reduced in *mdx* serum (Pan *et al.*, 2008). The cellular inhibitor of apoptosis 1 (cIAP1) protein is a regulator of NF- κ B signalling pathways. Enwere *et al.* (2013) examined if loss of cIAP1 in *mdx* mice would alleviate skeletal muscle dysfunction (Enwere *et al.*, 2013). Double mutant cIAP1/*mdx* mice presented with reduced immune cell invasion and decreased cytokine expression in the soleus muscle, together with reduced muscle fibre central nucleation compared with *mdx*. Remicade, a TNF blocking agent, showed modest benefits on skeletal muscle strength and fibrosis in *mdx* mice, however inhibition of Akt was observed in *mdx* mice, which negatively influences cardiac function (Ermolova *et al.*, 2014).

Non-steroidal anti-inflammatory drug (NSAID) treatment in *mdx* mice improved muscle morphology and reduced macrophage infiltration and necrosis, but had no beneficial effect on isometric force (Serra *et al.*, 2012). Inflammatory cytokines and cyclooxygenase-2 expression were decreased following NSAIDs in *mdx* skeletal muscle. The immunosuppressant drug rapamycin was administered to *mdx* mice to examine its effects on dystrophic muscles (Eghtesad *et al.*, 2011). Muscle fibre necrosis was significantly reduced in *mdx* diaphragm and limb muscle following rapamycin treatment and the infiltration of CD4⁺ and CD8⁺ T cells in skeletal muscle was decreased.

1.3.4 Cytokines

IL-15 is expressed in skeletal muscle and is known to have anabolic effects on muscle. Harcourt *et al.* (2005) demonstrated that four weeks of IL-15 administration in *mdx* mice improved diaphragm muscle strength, decreased collagen infiltration and increased muscle fibre cross-sectional area (Harcourt *et al.*, 2005). The anti-inflammatory cytokine IL-10 is elevated in skeletal muscle from *mdx* mice and localised to the surface of mono-nucleated cells in inflammatory lesions and regenerating

muscle fibres and myotubes (Villalta *et al.*, 2011; Pelosi *et al.*, 2017). Ablation of IL-10 in *mdx* mice resulted in increased muscle damage *in vivo* and poor muscular strength. The authors concluded that IL-10 has a regulatory role in *mdx* mice that may be executed by decreasing M1 macrophage activation and cyto-toxicity, increasing M2c macrophage activation and modulating muscle differentiation. In a similar study, ablation of IL-10 in *mdx* mice resulted in severe cardio-respiratory dysfunction (Nitahara-Kasahara *et al.*, 2014). The hearts of *mdx* mice lacking IL-10 were severely affected and exhibited extensive muscle degeneration and myofibre loss and functional reductions in percent fractional shortening and percent ejection fraction. Cytokines and chemokines were elevated in the diaphragm muscle of these mice and a significant reduction in tidal volume was reported compared with *mdx* mice. These data suggest a significant role for IL-10 as an immune-modulator in dystrophic muscle; it appears that susceptibility to inflammation in *mdx* mice is an important feature in the development of cardio-respiratory dysfunction. TNF- α deletion in *mdx* improved diaphragm muscle force and increased ventilatory capacity (Gosselin *et al.*, 2003).

1.3.5 Interleukin-6

IL-6 is a pleiotropic cytokine with anti- and pro-inflammatory actions in health and disease. IL-6 is secreted mainly from macrophages and T cells and plays a critical role in inflammation and tissue injury (Fisman & Tenenbaum, 2010). IL-6 signals through the IL-6 receptor (IL-6R), of which there are two subtypes, the soluble form (sIL-6R) and the transmembrane form (Scheller *et al.*, 2011). IL-6 signalling is complex and involves the signal transducing receptor glycoprotein 130 (gp130). The transmembrane IL-6R is mainly found in hepatocytes and leukocytes, with low expression in skeletal muscle (Keller *et al.*, 2005). The circulating sIL-6R is a ligand binding protein derived from the extracellular portion of the IL-6R by proteolytic cleavage or differential IL-6R mRNA splicing (Robson-Ansley *et al.*, 2010). IL-6 is released from muscle in response to exercise, injury and stress (Welc & Clanton, 2013). In chronic diseases such as DMD, IL-

IL-6 exerts pro-inflammatory actions. Binding of IL-6 to the IL-6 receptor activates the JAK/STAT signalling pathway (Pedersen & Febbraio, 2008).

IL-6 levels are increased in DMD and *mdx* mice (Rufo *et al.*, 2011; Cruz-Guzmán *et al.*, 2015; Pelosi *et al.*, 2015a). Blockade of IL-6 signalling in *mdx* mice using a neutralizing IL-6R antibody (αIL-6R) (Okazaki *et al.*, 2002) has proved beneficial to muscle physiology (Pelosi *et al.*, 2015a; Manning *et al.*, 2016, 2017). IL-6R neutralization improved diaphragm force generation (Manning *et al.*, 2017), restoration of gastrointestinal form and function (Manning *et al.*, 2016), improved treadmill exercise and decreased diaphragm muscle inflammation (Pelosi *et al.*, 2015a). Similarly, blockade of IL-6 in the *mdx/utrn*^{+/-} increased the area of embryonic MyHC-positive fibres, indicating muscle fibre regeneration, and reduced fibrosis in quadriceps muscle (Wada *et al.*, 2017). Serum creatine kinase was also reduced, indicating improved muscle integrity. Although significant improvements in limb muscle were noted, diaphragm and cardiac muscle pathology were not improved. Neutralisation of IL-6 in mice with cardio-toxin induced muscle damage was shown to promote muscle regeneration (Fujita *et al.*, 2014). Overexpression of IL-6 in *mdx* mice results in more severe muscle damage than that seen in *mdx* mice and an upregulation of genes related to antioxidant defence mechanisms (Pelosi *et al.*, 2015b; Pelosi *et al.*, 2017). These data suggest a contributing role for IL-6 in dystrophic muscle dysfunction.

1.3.6 Anabolic signalling in muscle

Muscle proteolysis occurs in DMD due to muscle damage and injury, there is increased serum creatine kinase due to decreased muscle integrity and activation of autophagy signalling pathways. Glucocorticoids are the gold standard treatment in DMD and are known to regulate protein metabolism in skeletal muscle, often promoting muscle atrophy. Targeting anabolic signalling in dystrophic muscle and supporting protein synthesis may be of potential benefit to skeletal muscle physiology.

Corticotrophin releasing factor (CRF) is known to have effects on skeletal and cardiac muscle signalling. CRF is released from the paraventricular nucleus of the hypothalamus in response to stress and hypothalamic-pituitary activation, and drives the release of adreno-corticotrophin hormone (ACTH) from the pituitary gland. CRF binds to CRF receptors (CRFR), of which there are two subtypes, CRFR1 and CRFR2. These are G-protein coupled receptors and CRF maintains high affinity for both CRFR1 and CRFR2, which on activation, activates adenylyl cyclase and increases cyclic AMP formation (Reutenauer-Patte *et al.*, 2012). Skeletal muscle expresses CRFR2 and CRFR2 agonists have the ability to modulate muscle mass. CRFR2 agonist treatment has been shown to promote increases in muscle mass and decrease muscle loss in atrophying conditions (Hinkle *et al.*, 2003a; Hinkle *et al.*, 2003b; Hinkle *et al.*, 2004). These effects are mediated by activation of anabolic signalling pathways and decreased proteolysis. Urocortin-2 is an endogenous peptide highly selective for CRFR2.

CRFR2 agonist treatment in *mdx* mice prevents diaphragm force loss and reduces muscle fibrosis, immune cell infiltration and immune cell-related gene expression (Hinkle *et al.*, 2007). Similarly, CRFR2 agonist treatment in *mdx* mice increased extensor digitorum longus and soleus muscle mass (Hall *et al.*, 2007). Urocortin-2 treatment in *mdx* mice increased skeletal muscle mass and reduced creatine kinase levels (Reutenauer-Patte *et al.*, 2012). Moreover, urocortin-2 reduced muscle fibre necrosis in the diaphragm. In models of myocardial infarction, urocortin-2 improves cardiac function and ameliorates cardiac remodelling (Ellmers *et al.*, 2015). In a similar manner, urocortin-2 is cardio-protective during ischemia reperfusion injury (Gao *et al.*, 2015).

Collectively, these data indicate a potential role for Urocortin-2 in stimulating anabolic signalling in dystrophic muscle and modulating muscle mass and fibre hypertrophy, along with improving muscle integrity.

1.3.7 Knowledge gaps addressed in this thesis

Currently, much remains to be examined in terms of respiratory system control in DMD and animal models of the dystrophinopathies. There are many knowledge gaps relating to the complete consequences of dystrophin deficiency on the respiratory control network. It is unclear if there are neural deficits or compensations in the control of breathing as a result of dystrophin deficiency. Dystrophic diaphragm muscle undergoes a progressive pathology, but it is unclear the extent to which ventilatory capacity is limited by profound diaphragm dysfunction in *mdx* mice. Given that inflammation is such a prominent feature of DMD and pathology in *mdx* mice, it is important to determine if there is evidence of neuroinflammation at sites related to respiratory control in *mdx* mice. Is there a capacity for neuromodulatory compensation in the motor pathway of breathing, in order to preserve ventilatory capacity? Can modulation of inflammatory-related and stress signalling using a combined anti-inflammatory and anti-stress intervention in *mdx* mice improve respiratory performance? These questions and several others posed in this review are addressed in this thesis.

1.4 Thesis structure and specific aims

The overall aim of this thesis was to investigate respiratory system control in a murine model of Duchenne muscular dystrophy - the *mdx* mouse. We sought to explore deficits and compensation within the respiratory control network, arising from dystrophin deficiency in young (8-week-old) *mdx* mice. Additionally, we sought to elucidate the putative contribution of mediators of inflammation and stress to respiratory deficits in *mdx* mice.

Chapter 2: Sensorimotor control of breathing in the *mdx* mouse model of Duchenne muscular dystrophy.

- Investigate chemo-afferent discharge from the carotid bodies of wild-type and *mdx* mice.
- Assess ventilation and metabolic activity during normoxia and in response to hypoxia in conscious wild-type and *mdx* mice.
- Characterise diaphragm muscle form and function in wild-type and *mdx*.
- Examine diaphragm EMG activity under basal conditions and in response to maximal chemostimulation in anaesthetised wild-type and *mdx* mice.

Chapter 4: Neuromechanical control of breathing in the dystrophin-deficient *mdx* mouse.

- Examine respiratory stability and ventilatory capacity in conscious wild-type and *mdx* mice.
- Investigate the neuro-mechanical control of breathing in wild-type and *mdx* mice.

- Examine the *mdx* cervical spinal cord (containing the phrenic motor nucleus) for evidence of inflammatory remodelling and apoptosis and monoamine concentrations compared with wild-type.

Chapter 5: Restoration of pharyngeal dilator muscle force in dystrophin-deficient (*mdx*) mice following co-treatment with neutralizing interleukin-6 receptor antibodies and urocortin-2.

- Assess the effects of blocking interleukin-6 receptor signalling and stimulating corticotrophin releasing factor receptor 2 with urocortin-2 on the form and function of wild-type and *mdx* sternohyoid muscle.

Chapter 6: Recovery of respiratory function in *mdx* mice co-treated with neutralizing interleukin-6 receptor antibodies and urocortin-2.

In wild-type and *mdx* mice, examine the effects of co-administration of neutralizing interleukin-6 receptor antibodies and urocortin-2 on:

- Diaphragm muscle force-generating capacity.
- Ventilation and metabolism in response to acute physiological gas challenges.
- Diaphragm muscle structure and MyHC isoform composition.
- Cytokine concentrations in the diaphragm.

1.5 References

- Abdel-Salam E, Abdel-Meguidr IE, Shatla R & Korraa SS. (2010). Stromal cell-derived factors in Duchenne muscular dystrophy. *Acta Myol* **29**, 398-403.
- Allen DG, Gervasio OL, Yeung EW & Whitehead NP. (2010). Calcium and the damage pathways in muscular dystrophy. *Can J Physiol Pharmacol* **88**, 83-91.
- Allen DG & Whitehead NP. (2011). Duchenne muscular dystrophy--what causes the increased membrane permeability in skeletal muscle? *Int J Biochem Cell Biol* **43**, 290-294.
- Almado CE, Machado BH & Leão RM. (2012). Chronic intermittent hypoxia depresses afferent neurotransmission in NTS neurons by a reduction in the number of active synapses. *J Neurosci* **32**, 16736-16746.
- Aloysius A, Born P, Kinali M, Davis T, Pane M & Mercuri E. (2008). Swallowing difficulties in Duchenne muscular dystrophy: indications for feeding assessment and outcome of videofluoroscopic swallow studies. *Eur J Paediatr Neurol* **12**, 239-245.
- Anderson JL, Head SI, Rae C & Morley JW. (2002). Brain function in Duchenne muscular dystrophy. *Brain* **125**, 4-13.
- Aranmolate A, Tse N & Colognato H. (2017). Myelination is delayed during postnatal brain development in the mdx mouse model of Duchenne muscular dystrophy. *BMC Neurosci* **18**, 63.
- Arens R & Muzumdar H. (2010). Sleep, sleep disordered breathing, and nocturnal hypoventilation in children with neuromuscular diseases. *Paediatr Respir Rev* **11**, 24-30.
- Attal P, Lambert F, Marchand-Adam S, Bobin S, Pourny JC, Chemla D, Lecarpentier Y & Coirault C. (2000). Severe mechanical dysfunction in pharyngeal muscle from adult mdx mice. *Am J Respir Crit Care Med* **162**, 278-281.
- Bach KB & Mitchell GS. (1996). Hypoxia-induced long-term facilitation of respiratory activity is serotonin dependent. *Respir Physiol* **104**, 251-260.
- Badr MS. (1996). Effect of ventilatory drive on upper airway patency in humans during NREM sleep. *Respir Physiol* **103**, 1-10.

- Baker-Herman TL, Fuller DD, Bavis RW, Zabka AG, Golder FJ, Doperalski NJ, Johnson RA, Watters JJ & Mitchell GS. (2004). BDNF is necessary and sufficient for spinal respiratory plasticity following intermittent hypoxia. *Nat Neurosci* **7**, 48-55.
- Baker-Herman TL & Mitchell GS. (2002). Phrenic long-term facilitation requires spinal serotonin receptor activation and protein synthesis. *J Neurosci* **22**, 6239-6246.
- Barbé F, Quera-Salva MA, McCann C, Gajdos P, Raphael JC, de Lattre J & Agustí AG. (1994). Sleep-related respiratory disturbances in patients with Duchenne muscular dystrophy. *Eur Respir J* **7**, 1403-1408.
- Barros Maranhão J, de Oliveira Moreira D, Maurício AF, de Carvalho SC, Ferretti R, Pereira JA, Santo Neto H & Marques MJ. (2015). Changes in caldesmon, TNF- α , TGF- β and MyoD levels during the progression of skeletal muscle dystrophy in mdx mice: a comparative analysis of the quadriceps, diaphragm and intrinsic laryngeal muscles. *Int J Exp Pathol* **96**, 285-293.
- Bates G, Sigurdardottir S, Kachmar L, Zitouni NB, Benedetti A, Petrof BJ, Rassier D & Lauzon AM. (2013). Molecular, cellular, and muscle strip mechanics of the mdx mouse diaphragm. *Am J Physiol Cell Physiol* **304**, C873-880.
- Bautista TG, Xing T, Fong AY & Pilowsky PM. (2012). Recurrent laryngeal nerve activity exhibits a 5-HT-mediated long-term facilitation and enhanced response to hypoxia following acute intermittent hypoxia in rat. *J Appl Physiol (1985)* **112**, 1144-1156.
- Baydur A, Gilgoff I, Prentice W, Carlson M & Fischer DA. (1990). Decline in respiratory function and experience with long-term assisted ventilation in advanced Duchenne's muscular dystrophy. *Chest* **97**, 884-889.
- Baydur A, Layne E, Aral H, Krishnareddy N, Topacio R, Frederick G & Bodden W. (2000). Long term non-invasive ventilation in the community for patients with musculoskeletal disorders: 46 year experience and review. *Thorax* **55**, 4-11.
- Beck J, Weinberg J, Hamnegård CH, Spahija J, Olofson J, Grimby G & Sinderby C. (2006). Diaphragmatic function in advanced Duchenne muscular dystrophy. *Neuromuscul Disord* **16**, 161-167.
- Bersanini C, Khirani S, Ramirez A, Lofaso F, Aubertin G, Beydon N, Mayer M, Maincent K, Boulé M & Fauroux B. (2012). Nocturnal hypoxaemia and hypercapnia in children with neuromuscular disorders. *Eur Respir J* **39**, 1206-1212.
- Birnkrant DJ, Ararat E & Mhanna MJ. (2016). Cardiac phenotype determines survival in Duchenne muscular dystrophy. *Pediatr Pulmonol* **51**, 70-76.

- Blake DJ, Weir A, Newey SE & Davies KE. (2002). Function and genetics of dystrophin and dystrophin-related proteins in muscle. *Physiol Rev* **82**, 291-329.
- Brünig I, Suter A, Knuesel I, Lüscher B & Fritschy JM. (2002). GABAergic terminals are required for postsynaptic clustering of dystrophin but not of GABA(A) receptors and gephyrin. *J Neurosci* **22**, 4805-4813.
- Bulfield G, Siller WG, Wight PA & Moore KJ. (1984). X chromosome-linked muscular dystrophy (mdx) in the mouse. *Proc Natl Acad Sci U S A* **81**, 1189-1192.
- Burns DP, Ali I, Rieux C, Healy J, Jasionek G & O'Halloran KD. (2017). Tempol Supplementation Restores Diaphragm Force and Metabolic Enzyme Activities in mdx Mice. *Antioxidants (Basel)* **6**.
- Burns DP, Edge D, O'Malley D & O'Halloran KD. (2015). Respiratory Control in the mdx Mouse Model of Duchenne Muscular Dystrophy. *Adv Exp Med Biol* **860**, 239-244.
- Burns DP & O'Halloran KD. (2016). Evidence of hypoxic tolerance in weak upper airway muscle from young mdx mice. *Respir Physiol Neurobiol* **226**, 68-75.
- Buyse GM, Goemans N, van den Hauwe M & Meier T. (2013). Effects of glucocorticoids and idebenone on respiratory function in patients with duchenne muscular dystrophy. *Pediatr Pulmonol* **48**, 912-920.
- Bye PT, Ellis ER, Issa FG, Donnelly PM & Sullivan CE. (1990). Respiratory failure and sleep in neuromuscular disease. *Thorax* **45**, 241-247.
- Canapari CA, Barrowman N, Hoey L, Walker SW, Townsend E, Tseng BS & Katz SL. (2015). Truncal fat distribution correlates with decreased vital capacity in Duchenne muscular dystrophy. *Pediatr Pulmonol* **50**, 63-70.
- Cantillon D & Bradford A. (1998). Effect of gender on rat upper airway muscle contractile properties. *Respir Physiol* **113**, 147-156.
- Cantillon D & Bradford A. (2000). Effects of age and gender on rat upper airway muscle contractile properties. *J Gerontol A Biol Sci Med Sci* **55**, B396-400.
- Capogrosso RF, Cozzoli A, Mantuano P, Camerino GM, Massari AM, Sblendorio VT, De Bellis M, Tamma R, Giustino A, Nico B, Montagnani M & De Luca A. (2016). Assessment of resveratrol, apocynin and taurine on mechanical-metabolic uncoupling and oxidative stress in a mouse model of duchenne muscular dystrophy: A comparison with the gold standard, α -methyl prednisolone. *Pharmacol Res* **106**, 101-113.

- Carretta D, Santarelli M, Vanni D, Carrai R, Sbriccoli A, Pinto F & Minciocchi D. (2001). The organisation of spinal projecting brainstem neurons in an animal model of muscular dystrophy. A retrograde tracing study on mdx mutant mice. *Brain Res* **895**, 213-222.
- Castele RJ, Connors AF & Altose MD. (1985). Effects of changes in CO₂ partial pressure on the sensation of respiratory drive. *J Appl Physiol (1985)* **59**, 1747-1751.
- Cerveri I, Fanfulla F, Zoia MC, Manni R & Tartara A. (1993). Sleep disorders in neuromuscular diseases. *Monaldi Arch Chest Dis* **48**, 318-321.
- Chan S & Head SI. (2011). The role of branched fibres in the pathogenesis of Duchenne muscular dystrophy. *Exp Physiol* **96**, 564-571.
- Chaussenot R, Edeline JM, Le Bec B, El Massioui N, Laroche S & Vaillend C. (2015). Cognitive dysfunction in the dystrophin-deficient mouse model of Duchenne muscular dystrophy: A reappraisal from sensory to executive processes. *Neurobiol Learn Mem* **124**, 111-122.
- Coirault C, Lambert F, Marchand-Adam S, Attal P, Chemla D & Lecarpentier Y. (1999). Myosin molecular motor dysfunction in dystrophic mouse diaphragm. *Am J Physiol* **277**, C1170-1176.
- Coirault C, Pignol B, Cooper RN, Butler-Browne G, Chabrier PE & Lecarpentier Y. (2003). Severe muscle dysfunction precedes collagen tissue proliferation in mdx mouse diaphragm. *J Appl Physiol (1985)* **94**, 1744-1750.
- Comim CM, Cassol-Jr OJ, Constantino LC, Constantino LS, Petronilho F, Tuon L, Vainzof M, Dal-Pizzol F & Quevedo J. (2009a). Oxidative variables and antioxidant enzymes activities in the mdx mouse brain. *Neurochem Int* **55**, 802-805.
- Comim CM, Tuon L, Stertz L, Vainzof M, Kapczinski F & Quevedo J. (2009b). Striatum brain-derived neurotrophic factor levels are decreased in dystrophin-deficient mice. *Neurosci Lett* **459**, 66-68.
- Cruz-Guzmán OeR, Rodríguez-Cruz M & Escobar Cedillo RE. (2015). Systemic Inflammation in Duchenne Muscular Dystrophy: Association with Muscle Function and Nutritional Status. *Biomed Res Int* **2015**, 891972.
- Cyrulnik SE & Hinton VJ. (2008). Duchenne muscular dystrophy: a cerebellar disorder? *Neurosci Biobehav Rev* **32**, 486-496.

- De Bruin PF, Ueki J, Bush A, Khan Y, Watson A & Pride NB. (1997). Diaphragm thickness and inspiratory strength in patients with Duchenne muscular dystrophy. *Thorax* **52**, 472-475.
- De Bruin PF, Ueki J, Bush A, Y Manzur A, Watson A & Pride NB. (2001). Inspiratory flow reserve in boys with Duchenne muscular dystrophy. *Pediatr Pulmonol* **31**, 451-457.
- De Paepe B, Creus KK, Martin JJ & De Bleecker JL. (2012). Upregulation of chemokines and their receptors in Duchenne muscular dystrophy: potential for attenuation of myofiber necrosis. *Muscle Nerve* **46**, 917-925.
- De Pasquale L, D'Amico A, Verardo M, Petrini S, Bertini E & De Benedetti F. (2012). Increased muscle expression of interleukin-17 in Duchenne muscular dystrophy. *Neurology* **78**, 1309-1314.
- Deconinck N & Dan B. (2007). Pathophysiology of duchenne muscular dystrophy: current hypotheses. *Pediatr Neurol* **36**, 1-7.
- Del Negro CA, Funk GD & Feldman JL. (2018). Breathing matters. *Nat Rev Neurosci* **19**, 351-367.
- Delfín DA, Zang KE, Schill KE, Patel NT, Janssen PM, Raman SV & Rafael-Fortney JA. (2012). Cardiomyopathy in the dystrophin/utrophin-deficient mouse model of severe muscular dystrophy is characterized by dysregulation of matrix metalloproteinases. *Neuromuscul Disord* **22**, 1006-1014.
- Demoule A, Divangahi M, Danialou G, Gvozdic D, Larkin G, Bao W & Petrof BJ. (2005). Expression and regulation of CC class chemokines in the dystrophic (mdx) diaphragm. *Am J Respir Cell Mol Biol* **33**, 178-185.
- Dempsey JA, Veasey SC, Morgan BJ & O'Donnell CP. (2010). Pathophysiology of sleep apnea. *Physiol Rev* **90**, 47-112.
- Devinney MJ, Huxtable AG, Nichols NL & Mitchell GS. (2013). Hypoxia-induced phrenic long-term facilitation: emergent properties. *Ann N Y Acad Sci* **1279**, 143-153.
- Dick TE, Hsieh YH, Wang N & Prabhakar N. (2007). Acute intermittent hypoxia increases both phrenic and sympathetic nerve activities in the rat. *Exp Physiol* **92**, 87-97.
- Dick TE & van Lunteren E. (1990). Fiber subtype distribution of pharyngeal dilator muscles and diaphragm in the cat. *J Appl Physiol (1985)* **68**, 2237-2240.

- Dougherty BJ, Lee KZ, Gonzalez-Rothi EJ, Lane MA, Reier PJ & Fuller DD. (2012). Recovery of inspiratory intercostal muscle activity following high cervical hemisection. *Respir Physiol Neurobiol* **183**, 186-192.
- Douglas NJ, White DP, Pickett CK, Weil JV & Zwillich CW. (1982a). Respiration during sleep in normal man. *Thorax* **37**, 840-844.
- Douglas NJ, White DP, Weil JV, Pickett CK, Martin RJ, Hudgel DW & Zwillich CW. (1982b). Hypoxic ventilatory response decreases during sleep in normal men. *Am Rev Respir Dis* **125**, 286-289.
- Douglas NJ, White DP, Weil JV, Pickett CK & Zwillich CW. (1982c). Hypercapnic ventilatory response in sleeping adults. *Am Rev Respir Dis* **126**, 758-762.
- Dudley RW, Danialou G, Govindaraju K, Lands L, Eidelman DE & Petrof BJ. (2006a). Sarcolemmal damage in dystrophin deficiency is modulated by synergistic interactions between mechanical and oxidative/nitrosative stresses. *Am J Pathol* **168**, 1276-1287; quiz 1404-1275.
- Dudley RW, Khairallah M, Mohammed S, Lands L, Des Rosiers C & Petrof BJ. (2006b). Dynamic responses of the glutathione system to acute oxidative stress in dystrophic mouse (mdx) muscles. *Am J Physiol Regul Integr Comp Physiol* **291**, R704-710.
- Dwinell MR, Huey KA & Powell FL. (2000). Chronic hypoxia induces changes in the central nervous system processing of arterial chemoreceptor input. *Adv Exp Med Biol* **475**, 477-484.
- Dwinell MR & Powell FL. (1999). Chronic hypoxia enhances the phrenic nerve response to arterial chemoreceptor stimulation in anesthetized rats. *J Appl Physiol (1985)* **87**, 817-823.
- Eckert DJ & Malhotra A. (2008). Pathophysiology of adult obstructive sleep apnea. *Proc Am Thorac Soc* **5**, 144-153.
- Edge D, Bradford A & O'Halloran KD. (2012). Chronic intermittent hypoxia increases apnoea index in sleeping rats. *Adv Exp Med Biol* **758**, 359-363.
- Edge D, Skelly JR, Bradford A & O'Halloran KD. (2010). Respiratory plasticity in the behaving rat following chronic intermittent hypoxia. *Adv Exp Med Biol* **669**, 267-270.
- Eghtesad S, Jhunjhunwala S, Little SR & Clemens PR. (2011). Rapamycin ameliorates dystrophic phenotype in mdx mouse skeletal muscle. *Mol Med* **17**, 917-924.

- Ehmsen J, Poon E & Davies K. (2002). The dystrophin-associated protein complex. *J Cell Sci* **115**, 2801-2803.
- El-Shafey AF, Armstrong AE, Terrill JR, Grounds MD & Arthur PG. (2011). Screening for increased protein thiol oxidation in oxidatively stressed muscle tissue. *Free Radic Res* **45**, 991-999.
- Eldridge FL & Millhorn DE. (1986). Oscillation, gating, and memory in the respiratory system. *Handbook of Physiology, The Respiratory System, Control of Breathing*, 93-114.
- Ellis ER, Bye PT, Bruderer JW & Sullivan CE. (1987). Treatment of respiratory failure during sleep in patients with neuromuscular disease. Positive-pressure ventilation through a nose mask. *Am Rev Respir Dis* **135**, 148-152.
- Ellmers LJ, Scott NJ, Cameron VA, Richards AM & Rademaker MT. (2015). Chronic urocortin 2 administration improves cardiac function and ameliorates cardiac remodeling after experimental myocardial infarction. *J Cardiovasc Pharmacol* **65**, 269-275.
- ElMallah MK, Stanley DA, Lee KZ, Turner SM, Streeter KA, Baekey DM & Fuller DD. (2016). Power spectral analysis of hypoglossal nerve activity during intermittent hypoxia-induced long-term facilitation in mice. *J Neurophysiol* **115**, 1372-1380.
- Enwere EK, Boudreault L, Holbrook J, Timusk K, Earl N, LaCasse E, Renaud JM & Korneluk RG. (2013). Loss of cIAP1 attenuates soleus muscle pathology and improves diaphragm function in mdx mice. *Hum Mol Genet* **22**, 867-878.
- Ermolova NV, Martinez L, Vetrone SA, Jordan MC, Roos KP, Sweeney HL & Spencer MJ. (2014). Long-term administration of the TNF blocking drug Remicade (cV1q) to mdx mice reduces skeletal and cardiac muscle fibrosis, but negatively impacts cardiac function. *Neuromuscul Disord* **24**, 583-595.
- Ervasti JM. (2007). Dystrophin, its interactions with other proteins, and implications for muscular dystrophy. *Biochim Biophys Acta* **1772**, 108-117.
- Ervasti JM & Campbell KP. (1991). Membrane organization of the dystrophin-glycoprotein complex. *Cell* **66**, 1121-1131.
- Fayssoil A, Abasse S & Silverston K. (2017). Cardiac Involvement Classification and Therapeutic Management in Patients with Duchenne Muscular Dystrophy. *J Neuromuscul Dis* **4**, 17-23.

- Feldman JL & Del Negro CA. (2006). Looking for inspiration: new perspectives on respiratory rhythm. *Nat Rev Neurosci* **7**, 232-242.
- Feldman JL, Del Negro CA & Gray PA. (2013). Understanding the rhythm of breathing: so near, yet so far. *Annu Rev Physiol* **75**, 423-452.
- Feldman JL, Mitchell GS & Nattie EE. (2003). Breathing: rhythmicity, plasticity, chemosensitivity. *Annu Rev Neurosci* **26**, 239-266.
- Fields DP & Mitchell GS. (2015). Spinal metaplasticity in respiratory motor control. *Front Neural Circuits* **9**, 2.
- Fink BR. (1961). The stimulant effect of wakefulness on respiration: clinical aspects. *Br J Anaesth* **33**, 97-101.
- Fisman EZ & Tenenbaum A. (2010). The ubiquitous interleukin-6: a time for reappraisal. *Cardiovasc Diabetol* **9**, 62.
- Fogel RB, Malhotra A, Pillar G, Edwards JK, Beauregard J, Shea SA & White DP. (2001). Genioglossal activation in patients with obstructive sleep apnea versus control subjects. Mechanisms of muscle control. *Am J Respir Crit Care Med* **164**, 2025-2030.
- Forbes SC, Willcocks RJ, Triplett WT, Rooney WD, Lott DJ, Wang DJ, Pollaro J, Senesac CR, Daniels MJ, Finkel RS, Russman BS, Byrne BJ, Finanger EL, Tennekoon GI, Walter GA, Sweeney HL & Vandenborne K. (2014). Magnetic resonance imaging and spectroscopy assessment of lower extremity skeletal muscles in boys with Duchenne muscular dystrophy: a multicenter cross sectional study. *PLoS One* **9**, e106435.
- Fregosi RF & Mitchell GS. (1994). Long-term facilitation of inspiratory intercostal nerve activity following carotid sinus nerve stimulation in cats. *J Physiol* **477 (Pt 3)**, 469-479.
- Fujita R, Kawano F, Ohira T, Nakai N, Shibaguchi T, Nishimoto N & Ohira Y. (2014). Anti-interleukin-6 receptor antibody (MR16-1) promotes muscle regeneration via modulation of gene expressions in infiltrated macrophages. *Biochim Biophys Acta* **1840**, 3170-3180.
- Fuller DD, Bach KB, Baker TL, Kinkead R & Mitchell GS. (2000). Long term facilitation of phrenic motor output. *Respir Physiol* **121**, 135-146.

- Fuller DD, Doperalski NJ, Dougherty BJ, Sandhu MS, Bolser DC & Reier PJ. (2008). Modest spontaneous recovery of ventilation following chronic high cervical hemisection in rats. *Exp Neurol* **211**, 97-106.
- Fuller DD & Mitchell GS. (2017). Respiratory neuroplasticity - Overview, significance and future directions. *Exp Neurol* **287**, 144-152.
- Funk GD, Parkis MA, Selvaratnam SR & Walsh C. (1997). Developmental modulation of glutamatergic inspiratory drive to hypoglossal motoneurons. *Respir Physiol* **110**, 125-137.
- Gao XF, Zhou Y, Wang DY, Lew KS, Richards AM & Wang P. (2015). Urocortin-2 suppression of p38-MAPK signaling as an additional mechanism for ischemic cardioprotection. *Mol Cell Biochem* **398**, 135-146.
- Gayraud J, Matecki S, Hnia K, Mornet D, Prefaut C, Mercier J, Michel A & Ramonatxo M. (2007). Ventilation during air breathing and in response to hypercapnia in 5 and 16 month-old mdx and C57 mice. *J Muscle Res Cell Motil* **28**, 29-37.
- Goodnough CL, Gao Y, Li X, Qutaish MQ, Goodnough LH, Molter J, Wilson D, Flask CA & Yu X. (2014). Lack of dystrophin results in abnormal cerebral diffusion and perfusion in vivo. *Neuroimage* **102 Pt 2**, 809-816.
- Gosselin LE, Barkley JE, Spencer MJ, McCormick KM & Farkas GA. (2003). Ventilatory dysfunction in mdx mice: impact of tumor necrosis factor-alpha deletion. *Muscle Nerve* **28**, 336-343.
- Gosselin LE & McCormick KM. (2004). Targeting the immune system to improve ventilatory function in muscular dystrophy. *Med Sci Sports Exerc* **36**, 44-51.
- Gosselin LE, Williams JE, Personius K & Farkas GA. (2007). A comparison of factors associated with collagen metabolism in different skeletal muscles from dystrophic (mdx) mice: impact of pirfenidone. *Muscle Nerve* **35**, 208-216.
- Guido AN, Campos GE, Neto HS, Marques MJ & Minatel E. (2010). Fiber type composition of the sternomastoid and diaphragm muscles of dystrophin-deficient mdx mice. *Anat Rec (Hoboken)* **293**, 1722-1728.
- Gutpell KM, Hrinivich WT & Hoffman LM. (2015). Skeletal muscle fibrosis in the mdx/utrn+/- mouse validates its suitability as a murine model of Duchenne muscular dystrophy. *PLoS One* **10**, e0117306.

- Hahn A, Bach JR, Delaubier A, Renardel-Irani A, Guillou C & Rideau Y. (1997). Clinical implications of maximal respiratory pressure determinations for individuals with Duchenne muscular dystrophy. *Arch Phys Med Rehabil* **78**, 1-6.
- Hall JE, Kaczor JJ, Hettinga BP, Isfort RJ & Tarnopolsky MA. (2007). Effects of a CRF2R agonist and exercise on mdx and wildtype skeletal muscle. *Muscle Nerve* **36**, 336-341.
- Harcourt LJ, Holmes AG, Gregorevic P, Schertzer JD, Stupka N, Plant DR & Lynch GS. (2005). Interleukin-15 administration improves diaphragm muscle pathology and function in dystrophic mdx mice. *Am J Pathol* **166**, 1131-1141.
- Harris JB, Wallace C & Wing J. (1972). Myelinated nerve fibre counts in the nerves of normal and dystrophic mouse muscle. *J Neurol Sci* **15**, 245-249.
- Henry CC, Martin KS, Ward BB, Handsfield GG, Peirce SM & Blemker SS. (2017). Spatial and age-related changes in the microstructure of dystrophic and healthy diaphragms. *PLoS One* **12**, e0183853.
- Hill NS, Redline S, Carskadon MA, Curran FJ & Millman RP. (1992). Sleep-disordered breathing in patients with Duchenne muscular dystrophy using negative pressure ventilators. *Chest* **102**, 1656-1662.
- Hinkle RT, Donnelly E, Cody DB, Bauer MB & Isfort RJ. (2003a). Urocortin II treatment reduces skeletal muscle mass and function loss during atrophy and increases nonatrophying skeletal muscle mass and function. *Endocrinology* **144**, 4939-4946.
- Hinkle RT, Donnelly E, Cody DB, Bauer MB, Sheldon RJ & Isfort RJ. (2004). Corticotropin releasing factor 2 receptor agonists reduce the denervation-induced loss of rat skeletal muscle mass and force and increase non-atrophying skeletal muscle mass and force. *J Muscle Res Cell Motil* **25**, 539-547.
- Hinkle RT, Donnelly E, Cody DB, Samuelsson S, Lange JS, Bauer MB, Tarnopolsky M, Sheldon RJ, Coste SC, Tobar E, Stenzel-Poore MP & Isfort RJ. (2003b). Activation of the CRF 2 receptor modulates skeletal muscle mass under physiological and pathological conditions. *Am J Physiol Endocrinol Metab* **285**, E889-898.
- Hinkle RT, Lefever FR, Dolan ET, Reichart DL, Dietrich JA, Gropp KE, Thacker RI, Demuth JP, Stevens PJ, Qu XA, Varbanov AR, Wang F & Isfort RJ. (2007). Corticotrophin releasing factor 2 receptor agonist treatment significantly slows disease progression in mdx mice. *BMC Med* **5**, 18.

- Hoffman EP, Brown RH & Kunkel LM. (1987). Dystrophin: the protein product of the Duchenne muscular dystrophy locus. *Cell* **51**, 919-928.
- Howell JM, Fletcher S, Kakulas BA, O'Hara M, Lochmuller H & Karpatis G. (1997). Use of the dog model for Duchenne muscular dystrophy in gene therapy trials. *Neuromuscul Disord* **7**, 325-328.
- Huang P, Cheng G, Lu H, Aronica M, Ransohoff RM & Zhou L. (2011). Impaired respiratory function in mdx and mdx/utrn(+/-) mice. *Muscle Nerve* **43**, 263-267.
- Huard J, Fortier LP, Labrecque C, Dansereau G & Tremblay JP. (1991). Is dystrophin present in the nerve terminal at the neuromuscular junction? An immunohistochemical study of the heterozygote dystrophic (mdx) mouse. *Synapse* **7**, 135-140.
- Hukins CA & Hillman DR. (2000). Daytime predictors of sleep hypoventilation in Duchenne muscular dystrophy. *Am J Respir Crit Care Med* **161**, 166-170.
- Ishizaki M, Suga T, Kimura E, Shiota T, Kawano R, Uchida Y, Uchino K, Yamashita S, Maeda Y & Uchino M. (2008). Mdx respiratory impairment following fibrosis of the diaphragm. *Neuromuscul Disord* **18**, 342-348.
- Ismail HM, Scapozza L, Ruegg UT & Dorchies OM. (2014). Diapocynin, a dimer of the NADPH oxidase inhibitor apocynin, reduces ROS production and prevents force loss in eccentrically contracting dystrophic muscle. *PLoS One* **9**, e110708.
- Jaros E & Jenkinson M. (1983). Quantitative studies of the abnormal axon-Schwann cell relationship in the peripheral motor and sensory nerves of the dystrophic mouse. *Brain Res* **258**, 181-196.
- Johnson RA & Mitchell GS. (2013). Common mechanisms of compensatory respiratory plasticity in spinal neurological disorders. *Respir Physiol Neurobiol* **189**, 419-428.
- Johnson SM & Mitchell GS. (2002). Activity-dependent plasticity in descending synaptic inputs to respiratory spinal motoneurons. *Respir Physiol Neurobiol* **131**, 79-90.
- Jordan D. (2001). Central nervous pathways and control of the airways. *Respir Physiol* **125**, 67-81.
- Kanagawa M & Toda T. (2006). The genetic and molecular basis of muscular dystrophy: roles of cell-matrix linkage in the pathogenesis. *J Hum Genet* **51**, 915-926.

- Katz S, Selvadurai H, Keilty K, Mitchell M & MacLusky I. (2004). Outcome of non-invasive positive pressure ventilation in paediatric neuromuscular disease. *Arch Dis Child* **89**, 121-124.
- Keller P, Penkowa M, Keller C, Steensberg A, Fischer CP, Giralt M, Hidalgo J & Pedersen BK. (2005). Interleukin-6 receptor expression in contracting human skeletal muscle: regulating role of IL-6. *FASEB J* **19**, 1181-1183.
- Khan Y & Heckmatt JZ. (1994). Obstructive apnoeas in Duchenne muscular dystrophy. *Thorax* **49**, 157-161.
- Khirani S, Ramirez A, Aubertin G, Boulé M, Chemouny C, Forin V & Fauroux B. (2014). Respiratory muscle decline in Duchenne muscular dystrophy. *Pediatr Pulmonol* **49**, 473-481.
- Kim JH, Kwak HB, Thompson LV & Lawler JM. (2013). Contribution of oxidative stress to pathology in diaphragm and limb muscles with Duchenne muscular dystrophy. *J Muscle Res Cell Motil* **34**, 1-13.
- Kim JH & Lawler JM. (2012). Amplification of proinflammatory phenotype, damage, and weakness by oxidative stress in the diaphragm muscle of mdx mice. *Free Radic Biol Med* **52**, 1597-1606.
- Kirk VG, Flemons WW, Adams C, Rimmer KP & Montgomery MD. (2000). Sleep-disordered breathing in Duchenne muscular dystrophy: a preliminary study of the role of portable monitoring. *Pediatr Pulmonol* **29**, 135-140.
- Kline DD. (2010). Chronic intermittent hypoxia affects integration of sensory input by neurons in the nucleus tractus solitarii. *Respir Physiol Neurobiol* **174**, 29-36.
- Kline DD, Ramirez-Navarro A & Kunze DL. (2007). Adaptive depression in synaptic transmission in the nucleus of the solitary tract after in vivo chronic intermittent hypoxia: evidence for homeostatic plasticity. *J Neurosci* **27**, 4663-4673.
- Klymiuk N, Blutke A, Graf A, Krause S, Burkhardt K, Wuensch A, Krebs S, Kessler B, Zakhartchenko V, Kurome M, Kemter E, Nagashima H, Schoser B, Herbach N, Blum H, Wanke R, Aartsma-Rus A, Thirion C, Lochmüller H, Walter MC & Wolf E. (2013). Dystrophin-deficient pigs provide new insights into the hierarchy of physiological derangements of dystrophic muscle. *Hum Mol Genet* **22**, 4368-4382.

- Knuesel I, Bornhauser BC, Zuellig RA, Heller F, Schaub MC & Fritschy JM. (2000). Differential expression of utrophin and dystrophin in CNS neurons: an in situ hybridization and immunohistochemical study. *J Comp Neurol* **422**, 594-611.
- Knuesel I, Mastrocola M, Zuellig RA, Bornhauser B, Schaub MC & Fritschy JM. (1999). Short communication: altered synaptic clustering of GABAA receptors in mice lacking dystrophin (mdx mice). *Eur J Neurosci* **11**, 4457-4462.
- Koenig M, Monaco AP & Kunkel LM. (1988). The complete sequence of dystrophin predicts a rod-shaped cytoskeletal protein. *Cell* **53**, 219-228.
- Kohn B, Guscetti F, Waxenberger M & Augsburg H. (1993). [Muscular dystrophy in a cat]. *Tierarztl Prax* **21**, 451-457.
- Kozakowska M, Pietraszek-Gremplewicz K, Jozkowicz A & Dulak J. (2015). The role of oxidative stress in skeletal muscle injury and regeneration: focus on antioxidant enzymes. *J Muscle Res Cell Motil* **36**, 377-393.
- Kravitz RM. (2009). Airway clearance in Duchenne muscular dystrophy. *Pediatrics* **123 Suppl 4**, S231-235.
- Kumar P & Prabhakar NR. (2012). Peripheral chemoreceptors: function and plasticity of the carotid body. *Compr Physiol* **2**, 141-219.
- Larcher T, Lafoux A, Tesson L, Remy S, Thepenier V, François V, Le Guiner C, Goubin H, Dutilleul M, Guigand L, Toumaniantz G, De Cian A, Boix C, Renaud JB, Cherel Y, Giovannangeli C, Concordet JP, Anegon I & Huchet C. (2014). Characterization of dystrophin deficient rats: a new model for Duchenne muscular dystrophy. *PLoS One* **9**, e110371.
- Lawler JM. (2011). Exacerbation of pathology by oxidative stress in respiratory and locomotor muscles with Duchenne muscular dystrophy. *J Physiol* **589**, 2161-2170.
- Lidov HG. (1996). Dystrophin in the nervous system. *Brain Pathol* **6**, 63-77.
- Lo Mauro A, D'Angelo MG, Romei M, Motta F, Colombo D, Comi GP, Pedotti A, Marchi E, Turconi AC, Bresolin N & Aliverti A. (2010). Abdominal volume contribution to tidal volume as an early indicator of respiratory impairment in Duchenne muscular dystrophy. *Eur Respir J* **35**, 1118-1125.
- Loehr JA, Wang S, Cully TR, Pal R, Larina IV, Larin KV & Rodney GG. (2018). NADPH oxidase mediates microtubule alterations and diaphragm dysfunction in dystrophic mice. *Elife* **7**.

- LoMauro A, D'Angelo MG & Aliverti A. (2017). Sleep Disordered Breathing in Duchenne Muscular Dystrophy. *Curr Neurol Neurosci Rep* **17**, 44.
- LoMauro A, Romei M, D'Angelo MG & Aliverti A. (2014). Determinants of cough efficiency in Duchenne muscular dystrophy. *Pediatr Pulmonol* **49**, 357-365.
- Lott DJ, Forbes SC, Mathur S, Germain SA, Senesac CR, Lee Sweeney H, Walter GA & Vandeborne K. (2014). Assessment of intramuscular lipid and metabolites of the lower leg using magnetic resonance spectroscopy in boys with Duchenne muscular dystrophy. *Neuromuscul Disord* **24**, 574-582.
- Lucking EF, O'Halloran KD & Jones JF. (2014). Increased cardiac output contributes to the development of chronic intermittent hypoxia-induced hypertension. *Exp Physiol* **99**, 1312-1324.
- Lynch GS, Hinkle RT, Chamberlain JS, Brooks SV & Faulkner JA. (2001). Force and power output of fast and slow skeletal muscles from mdx mice 6-28 months old. *J Physiol* **535**, 591-600.
- MacFarlane PM, Satriotomo I, Windelborn JA & Mitchell GS. (2009). NADPH oxidase activity is necessary for acute intermittent hypoxia-induced phrenic long-term facilitation. *J Physiol* **587**, 1931-1942.
- MacFarlane PM, Vinit S & Mitchell GS. (2014). Spinal nNOS regulates phrenic motor facilitation by a 5-HT_{2B} receptor- and NADPH oxidase-dependent mechanism. *Neuroscience* **269**, 67-78.
- Machado DL, Silva EC, Resende MB, Carvalho CR, Zanoteli E & Reed UC. (2012). Lung function monitoring in patients with duchenne muscular dystrophy on steroid therapy. *BMC Res Notes* **5**, 435.
- Mankodi A, Kovacs W, Norato G, Hsieh N, Bandettini WP, Bishop CA, Shimellis H, Newbould RD, Kim E, Fischbeck KH, Arai AE & Yao J. (2017). Respiratory magnetic resonance imaging biomarkers in Duchenne muscular dystrophy. *Ann Clin Transl Neurol* **4**, 655-662.
- Manni R, Ottolini A, Cerveri I, Bruschi C, Zoia MC, Lanzi G & Tartara A. (1989). Breathing patterns and HbSaO₂ changes during nocturnal sleep in patients with Duchenne muscular dystrophy. *J Neurol* **236**, 391-394.
- Manning J, Buckley MM, O'Halloran KD & O'Malley D. (2016). In vivo neutralization of IL-6 receptors ameliorates gastrointestinal dysfunction in dystrophin-deficient mdx mice. *Neurogastroenterol Motil* **28**, 1016-1026.

- Manning J, Buckley MM, O'Halloran KD & O'Malley D. (2017). Combined xIL-6R and urocortin-2 treatment restores mdx diaphragm muscle force. *Muscle Nerve*.
- Manning J & O'Malley D. (2015). What has the mdx mouse model of duchenne muscular dystrophy contributed to our understanding of this disease? *J Muscle Res Cell Motil*.
- Markham BE, Kernodle S, Nemzek J, Wilkinson JE & Sigler R. (2015). Chronic Dosing with Membrane Sealant Poloxamer 188 NF Improves Respiratory Dysfunction in Dystrophic Mdx and Mdx/Utrophin-/- Mice. *PLoS One* **10**, e0134832.
- Matecki S, Rivier F, Hugon G, Koechlin C, Michel A, Prefaut C, Mornet D & Ramonatxo M. (2005). The effect of respiratory muscle training with CO2 breathing on cellular adaptation of mdx mouse diaphragm. *Neuromuscul Disord* **15**, 427-436.
- Matsumura T, Saito T, Fujimura H, Shinno S & Sakoda S. (2012). Lung inflation training using a positive end-expiratory pressure valve in neuromuscular disorders. *Intern Med* **51**, 711-716.
- Mayer OH, Finkel RS, Rummey C, Benton MJ, Glanzman AM, Flickinger J, Lindström BM & Meier T. (2015). Characterization of pulmonary function in Duchenne Muscular Dystrophy. *Pediatr Pulmonol* **50**, 487-494.
- McDonald AA, Hebert SL, Kunz MD, Ralles SJ & McLoon LK. (2015). Disease course in mdx:utrophin+/- mice: comparison of three mouse models of Duchenne muscular dystrophy. *Physiol Rep* **3**.
- McGuire M, MacDermott M & Bradford A. (2002). Effects of chronic episodic hypoxia on rat upper airway muscle contractile properties and fiber-type distribution. *Chest* **122**, 1012-1017.
- Mead AF, Petrov M, Malik AS, Mitchell MA, Childers MK, Bogan JR, Seidner G, Kornegay JN & Stedman HH. (2014). Diaphragm remodeling and compensatory respiratory mechanics in a canine model of Duchenne muscular dystrophy. *J Appl Physiol (1985)* **116**, 807-815.
- Meier T, Rummey C, Leinonen M, Spagnolo P, Mayer OH, Buyse GM & Group DS. (2017). Characterization of pulmonary function in 10-18 year old patients with Duchenne muscular dystrophy. *Neuromuscul Disord* **27**, 307-314.
- Melacini P, Vianello A, Villanova C, Fanin M, Miorin M, Angelini C & Dalla Volta S. (1996). Cardiac and respiratory involvement in advanced stage Duchenne muscular dystrophy. *Neuromuscul Disord* **6**, 367-376.

- Mellies U, Dohna-Schwake C, Ragette R, Teschler H & Voit T. (2003a). [Nocturnal noninvasive ventilation of children and adolescents with neuromuscular diseases: effect on sleep and symptoms]. *Wien Klin Wochenschr* **115**, 855-859.
- Mellies U, Ragette R, Dohna Schwake C, Boehm H, Voit T & Teschler H. (2003b). Long-term noninvasive ventilation in children and adolescents with neuromuscular disorders. *Eur Respir J* **22**, 631-636.
- Mellies U, Ragette R, Schwake C, Boehm H, Voit T & Teschler H. (2003c). Daytime predictors of sleep disordered breathing in children and adolescents with neuromuscular disorders. *Neuromuscul Disord* **13**, 123-128.
- Messina S, Vita GL, Aguenouz M, Sframeli M, Romeo S, Rodolico C & Vita G. (2011). Activation of NF-kappaB pathway in Duchenne muscular dystrophy: relation to age. *Acta Myol* **30**, 16-23.
- Meza S, Giannouli E & Younes M. (1998). Control of breathing during sleep assessed by proportional assist ventilation. *J Appl Physiol (1985)* **84**, 3-12.
- Mifflin SW. (1990). Arterial chemoreceptor input to respiratory hypoglossal motoneurons. *J Appl Physiol (1985)* **69**, 700-709.
- Mitchell GS & Johnson SM. (2003). Neuroplasticity in respiratory motor control. *J Appl Physiol (1985)* **94**, 358-374.
- Mohr CH & Hill NS. (1990). Long-term follow-up of nocturnal ventilatory assistance in patients with respiratory failure due to Duchenne-type muscular dystrophy. *Chest* **97**, 91-96.
- Moraes DJ, Zoccal DB & Machado BH. (2012). Medullary respiratory network drives sympathetic overactivity and hypertension in rats submitted to chronic intermittent hypoxia. *Hypertension* **60**, 1374-1380.
- Mosqueira M, Baby SM, Lahiri S & Khurana TS. (2013). Ventilatory chemosensory drive is blunted in the mdx mouse model of Duchenne Muscular Dystrophy (DMD). *PLoS One* **8**, e69567.
- Muntoni F, Torelli S & Ferlini A. (2003). Dystrophin and mutations: one gene, several proteins, multiple phenotypes. *Lancet Neurol* **2**, 731-740.
- Mâncio RD, Hermes TA, Macedo AB, Mizobuti DS, Valduga AH, Rupcic IF & Minatel E. (2017). Vitamin E treatment decreases muscle injury in mdx mice. *Nutrition* **43-44**, 39-46.

- Nakae Y & Stoward PJ. (2016). The high correlation between counts and area fractions of lipofuscin granules, a biomarker of oxidative stress in muscular dystrophies. *Histochem Cell Biol* **146**, 627-634.
- Nakamura A & Takeda S. (2011). Mammalian models of Duchenne Muscular Dystrophy: pathological characteristics and therapeutic applications. *J Biomed Biotechnol* **2011**, 184393.
- Nichols B, Takeda S & Yokota T. (2015). Nonmechanical Roles of Dystrophin and Associated Proteins in Exercise, Neuromuscular Junctions, and Brains. *Brain Sci* **5**, 275-298.
- Nichols NL, Johnson RA, Satriotomo I & Mitchell GS. (2014). Neither serotonin nor adenosine-dependent mechanisms preserve ventilatory capacity in ALS rats. *Respir Physiol Neurobiol* **197**, 19-28.
- Nichols NL, Van Dyke J, Nashold L, Satriotomo I, Suzuki M & Mitchell GS. (2013). Ventilatory control in ALS. *Respir Physiol Neurobiol* **189**, 429-437.
- Nielsen AM, Bisgard GE & Vidruk EH. (1988). Carotid chemoreceptor activity during acute and sustained hypoxia in goats. *J Appl Physiol (1985)* **65**, 1796-1802.
- Nitahara-Kasahara Y, Hayashita-Kinoh H, Chiyo T, Nishiyama A, Okada H, Takeda S & Okada T. (2014). Dystrophic mdx mice develop severe cardiac and respiratory dysfunction following genetic ablation of the anti-inflammatory cytokine IL-10. *Hum Mol Genet* **23**, 3990-4000.
- Nowak KJ & Davies KE. (2004). Duchenne muscular dystrophy and dystrophin: pathogenesis and opportunities for treatment. *EMBO Rep* **5**, 872-876.
- O'Halloran KD, McGuire M, O'Hare T & Bradford A. (2002). Chronic intermittent asphyxia impairs rat upper airway muscle responses to acute hypoxia and asphyxia. *Chest* **122**, 269-275.
- Okazaki M, Yamada Y, Nishimoto N, Yoshizaki K & Mihara M. (2002). Characterization of anti-mouse interleukin-6 receptor antibody. *Immunol Lett* **84**, 231-240.
- Ozawa E, Hagiwara Y & Yoshida M. (1999). Creatine kinase, cell membrane and Duchenne muscular dystrophy. *Mol Cell Biochem* **190**, 143-151.
- Pan Y, Chen C, Shen Y, Zhu CH, Wang G, Wang XC, Chen HQ & Zhu MS. (2008). Curcumin alleviates dystrophic muscle pathology in mdx mice. *Mol Cells* **25**, 531-537.

- Papapetropoulos TA & Bradley WG. (1972). Spinal motor neurones in murine muscular dystrophy and spinal muscular atrophy. A quantitative histological study. *J Neurol Neurosurg Psychiatry* **35**, 60-65.
- Parames SF, Coletta-Yudice ED, Nogueira FM, Nering de Sousa MB, Hayashi MA, Lima-Landman MT, Lapa AJ & Souccar C. (2014). Altered acetylcholine release in the hippocampus of dystrophin-deficient mice. *Neuroscience* **269**, 173-183.
- Pedersen BK & Febbraio MA. (2008). Muscle as an endocrine organ: focus on muscle-derived interleukin-6. *Physiol Rev* **88**, 1379-1406.
- Pelosi L, Berardinelli MG, De Pasquale L, Nicoletti C, D'Amico A, Carvello F, Moneta GM, Catizone A, Bertini E, De Benedetti F & Musarò A. (2015a). Functional and Morphological Improvement of Dystrophic Muscle by Interleukin 6 Receptor Blockade. *EBioMedicine* **2**, 285-293.
- Pelosi L, Berardinelli MG, Forcina L, Spelta E, Rizzuto E, Nicoletti C, Camilli C, Testa E, Catizone A, De Benedetti F & Musarò A. (2015b). Increased levels of interleukin-6 exacerbate the dystrophic phenotype in mdx mice. *Hum Mol Genet* **24**, 6041-6053.
- Pelosi L, Forcina L, Nicoletti C, Scicchitano BM & Musarò A. (2017). Increased Circulating Levels of Interleukin-6 Induce Perturbation in Redox-Regulated Signaling Cascades in Muscle of Dystrophic Mice. *Oxid Med Cell Longev* **2017**, 1987218.
- Peng YJ, Nanduri J, Yuan G, Wang N, Deneris E, Pendyala S, Natarajan V, Kumar GK & Prabhakar NR. (2009). NADPH oxidase is required for the sensory plasticity of the carotid body by chronic intermittent hypoxia. *J Neurosci* **29**, 4903-4910.
- Peng YJ, Overholt JL, Kline D, Kumar GK & Prabhakar NR. (2003). Induction of sensory long-term facilitation in the carotid body by intermittent hypoxia: implications for recurrent apneas. *Proc Natl Acad Sci U S A* **100**, 10073-10078.
- Peng YJ, Yuan G, Jacono FJ, Kumar GK & Prabhakar NR. (2006a). 5-HT evokes sensory long-term facilitation of rodent carotid body via activation of NADPH oxidase. *J Physiol* **576**, 289-295.
- Peng YJ, Yuan G, Ramakrishnan D, Sharma SD, Bosch-Marce M, Kumar GK, Semenza GL & Prabhakar NR. (2006b). Heterozygous HIF-1 α deficiency impairs carotid body-mediated systemic responses and reactive oxygen species generation in mice exposed to intermittent hypoxia. *J Physiol* **577**, 705-716.

- Perronnet C, Chagneau C, Le Blanc P, Samson-Desvignes N, Mornet D, Laroche S, De La Porte S & Vaillend C. (2012). Upregulation of brain utrophin does not rescue behavioral alterations in dystrophin-deficient mice. *Hum Mol Genet* **21**, 2263-2276.
- Personius KE & Sawyer RP. (2006). Variability and failure of neurotransmission in the diaphragm of mdx mice. *Neuromuscul Disord* **16**, 168-177.
- Pescatori M, Broccolini A, Minetti C, Bertini E, Bruno C, D'amico A, Bernardini C, Mirabella M, Silvestri G, Giglio V, Modoni A, Pedemonte M, Tasca G, Galluzzi G, Mercuri E, Tonali PA & Ricci E. (2007). Gene expression profiling in the early phases of DMD: a constant molecular signature characterizes DMD muscle from early postnatal life throughout disease progression. *FASEB J* **21**, 1210-1226.
- Petrof BJ. (1998). The molecular basis of activity-induced muscle injury in Duchenne muscular dystrophy. *Mol Cell Biochem* **179**, 111-123.
- Petrof BJ, Shrager JB, Stedman HH, Kelly AM & Sweeney HL. (1993a). Dystrophin protects the sarcolemma from stresses developed during muscle contraction. *Proc Natl Acad Sci U S A* **90**, 3710-3714.
- Petrof BJ, Stedman HH, Shrager JB, Eby J, Sweeney HL & Kelly AM. (1993b). Adaptations in myosin heavy chain expression and contractile function in dystrophic mouse diaphragm. *Am J Physiol* **265**, C834-841.
- Phillips MF, Quinlivan RC, Edwards RH & Calverley PM. (2001). Changes in spirometry over time as a prognostic marker in patients with Duchenne muscular dystrophy. *Am J Respir Crit Care Med* **164**, 2191-2194.
- Pilgram GS, Potikanond S, Baines RA, Fradkin LG & Noordermeer JN. (2010). The roles of the dystrophin-associated glycoprotein complex at the synapse. *Mol Neurobiol* **41**, 1-21.
- Pinto ML, Tokunaga HH, Souccar C, Schoorlemmer GH & da Silva Lapa ReC. (2008). Loss of neuronal projections in the dystrophin-deficient mdx mouse is not progressive. *Brain Res* **1224**, 127-132.
- Pinto ML, Tokunaga HH, Souccar C, Schoorlemmer GH & Lapa ReC. (2007). Morphological changes in the trigemino-rubral pathway in dystrophic (mdx) mice. *Neurosci Lett* **416**, 175-179.
- Polla B, D'Antona G, Bottinelli R & Reggiani C. (2004). Respiratory muscle fibres: specialisation and plasticity. *Thorax* **59**, 808-817.

- Porter JD, Guo W, Merriam AP, Khanna S, Cheng G, Zhou X, Andrade FH, Richmonds C & Kaminski HJ. (2003). Persistent over-expression of specific CC class chemokines correlates with macrophage and T-cell recruitment in mdx skeletal muscle. *Neuromuscul Disord* **13**, 223-235.
- Powell FL, Huey KA & Dwinell MR. (2000). Central nervous system mechanisms of ventilatory acclimatization to hypoxia. *Respir Physiol* **121**, 223-236.
- Powell FL, Milsom WK & Mitchell GS. (1998). Time domains of the hypoxic ventilatory response. *Respir Physiol* **112**, 123-134.
- Prabhakar NR. (2011). Sensory plasticity of the carotid body: role of reactive oxygen species and physiological significance. *Respir Physiol Neurobiol* **178**, 375-380.
- Prabhakar NR & Peng YJ. (2004). Peripheral chemoreceptors in health and disease. *J Appl Physiol (1985)* **96**, 359-366.
- Prabhakar NR & Peng YJ. (2017). Oxygen Sensing by the Carotid Body: Past and Present. *Adv Exp Med Biol* **977**, 3-8.
- Prabhakar NR, Peng YJ, Jacono FJ, Kumar GK & Dick TE. (2005). Cardiovascular alterations by chronic intermittent hypoxia: importance of carotid body chemoreflexes. *Clin Exp Pharmacol Physiol* **32**, 447-449.
- Pratt SJ, Shah SB, Ward CW, Kerr JP, Stains JP & Lovering RM. (2015a). Recovery of altered neuromuscular junction morphology and muscle function in mdx mice after injury. *Cell Mol Life Sci* **72**, 153-164.
- Pratt SJ, Valencia AP, Le GK, Shah SB & Lovering RM. (2015b). Pre- and postsynaptic changes in the neuromuscular junction in dystrophic mice. *Front Physiol* **6**, 252.
- Rae C, Griffin JL, Blair DH, Bothwell JH, Bubb WA, Maitland A & Head S. (2002). Abnormalities in brain biochemistry associated with lack of dystrophin: studies of the mdx mouse. *Neuromuscul Disord* **12**, 121-129.
- Rae MG & O'Malley D. (2016). Cognitive dysfunction in Duchenne muscular dystrophy: a possible role for neuromodulatory immune molecules. *J Neurophysiol* **116**, 1304-1315.
- Raphael JC, Chevret S, Chastang C & Bouvet F. (1994). Randomised trial of preventive nasal ventilation in Duchenne muscular dystrophy. French Multicentre Cooperative Group on Home Mechanical Ventilation Assistance in Duchenne de Boulogne Muscular Dystrophy. *Lancet* **343**, 1600-1604.

- Reutenauer-Patte J, Boittin FX, Patthey-Vuadens O, Ruegg UT & Dorchie OM. (2012). Urocortins improve dystrophic skeletal muscle structure and function through both PKA- and Epac-dependent pathways. *Am J Pathol* **180**, 749-762.
- Roberto R, Fritz A, Hagar Y, Boice B, Skalsky A, Hwang H, Beckett L, McDonald C & Gupta M. (2011). The natural history of cardiac and pulmonary function decline in patients with duchenne muscular dystrophy. *Spine (Phila Pa 1976)* **36**, E1009-1017.
- Robson-Ansley P, Cockburn E, Walshe I, Stevenson E & Nimmo M. (2010). The effect of exercise on plasma soluble IL-6 receptor concentration: a dichotomous response. *Exerc Immunol Rev* **16**, 56-76.
- Rodillo EB, Fernandez-Bermejo E, Heckmatt JZ & Dubowitz V. (1988). Prevention of rapidly progressive scoliosis in Duchenne muscular dystrophy by prolongation of walking with orthoses. *J Child Neurol* **3**, 269-274.
- Rodrigues MR, Carvalho CR, Santaella DF, Lorenzi-Filho G & Marie SK. (2014). Effects of yoga breathing exercises on pulmonary function in patients with Duchenne muscular dystrophy: an exploratory analysis. *J Bras Pneumol* **40**, 128-133.
- Roy A, Farnham MMJ, Derakhshan F, Pilowsky PM & Wilson RJA. (2017). Acute intermittent hypoxia with concurrent hypercapnia evokes P2X and TRPV1 receptor-dependent sensory long-term facilitation in naïve carotid bodies. *J Physiol*.
- Rufo A, Del Fattore A, Capulli M, Carvello F, De Pasquale L, Ferrari S, Pierroz D, Morandi L, De Simone M, Rucci N, Bertini E, Bianchi ML, De Benedetti F & Teti A. (2011). Mechanisms inducing low bone density in Duchenne muscular dystrophy in mice and humans. *J Bone Miner Res* **26**, 1891-1903.
- Ryan CM & Bradley TD. (2005). Pathogenesis of obstructive sleep apnea. *J Appl Physiol* **99**, 2440-2450.
- Sandhu MS, Dougherty BJ, Lane MA, Bolser DC, Kirkwood PA, Reier PJ & Fuller DD. (2009). Respiratory recovery following high cervical hemisection. *Respir Physiol Neurobiol* **169**, 94-101.
- Sankri-Tarbichi AG. (2012). Obstructive sleep apnea-hypopnea syndrome: Etiology and diagnosis. *Avicenna J Med* **2**, 3-8.
- Sawnani H, Thampratankul L, Szczesniak RD, Fenchel MC & Simakajornboon N. (2015). Sleep disordered breathing in young boys with Duchenne muscular dystrophy. *J Pediatr* **166**, 640-645.e641.

- Scheller J, Chalaris A, Schmidt-Arras D & Rose-John S. (2011). The pro- and anti-inflammatory properties of the cytokine interleukin-6. *Biochim Biophys Acta* **1813**, 878-888.
- Schiaffino S & Reggiani C. (2011). Fiber types in mammalian skeletal muscles. *Physiol Rev* **91**, 1447-1531.
- Schwab RJ, Gupta KB, Gefter WB, Metzger LJ, Hoffman EA & Pack AI. (1995). Upper airway and soft tissue anatomy in normal subjects and patients with sleep-disordered breathing. Significance of the lateral pharyngeal walls. *Am J Respir Crit Care Med* **152**, 1673-1689.
- Sekiguchi M, Zushida K, Yoshida M, Maekawa M, Kamichi S, Sahara Y, Yuasa S, Takeda S & Wada K. (2009). A deficit of brain dystrophin impairs specific amygdala GABAergic transmission and enhances defensive behaviour in mice. *Brain* **132**, 124-135.
- Serra F, Quarta M, Canato M, Toniolo L, De Arcangelis V, Trotta A, Spath L, Monaco L, Reggiani C & Naro F. (2012). Inflammation in muscular dystrophy and the beneficial effects of non-steroidal anti-inflammatory drugs. *Muscle Nerve* **46**, 773-784.
- Seven YB, Nichols NL, Kelly MN, Hobson OR, Satriotomo I & Mitchell GS. (2018). Compensatory plasticity in diaphragm and intercostal muscle utilization in a rat model of ALS. *Exp Neurol* **299**, 148-156.
- Sharma P, Basu S, Mitchell RW, Stelmack GL, Anderson JE & Halayko AJ. (2014). Role of dystrophin in airway smooth muscle phenotype, contraction and lung function. *PLoS One* **9**, e102737.
- Shneerson JM. (1996). Is chronic respiratory failure in neuromuscular diseases worth treating? *J Neurol Neurosurg Psychiatry* **61**, 1-3.
- Skatrud JB & Dempsey JA. (1983). Interaction of sleep state and chemical stimuli in sustaining rhythmic ventilation. *J Appl Physiol Respir Environ Exerc Physiol* **55**, 813-822.
- Skelly JR, Edge D, Shortt CM, Jones JF, Bradford A & O'Halloran KD. (2012). Tempol ameliorates pharyngeal dilator muscle dysfunction in a rodent model of chronic intermittent hypoxia. *Am J Respir Cell Mol Biol* **46**, 139-148.
- Smith JC, Abdala AP, Rybak IA & Paton JF. (2009). Structural and functional architecture of respiratory networks in the mammalian brainstem. *Philos Trans R Soc Lond B Biol Sci* **364**, 2577-2587.

- Smith LR, Hammers DW, Sweeney HL & Barton ER. (2016). Increased collagen cross-linking is a signature of dystrophin-deficient muscle. *Muscle Nerve* **54**, 71-78.
- Smith PE, Calverley PM & Edwards RH. (1988). Hypoxemia during sleep in Duchenne muscular dystrophy. *Am Rev Respir Dis* **137**, 884-888.
- Smith PE, Edwards RH & Calverley PM. (1989a). Protriptyline treatment of sleep hypoxaemia in Duchenne muscular dystrophy. *Thorax* **44**, 1002-1005.
- Smith PE, Edwards RH & Calverley PM. (1989b). Ventilation and breathing pattern during sleep in Duchenne muscular dystrophy. *Chest* **96**, 1346-1351.
- Souza GM, Bonagamba LG, Amorim MR, Moraes DJ & Machado BH. (2015). Cardiovascular and respiratory responses to chronic intermittent hypoxia in adult female rats. *Exp Physiol* **100**, 249-258.
- Souza GM, Bonagamba LG, Amorim MR, Moraes DJ & Machado BH. (2016). Inspiratory modulation of sympathetic activity is increased in female rats exposed to chronic intermittent hypoxia. *Exp Physiol* **101**, 1345-1358.
- Stedman HH, Sweeney HL, Shrager JB, Maguire HC, Panettieri RA, Petrof B, Narusawa M, Leferovich JM, Sladky JT & Kelly AM. (1991). The mdx mouse diaphragm reproduces the degenerative changes of Duchenne muscular dystrophy. *Nature* **352**, 536-539.
- Stevens ED & Faulkner JA. (2000). The capacity of mdx mouse diaphragm muscle to do oscillatory work. *J Physiol* **522 Pt 3**, 457-466.
- Suresh S, Wales P, Dakin C, Harris MA & Cooper DG. (2005). Sleep-related breathing disorder in Duchenne muscular dystrophy: disease spectrum in the paediatric population. *J Paediatr Child Health* **41**, 500-503.
- Syabbalo N. (1998a). Assessment of respiratory muscle function and strength. *Postgrad Med J* **74**, 208-215.
- Syabbalo N. (1998b). Respiratory muscle function in patients with neuromuscular disorders and cardiopulmonary diseases. *Int J Clin Pract* **52**, 319-329.
- Teppema LJ & Dahan A. (2010). The ventilatory response to hypoxia in mammals: mechanisms, measurement, and analysis. *Physiol Rev* **90**, 675-754.
- Terada J & Mitchell GS. (2011). Diaphragm long-term facilitation following acute intermittent hypoxia during wakefulness and sleep. *J Appl Physiol (1985)* **110**, 1299-1310.

- Thibaud JL, Matot B, Barthélémy I, Fromes Y, Blot S & Carlier PG. (2017). Anatomical and mesoscopic characterization of the dystrophic diaphragm: An in vivo nuclear magnetic resonance imaging study in the Golden retriever muscular dystrophy dog. *Neuromuscul Disord* **27**, 315-325.
- Tidball JG. (2005). Inflammatory processes in muscle injury and repair. *Am J Physiol Regul Integr Comp Physiol* **288**, R345-353.
- Tidball JG & Wehling-Henricks M. (2007). The role of free radicals in the pathophysiology of muscular dystrophy. *J Appl Physiol (1985)* **102**, 1677-1686.
- Toussaint M, Davidson Z, Bouvoie V, Evenepoel N, Haan J & Soudon P. (2016). Dysphagia in Duchenne muscular dystrophy: practical recommendations to guide management. *Disabil Rehabil* **38**, 2052-2062.
- Toussaint M, Steens M & Soudon P. (2007). Lung function accurately predicts hypercapnia in patients with Duchenne muscular dystrophy. *Chest* **131**, 368-375.
- Vaillend C & Chaussonnet R. (2017). Relationships linking emotional, motor, cognitive and GABAergic dysfunctions in dystrophin-deficient mdx mice. *Hum Mol Genet* **26**, 1041-1055.
- van der Pijl EM, van Putten M, Niks EH, Verschuuren JJ, Aartsma-Rus A & Plomp JJ. (2016). Characterization of neuromuscular synapse function abnormalities in multiple Duchenne muscular dystrophy mouse models. *Eur J Neurosci* **43**, 1623-1635.
- Van Lunteren E & Vafaie H. (1993). Force potentiation in respiratory muscles: comparison of diaphragm and sternohyoid. *Am J Physiol* **264**, R1095-1100.
- Villalta SA, Rinaldi C, Deng B, Liu G, Fedor B & Tidball JG. (2011). Interleukin-10 reduces the pathology of mdx muscular dystrophy by deactivating M1 macrophages and modulating macrophage phenotype. *Hum Mol Genet* **20**, 790-805.
- Vizek M, Pickett CK & Weil JV. (1987). Increased carotid body hypoxic sensitivity during acclimatization to hypobaric hypoxia. *J Appl Physiol (1985)* **63**, 2403-2410.
- Vohra RS, Lott D, Mathur S, Senesac C, Deol J, Germain S, Bendixen R, Forbes SC, Sweeney HL, Walter GA & Vandenborne K. (2015). Magnetic Resonance Assessment of Hypertrophic and Pseudo-Hypertrophic Changes in Lower Leg Muscles of Boys with Duchenne Muscular Dystrophy and Their Relationship to Functional Measurements. *PLoS One* **10**, e0128915.

- Wada E, Tanihata J, Iwamura A, Takeda S, Hayashi YK & Matsuda R. (2017). Treatment with the anti-IL-6 receptor antibody attenuates muscular dystrophy via promoting skeletal muscle regeneration in dystrophin-/utrophin-deficient mice. *Skelet Muscle* **7**, 23.
- Wanke T, Toifl K, Merkle M, Formanek D, Lahrmann H & Zwick H. (1994). Inspiratory muscle training in patients with Duchenne muscular dystrophy. *Chest* **105**, 475-482.
- Welc SS & Clanton TL. (2013). The regulation of interleukin-6 implicates skeletal muscle as an integrative stress sensor and endocrine organ. *Exp Physiol* **98**, 359-371.
- Wellman A, Jordan AS, Malhotra A, Fogel RB, Katz ES, Schory K, Edwards JK & White DP. (2004). Ventilatory control and airway anatomy in obstructive sleep apnea. *Am J Respir Crit Care Med* **170**, 1225-1232.
- White DP. (2005). Pathogenesis of obstructive and central sleep apnea. *Am J Respir Crit Care Med* **172**, 1363-1370.
- White DP & Younes MK. (2012). Obstructive sleep apnea. *Compr Physiol* **2**, 2541-2594.
- Whitehead NP, Bible KL, Kim MJ, Odom GL, Adams ME & Froehner SC. (2016). Validation of ultrasonography for non-invasive assessment of diaphragm function in muscular dystrophy. *J Physiol* **594**, 7215-7227.
- Whitehead NP, Yeung EW & Allen DG. (2006). Muscle damage in mdx (dystrophic) mice: role of calcium and reactive oxygen species. *Clin Exp Pharmacol Physiol* **33**, 657-662.
- Wilkerson JE & Mitchell GS. (2009). Daily intermittent hypoxia augments spinal BDNF levels, ERK phosphorylation and respiratory long-term facilitation. *Exp Neurol* **217**, 116-123.
- Wilkerson JER, Devinney M & Mitchell GS. (2017). Intermittent but not sustained moderate hypoxia elicits long-term facilitation of hypoglossal motor output. *Respir Physiol Neurobiol*.
- Wilkinson KA, Huey K, Dinger B, He L, Fidone S & Powell FL. (2010). Chronic hypoxia increases the gain of the hypoxic ventilatory response by a mechanism in the central nervous system. *J Appl Physiol (1985)* **109**, 424-430.

- Willcocks RJ, Arpan IA, Forbes SC, Lott DJ, Senesac CR, Senesac E, Deol J, Triplett WT, Baligand C, Daniels MJ, Sweeney HL, Walter GA & Vandeborne K. (2014). Longitudinal measurements of MRI-T2 in boys with Duchenne muscular dystrophy: effects of age and disease progression. *Neuromuscul Disord* **24**, 393-401.
- Willmann R, Possekel S, Dubach-Powell J, Meier T & Ruegg MA. (2009). Mammalian animal models for Duchenne muscular dystrophy. *Neuromuscul Disord* **19**, 241-249.
- Worsnop C, Kay A, Pierce R, Kim Y & Trinder J. (1998). Activity of respiratory pump and upper airway muscles during sleep onset. *J Appl Physiol (1985)* **85**, 908-920.
- Xu R & Salpeter MM. (1997). Acetylcholine receptors in innervated muscles of dystrophic mdx mice degrade as after denervation. *J Neurosci* **17**, 8194-8200.
- Xu S, Shi D, Pratt SJ, Zhu W, Marshall A & Lovering RM. (2015). Abnormalities in brain structure and biochemistry associated with mdx mice measured by in vivo MRI and high resolution localized (1)H MRS. *Neuromuscul Disord* **25**, 764-772.
- Yiu EM & Kornberg AJ. (2008). Duchenne muscular dystrophy. *Neurol India* **56**, 236-247.
- Yiu EM & Kornberg AJ. (2015). Duchenne muscular dystrophy. *J Paediatr Child Health* **51**, 759-764.
- Zanardi MC, Tagliabue A, Orcesi S, Berardinelli A, Uggetti C & Pichiecchio A. (2003). Body composition and energy expenditure in Duchenne muscular dystrophy. *Eur J Clin Nutr* **57**, 273-278.

Chapter 2. Sensorimotor control of breathing in the *mdx* mouse model of Duchenne muscular dystrophy

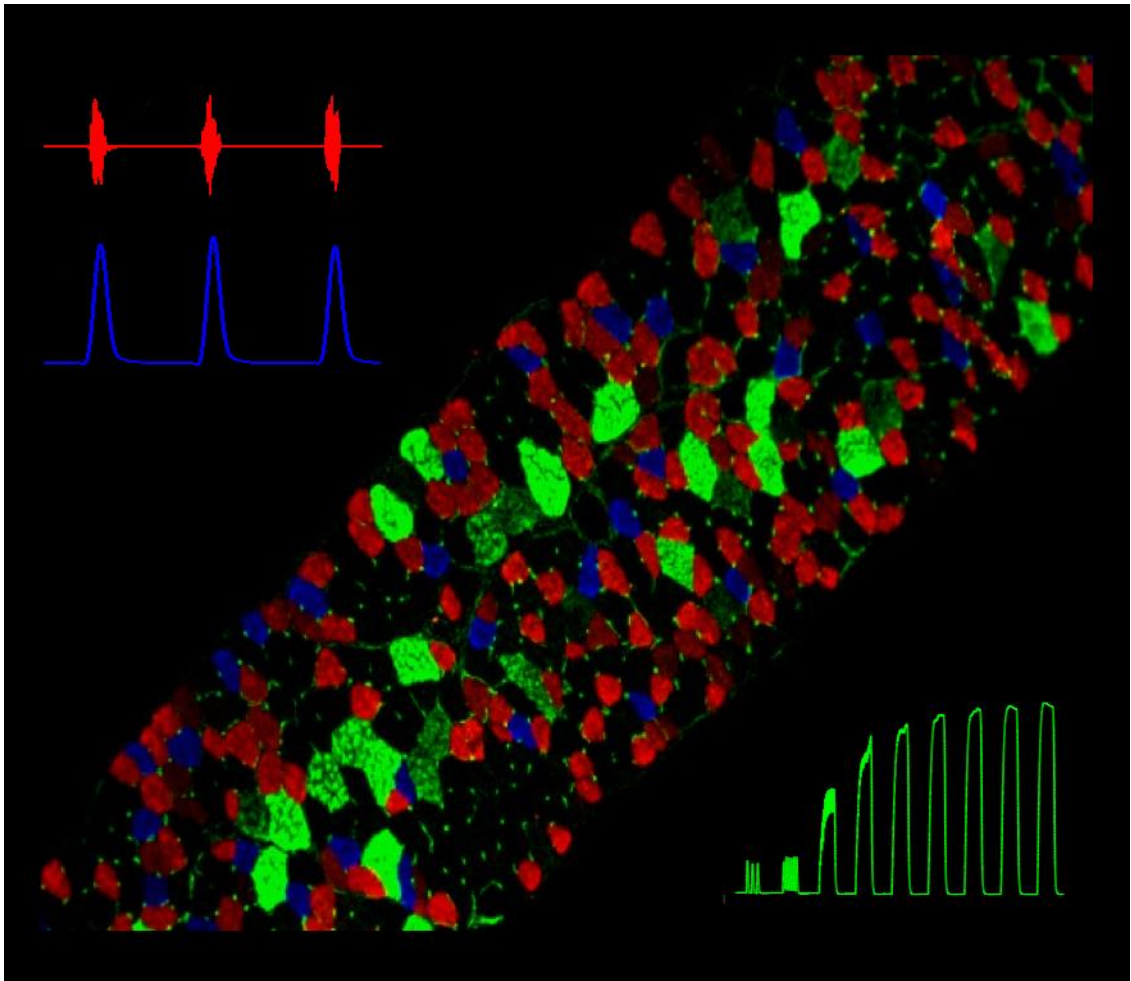
David P. Burns¹, Arijit Roy², Eric F. Lucking¹, Fiona B. McDonald², Sam Gray³, Richard J. Wilson², Deirdre Edge³ and Ken D. O'Halloran¹

¹*Department of Physiology, School of Medicine, College of Medicine and Health, University College Cork, Cork, Ireland.*

²*Hotchkiss Brain Institute, University of Calgary, Calgary, Alberta, Canada.*

³*Department of Physiology, School of Medicine, Trinity Biosciences Institute, Trinity College Dublin, the University of Dublin, Dublin, Ireland.*

Paper published in *The Journal of Physiology*.



Cover image shows representative immunofluorescent image of diaphragm muscle from a wild-type mouse. Murine diaphragm muscle expresses type I (blue), type IIa (red), type IIx (untagged, appearing black) and type IIb (green) myosin heavy chain isoforms. Top left shows representative traces for diaphragm raw (red) and integrated (blue) EMG activity in an anaesthetised mouse. Bottom right shows original trace of diaphragm force-frequency relationship ex vivo (green).

Key points

- Respiratory failure is a leading cause of mortality in Duchenne muscular dystrophy (DMD), but little is known about the control of breathing in DMD and animal models.
- We show that young (8 weeks of age) *mdx* mice hypoventilate during basal breathing due to reduced tidal volume. Basal CO₂ production is equivalent in wild-type and *mdx* mice.
- We show that carotid bodies from *mdx* mice have blunted responses to hyperoxia, revealing hypoactivity in normoxia. However, carotid body, ventilatory and metabolic responses to hypoxia are equivalent in wild-type and *mdx* mice.
- Our study revealed profound muscle weakness and muscle fibre remodelling in young *mdx* diaphragm suggesting severe mechanical disadvantage in *mdx* mice at an early age.
- Our study reveals a potentiated neural motor drive to breathe in *mdx* mice during maximal chemoactivation, suggesting compensatory neuroplasticity enhancing respiratory motor output to the diaphragm and likely other accessory muscles.

Abbreviations: AUC, area under the curve; CSA, cross-sectional area; CSN, carotid sinus nerve; CT, contraction time; DMD, Duchenne muscular dystrophy; EMG, electromyogram; f_R , respiratory frequency; F_iO_2 , fractional inspired oxygen concentration; Hb, haemoglobin; HCO_3^- , bicarbonate; L_o , optimum length; MFO, mean frequency oscillation; PCO_2 , partial pressure of CO_2 ; PO_2 , partial pressure of O_2 ; P_t , isometric twitch force; SpO_2 , arterial O_2 percent saturation; TCO_2 , total CO_2 ; V_E , minute ventilation; V_E/VCO_2 , ventilatory equivalent for CO_2 ; V_E/VO_2 , ventilatory equivalent for O_2 ; VCO_2 , carbon dioxide production; VO_2 , oxygen consumption; V_T , tidal volume; $\frac{1}{2} RT$, half-relaxation time.

Abstract

Patients with Duchenne muscular dystrophy (DMD) hypoventilate with consequential arterial blood gas derangement relevant to disease progression. Whereas deficits in DMD diaphragm are recognized, there is a paucity of knowledge in respect of the neural control of breathing in dystrophinopathies. We sought to perform an analysis of respiratory control in a model of DMD, the *mdx* mouse. In eight week old male wild-type and *mdx* mice, ventilation and metabolism, carotid body afferent activity, and diaphragm muscle force-generating capacity, and muscle fibre size, distribution and centronucleation were determined. Diaphragm EMG activity and responsiveness to chemostimulation was determined. During normoxia, *mdx* mice hypoventilated, owing to a reduction in tidal volume. Basal CO₂ production was not different between wild-type and *mdx* mice. Carotid sinus nerve responses to hyperoxia were blunted in *mdx* suggesting hypoactivity. However, carotid body, ventilatory and metabolic responses to hypoxia were equivalent in wild-type and *mdx* mice. Diaphragm force was severely depressed in *mdx* mice, with evidence of fibre remodelling and damage. Diaphragm EMG responses to chemoactivation were enhanced in *mdx* mice. We conclude that there is evidence of chronic hypoventilation in young *mdx* mice. Diaphragm dysfunction confers mechanical deficiency in *mdx* resulting in impaired capacity to generate normal tidal volume at rest and decreased absolute ventilation during chemoactivation. Enhanced *mdx* diaphragm EMG responsiveness suggests compensatory neuroplasticity facilitating respiratory motor output, which may extend to accessory muscles of breathing. Our results may have relevance to emerging treatments for human DMD aiming to preserve ventilatory capacity.

Keywords: Duchenne muscular dystrophy, *mdx*, hypoventilation, carotid body, diaphragm, EMG

2.1 Introduction

Duchenne muscular dystrophy (DMD) is a fatal X-linked neuromuscular disease characterized by dystrophin deficiency. Deficits in this structural protein lead to aberrant structural remodelling and damage in skeletal and other muscles (Muntoni *et al.*, 2003; Deconinck & Dan, 2007; Ervasti, 2007; Mosqueira *et al.*, 2013b), with consequential profound muscle weakness extending to the striated muscles of breathing—the final effectors in the respiratory control network. Respiratory insufficiency is a hallmark of DMD (Baydur *et al.*, 1990; Bersanini *et al.*, 2012). Whereas diaphragm dysfunction is a recognized primary morbid feature in DMD (De Bruin *et al.*, 1997; Beck *et al.*, 2006; Khirani *et al.*, 2014), there is a paucity of knowledge in respect of the neural control of breathing in the human dystrophinopathies. Of note, DMD patients hypoventilate with resultant hypoxaemia (Smith *et al.*, 1989a, b; Melacini *et al.*, 1996), a symptom which may have particular relevance to muscle pathology and disease progression, in the light of data from rodent models revealing hypoxia-induced respiratory muscle weakness (McMorrow *et al.*, 2011; Skelly *et al.*, 2012; Shortt *et al.*, 2014) due to altered redox signalling and overt oxidative stress (Lewis *et al.*, 2015; Lewis *et al.*, 2016), which are features of DMD.

Respiratory failure in DMD results in premature death. Yet, the early impact of dystrophin deficiency on the respiratory control network is unclear. This knowledge gap is significant and has potential relevance to the treatment of DMD. It is not known if dystrophin deficiency has consequences for sensorimotor control of breathing. There is ample evidence in support of remarkable capacity for plasticity within the respiratory control network governing arterial blood gas and pH homeostasis in health and disease (Mitchell & Johnson, 2003; Kumar & Prabhakar, 2012; Fuller & Mitchell, 2017). Sensory and motor plasticity is context-dependent, with a capacity for adaptive or maladaptive outcomes. Compensatory neuroplasticity at one or more sites of the respiratory control network could ameliorate respiratory muscle deficits in early stages of DMD. Conversely, sensorimotor deficits could exacerbate aberrant respiratory control in

DMD and contribute to disease progression. Dystrophin is present in the carotid body (Mosqueira *et al.*, 2013a), the primary blood oxygen sensor, but it is unclear if dystrophin deficiency affects chemoafferent discharge and as such, the control of breathing. Dystrophin is also present in neurons (Lidov, 1996), but it is not known if central respiratory motor drive is affected by dystrophinopathies, potentiating or ameliorating impaired respiratory mechanics due to respiratory muscle weakness. A greater understanding of the control of breathing in DMD is likely to prove important to therapeutic strategies, and might offer novel targets in interventional therapies particularly early in disease onset before the establishment of overt respiratory pathology.

We sought to perform an assessment of respiratory control in a young murine model of DMD—the *mdx* mouse. Whereas, diaphragm dysfunction faithfully recapitulating the human condition has been established in the model, assessment of respiratory control, especially in young animals, is lacking. We hypothesized that there should be evidence of neuroplasticity in the respiratory control network of the *mdx* mouse.

2.2 Methods

2.2.1 Ethical approval

Procedures concerning live animals were performed under licence in accordance with Irish and European directive 2010/63/EU following approval by University College Cork animal research ethics committee. Carotid body recordings were performed in accordance with The Canadian Council on Animal Care Guidelines and were approved locally by the Animal Care Committee of the Cumming School of Medicine, University of Calgary, Canada.

2.2.2 Experimental animals

Male and female wild-type (C57BL/10ScSnJ) and *mdx* (C57BL/10ScSn-Dmd^{mdx}/J) mice were purchased from the Jackson Laboratory (Bar Harbor, ME, USA) and bred at University College Cork's animal housing facility. Eight-week-old male wild-type (n = 53) and *mdx* (n = 52) mice were studied for respiratory and metabolism measurements, *ex vivo* muscle function tests, tissue harvesting for immunohistochemistry, *in vivo* EMG recordings and arterial blood gas analysis. For carotid body-carotid sinus nerve preparations, male wild-type (n = 6) and *mdx* (n = 6) mice were purchased from the Jackson Laboratory and transferred to the University of Calgary for subsequent experiments at eight weeks of age. Animals were housed conventionally in temperature- and humidity-controlled facilities, operating on a 12 h light: 12 h dark cycle with food and water available *ad libitum*.

2.2.3 Respiratory recordings

Respiratory flow recordings were performed using whole-body plethysmography in unrestrained, unanaesthetised mice during quiet rest. Wild-type (n = 13) and *mdx* (n = 12) mice were introduced into plethysmograph chambers (Model PLY4211; volume=600mL, Buxco Research Systems, Wilmington, NC, USA) and allowed a 60-90 minute acclimation period until sufficiently settled, with room air passing through each chamber (1 L/min). Recordings were typically performed in parallel, with

contemporaneous assessment of breathing in one wild-type mouse and one *mdx* mouse using a two chamber set-up. For successive recording sessions, mice were assigned to chambers based on genotype in an alternating fashion to avoid any potential bias associated with a given chamber. *Post hoc* analysis of breathing within each genotype confirmed no difference in parameters recorded comparing data derived from the two chambers.

Experimental protocol: Following the acclimation period, a 20-30-minute baseline recording was performed in normoxia. This was followed by a 20-minute hypoxic challenge ($F_{iO_2} = 0.1$; balance N_2). Following a 60-minute recovery period in normoxia, a 20-30 minute normoxic baseline period was recorded. This was followed by a graded hypoxic challenge in which animals were challenged with decreasing levels of inspired oxygen: $F_{iO_2} = 0.15, 0.12, 0.10,$ and 0.08 (balance N_2) consecutively for 5 minutes each. Respiratory parameters including respiratory frequency (f_R), tidal volume (V_T) and minute ventilation (V_E) were recorded on a breath-by-breath basis for analysis offline.

Data analysis: To maximize the recording period for the assessment of ventilatory parameters in normoxia, both normoxic bouts were pooled to generate one set of baseline (normoxia) data; there was no significant difference for ventilatory parameters between the two normoxic periods. Based on the time constant for the plethysmograph chambers and that gases were thoroughly mixed before entry to the plethysmograph chambers, we assumed complete gas mixing during gas challenges by ~ 3 minutes of exposure. For the sustained (20 minute) hypoxic challenge, data are shown after 5 minutes of exposure and are presented on a minute-by-minute basis thereafter. For the graded hypoxic challenge, measurements were taken during the 5th minute of exposure to the given F_{iO_2} challenge. For each of the hypoxic challenges (sustained and graded), data during hypoxic exposure were compared with the preceding 5 minutes of baseline ($F_{iO_2}: 0.21$). In a separate historical cohort of wild-type ($n = 10$) and *mdx* ($n = 11$) mice (Burns *et al.*, 2015), we assessed the ventilatory

response to a 10 minute hypercapnic gas challenge (5% CO₂, balance O₂). V_T and V_E were normalised for body mass (g).

2.2.4 Metabolism measurements

O₂ consumption (VO₂) and CO₂ production (VCO₂) were measured in wild-type (n = 13) and *mdx* (n = 12) mice undergoing the whole-body plethysmography protocol. Airflow through the chamber was maintained at 1 L/min. Fractional concentrations of O₂ and CO₂ were measured in air entering and exiting the plethysmograph (O₂ and CO₂ analyzer; ADInstruments, Colorado Springs, CO, USA) similar to that previously described (Bavis *et al.*, 2010; Bavis *et al.*, 2014).

Data analysis: calculation of VO₂ and VCO₂ was performed as previously described (Haouzi *et al.*, 2009). For the sustained (20 minute) hypoxic challenge data are shown after 5 minutes of exposure and are presented on a minute-by-minute basis thereafter. For the graded hypoxic challenge, measurements were taken during the 5th minute of exposure to the given F_iO₂ challenge. For each of the hypoxic challenges (sustained and graded), data during hypoxic exposure were compared with the preceding 5 minutes of baseline (F_iO₂: 0.21). VO₂ and VCO₂ were normalised for body mass (g).

2.2.5 Blood gas analysis

Wild-type (n = 7) and *mdx* (n = 7) mice were anaesthetised with 5% isoflurane in air. A laparotomy was performed and cardiac puncture was performed by advancing a 25G needle through the diaphragm and into the apex of the heart for blood sampling for analysis. 0.2ml of blood was collected and used to measure pH, the partial pressure of O₂ (PO₂) and CO₂ (PCO₂), total CO₂ (TCO₂), bicarbonate concentration [HCO₃⁻], arterial saturation (SaO₂), sodium ion concentration [Na⁺], potassium ion concentration [K⁺], haematocrit and haemoglobin concentration [Hb] using a blood gas analyzer (i-Stat; Heska, Fort Collins, CO, USA). Animals were killed by cervical dislocation.

2.2.6 Arterially perfused ex vivo carotid body-carotid sinus nerve preparation

At the University of Calgary, wild-type (n = 6) and *mdx* (n = 6) mice were heavily anaesthetised with isoflurane and then decapitated (lower cervical level). The carotid bifurcation, including the carotid body-carotid sinus nerve-superior cervical ganglion, was quickly isolated *en bloc* for *in vitro* perfusion as described previously (Roy *et al.*, 2012). The carotid bifurcation was then transferred to a dissection dish containing physiological saline (in mM: 1 MgSO₄, 1.25 NaH₂PO₄, 4 KCl, 24 NaHCO₃, 115 NaCl, 10 glucose, 12 sucrose, and 2 CaCl₂) and equilibrated with hyperoxia (95% O₂/5% CO₂). After 15-20 minutes, the isolated tissue was transferred to a recording chamber with a built-in water-fed heating circuit and the common carotid artery was immediately cannulated for luminal perfusion with physiological saline equilibrated with 100 mmHg PO₂ and 36 mmHg PCO₂ (balance N₂). The carotid sinus nerve was then carefully desheathed and the carotid sinus region was bisected. The occipital, internal, and external arteries were ligated, and small incisions were made on the internal and external carotid arteries to allow perfusate to exit. A peristaltic pump was used to set the perfusion rate at ~10 ml/min, which was sufficient to maintain a constant pressure of 90-100 mmHg at the tip of the cannula. The perfusate was equilibrated with computer-controlled gas mixtures monitored using CO₂ and O₂ gas analyzers (models CA-2A and PA1B, respectively, Sable Systems, Las Vegas, NV, USA); a gas mixture of 100 mmHg PO₂ and 36 mmHg PCO₂ (balance N₂) was used to start the experiments (yielding pH ~7.4). Before reaching the cannula, the perfusate was passed through a bubble trap and heat exchanger. The temperature of the perfusate, measured continuously as it departed the preparation, was maintained at 37 ± 0.5°C. The effluent from the chamber was recirculated.

Chemosensory discharge was recorded extracellularly from the whole desheathed carotid sinus nerve, which was placed on a platinum electrode and lifted into a thin film of paraffin oil. A reference electrode was placed close to the bifurcation. Carotid sinus nerve activity was monitored using a differential AC amplifier (model 1700, AM

Systems) and a secondary amplifier (model AM502, Tektronix, Beaverton, OR). The neural activity was amplified, filtered (300-Hz low cutoff, 5-kHz high cutoff), displayed on an oscilloscope, rectified, integrated (200-ms time constant), and stored on a computer using an analogue-to-digital board (Digidata 1322A, Axon Instruments, Union City, CA, USA) and data acquisition software (Axoscope 9.0). Preparations were left undisturbed for 45 minutes to stabilize before the experimental protocol began.

Experimental protocol: The following protocol was used for all experiments: 1) the carotid body was perfused for 5 minutes with normoxia (100 mmHg PO₂ and 36 mmHg PCO₂; balance N₂) to determine baseline carotid sinus nerve activity; 2) neural responses were obtained by challenging the carotid body for 5 minutes with mild, moderate and severe hypoxia (80, 60 & 40 mmHg, respectively) interspersed with normoxia; 3) finally a hyperoxic (500 mmHg PO₂ and 36 mmHg PCO₂; balance N₂) challenge was given for 5 minutes to examine the sensitivity of the carotid body (Dejours test).

Data analysis: Data were analyzed offline using custom software (written by R.J.A. Wilson). Carotid sinus nerve activity was divided into 2 second time bins, and activity in each bin was rectified and summed (expressed as integrated neural discharge). Data are shown as absolute carotid sinus nerve discharge frequencies in each of the different conditions in the protocol. Neural responses to PO₂ challenge were determined by comparing absolute discharge frequencies and also responses normalised to the hyperoxic condition, and separately to the normoxic condition.

2.2.7 Ex vivo muscle function tests

Diaphragm muscle function was examined *ex vivo* under isometric conditions using a standardized protocol as previously described (Shortt *et al.*, 2014). Wild-type (n = 7) and *mdx* (n = 7) mice were anaesthetised with 5% isoflurane by inhalation in air and euthanized by cervical dislocation. The diaphragm muscle was excised immediately

with rib and central tendon attached. Longitudinally arranged bundles were prepared for assessment of contractile function and were suspended vertically between two platinum plate electrodes. The rib was attached to a fixed hook at one end and the central tendon was attached to a force transducer with non-elastic string at the other end. Muscle baths contained Krebs solution (in mM: 120 NaCl, 5 KCl, 2.5 Ca²⁺, 1.2 MgSO₄, 1.2 NaH₂PO₄, 25 NaHCO₃, 11.5 glucose) and D-tubocurarine (25µM) and were equilibrated under hyperoxic conditions (95% O₂/ 5% CO₂). The optimum length (L_o) was determined by adjusting the position of the force transducer, and hence the length of the muscle preparations, by use of a micro-positioner between intermittent twitch contractions (Burns & O'Halloran, 2016; Burns *et al.*, 2017). L_o was taken as the muscle length associated with maximal isometric twitch force in response to single isometric twitch stimulation (supramaximal stimulation, 1ms duration). Once L_o was determined, the muscle was held at this length for the duration of the protocol.

Experimental protocol: A single isometric twitch was measured. Peak isometric twitch force (P_t), contraction time (CT; time to peak force) and half-relaxation time (½ RT; time for peak force to decay by 50%) were determined. The force-frequency relationship was determined by sequentially stimulating the muscle at 10, 20, 40, 60, 80, 100, 120, 140, 160 Hz (300ms train duration), allowing a 1 minute interval between stimulation.

Data analysis: Specific force was calculated in N/cm² of muscle cross-sectional area (CSA). The CSA of each strip was determined by dividing the muscle mass (weight in grams) by the product of muscle L_o (cm) and muscle density (assumed to be 1.06 g/cm³). The CT and ½ RT were measured as indices of isometric twitch kinetics. Normalisation of diaphragm forces to CSA was principally a means of standardizing the *ex vivo* muscle preparations. It should be noted that tissue, and not muscle fibre CSA was estimated with this approach and our data do not provide information on the specific force of muscle fibres *per se*, which might also require consideration of revised

muscle density values in *mdx*. Absolute muscle forces (N) were also assessed and compared in our study.

2.2.8 Muscle immunohistochemistry

Wild-type (n = 8) and *mdx* (n = 8) mice were anaesthetised with 5% isoflurane by inhalation in air and euthanized by cervical dislocation. Diaphragm muscle was excised immediately and a section of the hemi-diaphragm was mounted on a block of liver. Tissue samples were embedded in optimum cutting temperature (OCT; VWR International, Dublin, Ireland) embedding medium, frozen in isopentane (Sigma Aldrich, Wicklow, Ireland) cooled in liquid nitrogen and stored at -80°C for subsequent structural analysis. Serial transverse muscle sections (10µm) were cryosectioned (Leica CM3050; Leica Microsystems, Nussloch, Germany) at -22°C and mounted on polylysine-coated glass slides (VWR International, Dublin, Ireland). Slides were immersed in PBS (0.01 M) containing 1% bovine serum albumin (BSA) for 15 minutes. After 3x5 minute PBS washes, slides were immersed in PBS containing 5% normal goat serum (Sigma Aldrich, Wicklow, Ireland) for 30 minutes. Slides then underwent a further 3x5 minute PBS washes prior to application of the primary antibody (rabbit anti-laminin, 1:500; Sigma Aldrich, Wicklow, Ireland), diluted in PBS and 1% BSA. Slides were incubated overnight at 4°C in a humidity chamber. After the incubation period, slides were washed with PBS for 3x5 minutes before the secondary antibody (FITC-conjugated goat anti-rabbit; 1:250, Sigma Aldrich, Wicklow, Ireland), diluted in PBS and 1% BSA, was applied. Slides were incubated for 1 hour in the dark at room temperature. To identify myonuclei, the nuclear stain Hoechst (Sigma Aldrich, Wicklow, Ireland) was diluted in PBS (1:4) and applied to a subset of muscle sections for 10 minutes. Slides were rinsed with PBS for 5 minutes, cover-slipped with polyvinyl alcohol mounting medium with DABCO® anti-fade (Sigma Aldrich, Wicklow, Ireland).

Data analysis: Muscle sections were viewed at x10 magnification and images captured using an Olympus BX51 microscope and an Olympus DP71 camera. For each animal, 3-

4 images were captured for analysis from multiple muscle sections. For measurements, a square test frame of (600 x 600 μm), with inclusion and exclusion boundaries, was placed randomly over each image (Shortt et al., 2014). To determine the size distribution of muscle fibres within the diaphragm the individual fibre boundaries were determined using Imaris software. From this, the fibre cross-sectional area as well as Feret's minimal diameter were determined (Dubach-Powell, 2008). The coefficient of variation of muscle fibre minimal Feret's diameter, was also constructed for wild-type and *mdx*. In a subset of animals (n = 5 per genotype) centrally nucleated muscle fibres were identified using ImageJ software on merged laminin and hoescht stained images. The proportion of centrally nucleated muscle fibres was expressed relative to the total number of myofibres analyzed per image. Data generated from multiple images was averaged per animal before computing group means.

2.2.9 Diaphragm EMG activity and responsiveness

Anaesthesia was induced with 5% isoflurane in 60% O₂ (balance N₂) followed by urethane (1.8 g/kg i.p.). Wild-type (n = 8) and *mdx* (n = 7) mice were then placed in the supine position, gradually weaned off the isoflurane and body temperature was maintained at 37°C via a rectal probe and thermostatically-controlled heating blanket (Harvard Apparatus, Holliston, MA, USA). Supplemental anaesthetic was administered if necessary to maintain a surgical plane of anaesthesia, which was assessed by assessment of pedal withdrawal reflex to noxious pinch. A pulse oximeter clip (MouseOx™, Starr Life Sciences Corporation, Oakmount, PA, USA) was placed on the thigh of each mouse for the measurement of arterial O₂ saturation. A mid-cervical tracheotomy was performed to avoid upper airway obstruction. All animals were maintained with a bias flow of supplemental O₂ (FiO₂ = 0.60) unless otherwise stated. Concentric needle electrodes (26G; Natus Manufacturing Ltd, Ireland) were inserted into the costal diaphragm for the continuous measurement of diaphragm EMG activity which was amplified (x5,000), filtered (500Hz low cut-off to 5,000Hz high cut-off) and integrated (50ms time constant; Neurolog system, Digitimer Ltd, UK). All signals were

passed through an analogue-to-digital converter (r8/30; ADInstruments, Colorado Springs, CO, USA) and were acquired using LabChart 7 (ADInstruments, Colorado Springs, CO, USA).

Experimental protocol: Spontaneously breathing animals were vagotomized and allowed to stabilize for a minimum of 5 minutes before baseline parameters were measured. It is established that chemostimulation in spontaneously breathing mice elicits a significantly greater phrenic motor response following vagotomy compared with vagi intact (Kline *et al.*, 2002). Next, animals were sequentially challenged with hypercapnia (5% CO₂ and 10% CO₂; 2min each), hypoxia (15% O₂; 1min), and asphyxia (15% O₂/5% CO₂; 1min) to examine the effects of chemostimulation on diaphragm EMG activity. Following completion of diaphragm EMG recordings, animals were euthanized via cervical dislocation.

Data analysis: Amplitude and area under the curve (AUC) of integrated respiratory EMG activity was analyzed and averaged under steady-state basal conditions, and for 1 minute of baseline immediately prior to chemostimulation challenges. Amplitude and AUC of integrated respiratory EMG activity was analyzed and averaged for the final 15 breaths (maximal response) of the chemostimulation challenges. Baseline data were reported in absolute units. Responses to chemostimulation were expressed as percent change from the preceding baseline value. This portrayal of the data was considered appropriate given that baseline EMG activity was found to be equivalent in wild-type and *mdx* mice. As such, percent change from baseline is in effect equivalent to Δ EMG activity and importantly, a difference in the percent change between groups corresponds to a true difference in total EMG activity, important in the context of a transduction of neuromuscular-to-mechanical activity. Because we tested the hypothesis that diaphragm EMG activity would be altered in *mdx* mice compared with wild-type mice we did not normalise EMG data to a maximum reference value within each preparation (e.g. augmented breath or swallow), because such a maximum value

could itself be changed in *mdx* mice resulting from neuroplasticity. Our principal focus was the level of EMG activity *per se*. In 1 *mdx* and 2 wild-type mice, the EMG response to gas challenges was characterized by tachypnoea and reduced EMG amplitude. Since our aim was to compare the magnitude of the increase in EMG amplitude (motor recruitment) during chemostimulation, we established *a priori* that trials characterized by frequency-only responses to gas challenge (tachypnoea) would be excluded from group analysis of the effects of chemostimulation on EMG amplitude and area under the curve in wild-type and *mdx* mice.

2.2.10 Statistical analysis

Values are expressed as mean \pm SD or as box and whiskers plot (median, 25-75% centiles and minimum and maximum values). Data were statistically analyzed by Prism 6.0 (Graphpad Software, San Diego, CA, USA). For measures of baseline ventilation and metabolism, basal carotid sinus nerve activity during normoxia and hyperoxia, basal diaphragm EMG activity, diaphragm muscle twitch force and contractile kinetics, diaphragm muscle fibres, and arterial blood gas analysis, all data for wild-type and *mdx* groups were tested for normal distribution and equal variances and were statistically compared using unpaired two-tailed Student's *t* tests, with Welch's correction for unequal variances used as appropriate. Ventilatory and metabolic responsiveness to hypoxia (separate sustained and graded challenges), carotid sinus nerve activity response to hypoxic challenge, diaphragm muscle force-frequency relationship, and diaphragm EMG responses to chemostimulation in wild-type and *mdx* groups were statistically compared by repeated measures two-way ANOVA (gas x gene) with Bonferroni *post hoc* test. Data for absolute carotid sinus nerve activity were non-parametric and therefore were log transformed. $P < 0.05$ was considered statistically significant in all tests.

2.3 Results

2.3.1 Baseline ventilation and metabolism

Representative respiratory flow traces for wild-type and *mdx* mice during baseline (normoxic) ventilation are shown in Fig. 2.1A. Minute ventilation during baseline conditions (combined normoxic bouts) was significantly reduced in *mdx* compared with wild-type mice ($P = 0.0001$; unpaired Student's t test; Fig. 2.1D). This reduction in normoxic V_E in *mdx* mice was the result of a lower V_T ($P = 0.0003$; Fig. 2.1C); f_R did not differ significantly between groups ($P = 0.2612$; Fig. 2.1B). Performing this analysis on absolute volume data (not normalised for body mass) yielded similar effects for both V_E and V_T (data not shown).

Respiratory and metabolic parameters are shown in Table 2.1. Assessment of O_2 consumption (VO_2) and CO_2 production (VCO_2) revealed minimal differences between wild-type and *mdx* mice. VO_2 (normalised to body mass) was significantly reduced for *mdx* ($P = 0.0043$) compared with wild-type, but not when expressed in absolute terms of oxygen consumed ($P = 0.6985$). No difference was noted for VCO_2 between groups when analysis was performed on absolute and normalised values. Carbon dioxide production, chosen *a priori* as the preferred index of metabolism, was effectively unchanged between wild-type and *mdx* mice. The ventilatory equivalent for CO_2 (V_E/VCO_2) was significantly reduced for *mdx* ($P = 0.0243$) compared with wild-type mice, indicative of hypoventilation in *mdx* mice. The ratio of VCO_2 to VO_2 (respiratory exchange ratio) was not different between groups.

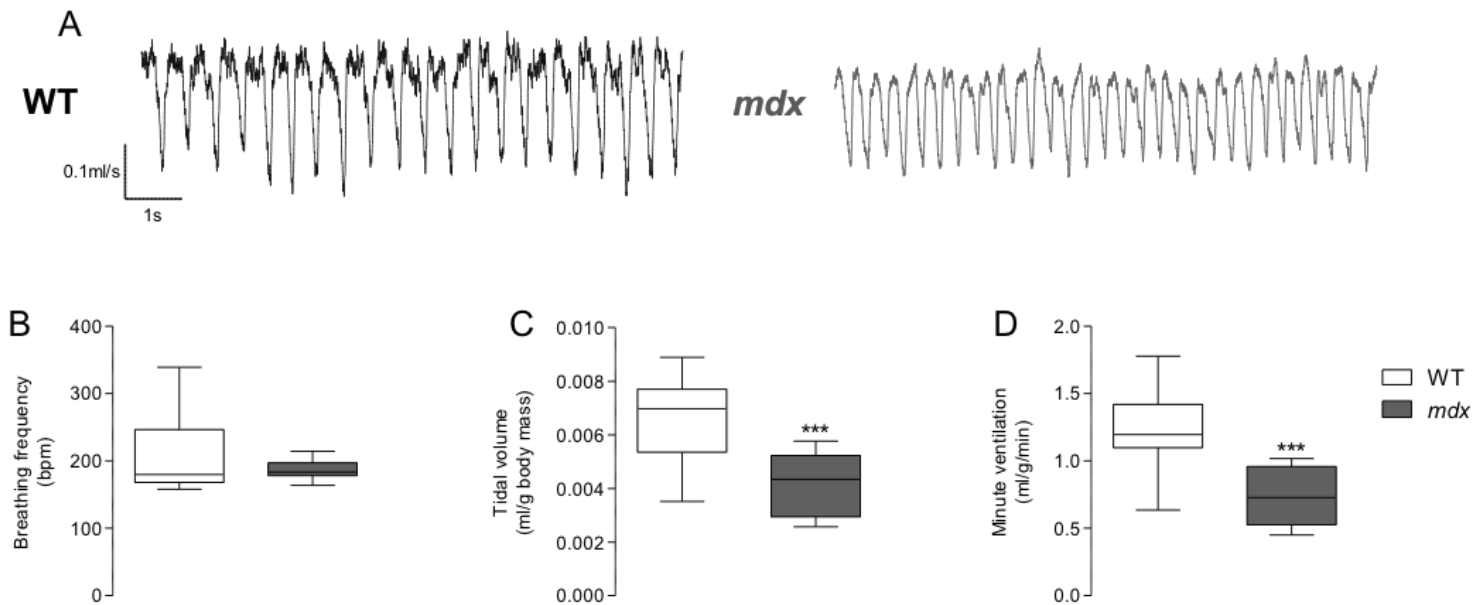


Figure 2.1 Baseline ventilation in conscious mice

A: representative respiratory flow traces during normoxic ventilation in a wild-type (WT) mouse (black) and *mdx* mouse (grey); inspiration downwards. B, C and D: breathing frequency (B), tidal volume (C) and minute ventilation (D) for WT (n = 13) and *mdx* (n = 12) mice during normoxic ventilation. Values (B-D) are expressed as box and whisker plots (median, 25-75% centiles and minimum and maximum values) and data were statistically compared by unpaired Student's *t* tests with Welch's correction used where appropriate. ****P* < 0.001 compared with WT.

	WT (n = 13)	mdx (n = 12)	Student's <i>t</i> tests
VO ₂ (ml/min)	1.6 ± 0.2	1.5 ± 0.3	<i>P</i> = 0.6985
VO ₂ (ml/g/min)	0.072 ± 0.01	0.058 ± 0.01	<i>P</i> = 0.0043
VCO ₂ (ml/min)	0.86 ± 0.18	0.94 ± 0.25	<i>P</i> = 0.3570
VCO ₂ (ml/g/min)	0.040 ± 0.009	0.036 ± 0.009	<i>P</i> = 0.2404
VCO ₂ /VO ₂	0.6 ± 0.1	0.6 ± 0.1	<i>P</i> = 0.2228
V _E /VO ₂	17.5 ± 5.4	13.6 ± 5.5	<i>P</i> = 0.0819
V _E /VCO ₂	32.4 ± 11.5	22.4 ± 8.8	<i>P</i> = 0.0243
Body mass (g)	22.0 ± 1.7	26.3 ± 1.4	<i>P</i> < 0.0001

Table 2.1 Baseline ventilation and metabolic measurements

Definition of abbreviations: VO₂, oxygen consumption; VCO₂, carbon dioxide production; VCO₂/VO₂, respiratory exchange ratio (RER); V_E/VO₂, ventilatory equivalent for O₂; V_E/VCO₂, ventilatory equivalent for CO₂; WT, wild-type. Data are shown as mean ± SD and were statistically compared using unpaired Student's *t* tests.

2.3.2 Blood gas analysis

Intra-cardiac blood gas data for wild-type and *mdx* mice are shown in Table 2.2. Haematocrit was significantly lower in *mdx* ($P = 0.0005$; unpaired Student's *t* test) compared with wild-type, but haemoglobin concentration was equivalent between the two groups. Significant increases in blood values for $[\text{HCO}_3^-]$ ($P = 0.0496$), TCO_2 ($P = 0.00382$), $[\text{K}^+]$ ($P = 0.0078$), and $[\text{Na}^+]$ ($P = 0.0442$) were observed in *mdx* compared with wild-type.

	WT (n = 7)	<i>mdx</i> (n = 7)	Student's <i>t</i> tests
pH	7.37 ± 0.03	7.37 ± 0.01	$P = 0.5815$
PCO ₂ (mmHg)	35.2 ± 4.7	38.3 ± 2.0	$P = 0.1248$
PO ₂ (mmHg)	107.1 ± 13.7	96.7 ± 6.2	$P = 0.0920$
HCO ₃ ⁻ (mmol/L)	20.0 ± 2.4	22.3 ± 1.4	$P = 0.0496$
TCO ₂ (mmol/L)	21.0 ± 2.4	23.4 ± 1.4	$P = 0.0382$
SaO ₂ (%)	97.9 ± 0.9	97.3 ± 0.8	$P = 0.2225$
Na ⁺ (mmol/L)	143.0 ± 1.2	144.1 ± 0.7	$P = 0.0442$
K ⁺ (mmol/L)	4.4 ± 0.2	5.0 ± 0.4	$P = 0.0078$
Haematocrit (%)	39.7 ± 1.4	36.0 ± 1.5	$P = 0.0005$
Hb (g/dl)	13.5 ± 0.5	13.0 ± 2.1	$P = 0.5080$

Table 2.2 Intra-cardiac blood gas analysis

Definition of abbreviations: PCO₂, partial pressure of CO₂; PO₂, partial pressure of O₂; HCO₃⁻, bicarbonate; TCO₂, total CO₂; SaO₂, arterial oxygen saturation; Na⁺, sodium; K⁺, potassium; Hb, haemoglobin; WT, wild-type. Data are shown as mean ± SD and were statistically compared using unpaired Student's *t* tests.

2.3.3 Carotid sinus nerve discharge

Figure 2.2 shows representative traces from wild-type (A) and *mdx* (B) carotid body-carotid sinus nerve preparations *ex vivo*. Group data for carotid sinus nerve activity (normalised to hyperoxia) for wild-type and *mdx* preparations during normoxia (100 mmHg) and in response to a graded hypoxic challenge (80, 60 and 40 mmHg) are shown in Fig. 2.2C. Of note during normoxia, carotid sinus nerve activity was ~30% less in *mdx* compared with wild-type preparations ($P = 0.0064$; unpaired Student's *t* test), revealing a relative hypoactivity of carotid body afferent discharge in normoxia. Both wild-type and *mdx* preparations responded to decreasing levels of O₂ by corresponding increases in carotid sinus nerve activity ($P < 0.0001$; two-way ANOVA); however, no significant difference in hypoxic responsiveness was noted between wild-type and *mdx* (gas x gene $P = 0.6452$). Statistical judgment of the data was equivalent whether normalised to hyperoxia or normoxia.

Data for absolute carotid sinus nerve discharge frequencies in each condition are shown in Table 2.3. Consistent with the normalised data, there was no statistical difference in hypoxic responsiveness between wild-type and *mdx* preparations (Table 2.3). The carotid sinus nerve discharge frequency response to hyperoxia (Dejours test) was significantly blunted in *mdx* compared with wild-type (-18.7 ± 7.2 vs. -7.7 ± 3.1 Δ impulses per min, unpaired Student's *t* test, $P = 0.011$ for wild-type ($n = 6$) vs. *mdx* ($n = 6$) mice), further suggestive of a relative hypoactivity during normoxia in *mdx* carotid body.

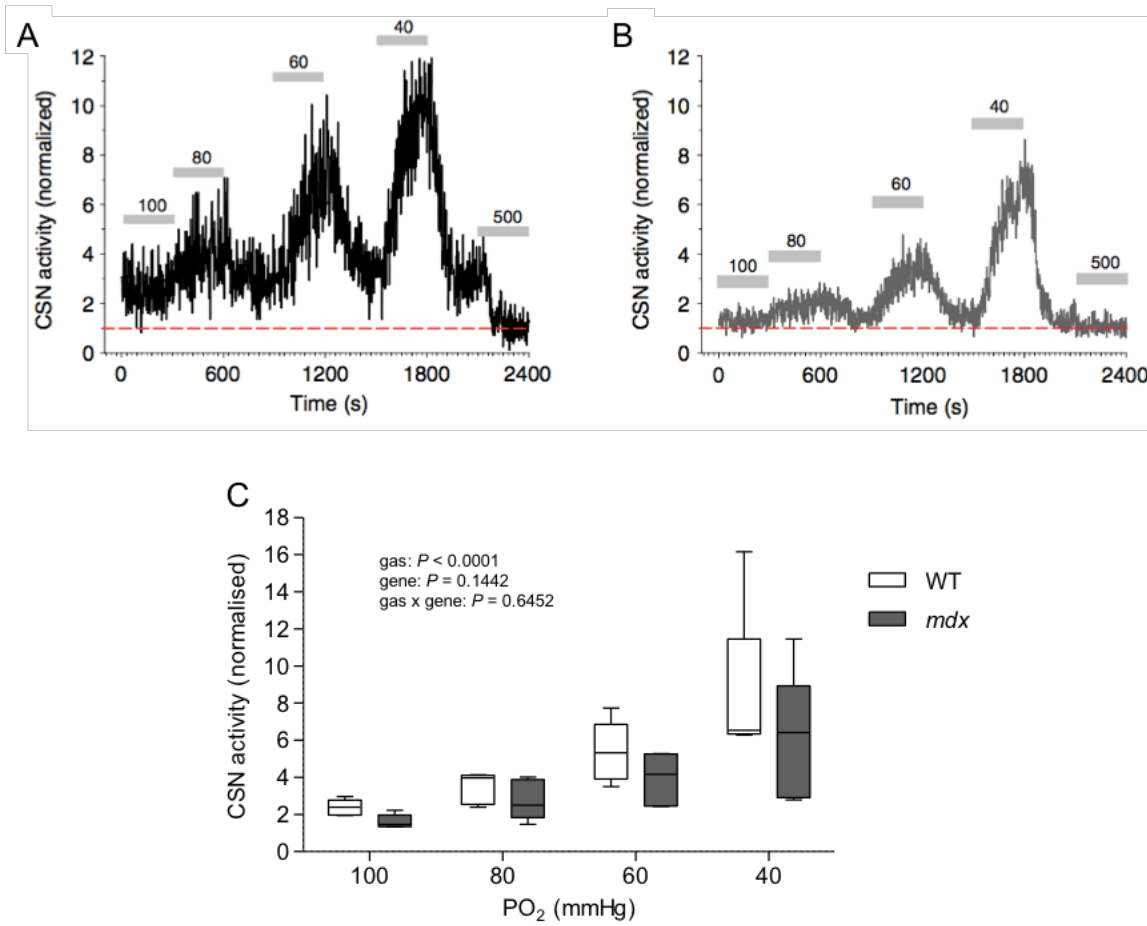


Figure 2.2 *Ex vivo* carotid sinus nerve discharge

A and B: representative recordings of integrated carotid sinus nerve (CSN) activity *ex vivo* in a wild-type mouse (A) and *mdx* mouse (B) during normoxia (100 mmHg) and mild (80 mmHg), moderate (60 mmHg) and severe (40 mmHg) hypoxia. CSN activity was normalised to activity in hyperoxia (500 mmHg), illustrated by the horizontal dashed line. C: group data of CSN activity for wild-type (WT, $n = 6$) and *mdx* ($n = 6$) during normoxia (100 mmHg) and graded hypoxia (80, 60, 40 mmHg). Values are expressed as box and whisker plots (median, 25-75% centiles and minimum and maximum values). Data were statistically compared by repeated measures two-way ANOVA (gas x gene).

		100 mmHg	80 mmHg	60 mmHg	40 mmHg	Two-way RMANOVA
Discharge frequency (impulses/min)	WT	37.4 ± 20.7	53.2 ± 23.9	82.3 ± 39.9	122.2 ± 73.1	Gas $P < 0.001$ Gene $P = 0.327$ Gas x gene $P = 0.953$
	<i>mdx</i>	23.8 ± 11.5	36.2 ± 14.5	54.9 ± 22.4	80.0 ± 39.6	
Δ discharge frequency (impulses/min)	WT	-	15.8 ± 7.8	44.9 ± 26.2	84.8 ± 59.6	Gas $P < 0.001$ Gene $P = 0.357$ Gas x gene $P = 0.228$
	<i>mdx</i>	-	12.5 ± 8.1	31.3 ± 16.2	56.3 ± 36.2	

Table 2.3 Carotid sinus nerve afferent discharge in normoxia and hypoxia

Definition of abbreviations: WT, wild-type. Data are shown as mean ± SD and were statistically compared by repeated measures two-way ANOVA (gas x gene). Responses to hypoxia are expressed as Δ impulses per min from baseline (normoxia) values.

2.3.4 Ventilatory responsiveness to hypoxia and hypercapnia

Figure 2.3 shows ventilatory and metabolic data during normoxia and in response to graded hypoxia. Minute ventilation was lower in *mdx* ($P = 0.0054$; two-way ANOVA) compared with wild-type, attributed to a lower tidal volume in *mdx* mice. V_{CO_2} decreased in response to hypoxia in wild-type and *mdx* mice ($P < 0.0001$). V_E/V_{CO_2} increased for both wild-type and *mdx* mice with decreasing levels of inspired O_2 ($P < 0.0001$). No significant difference in V_E/V_{CO_2} was observed between wild-type and *mdx* mice in response to graded hypoxia. Fig. 2.4 shows the time course of minute ventilation to a 20-minute sustained hypoxic challenge ($F_{iO_2} = 0.1$; balance N_2). Ventilation increased rapidly in wild-type and *mdx* mice at the onset of hypoxia ($P < 0.0001$) and then declined towards baseline values (Fig. 2.4). A significantly lower V_E in *mdx* compared with wild-type mice was observed during gas challenge ($P = 0.03$), owing to reduced V_T in *mdx* mice (Fig. 2.4). The peak hypoxic ventilatory response was not different between strains (delta V_E was $+1.44 \pm 0.80$ vs. $+0.90 \pm 0.70$ ml/min/g, unpaired Student's *t* test, $P = 0.07$ for wild-type ($n = 13$) vs. *mdx* ($n = 12$); % change from baseline was $+131.8 \pm 52.1\%$ vs. $+111.7 \pm 69.6\%$, $P = 0.4185$). Figure 2.5 shows data for V_E during baseline and hypercapnic gas challenge. Minute ventilation was increased significantly both in wild-type and *mdx* mice during CO_2 exposure. Minute ventilation remained significantly lower in *mdx* compared with wild-type mice during hypercapnic breathing, but the ventilatory response to hypercapnia was not different between wild-type and *mdx* mice (delta V_E was $+1.9 \pm 0.8$ vs. $+1.7 \pm 0.6$ ml/min/g, unpaired Student's *t* test, $P = 0.5768$ for wild-type ($n = 10$) vs. *mdx* mice ($n = 11$); % change from baseline was $+131 \pm 47\%$ vs. $+178 \pm 80\%$, $P = 0.1194$).

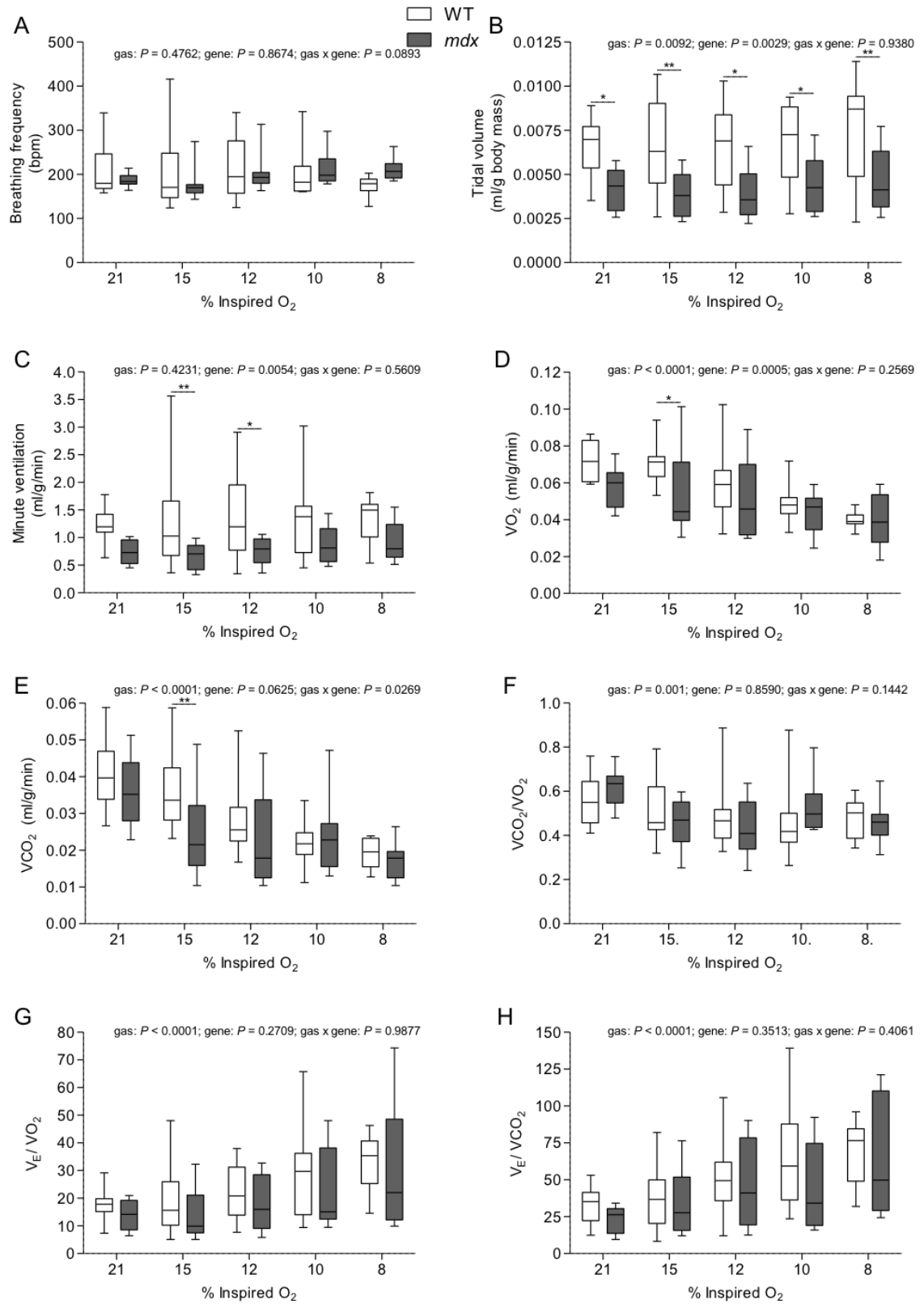


Figure 2.3 Ventilatory and metabolic responsiveness to graded hypoxia

Figure 2.3 A-H: group data for breathing frequency (A), tidal volume (B), minute ventilation (C), oxygen consumption (D; $\dot{V}O_2$), carbon dioxide production (E; $\dot{V}CO_2$), respiratory exchange ratio (F; $\dot{V}CO_2/\dot{V}O_2$), ventilatory equivalent for oxygen (G; $\dot{V}_E/\dot{V}O_2$) and ventilatory equivalent for carbon dioxide (H; $\dot{V}_E/\dot{V}CO_2$) for wild-type (WT, n = 13) and *mdx* (n = 12) mice during normoxia (21% inspired O_2 ; balance N_2) and graded hypoxia (15, 12, 10 and 8% inspired O_2 ; balance N_2). Values expressed as box and whisker plots (median, 25-75% centiles and minimum and maximum values). Data were statistically compared by repeated measures two-way ANOVA (gas x gene) with Bonferroni *post hoc* test. * $P < 0.05$, ** $P < 0.01$ compared with corresponding WT value.

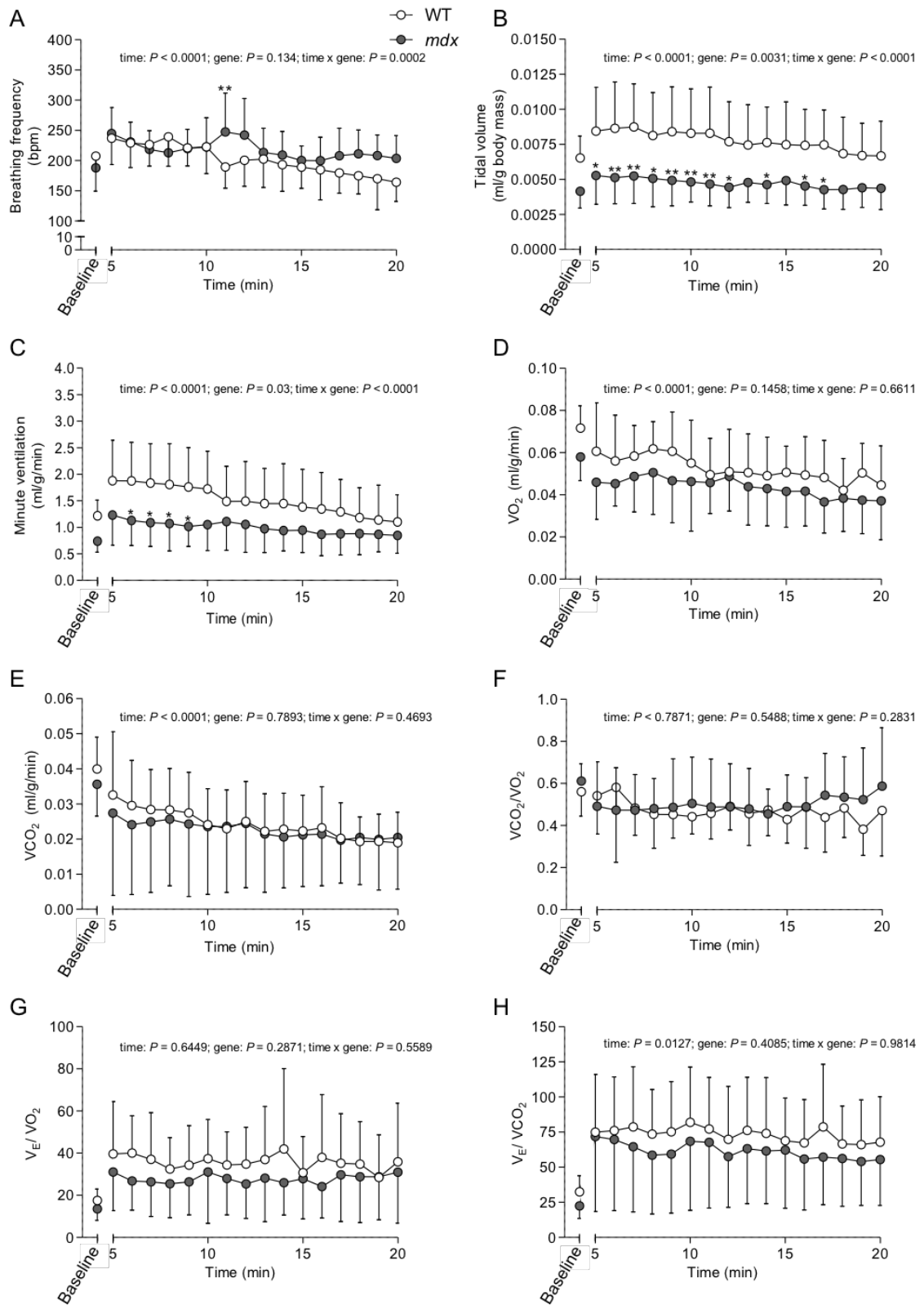


Figure 2.4 Ventilatory and metabolic responsiveness to sustained hypoxia

Figure 2.4 A-H: group data (mean \pm SD) for breathing frequency (A), tidal volume (B), minute ventilation (C), oxygen consumption (D; $\dot{V}O_2$), carbon dioxide production (E; $\dot{V}CO_2$), respiratory exchange ratio (F; $\dot{V}CO_2/\dot{V}O_2$), ventilatory equivalent for oxygen (G; $\dot{V}_E/\dot{V}O_2$) and ventilatory equivalent for carbon dioxide (H; $\dot{V}_E/\dot{V}CO_2$) for wild-type (WT, n = 13) and *mdx* (n = 12) mice during baseline and after 5-20 min of exposure to hypoxia (10% O₂ inspired oxygen; balance N₂). Data were statistically compared by repeated measures two-way ANOVA (gas x gene) with Bonferroni *post-hoc* test. **P* < 0.05, ***P* < 0.01 compared with corresponding WT value.

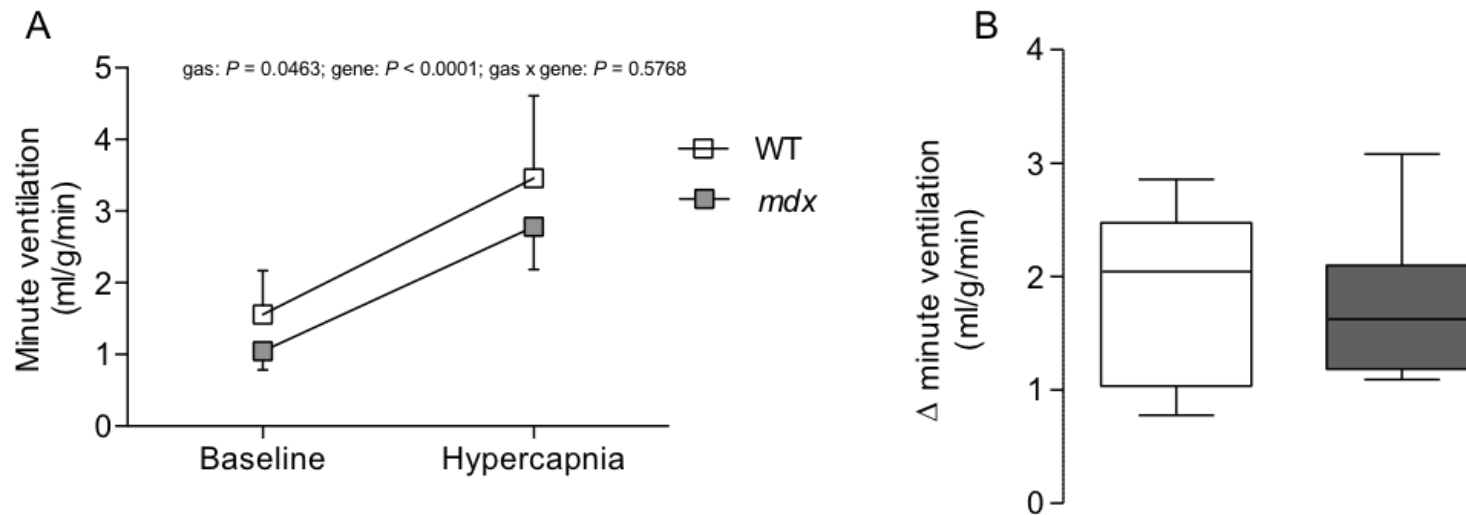


Figure 2.5 Ventilatory responsiveness to hypercapnia

A: group data (mean \pm SD) for minute ventilation in wild-type (WT, $n = 10$) and *mdx* ($n = 11$) mice during baseline (air) and hypercapnia (5% CO₂, balance N₂). Data were statistically compared using repeated measures two-way ANOVA. B: group data (mean \pm SD) for ventilatory responsiveness to hypercapnia (ΔV_E) in WT ($n = 10$) and *mdx* ($n = 11$) mice. Values are expressed as box and whisker plots (median, 25-75% centiles and minimum and maximum values). Data were statistically compared by unpaired Student's *t* tests.

2.3.5 Diaphragm muscle function

Representative original traces for wild-type and *mdx* diaphragm twitch contraction (A) and force-frequency relationship (B) are shown in Fig. 2.6. Isometric twitch force and contractile kinetics for wild-type and *mdx* mice are shown in Table 2.4. Twitch contraction time was significantly prolonged in *mdx* compared with wild-type diaphragms ($P = 0.0155$; unpaired Student's *t* test). Twitch force was significantly reduced in *mdx* diaphragm muscle preparations ($P = 0.0292$). For force-frequency relationship, diaphragm specific force was significantly depressed in *mdx* compared with wild-type preparations ($P = 0.0002$, repeated measures two-way ANOVA). *Post-hoc* analysis revealed significant differences between wild-type and *mdx* diaphragm force generation across a broad stimulus range (40-160 Hz). Absolute measurements of diaphragm force (N), prior to normalisation to CSA, were significantly depressed in *mdx* compared with wild-type.

	WT (n = 7)	<i>mdx</i> (n = 7)	Student's <i>t</i> tests
CT (ms)	15.4 ± 1.3	18.9 ± 3.0	$P = 0.0155$
½ RT (ms)	19.9 ± 3.0	19.1 ± 2.9	$P = 0.5975$
P _t (N/cm ²)	2.7 ± 0.7	1.8 ± 0.8	$P = 0.0292$

Table 2.4 Diaphragm muscle twitch force and contractile kinetics

Definition of abbreviations: CT, contraction time; ½ RT, half-relaxation time; P_t, twitch force; WT, wild-type. Data are shown as mean ± SD and were statistically compared using unpaired Student's *t* tests.

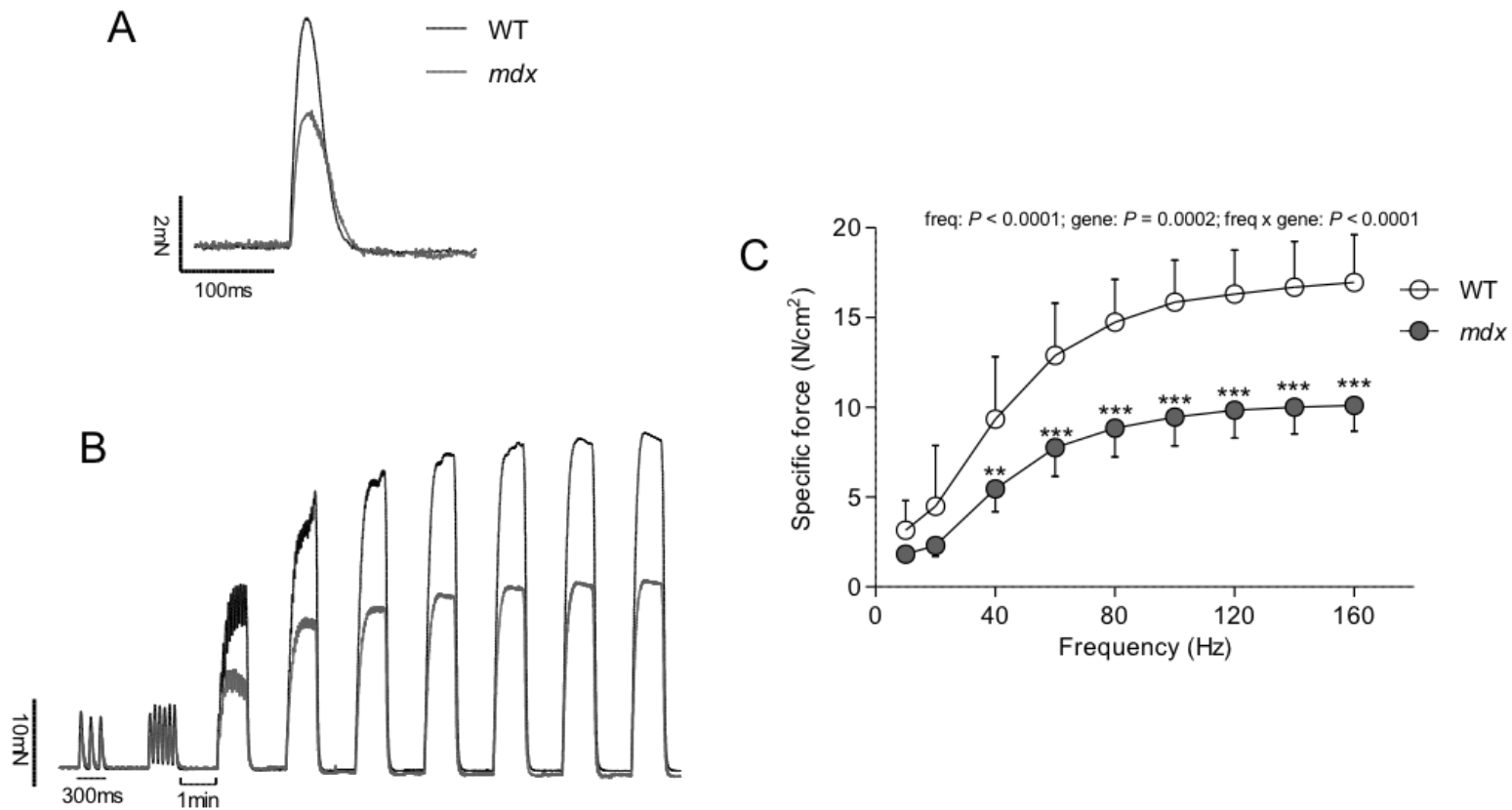


Figure 2.6 Ex vivo diaphragm muscle contractile function

A and B: original traces of *ex vivo* diaphragm muscle twitch contraction (A) and force-frequency relationship (B) for wild-type (WT) (black) and *mdx* (grey) preparations. C, group data (mean \pm SD; $n = 7$ for both groups) for diaphragm muscle force-frequency relationship *ex vivo* in WT (open) and *mdx* (grey) muscle preparations. Data were statistically compared by repeated measures two-way ANOVA (frequency \times gene) followed by Bonferroni *post-hoc* test. ** $P < 0.01$, *** $P < 0.001$ compared with corresponding WT values.

2.3.6 Diaphragm muscle fibre size and distribution

Representative immunofluorescence images from wild-type and *mdx* diaphragm muscle are shown in figure 2.7. Dystrophin deficiency in *mdx* diaphragm resulted in a significant increase in the coefficient of variation of muscle fibre size ($P < 0.0001$; unpaired Student's *t* test), as measured by minimal Feret's diameter (Fig. 2.7C). There was a significantly increased proportion of centralized myonuclei, indicative of muscle damage in *mdx* compared with wild-type ($P = 0.0005$; Fig. 2.7D). A leftward shift in the frequency distribution of muscle fibre size was evident in *mdx* diaphragm, based on minimal Feret's diameter (Fig. 2.7E) or CSA (Fig. 2.7F).

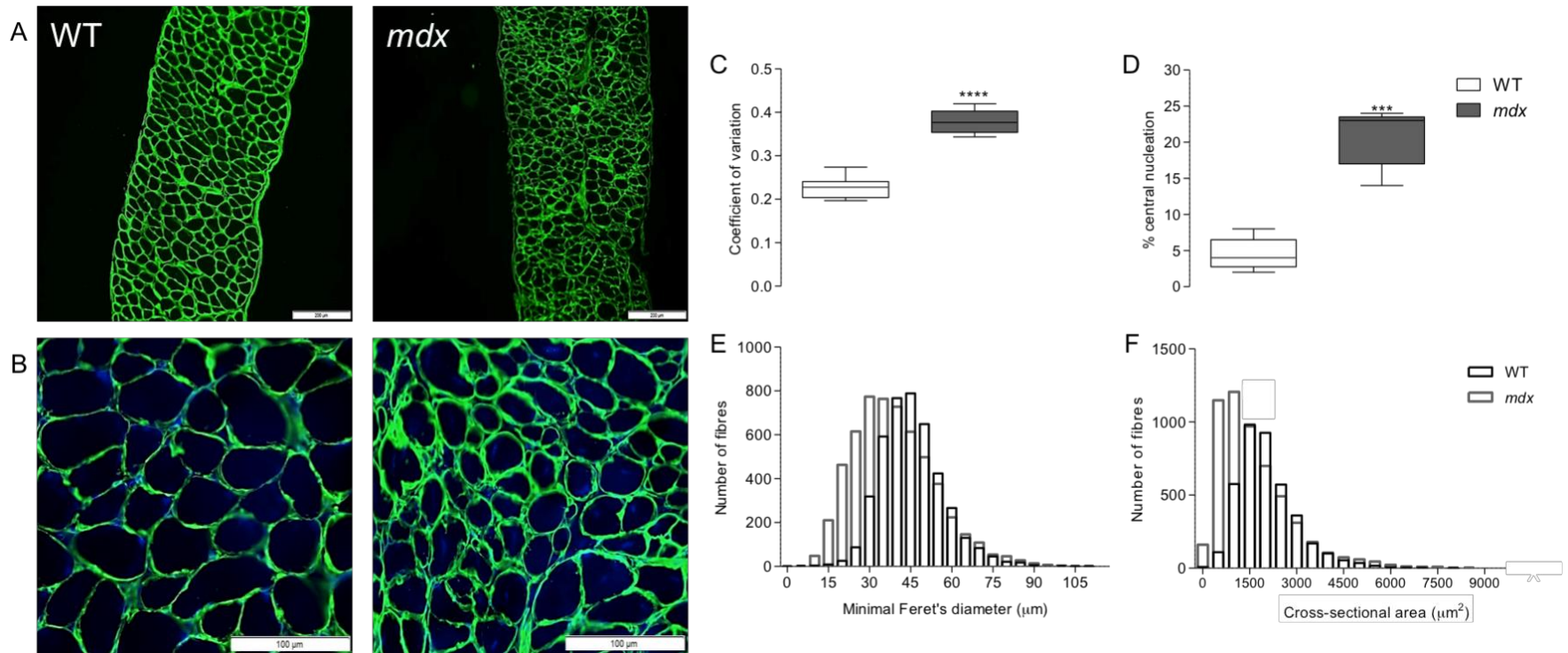


Figure 2.7 Diaphragm muscle structure

A: representative images of diaphragm muscle immunofluorescently labelled for laminin from wild-type (WT) (top left) and *mdx* (top right) mice. B: representative images of diaphragm muscle immunofluorescently labelled for laminin (green) and myonuclei (blue) from WT (bottom left) and *mdx* (bottom right) mice. C: group data for coefficient of variation of diaphragm muscle fibre size as measured by minimal Feret's diameter for WT (n = 8) and *mdx* (n = 8) mice. D: group data for percentage of fibres with centralized myonuclei in diaphragm muscle of WT (n = 6) and *mdx* (n = 5) mice. Values are expressed as box and whisker plots (median, 25-75% centiles and minimum and maximum values). Data were statistically compared by unpaired Student's *t* tests. E and F: frequency distribution of WT and *mdx* diaphragm muscle fibre size as measured by minimal Feret's diameter (E) and cross-sectional area (F). *** $P = 0.0005$, **** $P < 0.0001$ compared with corresponding WT value.

2.3.7 Diaphragm EMG responsiveness

Representative original diaphragm EMG traces during baseline and in response to chemostimulation are shown in figure 2.8A. Diaphragm EMG activity was examined in wild-type and *mdx* mice during baseline (60% O₂) and in response to chemostimulation challenges. Basal diaphragm EMG amplitude and AUC was not different between wild-type and *mdx* mice (Fig. 2.8B, inset). Gas challenges typically increased EMG responsiveness for both wild-type and *mdx* for amplitude ($P = 0.0202$; repeated measures two-way ANOVA; Fig. 2.8B) and AUC ($P = 0.0531$; Fig. 2.8C). For AUC, a significant genotype difference was noted ($P = 0.0452$) and *post-hoc* analysis revealed EMG responsiveness to maximal chemostimulation (asphyxia) was significantly enhanced in *mdx* compared with wild-type mice ($P < 0.05$; two-way ANOVA with Bonferroni *post hoc* test).

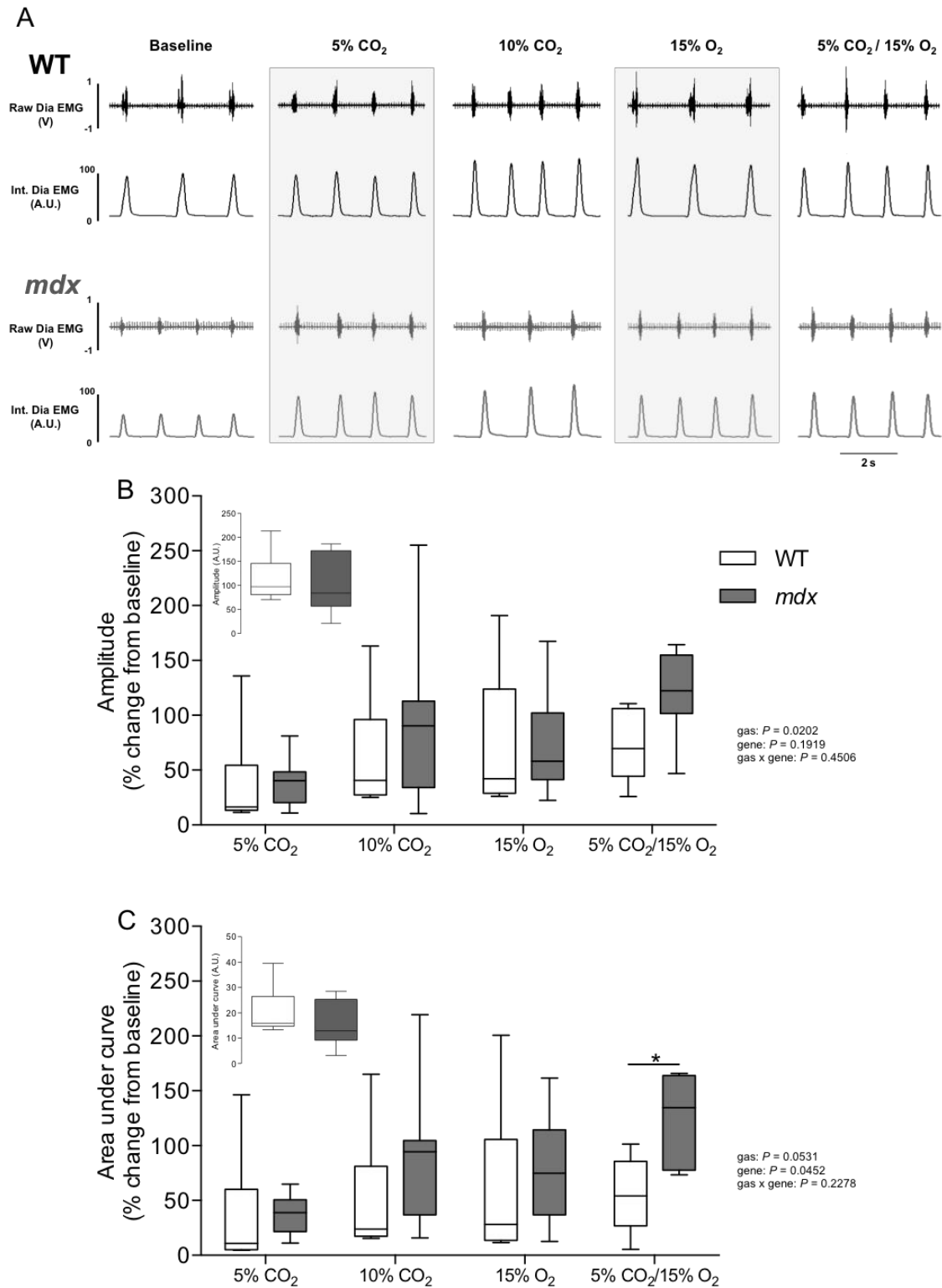


Figure 2.8 Diaphragm EMG

A: representative traces of diaphragm (Dia) muscle raw and integrated (Int.) EMG activity for a wild-type (WT) mouse (black) and *mdx* mouse (grey) during baseline (60% inspired O₂), hypercapnia (5% and 10% CO₂), hypoxia (15% O₂) and asphyxia (15%

O₂/5% CO₂). B and C: diaphragm muscle integrated EMG activity expressed as amplitude (B) and area under the curve (C) for WT (n = 8) and *mdx* (n = 7) mice during baseline (inset), hypercapnia (5% CO₂ and 10% CO₂), hypoxia (15% O₂) and asphyxia (15% O₂/5% CO₂). Baseline data are reported as absolute units. Note that there was no significant difference in baseline data comparing WT and *mdx* mice. Gas challenges are expressed as % change from baseline. All values are presented as box and whisker plots (median, 25-75% centiles and minimum and maximum values). Baseline data were statistically compared by unpaired Student's *t* tests. Gas challenges were statistically compared by repeated measures two-way ANOVA with Bonferroni *post-hoc* test. **P* < 0.05 compared with WT.

2.4 Discussion

The main findings of our study are: 1) young (eight week old) *mdx* mice hypoventilate during basal breathing, owing to reduced tidal volume; 2) intra-cardiac blood total CO₂ and [HCO₃⁻] are elevated in young *mdx* mice suggesting compensated respiratory acidosis; 3) the carotid body response to hyperoxia is depressed in young *mdx* mice; 4) chemosensory, ventilatory, and metabolic responses to hypoxia are unaffected in young *mdx* mice; 5) there is profound diaphragm muscle weakness, fibre remodelling and damage in young *mdx* mice; 6) diaphragm EMG responsiveness to chemostimulation is enhanced in young *mdx* mice suggesting compensatory neuroplasticity.

Overall, our study revealed that basal CO₂ production was unaffected in *mdx* mice, but *mdx* mice had a substantial reduction in tidal volume that was not compensated for by increased breathing frequency resulting in reduced minute ventilation. Thus, *mdx* mice hypoventilate by 8 weeks of age i.e. inadequate ventilation to meet metabolic demand, which is suggested by the data for reduced ventilatory equivalent for carbon dioxide (V_E/V_{CO_2}) in *mdx* mice. Cardiac puncture for blood gas analysis under isoflurane anaesthesia (breathing air) revealed a trend towards decreased PO₂ and increased PCO₂ in *mdx*, but the changes were modest in comparison to the ventilatory data derived by plethysmography. There are at least three factors to consider. First, the blood was sampled from anaesthetised animals, and anaesthesia has pronounced inhibitory effects on ventilation, though this might be expected to potentiate respiratory depression in *mdx* mice. Second, there may be cardio-pulmonary adjustments that compensate for mechanical deficits in young *mdx* mice. Third, the sample size may have been too small to reveal statistical significance in some key parameters (PO₂ and PCO₂) that did change in a manner consistent with hypoventilation. Nonetheless, total CO₂ and [HCO₃⁻] were significantly elevated in *mdx* mice suggesting the development of a compensated respiratory acidosis secondary to chronic hypoventilation. Persistent hypoventilation and resultant hypoxaemia, which have been described in *mdx* mice at 6 months of age (Mosqueira et al., 2013a), would be expected to cause increased haematocrit and haemoglobin concentration. Of interest, we noted significantly

enlarged, darkened spleens in *mdx* mice, which may have implications for the control of circulating red blood cells. It would be interesting to determine if *mdx* mice are chronically hypoxic in early life, as hypoxic stress has the capacity to drive plasticity at multiple sites within the respiratory control network.

Sensory inputs from the peripheral chemoreceptors are generally regarded as providing a tonic drive to “eupnoeic” breathing. Moreover, while they primarily detect hypoxia, their sensitivity is strongly modulated by PaCO₂ and they have powerful non-linear interactions with central (brainstem) chemoreceptors that also detect CO₂ concentration (Wilson & Teppema, 2016). Therefore, the relative hypoactivity of *mdx* compared with wild-type carotid bodies might have contributed to the resting hypoventilation of *mdx* mice. Carotid body responses to hypoxia (mild, moderate and severe), whether assessed as absolute or normalised data, were equivalent in *mdx* and wild-type mice with no statistical genotype or genotype x gas effect. Of note, carotid sinus nerve afferent discharge was less at all PO₂ levels in *mdx* preparations, such that chemoafferent drive to the respiratory centres was lower in *mdx* compared with wild-type representing a potentially physiologically relevant sensory deficit in the control of breathing. Interestingly, ventilatory responsiveness to sustained and graded hypoxia was equivalent in *mdx* and wild-type mice with no genotype effect. Of note, however, ventilation was reduced in *mdx* due to significant reductions in tidal volume at all levels of hypoxic ventilation, which may relate to sensory deficit as well as mechanical disadvantage in *mdx* over a range of ventilations compared with wild-type. Metabolism and metabolic responses to hypoxia were generally equivalent between wild-type and *mdx* mice.

While our report is the first to characterize respiratory and metabolic parameters in young *mdx* mice and describe that a significant respiratory phenotype presents as early as 8 weeks of age, our data are generally consistent with reports of hypoventilation in older (6-12 months of age) *mdx* mice (Huang *et al.*, 2011; Mosqueira *et al.*, 2013a). When viewed together, the implication of these findings is that respiratory insufficiency presents early in the *mdx* model, and thus likely

impacts on the progression and manifestation of respiratory morbidity typically reported in older animals.

Our study confirmed profound diaphragm weakness in *mdx* mice. Coirault et al. (1999) have previously reported reduced strength in *mdx* diaphragm which was associated with a reduction in the number of cross bridges generating contractile force and in the elementary force generated per actomyosin interaction. These functional changes were associated with changes in myosin isoform composition (shift from myosin heavy chain type IIa to IIa). Interestingly, diaphragm mechanical dysfunction is present at a young age (6 weeks) when muscle fibre necrosis and/or fibrosis remain limited (Coirault *et al.*, 2003). Diaphragm force-generating capacity in the present study was depressed across a broad range of stimulation frequencies including the range relevant to basal breathing. Respiratory nerve activity in mice displays medium frequency oscillations (MFOs) in the range of 20-50Hz (O'Neal *et al.*, 2005; ElMallah *et al.*, 2016), which are believed to reflect the underlying motor neuron discharge rates (Christakos *et al.*, 1991). The severe weakness in *mdx* diaphragm at this early age appears primarily responsible for the mechanical disadvantage manifest in reduced tidal volumes in freely-behaving mice. Force increases as a function of stimulation frequency in *mdx* mice, which provides capacity to increase breathing in response to increased neural drive. However, the intrinsic weakness in *mdx* diaphragm is impressive even at this early stage, presumably placing a limit on ventilatory capacity. Moreover, force-generating capacity remains severely compromised at higher stimulation frequencies.

There are few studies examining the hypoxic ventilatory response in *mdx* (Mosqueira *et al.*, 2013a; Burns *et al.*, 2015). The hypometabolic response to hypoxia in mice is such that ventilatory responses to hypoxia are modest. Indeed, tidal volume and ventilation do not increase much above baseline in response to graded hypoxia, and the ventilatory response to sustained hypoxia is primarily driven by increased respiratory frequency. Therefore, it is difficult to discern from ventilatory responses to hypoxia if *mdx* mice are capable of transducing increased diaphragm force-generating capacity resulting from motor recruitment to increase

ventilation. To examine this further, we assessed hypercapnic ventilatory responses in wild-type and *mdx* mice. Ventilation increased in response to hypercapnic challenge, due to increases in respiratory frequency and tidal volume, and the response was equivalent in the two groups. The data reveal that *mdx* mice are capable of increasing tidal volume during chemostimulation. Although, ventilation remains significantly lower in *mdx* compared with wild-type mice during hypercapnic breathing, the ventilatory response to hypercapnia is not different between the two groups of mice. This reveals an interesting feature of respiratory control in the young *mdx* mouse, namely that a considerable reserve in ventilatory capacity prevails, which presumably extends to accessory muscles of breathing given the profound weakness noted in the diaphragm muscle. Analysis of fibre size and distribution in diaphragm muscle revealed considerable fibre remodelling and evidence of centronucleation, which is a hallmark of fibre necrosis. Diaphragm muscle structure of *mdx* mice has been well described with muscle fibres undergoing inflammatory cell infiltration, fibrosis and necrosis (Gayraud *et al.*, 2007; Ishizaki *et al.*, 2008; Huang *et al.*, 2011). In addition to structural abnormalities in *mdx* resulting in loss of function, there is growing evidence implicating oxidative stress in dystrophic diaphragm pathology (Kim & Lawler, 2012; Kim *et al.*, 2013).

In anaesthetised mice, we examined respiratory neural drive to the diaphragm under baseline conditions and in response to chemostimulation with hypoxia, hypercapnia, and asphyxia. Baseline diaphragm EMG activity was equivalent in wild-type and *mdx* mice (although respiratory frequency was higher in *mdx* mice), but since anaesthetised animals breathed 60% oxygen under baseline conditions, it is likely that carotid body chemoafferent input was depressed in our studies such that putative differences in peripheral control of breathing between *mdx* and wild-type (i.e. sensory deficit suggested by carotid body preparations) would not have contributed to the EMG findings. We further acknowledge the recognized limitations in respect of comparisons of EMG activity between animals. Whether dystrophin deficiency affects central respiratory motor outflow in normoxia was not established in our studies; however, given the significance of this observation, it is

worthy of future investigation. Chemoactivation of diaphragm EMG activity was enhanced in *mdx*, with EMG activity considerably potentiated under maximal chemostimulation with asphyxia. The potentiated response, which revealed a true increase in absolute EMG activity, reveals compensatory plasticity in *mdx* either in the central brainstem respiratory network and/or at the level of the phrenic motor nucleus. Potentiated motor outflow in response to chemostimulation may serve to facilitate increased ventilation by providing greater neural drive via phrenic motor neurons to diaphragm, facilitating the transduction of neuromuscular-to-mechanical events during chemostimulation challenge. Perhaps in this manner the potentiated output facilitates equivalent increases in ventilation (ΔV_E) during chemostimulation despite the mechanical disadvantage presenting in *mdx* mice.

However, it is important to recognize that the force-generating capacity of the *mdx* diaphragm is severely compromised. It is evident from analysis of force-frequency relationship in *mdx* diaphragm that increased frequency of stimulation results in little gain in force. As such, there may be little mechanical advantage to increased activation of the diaphragm, which suggests that activation of accessory muscles of breathing may be especially important in *mdx* (and DMD) to support increased tidal volume during respiratory stimulation. We acknowledge that aberrant motor unit potentials in dystrophic *mdx* muscle (Han *et al.*, 2006) could have contaminated diaphragm EMG recordings such that comparisons between wild-type and *mdx* may not be entirely appropriate in respect of the issue of neuroplasticity, an issue further complicated by potential changes at the neuromuscular junction (Pratt *et al.*, 2015). Recordings of phrenic motor discharge are required to definitively determine if central respiratory drive is elevated in *mdx* and this is an area worthy of future study. Assessment of motor drive in accessory pathways contributing to ventilation is also worthy of pursuit. It would also be very interesting to characterize motor unit potentials in respiratory EMGs of young *mdx* mice.

Limitations

Whole-body plethysmography provides an estimate of tidal volume, which is dependent on a number of assumptions (Mortola & Frappell, 1998; Stephenson &

Gucciardi, 2002). The calculation depends on knowledge of chamber temperature and humidity, and animal airway temperatures. Whereas the former were measured in our studies (~22°C), animal body temperature, a surrogate for alveolar temperature, was estimated (37.5°C) for both groups in our study for the purpose of the calculation of tidal volume. This additional limitation raises concern over the accuracy of our estimation of tidal volume, important to address since we report that tidal volume was significantly different between wild-type and *mdx* mice. Direct airflow measurement with a pneumotachometer or assessment of breathing using head-out plethysmography would provide accurate measures of tidal volumes, worthy of pursuit into the future, but it is recognized that these techniques are not without limitations associated with anaesthesia and restraint, respectively. Of note for the present study, errors in body temperature could conceivably have accounted for a substantive proportion of the difference reported between wild-type and *mdx* mice (Mortola & Frappell, 1998). We determined that basal CO₂ production was equivalent in both groups, but we assumed for the purpose of tidal volume calculation that body temperature was also equivalent, which we acknowledge is an assumption of major significance in the calculation of tidal volume. Body temperature likely decreased during the hypoxic challenges. Indeed, we report a significant decrease in CO₂ production during both sustained and graded hypoxia. Whereas, the hypometabolic response (decreased CO₂ production) was equivalent in wild-type and *mdx* mice, we assumed (because we did not measure) that the presumed hypothermic response was also equivalent between wild-type and *mdx* mice. Our assumption does not account for potential differences in body temperature between wild-type and *mdx* mice at rest and/or in response to gas challenge. Of interest, a significant difference in resting body temperature between wild-type and *mdx* mice was reported in a previous study (Helliwell *et al.*, 1996). However, such a difference if it existed in our study would on average have resulted in an under-estimation of the magnitude of the reduction in tidal volume in *mdx* mice compared with wild-type during normoxia. It is also probable that our use of a single estimated body temperature for all animals in the study introduced errors and thus variability within and not just between groups, which might have obscured the genotype effect. It remains possible that a

component ---perhaps substantial--- of the difference in tidal volume reported in the present study relates to temperature differences between wild-type and *mdx* mice and hence errors related to the assumptions made herein. This issue should be addressed in future studies, notwithstanding the inherent limitations of the technique of whole-body plethysmography for the estimation of tidal volume even with incorporation of body temperature.

We acknowledge the apparent discrepancy in the strength of the conclusions drawn from plethysmography and intra-cardiac blood gas analysis, particularly in the light of the limitations described above. We have favoured the conclusion that *mdx* animals hypoventilate based on the significant decrease in V_E/V_{CO_2} measurements derived by plethysmography. Yet, the blood gas data, which are ordinarily taken as the gold standard, suggest modest differences in PO_2 and PCO_2 but with additional supporting evidence suggesting a compensated respiratory acidosis. We suggest that blood gas data should be viewed cautiously in our study, acknowledging that sample size was a limiting factor, but again we emphasize that the magnitude of the hypoventilation reported in our study by use of whole-body plethysmography may have been over-estimated. Arterial blood gas sampling in conscious mice during ventilatory and metabolic assessment by plethysmography represents the gold standard for comparisons and would be required to convincingly demonstrate hypoventilation in young *mdx* mice.

Our EMG study suggests compensatory neuroplasticity in respiratory motor output in *mdx* mice in response to chemostimulation. We acknowledge that recordings of respiratory motor nerves in reduced preparations, complemented by respiratory EMGs in intact spontaneously breathing preparations, extending to contemporaneous recordings of respiratory EMGs and breathing across the sleep-wake cycle would lend further credence to this novel observation.

Relevance to DMD

Our study in the *mdx* mouse raises interesting issues of potential relevance to human DMD. Dystrophin deficiency results in respiratory insufficiency early in life,

which could establish blood gas disturbances with relevance to neuromuscular performance. Hypoxia-induced respiratory muscle dysfunction may be an important and under-recognised feature of DMD. Dystrophin deficiency may adversely affect basal sensory control of breathing, but the preserved capacity for carotid body chemoaerents to respond to hypoxia and therefore presumably other stimulants, suggests that pharmacotherapies that enhance carotid body activity may have some application in the treatment of DMD. It is apparent that dystrophin deficiency results in profound diaphragm dysfunction, which appears early in the mouse model. The severe mechanical disadvantage presents across a range of stimulations, but a preserved capacity to raise ventilation suggests support from accessory muscles of breathing, which may have relevance to DMD. Our study revealed a potentiated neural drive to breathe in *mdx* during maximal chemoactivation, suggesting compensatory neuroplasticity enhancing respiratory motor output to the diaphragm and perhaps other respiratory muscles, which should serve to facilitate ventilation in response to challenge. If neuroplasticity is a feature of DMD, it may be possible to boost motor facilitation of breathing through safe interventions, and in this way preserve or limit deficiencies in respiratory capacity.

2.5 Translational Perspective

Duchenne muscular dystrophy (DMD) is an X-linked fatal neuromuscular disease, which commonly culminates in respiratory failure. Whereas respiratory muscle dysfunction is recognized in DMD, a comprehensive assessment of respiratory control is lacking. The dystrophin-deficient *mdx* mouse has proved to be a useful pre-clinical model of DMD, principally because diaphragm muscle dysfunction recapitulates features of the human disease. We set out to interrogate sensory and motor control of breathing in young *mdx* mice. We hypothesized that there would be evidence of plasticity in the neural control of breathing. Our study reveals that *mdx* mice hypoventilate as early as 8 weeks of age (equivalent to young adult). We revealed evidence of sensory deficit in *mdx* mice which may partly contribute to resting hypoventilation, but sensory responses to oxygen deprivation (hypoxia) are normal. Ventilatory responses to respiratory-relevant chemical activation of breathing are normal in *mdx* mice, revealing ventilatory reserve, although ventilation is lower in *mdx* mice compared with wild-type mice at all levels of ventilation. Assessment of diaphragm electromyogram activity revealed enhanced motor drive to the respiratory pump muscle during maximum chemoactivation, revealing a compensatory phenomenon in neuromechanical control of ventilation in *mdx* mice. Profound diaphragm weakness in young *mdx* mice suggests that enhanced recruitment of accessory muscles of breathing may be especially important in facilitating enhanced lung ventilation during chemoactivation. Our novel findings have implications for human DMD. Safe interventional therapies that serve to boost breathing may preserve or limit deficiencies in respiratory capacity in DMD patients reducing morbidity and mortality.

2.6 Additional information

Competing interests

The authors have no financial, professional or personal conflicts relating to this publication.

Author contributions

DPB: experimental design; acquisition of data; data and statistical analysis and interpretation of data; drafting of the original manuscript; AR: carotid body studies: experimental design; acquisition of data; analysis; drafting of the original manuscript; DE: muscle histology: experimental design; data acquisition; interpretation of data; SG: muscle histology: data acquisition; data analysis; EFL: experimental design; acquisition of data; FBMcD: carotid body studies: experimental design; analysis; RJW: carotid body studies: experimental design; critical revision of the manuscript for important intellectual content; KDOH: experimental design; statistical analysis and interpretation of data; drafting and critical revision of the manuscript for important intellectual content.

Acknowledgements

We are grateful to staff of the Biological Services Unit, University College Cork for their support in the breeding and maintenance of the murine colonies. DPB was supported by funding from the Department of Physiology, UCC. Salary support for RJW provided by Alberta Innovates Health Solutions and work in Calgary was funded by the Canadian Institutes for Health Research.

2.7 References

- Bavis RW, van Heerden ES, Brackett DG, Harmeling LH, Johnson SM, Blegen HJ, Logan S, Nguyen GN & Fallon SC. (2014). Postnatal development of eupneic ventilation and metabolism in rats chronically exposed to moderate hyperoxia. *Respir Physiol Neurobiol* **198**, 1-12.
- Bavis RW, Young KM, Barry KJ, Boller MR, Kim E, Klein PM, Ovrutsky AR & Rampersad DA. (2010). Chronic hyperoxia alters the early and late phases of the hypoxic ventilatory response in neonatal rats. *J Appl Physiol (1985)* **109**, 796-803.
- Baydur A, Gilgoff I, Prentice W, Carlson M & Fischer DA. (1990). Decline in respiratory function and experience with long-term assisted ventilation in advanced Duchenne's muscular dystrophy. *Chest* **97**, 884-889.
- Beck J, Weinberg J, Hamnegård CH, Spahija J, Olofson J, Grimby G & Sinderby C. (2006). Diaphragmatic function in advanced Duchenne muscular dystrophy. *Neuromuscul Disord* **16**, 161-167.
- Bersanini C, Khirani S, Ramirez A, Lofaso F, Aubertin G, Beydon N, Mayer M, Maincent K, Boulé M & Fauroux B. (2012). Nocturnal hypoxaemia and hypercapnia in children with neuromuscular disorders. *Eur Respir J* **39**, 1206-1212.
- Burns DP, Edge D, O'Malley D & O'Halloran KD. (2015). Respiratory control in the mdx mouse model of Duchenne muscular dystrophy. *Adv Exp Med Biol* **860**, 239-244.
- Burns DP & O'Halloran KD. (2016). Evidence of hypoxic tolerance in weak upper airway muscle from young mdx mice. *Respir Physiol Neurobiol* **226**, 68-75.
- Burns DP, Rowland J, Canavan L, Murphy KH, Brannock M, O'Malley D, O'Halloran KD & Edge D. (2017). Restoration of pharyngeal dilator muscle force in dystrophin deficient (mdx) mice following co-treatment with neutralizing IL-6 receptor antibodies and Urocortin-2. *Exp Physiol*, doi: 10.1113/EP086232.
- Christakos CN, Cohen MI, Barnhardt R & Shaw CF. (1991). Fast rhythms in phrenic motoneuron and nerve discharges. *J Neurophysiol* **66**, 674-687.
- Coirault C, Pignol B, Cooper RN, Butler-Browne G, Chabrier PE & Lecarpentier Y. (2003). Severe muscle dysfunction precedes collagen tissue proliferation in mdx mouse diaphragm. *J Appl Physiol (1985)* **94**, 1744-1750.
- De Bruin PF, Ueki J, Bush A, Khan Y, Watson A & Pride NB. (1997). Diaphragm thickness and inspiratory strength in patients with Duchenne muscular dystrophy. *Thorax* **52**, 472-475.

- Deconinck N & Dan B. (2007). Pathophysiology of duchenne muscular dystrophy: current hypotheses. *Pediatr Neurol* **36**, 1-7.
- Dubach-Powell J. (2008). Quantitative determination of muscle fibre diameter (minimal Feret's diameter) and percentage of centralised nuclei, pp. 14. TREAT-NMD Neuromuscular Network.
- ElMallah MK, Stanley DA, Lee KZ, Turner SM, Streeter KA, Baekey DM & Fuller DD. (2016). Power spectral analysis of hypoglossal nerve activity during intermittent hypoxia-induced long-term facilitation in mice. *J Neurophysiol* **115**, 1372-1380.
- Ervasti JM. (2007). Dystrophin, its interactions with other proteins, and implications for muscular dystrophy. *Biochim Biophys Acta* **1772**, 108-117.
- Fuller DD & Mitchell GS. (2017). Respiratory neuroplasticity - Overview, significance and future directions. *Exp Neurol* **287**, 144-152.
- Gayraud J, Matecki S, Hnia K, Mornet D, Prefaut C, Mercier J, Michel A & Ramonatxo M. (2007). Ventilation during air breathing and in response to hypercapnia in 5 and 16 month-old mdx and C57 mice. *J Muscle Res Cell Motil* **28**, 29-37.
- Han JJ, Carter GT, Ra JJ, Abresch RT, Chamberlain JS & Robinson LR. (2006). Electromyographic studies in mdx and wild-type C57 mice. *Muscle Nerve* **33**, 208-214.
- Haouzi P, Bell HJ, Notet V & Bihain B. (2009). Comparison of the metabolic and ventilatory response to hypoxia and H₂S in unsedated mice and rats. *Respir Physiol Neurobiol* **167**, 316-322.
- Helliwell TR, MacLennan PA, McArdle A, Edwards RH & Jackson MJ. (2006). Fasting increases the extent of muscle necrosis in the mdx mouse. *CLin Sci* **90**, 467-472.
- Huang P, Cheng G, Lu H, Aronica M, Ransohoff RM & Zhou L. (2011). Impaired respiratory function in mdx and mdx/utrn(+/-) mice. *Muscle Nerve* **43**, 263-267.
- Ishizaki M, Suga T, Kimura E, Shiota T, Kawano R, Uchida Y, Uchino K, Yamashita S, Maeda Y & Uchino M. (2008). Mdx respiratory impairment following fibrosis of the diaphragm. *Neuromuscul Disord* **18**, 342-348.
- Khirani S, Ramirez A, Aubertin G, Boulé M, Chemouny C, Forin V & Fauroux B. (2014). Respiratory muscle decline in Duchenne muscular dystrophy. *Pediatr Pulmonol* **49**, 473-481.

- Kim JH, Kwak HB, Thompson LV & Lawler JM. (2013). Contribution of oxidative stress to pathology in diaphragm and limb muscles with Duchenne muscular dystrophy. *J Muscle Res Cell Motil* **34**, 1-13.
- Kim JH & Lawler JM. (2012). Amplification of proinflammatory phenotype, damage, and weakness by oxidative stress in the diaphragm muscle of mdx mice. *Free Radic Biol Med* **52**, 1597-1606.
- Kline DD, Peng YJ, Manalo DJ, Semenza GL & Prabhakar NR. (2002). Defective carotid body function and impaired ventilatory responses to chronic hypoxia in mice partially deficient for hypoxia-inducible factor 1 alpha. *Proc Natl Acad Sci U S A* **99**, 821-826.
- Kumar P & Prabhakar NR. (2012). Peripheral chemoreceptors: function and plasticity of the carotid body. *Compr Physiol* **2**, 141-219.
- Lewis P, Sheehan D, Soares R, Coelho AV & O'Halloran KD. (2016). Redox remodeling is pivotal in murine diaphragm muscle adaptation to chronic sustained hypoxia. *Am J Respir Cell Mol Biol* **55**, 12-23.
- Lewis P, Sheehan D, Soares R, Varela Coelho A & O'Halloran KD. (2015). Chronic sustained hypoxia-induced redox remodeling causes contractile dysfunction in mouse sternohyoid muscle. *Front Physiol* **6**, 122.
- Lidov HG. (1996). Dystrophin in the nervous system. *Brain Pathol* **6**, 63-77.
- McMorrow C, Fredsted A, Carberry J, O'Connell RA, Bradford A, Jones JF & O'Halloran KD. (2011). Chronic hypoxia increases rat diaphragm muscle endurance and sodium-potassium ATPase pump content. *Eur Respir J* **37**, 1474-1481.
- Melacini P, Vianello A, Villanova C, Fanin M, Miorin M, Angelini C & Dalla Volta S. (1996). Cardiac and respiratory involvement in advanced stage Duchenne muscular dystrophy. *Neuromuscul Disord* **6**, 367-376.
- Mitchell GS & Johnson SM. (2003). Neuroplasticity in respiratory motor control. *J Appl Physiol (1985)* **94**, 358-374.
- Mortola JP & Frappell PB. (1998). On the barometric method for measurements of ventilation, and its use in small animals. *Can J Physiol Pharmacol* **76**, 937-944.
- Mosqueira M, Baby SM, Lahiri S & Khurana TS. (2013a). Ventilatory chemosensory drive is blunted in the mdx mouse model of Duchenne Muscular Dystrophy (DMD). *PLoS One* **8**, e69567.

- Mosqueira M, Zeiger U, Förderer M, Brinkmeier H & Fink RH. (2013b). Cardiac and respiratory dysfunction in Duchenne muscular dystrophy and the role of second messengers. *Med Res Rev* **33**, 1174-1213.
- Muntoni F, Torelli S & Ferlini A. (2003). Dystrophin and mutations: one gene, several proteins, multiple phenotypes. *Lancet Neurol* **2**, 731-740.
- O'Neal MH, Spiegel ET, Chon KH & Solomon IC. (2005). Time-frequency representation of inspiratory motor output in anesthetized C57BL/6 mice in vivo. *J Neurophysiol* **93**, 1762-1775.
- Pratt SJ, Valencia AP, Le GK, Shah SB & Lovering RM. (2015). Pre- and postsynaptic changes in the neuromuscular junction in dystrophic mice. *Front Physiol* **6**, 252.
- Roy A, Mandadi S, Fiamma MN, Rodikova E, Ferguson EV, Whelan PJ & Wilson RJ. (2012). Anandamide modulates carotid sinus nerve afferent activity via TRPV1 receptors increasing responses to heat. *J Appl Physiol (1985)* **112**, 212-224.
- Shortt CM, Fredsted A, Chow HB, Williams R, Skelly JR, Edge D, Bradford A & O'Halloran KD. (2014). Reactive oxygen species mediated diaphragm fatigue in a rat model of chronic intermittent hypoxia. *Exp Physiol* **99**, 688-700.
- Skelly JR, Edge D, Shortt CM, Jones JF, Bradford A & O'Halloran KD. (2012). Tempol ameliorates pharyngeal dilator muscle dysfunction in a rodent model of chronic intermittent hypoxia. *Am J Respir Cell Mol Biol* **46**, 139-148.
- Smith PE, Edwards RH & Calverley PM. (1989a). Oxygen treatment of sleep hypoxaemia in Duchenne muscular dystrophy. *Thorax* **44**, 997-1001.
- Smith PE, Edwards RH & Calverley PM. (1989b). Ventilation and breathing pattern during sleep in Duchenne muscular dystrophy. *Chest* **96**, 1346-1351.
- Stephenson R & Gucciardi EJ. (2002). Theoretical and practical considerations in the application of whole body plethysmography to sleep research. *Eur J Appl Physiol* **87**, 207-219.
- Wilson RJ & Teppema LJ. (2016). Integration of central and peripheral respiratory chemoreflexes. *Compr Physiol* **6**, 1005-1041.

Chapter 3. Breathing with neuromuscular disease: Does compensatory plasticity in the motor drive to breathe offer a potential therapeutic target in muscular dystrophy?

Ken D. O'Halloran and David P. Burns

*Department of Physiology, School of Medicine, College of Medicine and Health,
University College Cork, Cork, Ireland.*

Review article published in *Respiratory Physiology and Neurobiology*.

Highlights

- Dystrophin deficiency in *mdx* mice results in deficits at multiple sites of the respiratory control system.
- Evidence suggests compensatory neuroplasticity in the motor drive to the diaphragm muscle during maximal chemoactivation in *mdx* mice.
- Understanding intrinsic physiological compensatory mechanisms in *mdx* mice is important in the context of interventional strategies in animal models and human dystrophinopathies.

Abbreviations: DMD, Duchenne muscular dystrophy; EMG, electromyography; LTF, long-term facilitation; MyHC, myosin heavy chain; V_E/V_{CO_2} , ventilatory equivalent for carbon dioxide; WT, wild-type.

Abstract

Duchenne muscular dystrophy (DMD) is a fatal neuromuscular disease associated with respiratory-related morbidity and mortality. Herein, we review recent work by our group exploring deficits and compensation in the respiratory control network governing respiratory homeostasis in a pre-clinical model of DMD, the *mdx* mouse. Deficits at multiple sites of the network provide considerable challenges to respiratory control. However, our work has also revealed evidence of compensatory neuroplasticity in the motor drive to breathe enhancing diaphragm muscle activity during increased chemical drive. The finding may explain the preserved capacity for *mdx* mice to increase ventilation in response to chemoactivation. Given the profound dysfunction in the primary pump muscle of breathing, we argue that activation of accessory muscles of breathing may be especially important in *mdx* (and perhaps DMD). Notwithstanding the challenges offered by respiratory muscle dysfunction, it may be possible to further leverage intrinsic physiological mechanisms serving to compensate for weak muscles in attempts to restore or preserve ventilatory capacity. We discuss current knowledge gaps and the need to better appreciate fundamental aspects of respiratory control in pre-clinical models so as to better inform intervention strategies in human DMD.

Keywords: Duchenne muscular dystrophy; diaphragm; electromyogram; *mdx* mouse; neuroplasticity

3.1 Duchenne muscular dystrophy (DMD): Respiratory morbidity and mortality

Dystrophin is a structural protein involved in preventing stretch-induced muscle damage during contraction via anchoring the actin cytoskeleton to the sarcolemma (Petrof *et al.*, 1993). In the absence of dystrophin, muscle damage occurs, resulting in muscle fibre necrosis and extensive muscle weakness. Skeletal muscle function is adversely affected in the dystrophinopathies, with attendant muscle fibrosis and secondary inflammation. The striated muscles of breathing are implicated in the disease with evidence of diaphragm muscle weakness (Khirani *et al.*, 2014), which has major implications for the control of breathing in DMD.

Respiratory morbidity and mortality are common features of many neuromuscular diseases (Bye *et al.*, 1990). Many boys with DMD experience respiratory disturbances during life, while cardio-respiratory failure remains the leading cause of death. Pulmonary function peaks when patients are in their mid-teens, although forced vital capacity values remain lower than predicted (De Bruin *et al.*, 2001; Phillips *et al.*, 2001; Khirani *et al.*, 2014). Thereafter, there is a steady decrease in lung volumes with increasing age. Trans-diaphragmatic pressure during sniff behaviours are reported to be low in DMD and declined steadily once DMD boys reached 10 years of age (Khirani *et al.*, 2014), revealing impaired mechanical function of the diaphragm.

Patients with DMD experience disruptions to breathing, particularly during sleep (Arens & Muzumdar, 2010). Patients are known to suffer from sleep apnoea and both obstructive and central apnoeas have been described with subsequent disruptions to arterial blood oxygenation levels (Barbé *et al.*, 1994; Khan & Heckmatt, 1994). Evidence suggests that patients have a greater risk of oxygen desaturation during sleep with increasing age (Khan & Heckmatt, 1994), which is most likely due to obstructive apnoea during the first decade of life (Suresh *et al.*, 2005). As patients reach the second decade of life, they are at an increased risk of hypoventilation during sleep (Smith *et al.*, 1989; Suresh *et al.*, 2005), likely due to inadequate diaphragm muscle performance. Patients are known to develop scoliosis, further impacting on respiratory function.

3.2 The dystrophin-deficient *mdx* mouse: Diaphragm dysfunction recapitulating human DMD

The *mdx* mouse is a mutant model of DMD. Dystrophic diaphragm muscle from *mdx* mice exhibits severe mechanical dysfunction and muscle weakness from a young age (Coirault *et al.*, 2003). Moreover, *mdx* diaphragm shows evidence of inflammation, centralised myonuclei and fibrosis (Stedman *et al.*, 1991; Coirault *et al.*, 2003; Huang *et al.*, 2009). Structural alterations in myosin heavy chain (MyHC) isoform composition are observed, with dystrophic diaphragm expressing a reduced number of MyHC IIx fibres and increased MyHC IIa fibres (Coirault *et al.*, 1999) compared with wild-type, likely related to a lack of maturation of muscle fibres due to ongoing damage and repair processes. Few studies have examined the functional consequences of dystrophin deficiency on ventilatory capacity in *mdx* mice. Impaired normoxic ventilation was reported in 2 month old and 6 month old *mdx* mice (Mosqueira *et al.*, 2013; Burns *et al.*, 2015). In addition to diaphragm muscle weakness, the musculature of the upper airway is also compromised by dystrophin deficiency in the *mdx* mouse (Attal *et al.*, 2000; Burns & O'Halloran, 2016). Muscle weakness, inflammation, fibrosis and central nucleation are described in the dystrophic sternohyoid muscle, a representative pharyngeal dilator (Burns *et al.*, 2017a).

3.3 Control of breathing in the *mdx* mouse: Neural adaptation or maladaptation?

There is now a large body of evidence revealing a remarkable capacity for plasticity at multiple sites within the respiratory control network governing control of arterial blood gases and pH (Huey *et al.*, 2003; Mitchell & Johnson, 2003; Bavis *et al.*, 2007; Kumar & Prabhakar, 2012; Fuller & Mitchell, 2017). Sensory and motor plasticity is context-dependent and can elaborate overt adaptive or maladaptive outcomes (Baker *et al.*, 2001; Peng *et al.*, 2003; Prabhakar, 2011; Wilkerson *et al.*, 2017). Compensatory neuroplasticity at one or more sites of the integrative network could ameliorate respiratory system compromise in DMD. Conversely, deficits in sensorimotor control of breathing could further compound respiratory morbidity, disrupting respiratory homeostasis potentially establishing a spiral of disability. Until recently, the impact of dystrophin deficiency on the neural control of

breathing was unclear. We performed the first broad assessment of sensorimotor control of breathing in *mdx* mice (Burns *et al.*, 2017b). We reasoned that there would be evidence of neuroplasticity of relevance to respiratory homeostasis at one or more sites of the respiratory control network of the *mdx* mouse.

3.4 Control of breathing in the *mdx* mouse: Deficits and dysfunction

We studied young adult male *mdx* mice given our interest in the early impact of dystrophin deficiency on the control of breathing. In *mdx* mice at 8 weeks of age, we confirmed the appearance of profound diaphragm muscle weakness. Isometric force-generating capacity of *ex vivo* diaphragm preparations was depressed by ~40% compared with age-matched wild-type control diaphragms (Burns *et al.*, 2017b). Immunohistochemistry performed on diaphragm muscle cross-sections revealed a greater abundance of small diameter fibres and increased coefficient of variation of muscle fibre size, which together with an increased density of centrally-nucleated fibres (indicative of myonecrosis) demonstrated considerable muscle remodelling in the *mdx* diaphragm (Burns *et al.*, 2017b). The intrinsic weakness in diaphragm is substantial at a young age and would be expected to place considerable limits on ventilatory performance.

Indeed, mechanical disadvantage in *mdx* at 8 weeks of age was suggested by our study with evidence, using whole-body plethysmography, of hypoventilation during baseline normoxic breathing in *mdx* mice compared with wild-type mice (Burns *et al.*, 2017b). There was a significant decrease in the ventilatory equivalent for carbon dioxide (V_E/V_{CO_2}) in *mdx* mice, the principal deficit arising from a significant reduction in baseline tidal volume. Intra-cardiac blood gas analysis in isoflurane anaesthetised *mdx* mice demonstrated the development of a compensated respiratory acidosis.

Dystrophin is expressed in the carotid body (Mosqueira *et al.*, 2013). We explored carotid body afferent discharge frequency and responsiveness to hypoxia in isolated perfused carotid body-carotid sinus nerve preparations to determine if sensory deficit presents and contributes to ventilatory impairment in *mdx* mice

(Burns *et al.*, 2017b). A relative hypoactivity of the carotid body was revealed during normoxia, with evidence of a blunted inhibitory response to hyperoxia in *mdx* preparations compared with wild-type preparations. However, the classic excitatory chemosensory response to hypoxia was not significantly different between *mdx* and wild-type carotid bodies. The latter finding was consistent with observations of equivalent hypoxic ventilatory responses in *mdx* and wild-type mice (Burns *et al.*, 2017b). Since sensory inputs from the peripheral chemoreceptors provide tonic drive to eupnoeic breathing, carotid body hypoactivity might contribute, at least in part, to resting hypoventilation in *mdx*.

3.5 Control of breathing in the *mdx* mouse: Compensation and limitations

In our recent study (Burns *et al.*, 2017b), we recorded diaphragm EMG activity during baseline and in response to chemoactivation of breathing during asphyxic challenge. Baseline activity was equivalent between wild-type and *mdx* mice, but the increased EMG activity in response to asphyxia was significantly enhanced in *mdx* mice. The response is suggestive of compensatory neuroplasticity in the motor control of breathing. Since chemosensory responses were equivalent between wild-type and *mdx* mice, we concluded that increased neural drive was reflective of an increased gain in the control system at the level of key integrative sites in the brainstem network and/or at the level of the spinal phrenic motor pool innervating the diaphragm.

Whereas diaphragm EMG responsiveness was significantly increased in *mdx*, the profound weakness of the major muscle of breathing is such that transduction of enhanced neural drive to the mechanical act of breathing is likely severely compromised. Yet, of note, *mdx* mice are capable of increasing ventilation in response to increased chemical drive to breathe. In our study, the ventilatory response to hypercapnia was equivalent in wild-type and *mdx* mice (Burns *et al.*, 2017b). It is established that motor recruitment of the diaphragm in response to hypercapnia is submaximal, operating below 30% of the maximum capacity of the system (Mantilla *et al.*, 2010; Greising *et al.*, 2013). As such, increased neural drive and a right-ward shift of the force-frequency relationship in *mdx* diaphragm might

provide increased diaphragm force-generating capacity, notwithstanding the significant deficit in *mdx* muscle compared with wild-type (Figure 3.1). It is also conceivable that increased drive in motor pathways to accessory muscles of breathing facilitates tidal breathing in *mdx* mice. If neuroplasticity extends to multiple parallel efferent pathways, arising for example from enhanced central respiratory drive to breathe during chemoactivation, recruitment of accessory inspiratory muscles of breathing might help to preserve ventilatory capacity in response to chemoactivation. Activation of accessory muscles of breathing may be especially important in *mdx* (and perhaps DMD) allowing for greater efficiency in neuromechanical coupling compared with outcomes dependent on the dysfunctional diaphragm. Interestingly, there is evidence of expiratory muscle recruitment to facilitate ventilation in the Golden Retriever model of muscular dystrophy (Mead *et al.*, 2014). If compensatory neuroplasticity presents in efferent motor pathways in DMD, it may be possible to further boost neural drive to breathe and in this way help preserve ventilatory capacity. A major drawback with such an approach are the limits afforded by the final effector organs, the respiratory muscles, and potential concerns associated with activity-induced damage, since it is known that exercise in *mdx* mice exacerbates muscle dysfunction, including diaphragm dysfunction (Selsby *et al.*, 2013). However, harnessing putative plasticity in accessory pathways may offer an attractive therapeutic strategy in DMD.

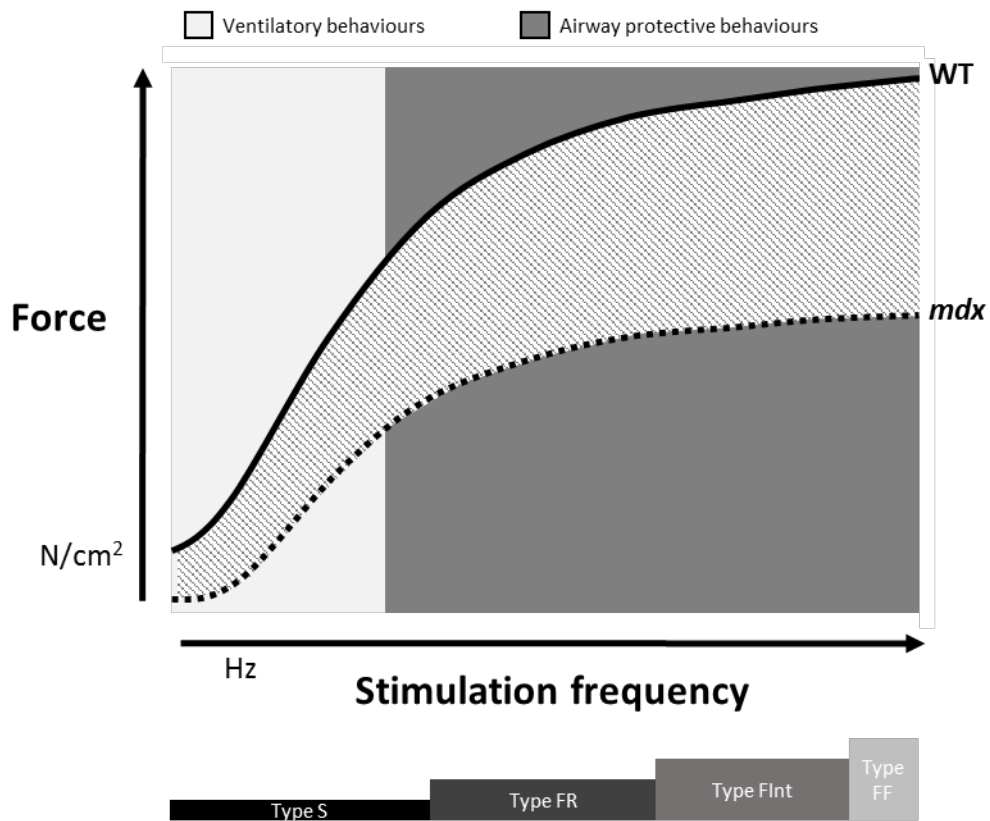


Figure 3.1 Diaphragm muscle weakness in dystrophin-deficient *mdx* mice.

Schematic representation of diaphragm force-frequency relationship in wild-type (WT) and dystrophin-deficient *mdx* mice. Deficits in force-generating capacity are seen in the range relevant to ventilation and airway protective behaviours. Enhanced neural drive during chemoactivation has limited capacity to increase diaphragm force, compared with wild-type, suggesting that preserved ventilatory capacity in *mdx* during chemostimulation may be especially dependent on accessory muscles of breathing. Adapted from data presented in (Burns *et al.*, 2017b). The bottom schematic, informed by the studies of Sieck and Mantilla (Mantilla *et al.*, 2010), illustrates the major motor unit types associated with graded force-generating capacity of the *in vivo* diaphragm.

3.6 Control of breathing in the *mdx* mouse: Knowledge gaps

There is a surprising dearth of information in respect of the neural control of breathing in the dystrophinopathies, notwithstanding that respiratory morbidity and mortality are dominant features. More studies are required to understand the extent of respiratory system deficit and compensation, and the temporal changes over the course of disease progression. Knowledge of fundamental aspects of respiratory control is essential in the consideration of respiratory management of patients with neuromuscular disease. Moreover, a better appreciation of the intrinsic compensatory processes at play in DMD should help inform therapeutic strategies. Our study revealed enhanced diaphragm EMG responsiveness in *mdx* mice suggestive of compensatory neuroplasticity. However, in a myopathy model such as *mdx*, EMG recordings may be contaminated by aberrant motor unit potentials associated with dynamic degeneration and regeneration of muscle fibres. It will be important to establish if increased efferent drive is revealed in phrenic neurogram recordings. We are currently exploring this issue with evidence of potentiated phrenic neurogram activity in *mdx* mice in response to maximum chemostimulation (Burns et al., unpublished observations). It is unclear whether motor activation of accessory muscles is altered in *mdx* and this represents an important gap in the understanding of respiratory control in dystrophin-deficient neuromuscular disease. Studies are required to address this issue and determine if therapeutic strategies exploiting these pathways represents a viable interventional option aimed at increasing ventilatory capacity, with a view to treatment options for DMD patients. A summary of the effects of dystrophin-deficiency on respiratory control in young adult *mdx* mice is shown in Figure 3.2.

3.7 Control of breathing in the *mdx* mouse: Therapeutic intermittent hypoxia to boost respiratory drive?

In recent years, Mitchell and colleagues have pioneered the understanding and potential exploitation of mechanisms of motor plasticity to enhance respiratory motor output (Fuller & Mitchell, 2017). Manipulating environmental oxygen in the form of acute bouts of intermittent hypoxia has the capacity to evoke ventilatory long-term facilitation (LTF) in behaving rodents (Edge & O'Halloran, 2015).

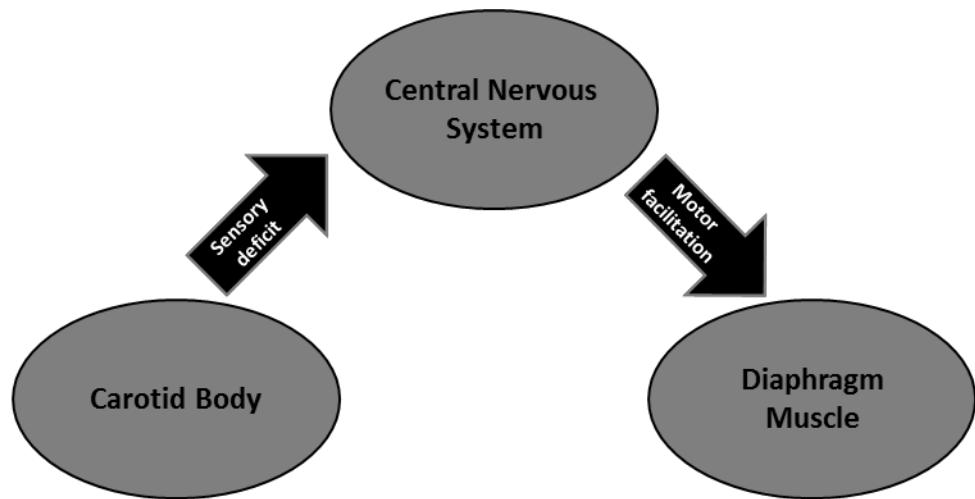
Furthermore, intermittent hypoxia-induced LTF is well described in motor pathways of the diaphragm (Fuller *et al.*, 2000), upper airway (Wilkerson *et al.*, 2017) and accessory muscles of breathing such as the intercostal muscles (Navarrete-Opazo & Mitchell, 2014). We reason that safe interventions aimed at evoking LTF in the motor pathways of breathing may have therapeutic capacity to facilitate breathing in *mdx* mice, as has been elegantly demonstrated in rodent models of motor neuron loss (Nichols *et al.*, 2013; Nichols *et al.*, 2015) and spinal cord injury (Dougherty *et al.*, 2017). This warrants attention in future studies.

3.8 Conclusion

Dystrophin-deficiency has detrimental consequences for respiratory control, principally owing to respiratory muscle dysfunction. We have revealed a broader vista of the deficits that present early in a pre-clinical model of neuromuscular disease, the *mdx* mouse. We also have revealed, for the first time, compensatory adjustments in the nervous system control of respiratory muscles in *mdx* mice striving for homeostatic control of breathing. We suggest that it may be possible to exploit intrinsic physiological mechanisms serving to boost breathing in the development of therapeutic strategies for DMD, through the use of safe interventional therapies such as intermittent hypoxia.

Acknowledgements

We are grateful to our co-authors on the original article (Burns *et al.*, 2017b) reviewed herein for their important contributions to the study. DPB is supported by the Department of Physiology, University College Cork, Ireland.



Deficits

- Carotid body hypoactivity
- Hypoventilation
- Diaphragm myofibre remodelling and muscle weakness

Compensation

- Potentiated diaphragm EMG responsiveness
- Preserved chemosensory and ventilatory responsiveness to hypoxia
- Preserved ventilatory response to hypercapnia

Compensatory neuroplasticity limits ventilatory deficit in young *mdx* mice

Figure 3.2 Summary of the effects of dystrophin-deficiency on respiratory control in young *mdx* mice.

Summary of the deficits and compensation in respiratory control in young adult *mdx* mice. Adapted from data presented in (Burns *et al.*, 2017b).

3.9 References

- Arens R & Muzumdar H. (2010). Sleep, sleep disordered breathing, and nocturnal hypoventilation in children with neuromuscular diseases. *Paediatr Respir Rev* **11**, 24-30.
- Attal P, Lambert F, Marchand-Adam S, Bobin S, Pourny JC, Chemla D, Lecarpentier Y & Coirault C. (2000). Severe mechanical dysfunction in pharyngeal muscle from adult mdx mice. *Am J Respir Crit Care Med* **162**, 278-281.
- Baker TL, Fuller DD, Zabka AG & Mitchell GS. (2001). Respiratory plasticity: differential actions of continuous and episodic hypoxia and hypercapnia. *Respir Physiol* **129**, 25-35.
- Barbé F, Quera-Salva MA, McCann C, Gajdos P, Raphael JC, de Lattre J & Agustí AG. (1994). Sleep-related respiratory disturbances in patients with Duchenne muscular dystrophy. *Eur Respir J* **7**, 1403-1408.
- Bavis RW, Powell FL, Bradford A, Hsia CC, Peltonen JE, Soliz J, Zeis B, Fergusson EK, Fu Z, Gassmann M, Kim CB, Maurer J, McGuire M, Miller BM, O'Halloran KD, Paul RJ, Reid SG, Rusko HK, Tikkanen HO & Wilkinson KA. (2007). Respiratory plasticity in response to changes in oxygen supply and demand. *Integr Comp Biol* **47**, 532-551.
- Burns DP, Edge D, O'Malley D & O'Halloran KD. (2015). Respiratory Control in the mdx Mouse Model of Duchenne Muscular Dystrophy. *Adv Exp Med Biol* **860**, 239-244.
- Burns DP & O'Halloran KD. (2016). Evidence of hypoxic tolerance in weak upper airway muscle from young mdx mice. *Respir Physiol Neurobiol* **226**, 68-75.
- Burns DP, Rowland J, Canavan L, Murphy KH, Brannock M, O'Malley D, O'Halloran KD & Edge D. (2017a). Restoration of pharyngeal dilator muscle force in dystrophin-deficient (mdx) mice following co-treatment with neutralizing interleukin-6 receptor antibodies and urocortin 2. *Exp Physiol* **102**, 1177-1193.
- Burns DP, Roy A, Lucking EF, McDonald FB, Gray S, Wilson RJ, Edge D & O'Halloran KD. (2017b). Sensorimotor control of breathing in the mdx mouse model of Duchenne muscular dystrophy. *J Physiol*.
- Bye PT, Ellis ER, Issa FG, Donnelly PM & Sullivan CE. (1990). Respiratory failure and sleep in neuromuscular disease. *Thorax* **45**, 241-247.
- Coirault C, Lambert F, Marchand-Adam S, Attal P, Chemla D & Lecarpentier Y. (1999). Myosin molecular motor dysfunction in dystrophic mouse diaphragm. *Am J Physiol* **277**, C1170-1176.

- Coirault C, Pignol B, Cooper RN, Butler-Browne G, Chabrier PE & Lecarpentier Y. (2003). Severe muscle dysfunction precedes collagen tissue proliferation in mdx mouse diaphragm. *J Appl Physiol (1985)* **94**, 1744-1750.
- De Bruin PF, Ueki J, Bush A, Y Manzur A, Watson A & Pride NB. (2001). Inspiratory flow reserve in boys with Duchenne muscular dystrophy. *Pediatr Pulmonol* **31**, 451-457.
- Dougherty BJ, Terada J, Springborn SR, Vinit S, MacFarlane PM & Mitchell GS. (2017). Daily acute intermittent hypoxia improves breathing function with acute and chronic spinal injury via distinct mechanisms. *Respir Physiol Neurobiol*.
- Edge D & O'Halloran KD. (2015). Chronic Intermittent Hypoxia Blunts the Expression of Ventilatory Long Term Facilitation in Sleeping Rats. *Adv Exp Med Biol* **860**, 335-342.
- Fuller DD, Bach KB, Baker TL, Kinkead R & Mitchell GS. (2000). Long term facilitation of phrenic motor output. *Respir Physiol* **121**, 135-146.
- Fuller DD & Mitchell GS. (2017). Respiratory neuroplasticity - Overview, significance and future directions. *Exp Neurol* **287**, 144-152.
- Greising SM, Sieck DC, Sieck GC & Mantilla CB. (2013). Novel method for transdiaphragmatic pressure measurements in mice. *Respir Physiol Neurobiol* **188**, 56-59.
- Huang P, Zhao XS, Fields M, Ransohoff RM & Zhou L. (2009). Imatinib attenuates skeletal muscle dystrophy in mdx mice. *FASEB J* **23**, 2539-2548.
- Huey KA, Szewczak JM & Powell FL. (2003). Dopaminergic mechanisms of neural plasticity in respiratory control: transgenic approaches. *Respir Physiol Neurobiol* **135**, 133-144.
- Khan Y & Heckmatt JZ. (1994). Obstructive apnoeas in Duchenne muscular dystrophy. *Thorax* **49**, 157-161.
- Khirani S, Ramirez A, Aubertin G, Boulé M, Chemouny C, Forin V & Fauroux B. (2014). Respiratory muscle decline in Duchenne muscular dystrophy. *Pediatr Pulmonol* **49**, 473-481.
- Kumar P & Prabhakar NR. (2012). Peripheral chemoreceptors: function and plasticity of the carotid body. *Compr Physiol* **2**, 141-219.
- Mantilla CB, Seven YB, Zhan WZ & Sieck GC. (2010). Diaphragm motor unit recruitment in rats. *Respir Physiol Neurobiol* **173**, 101-106.

- Mead AF, Petrov M, Malik AS, Mitchell MA, Childers MK, Bogan JR, Seidner G, Kornegay JN & Stedman HH. (2014). Diaphragm remodeling and compensatory respiratory mechanics in a canine model of Duchenne muscular dystrophy. *J Appl Physiol* (1985) **116**, 807-815.
- Mitchell GS & Johnson SM. (2003). Neuroplasticity in respiratory motor control. *J Appl Physiol* (1985) **94**, 358-374.
- Mosqueira M, Baby SM, Lahiri S & Khurana TS. (2013). Ventilatory chemosensory drive is blunted in the mdx mouse model of Duchenne Muscular Dystrophy (DMD). *PLoS One* **8**, e69567.
- Navarrete-Opazo A & Mitchell GS. (2014). Recruitment and plasticity in diaphragm, intercostal, and abdominal muscles in unanesthetized rats. *J Appl Physiol* (1985) **117**, 180-188.
- Nichols NL, Gowing G, Satriotomo I, Nashold LJ, Dale EA, Suzuki M, Avalos P, Mulcrone PL, McHugh J, Svendsen CN & Mitchell GS. (2013). Intermittent hypoxia and stem cell implants preserve breathing capacity in a rodent model of amyotrophic lateral sclerosis. *Am J Respir Crit Care Med* **187**, 535-542.
- Nichols NL, Satriotomo I, Harrigan DJ & Mitchell GS. (2015). Acute intermittent hypoxia induced phrenic long-term facilitation despite increased SOD1 expression in a rat model of ALS. *Exp Neurol* **273**, 138-150.
- Peng YJ, Overholt JL, Kline D, Kumar GK & Prabhakar NR. (2003). Induction of sensory long-term facilitation in the carotid body by intermittent hypoxia: implications for recurrent apneas. *Proc Natl Acad Sci U S A* **100**, 10073-10078.
- Petrof BJ, Shrager JB, Stedman HH, Kelly AM & Sweeney HL. (1993). Dystrophin protects the sarcolemma from stresses developed during muscle contraction. *Proc Natl Acad Sci U S A* **90**, 3710-3714.
- Phillips MF, Quinlivan RC, Edwards RH & Calverley PM. (2001). Changes in spirometry over time as a prognostic marker in patients with Duchenne muscular dystrophy. *Am J Respir Crit Care Med* **164**, 2191-2194.
- Prabhakar NR. (2011). Sensory plasticity of the carotid body: role of reactive oxygen species and physiological significance. *Respir Physiol Neurobiol* **178**, 375-380.
- Selsby JT, Acosta P, Sleeper MM, Barton ER & Sweeney HL. (2013). Long-term wheel running compromises diaphragm function but improves cardiac and plantarflexor function in the mdx mouse. *J Appl Physiol* (1985) **115**, 660-666.

- Smith PE, Edwards RH & Calverley PM. (1989). Ventilation and breathing pattern during sleep in Duchenne muscular dystrophy. *Chest* **96**, 1346-1351.
- Stedman HH, Sweeney HL, Shrager JB, Maguire HC, Panettieri RA, Petrof B, Narusawa M, Leferovich JM, Sladky JT & Kelly AM. (1991). The mdx mouse diaphragm reproduces the degenerative changes of Duchenne muscular dystrophy. *Nature* **352**, 536-539.
- Suresh S, Wales P, Dakin C, Harris MA & Cooper DG. (2005). Sleep-related breathing disorder in Duchenne muscular dystrophy: disease spectrum in the paediatric population. *J Paediatr Child Health* **41**, 500-503.
- Wilkerson JER, Devinney M & Mitchell GS. (2017). Intermittent but not sustained moderate hypoxia elicits long-term facilitation of hypoglossal motor output. *Respir Physiol Neurobiol*.

Chapter 4. Neuromechanical control of breathing in the dystrophin-deficient *mdx* mouse

David P. Burns¹, Eabha O'Driscoll², Kevin H. Murphy¹, Karen M. O'Connor^{1,3}, Eric F. Lucking¹, Pardeep Dhaliwal¹, Gerard Clarke^{3,4}, Deirdre Edge² and Ken D. O'Halloran¹

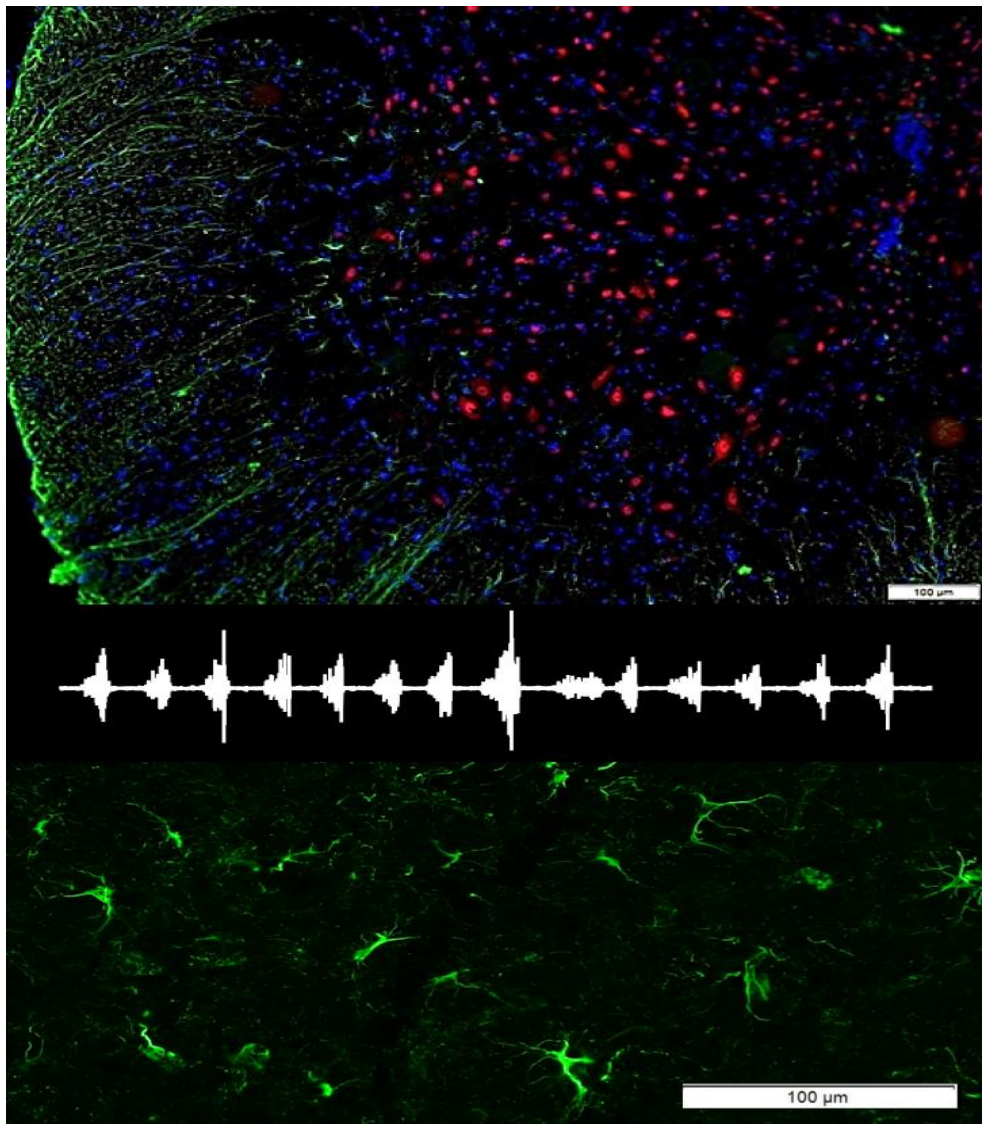
¹*Department of Physiology, School of Medicine, University College Cork, Cork, Ireland.*

²*Department of Physiology, School of Medicine, Trinity Biosciences Institute, Trinity College Dublin, the University of Dublin, Dublin, Ireland.*

³*APC Microbiome Institute, University College Cork, Cork, Ireland.*

⁴*Department of Psychiatry and Neurobehavioural Science, School of Medicine, University College Cork, Cork, Ireland.*

Paper currently under consideration.



Top image shows immunofluorescent image of spinal cord labelled for green fibrillary acidic protein (GFAP, green), NeuN (red) and DAPI (nuclear stain, blue). Trace shows diaphragm raw EMG activity in an anaesthetised mouse. Bottom image shows astrocytes labelled using GFAP.

Key points

- Respiratory muscle weakness is a major feature of Duchenne muscular dystrophy (DMD), but little is known about the neural control of respiratory muscles in DMD and animal models.
- Although extensive diaphragm muscle weakness is apparent in young (8-week-old) *mdx* mice, ventilatory capacity in response to maximum chemostimulation is preserved, with no evidence of perturbed respiratory rhythm.
- In *mdx* mice, peak inspiratory oesophageal pressure generation is maintained during basal and chemoactivated breathing and peak sub-atmospheric pressure during augmented breaths is greater compared with wild-type mice; diaphragm EMG activity is equivalent between groups.
- Monoamine concentrations are increased and the density of activated astrocytes and microglia and pro-inflammatory gene expression is equivalent in the C3-C5 spinal cord of *mdx* mice compared with wild-type mice.
- Our finding of enhanced inspiratory pressure generation in *mdx* mice, despite substantial diaphragm weakness, suggests enhanced accessory respiratory motor drive preserving ventilatory capacity.

Abbreviations: $\frac{1}{2}$ RT, half-relaxation time; 5-HT, 5-hydroxytryptamine; ANOVA, analysis of variance; AUC, area under the curve; BB_n , breath-to-breath; BB_{n+1} , breath-to-breath interval; CSA, cross-sectional area; CT, contraction time; DMD, Duchenne muscular dystrophy; EMG, electromyogram; $ETCO_2$, end-tidal CO_2 ; f_R , respiratory frequency; F_iO_2 , fractional inspired oxygen concentration; GFAP, glial fibrillary acidic protein; HIAA, 5-hydroxyindoleacetic acid; HIF, hypoxia-inducible factor; HPLC, high performance liquid chromatography; Iba-1, ionizing calcium-binding adaptor molecule 1; IL, interleukin; iNOS, inducible nitric oxide synthase; L_o , optimum length; NA, noradrenaline; $NF\kappa B$, nuclear factor kappa-light-chain-enhancer of activated B cells; OCT, optimum cutting temperature; P_t , twitch force; P_o , tetanic force; SD1, short-term variability; SD2, long-term variability; S_{max} , maximum total shortening; SpO_2 , peripheral capillary oxygen saturation; T_e , expiratory duration; T_i , inspiratory duration; $TNF-\alpha$, tumour necrosis factor alpha; TUNEL, terminal deoxynucleotidyl transferase dUTP nick end labelling; V_E , minute ventilation; V_{max} , maximum shortening velocity; V_T , tidal volume; WT, wild-type.

Abstract

Diaphragm dysfunction is recognised in the *mdx* mouse model of muscular dystrophy, however there is a paucity of information concerning neural control of the respiratory muscles. In young adult (8 weeks of age) wild-type and *mdx* mice, we sought to assess respiratory rhythm stability, ventilatory capacity, neural activation of the diaphragm and inspiratory pressure-generating capacity. In C3-C5 spinal cord containing the phrenic motor nucleus, monoamine concentrations, the density of activated astrocytes and microglia, and pro-inflammatory gene expression was assessed. We hypothesised that increased motor recruitment of the diaphragm limits ventilatory decline in *mdx* mice. Poincaré analysis of respiratory timing revealed no evidence of perturbed respiratory rhythm in *mdx* mice, which retained a remarkable capacity to enhance ventilation despite substantial diaphragm muscle weakness. In *mdx* mice, peak inspiratory oesophageal pressure generation was preserved during basal and chemoactivated breathing and was significantly greater during augmented breaths compared with wild-type mice. Monoamine concentrations were significantly increased in the cervical spinal cord of *mdx* mice, and the density of activated glial cells and expression of pro-inflammatory genes was unchanged, revealing no evidence of neuroinflammation, but *mdx* diaphragm EMG activity was not potentiated compared with wild-type across the range of ventilatory behaviours. We reason that compensatory neuroplasticity in accessory motor pathways preserves ventilatory capacity in *mdx* mice despite profound diaphragm muscle weakness, which may have relevance to the development of interventional strategies designed to alleviate respiratory insufficiency in the human dystrophinopathies.

Keywords: DMD; *mdx*; plasticity; breathing; spinal cord; oesophageal pressure; EMG; diaphragm

4.1 Introduction

Dystrophin is a structural protein found in muscle and the central nervous system (Lidov, 1996; Muntoni *et al.*, 2003). Duchenne muscular dystrophy (DMD) is a severe neuromuscular disease caused by dystrophin deficiency (Hoffman *et al.*, 1987; Ervasti, 2007). Respiratory muscle dysfunction is described in DMD patients (De Bruin *et al.*, 1997; Beck *et al.*, 2006) with deleterious consequences for respiratory system performance (Mayer *et al.*, 2015). Loss of ambulation and cardio-respiratory failure are cardinal features of DMD (Yiu & Kornberg, 2008). Life expectancy for DMD boys is severely curtailed and there is no cure for the devastating disease.

Substantial diaphragm muscle weakness is reported in patients and animal models of DMD (Stedman *et al.*, 1991; Khirani *et al.*, 2014). However, there remains an incomplete understanding of the neural control of breathing, where further deficits or compensation may arise with implications for respiratory performance (Burns *et al.*, 2017c). A thorough understanding of the consequences of dystrophin deficiency on the neuromechanical control of breathing is essential in the consideration of disease progression and therapeutic strategies to combat respiratory insufficiency in DMD.

Dystrophin is highly enriched post-synaptically in the central nervous system. In the *mdx* mouse model of DMD, studies indicate reduced cortico-spinal neurons (Sbriccoli *et al.*, 1995), damage to motor pathways (Carretta *et al.*, 2001), loss of neuronal projections (Pinto *et al.*, 2008), GABAergic dysfunction (Sekiguchi *et al.*, 2009; Vaillend & Chaussonot, 2017) and cognitive deficits (Chaussonot *et al.*, 2015). It is unclear if dystrophin deficiency affects central respiratory rhythm and pattern generation and propensity for apnoea, notwithstanding that sleep-disordered breathing is common in DMD (Barbé *et al.*, 1994; Suresh *et al.*, 2005; Sawhani *et al.*, 2015). Clearly, aberrant neural control of breathing could serve to exacerbate respiratory morbidity in DMD, compounding mechanical constraints arising from respiratory muscle dysfunction.

Respiratory neuromechanical coupling in DMD and animal models is understudied. A comprehensive understanding of the motor control of the dystrophin deficient respiratory musculature is lacking. It is essential to determine if dystrophin deficiency is deleterious to the motor control of breathing, or if there is intrinsic compensation within the neural control circuits, or perhaps a capacity to evoke compensation, with consequences for the mechanics of breathing. Recently we described evidence of enhanced motor drive to the *mdx* diaphragm during enhanced chemoactivation of breathing (Burns *et al.*, 2017c), suggesting intrinsic compensation in the neural control of ventilation in dystrophin deficient mice. Our study revealed hypoventilation during basal breathing in conscious mice, but a retained capacity in *mdx* mice to increase ventilation in response to modest chemostimulation (Burns *et al.*, 2017c). However, the extent to which dystrophin deficiency affects inspiratory pressure-generating capacity, or if enhanced phrenic recruitment of the diaphragm contributes to preservation of mechanical capacity during increased ventilatory drive is unclear, but important to establish. It is not known if altered neuromodulatory signalling to the phrenic motor neuronal pool underpins the expression of evoked motor facilitation of breathing in *mdx* mice (Burns *et al.*, 2017c).

Systemic and muscle inflammation are prominent features of DMD and *mdx* mice, due to muscle fibre damage (Messina *et al.*, 2011; Rufo *et al.*, 2011; Cruz-Guzmán *et al.*, 2015). Blood brain barrier function is impaired in *mdx* mice due to dystrophin deficiency (Goodnough *et al.*, 2014). There is mounting evidence that inflammation suppresses the expression of respiratory motor facilitation (Huxtable *et al.*, 2011; Huxtable *et al.*, 2013; Huxtable *et al.*, 2015) and increased understanding of the pivotal role of neuroimmune interactions for the control of breathing (Popa *et al.*, 2011; MacFarlane *et al.*, 2016; Stokes *et al.*, 2017; Sheikhabaei *et al.*, 2018). If enhanced motor facilitation of the weakened diaphragm is an intrinsic compensatory feature in *mdx* mice to preserve breathing or limit ventilatory insufficiency (Burns *et al.*, 2017c), then it is important to discern if there is neuroinflammation in the cervical spinal phrenic motor pool, which may suppress the capacity for neuroplasticity.

We sought to address these knowledge gaps. We assessed respiratory stability in conscious *mdx* mice and determined ventilatory capacity during hypercapnic hypoxic breathing. In anaesthetised mice, we sought to determine peak inspiratory pressure-generating capacity with contemporaneous measurement of diaphragm electromyogram (EMG) activity, to consider neuromechanical coupling. The concentrations of neuromodulatory monoamines together with assessment of the neuroinflammatory status was determined in cervical spinal cord containing the phrenic motor nucleus. Our principal objective was to perform an assessment of the neuromechanical control of breathing in the *mdx* mouse model of DMD. We hypothesized that potentiated motor facilitation of the diaphragm during increased ventilatory demand limits ventilatory insufficiency in *mdx* mice.

4.2 Methods

4.2.1 Ethical approval

Procedures on live animals were performed under licence in accordance with Irish and European law following approval by University College Cork animal research ethics committee.

4.2.2 Experimental animals

Male and female wild-type (C57BL/10ScSnJ) and *mdx* (C57BL/10ScSn-Dmd^{mdx}/J) mice were purchased from the Jackson Laboratory (Bar Harbor, ME, USA) and bred at University College Cork's animal housing facility. Eight-week-old male wild-type (n = 23) and *mdx* (n = 21) mice were studied for respiratory recordings examining breathing stability and subsequent tissue harvesting for immunohistochemistry and gene expression analyses. Animals were housed conventionally. In addition, male wild-type (n = 18) and *mdx* (n = 16) mice were purchased directly from the Jackson Laboratory for respiratory measurements examining ventilatory capacity, *in vivo* oesophageal pressure and EMG recordings, *ex vivo* diaphragm muscle function and tissue harvesting for monoamine analysis. The latter animals were housed in individually ventilated cages in our institution's animal housing facility. All animals were housed in temperature and humidity-controlled rooms, operating on a 12 h light/ 12 h dark cycle with food and water available *ad libitum*.

4.2.3 Whole-body plethysmography

Whole-body plethysmography was used to assess respiratory flow in unrestrained and unanaesthetised mice during quiet rest. Mice were introduced into plethysmograph chambers (Model PLY4211; volume 600ml, Buxco Research Systems, Wilmington, NC, USA) and allowed 60-90 min to acclimate to the chamber environment. Following exploration and grooming behaviours mice settled and were studied during quiet rest. Recordings were typically performed in a wild-type and *mdx* mouse contemporaneously in parallel using a pair of plethysmograph chambers.

4.2.3.1 Respiratory stability

Experimental protocol: Respiratory flow recordings were performed in wild-type (n = 13) and *mdx* (n = 12) mice during normoxia (21% O₂) for 20-30 min to assess respiratory stability.

Data analysis: The breath-to-breath (BB_n) and subsequent interval (BB_{n+1}) of 200 breaths were analyzed as previously described (Peng *et al.*, 2011; Souza *et al.*, 2015). Poincaré plots expressing BB_n versus BB_{n+1} for 200 consecutive breaths were plotted for wild-type and *mdx* mice. Short-term variability (SD1) and long-term variability (SD2) were calculated as indices of breathing variability in wild-type and *mdx* mice. The frequency of augmented breaths, defined as an increase in tidal volume to at least twice the amplitude observed in a eupnoeic breath, was recorded. In addition, the frequency and duration of spontaneous and post-sigh apnoeas were determined. An apnoea was defined as a period of breathing cessation of at least two missed breaths. A study of ventilatory and metabolic responsiveness to hypoxia in these mice was previously reported (Burns *et al.*, 2017c).

4.2.3.2 Ventilatory responsiveness to chemostimulation

Experimental protocol: Mice were introduced into plethysmograph chambers as described above. Following acclimation and a settling period, a 20-min baseline recording was performed in normoxia. This was followed by a graded hypercapnic challenge in which animals were challenged with increasing levels of inspired carbon dioxide: F_ICO₂ = 0.02, 0.04 and 0.06 (in 21% O₂) consecutively for 5 min each. This was immediately followed by maximal chemoreceptor stimulation with asphyxia (10% O₂/ 6% CO₂) for 5 minutes, to examine ventilatory capacity in wild-type (n = 9) and *mdx* (n = 7) mice. Mice were subsequently euthanized by urethane overdose.

Data analysis: Peak ventilation during graded hypercapnia and asphyxia was determined and compared with the preceding baseline normoxic period.

Ventilatory responsiveness to chemostimulation was expressed as % change from baseline.

4.2.4 Diaphragm EMG and oesophageal pressure recordings

Anaesthesia was induced with 5% isoflurane in 60% O₂ (balance N₂) followed by urethane (1.7g/kg i.p.). Wild-type (n = 9) and *mdx* (n = 9) mice were then placed in the supine position, gradually weaned from the isoflurane and body temperature was maintained at 37°C via a rectal probe and thermostatically-controlled heating blanket (Harvard Apparatus, Holliston, MA, USA). Supplemental anaesthetic was administered if necessary to maintain a surgical plane of anaesthesia, which was assessed by assessment of pedal withdrawal reflex to noxious pinch. A pulse oximeter clip (MouseOx™, Starr Life Sciences Corporation, Oakmount, PA, USA) was placed on a shaved thigh of each mouse for the measurement of peripheral capillary O₂ saturation (SpO₂). A mid-cervical tracheotomy was performed. All animals were maintained with a bias flow of supplemental O₂ (FiO₂ = 0.60) under baseline conditions. End-tidal carbon dioxide (ETCO₂) was measured using a MicroCapStar (CWE, Ardmore, PA). To estimate intra-pleural subatmospheric pressure generated by the respiratory musculature during inspiration, we measured oesophageal pressure using a pressure-tip catheter (Mikro-Tip, Millar Inc., Houston, TX, USA), which was positioned in the thoracic oesophagus through the mouth. During inspiratory activity, oesophageal recordings displayed phasic subatmospheric pressure swings. Concentric needle electrodes (26G; Natus Manufacturing Ltd, Ireland) were inserted into the costal diaphragm for the continuous measurement of diaphragm EMG activity, which was amplified (x5,000), filtered (500Hz low cut-off to 5,000Hz high cut-off) and integrated (50ms time constant; Neurolog system, Digitimer Ltd, UK). All signals were passed through an analogue-to-digital converter (r8/30; ADInstruments, Colorado Springs, CO, USA) and were acquired using LabChart 7 (ADInstruments, Colorado Springs, CO, USA).

Experimental protocol: Following instrumentation, animals were allowed at least 10 minutes to stabilize before baseline parameters were measured for a period of 10 minutes. Next, animals were challenged with asphyxia (15% O₂/5% CO₂; 1min) to

examine the effects of chemostimulation on diaphragm EMG activity and oesophageal pressure generation. Following the experimental protocol, mice were euthanised by decapitation. Diaphragm muscle was excised for *ex vivo* functional analysis (section 4.2.5). Cervical spinal cord was collected for the determination of monoamine concentrations (section 4.2.9).

Data analysis: The amplitudes of integrated inspiratory diaphragm EMG activity and peak inspiratory subatmospheric oesophageal pressure were analyzed and averaged under steady-state basal conditions, and for 1 minute of baseline immediately prior to chemostimulation challenges. The amplitude of integrated inspiratory diaphragm EMG activity and peak inspiratory subatmospheric oesophageal pressure were analyzed and averaged for the final 15 breaths (maximal response) of the asphyxic challenge. Baseline EMG data and oesophageal pressure are reported in absolute units. Responses to chemostimulation are expressed as absolute change from the preceding baseline value. Spontaneous augmented breaths (sighs) observed during baseline conditions were analysed and compared with the average of the preceding five breaths. Augmented breaths were classified as breaths with more than double baseline EMG amplitude a (Mantilla *et al.*, 2011; Seven *et al.*, 2014).

4.2.5 *Ex vivo diaphragm muscle function*

Diaphragm muscle was excised with rib and central tendon attached. Muscle bundles with longitudinally arranged muscle fibres were prepared for functional assessment and suspended vertically between two platinum plate electrodes. The rib was attached to an immobile hook and the central tendon was attached to a dual-mode force transducer (Aurora Scientific Inc.; Aurora, ON, Canada) with non-elastic string. Diaphragm muscle preparations from wild-type ($n = 8$) and *mdx* ($n = 9$) mice were studied in a water-jacketed tissue bath at 35°C containing Krebs solution (in mM: 120 NaCl, 5 KCl, 2.5 Ca²⁺, 1.2 MgSO₄, 1.2 NaH₂PO₄, 25 NaHCO₃, 11.5 glucose) and D-tubocurarine (25 µm) and were continuously aerated with hyperoxia (95% O₂/ 5% CO₂). Muscle optimum length (L_0) was determined by adjusting the position of the force transducer, in turn adjusting the length of the

muscle preparations, using a micro-positioner between intermittent twitch contractions (Burns & O'Halloran, 2016; Burns *et al.*, 2017b). L_0 was determined as the muscle length which revealed maximal isometric twitch force in response to single isometric twitch stimulation (supramaximal stimulation, 1ms duration). Preparations remained at L_0 for the duration of the protocol.

Experimental protocol: A single isometric twitch contraction was measured. Peak isometric twitch force (P_t), contraction time (CT) and half-relaxation time ($1/2$ RT) were determined. Peak isometric force at 100Hz (P_o) was determined. The force-frequency relationship was examined by stimulating the muscle sequentially at 10, 20, 40, 60, 80, 100, 120, 140 and 160 Hz (300ms train duration). Contractions were interspersed by a 1 min interval. Next, an isotonic contraction was elicited in preparations at 0% load to examine maximum unloaded muscle shortening and velocity of shortening (Burns & O'Halloran, 2016; Burns *et al.*, 2017b).

Data analysis: Muscle force was normalised for muscle cross-sectional area (CSA) and expressed as specific force (N/cm^2). The CSA of each muscle bundle was determined by dividing muscle mass (weight in grams) by the product of muscle L_0 (cm) and muscle density (assumed to be $1.06 g/cm^3$). CT and $1/2$ RT were measured as indices of isometric twitch kinetics. Total muscle shortening was determined as the maximum distance shortened during contraction. Shortening velocity was determined as the distance shortened during the initial 30 ms of shortening (Lewis *et al.*, 2015). Total muscle shortening was normalised to L_0 and expressed in L/L_0 . Shortening velocity was normalised to L_0 and expressed in L_0/s

4.2.6 Tissue collection

Real time polymerase chain reaction (RT-PCR) analysis: wild-type ($n = 7$) and *mdx* ($n = 6$) mice were anaesthetised with 5% isoflurane by inhalation in oxygen and euthanized by decapitation. The cervical spinal cord was isolated at the level of C3-C5 and immediately snap frozen in liquid nitrogen. This region of the spinal cord contains the phrenic motor nuclei in the mouse (Qiu *et al.*, 2010).

Immunohistochemical experiments: wild-type (n = 3) and *mdx* (n = 3) mice were deeply anaesthetised with 60mg/kg i.p. sodium pentobarbital (Euthatal; Abbeyville Veterinary Clinic, Cork, Ireland). Mice were transcardially perfused with saline (100 ml) followed by perfusion with 4% Paraformaldehyde (PFA). Spinal cord (C3-C5) was harvested and post-fixed overnight in 4% PFA at 4°C and then transferred to a 20% sucrose solution for cryo-protection for ~72hrs at 4°C. Spinal cords were embedded in optimum cutting temperature (OCT; VWR International, Dublin, Ireland) and frozen in isopentane (Sigma Aldrich, Wicklow, Ireland) cooled on dry ice. All tissues were then stored at -80°C until required for cryo-sectioning.

4.2.7 Spinal cord immunostaining

Spinal cord samples were removed from the -80°C and allowed to equilibrate at -22°C in a cryostat (Leica CM3050 S, Leica Biosystems). Samples were orientated to enable transverse sections to be obtained. Serial sections of 20 µm thickness were obtained starting at C5 and moving in a caudal to rostral fashion were collected and mounted on polysine-coated glass slides (VWR International, Dublin, Ireland). Sections were collected in series, with 4 sections per slide ensuring a difference of 100µm between each tissue section on a given slide. This allowed for a good distribution of key nuclei across multiple slides for comparative immunohistochemical investigation. Slides were allowed to dry at room temperature for 30 min before being stored at -80°C until required for staining. To examine astrocytes and microglia within the putative phrenic motor nucleus, sections were double-labelled with the neuronal marker NeuN (Millipore – 2726770), and glial fibrillary acidic protein (GFAP – DAKO – Z0334) or ionizing calcium-binding adaptor molecule 1 (Iba-1 – Wako - LAR1186). GFAP is a pan reactive astrocytic marker and Iba-1, is a microglia-specific calcium binding protein. Slides were removed from the -80°C and equilibrated at room temperature before staining. Transverse sections throughout the extent of C3-C5, were stained from wild-type and *mdx* mice (n = 3 per group). Individual sections were circled using a hydrophobic pap pen (Liquid Blocker Super PAP Pen, Ted Palla, Inc). Slides were washed with 0.1M PBS twice for 5 min. All sections were then blocked with 3% goat serum (Sigma G9023) and 20% Triton® X-100 (Tx-100) (Acrös 215682500) in 0.1M

PBS for 1 hour at room temperature. Following a wash with 0.1M PBS 2 x 5 min, primary antibodies were applied in a cocktail of (NeuN 1:200 and GFAP 1:1000) or (NeuN 1:200 and Iba1 1:800) in 0.1M PBS containing 0.1% Tx-100 (PBT). Negative control sections were run in parallel with omission of the primary antibodies. Following an overnight incubation at 4°C, slides were washed with PBT 3 x 10 min, then dH₂O x 5 min before application of specific secondary antibodies, Alexa flour 594 (1:100; Jackson 115585205) and a Fluorescein isothiocyanate (FITC) conjugated goat anti-rabbit IgG (1:500; Sigma F9887) for 90 min in the dark, at room temperature. Following a PBST 2 x 5 min wash slides were incubated with DAPI (1:500 in 0.1M PBS), washed with PBS (5 min) before cover slipping with Fluoromount (Sigma F460).

Image analysis: All slides were viewed and images were digitally captured using an Olympus BX51 microscope and an Olympus DP71 and camera. Images were taken of each region of interest at x10/x20 magnification. Quantitative analysis of GFAP and Iba-1 positive cell numerical density (%) was measured using Image J, by analysing cell counts of 8-bit FITC (green) channel, within a 250µm² discrete area of motor nuclei by counting the number of GFAP- or Iba-1 positive cells and expressing them as a % of the total nuclei x 100 per area. Only cells which displayed activated morphology (astrocytes: 3 or more projections, and microglia: amoeboid in shape) were included in the analysis. Multiple images were captured and averaged per animal before comparing group means.

4.2.8 Terminal deoxynucleotidyl Transferase (TdT) dUTP Nick-End Labelling assay (TUNEL assay)

To investigate cellular apoptosis in the spinal cord, TUNEL (terminal deoxynucleotide transferase-mediated dUTP nick end labelling) staining was performed. Transverse sections throughout the C3-C5 region were stained from wild-type and *mdx* mice (n = 3 per group). Slides were removed from the -80°C and equilibrated at room temperature before staining using the ApopTag® Peroxidase *In Situ* Apoptosis Detection Kit (Millipore S7100) according to the manufacturer's instructions. DNAase-treated slides were used as a positive control (Fig. 4.6B).

4.2.9 High performance liquid chromatography (HPLC)

Monoamines and metabolites important in the neurochemical control of breathing, including noradrenaline (NA), 5-hydroxytryptamine (5-HT) and 5-hydroxyindoleacetic acid (5-HIAA), were quantified using high performance liquid chromatography (HPLC), as previously described, in the cervical spinal cord (C3-C5 region) of wild-type (n = 9) and *mdx* (n = 9) mice.

Experimental protocol: Frozen samples were thawed in 500 μ l of chilled homogenising buffer spiked with 2ng/20 μ l of N-Methyl 5-HT (Sigma, UK) as internal standard, sonicated for 2 x 4 s bursts (Bandelin Sonoplus HD 2070) and centrifuged at 14,000 RPM for 20 mins at 8°C (MIKRO 22 R refrigerated centrifuge). 20 μ l of supernatant was injected onto the HPLC system (Electrochemical Detection). The mobile phase contained 0.1M citric acid, 0.1M sodium dihydrogen phosphate, 0.01mM EDTA (Fisher Scientific Ireland), 5.6mM octane-1-sulphonic acid (Sigma) and 11% (v/v) HPLC-grade methanol (Fisher Scientific IRELAND), and was adjusted to pH 2.8 using 4N sodium hydroxide (Alkem/Reagecon). A reverse-phase column (Kinetex 2.6u C18 100 x 4.6mm, Phenomenex, UK) maintained at 30°C was employed in the separation (Flow rate 0.9ml/min), the glassy carbon working electrode combined with an Ag/AgCL reference electrode (Shimadzu) was operated at +0.8V and the chromatograms generated were analysed using Class-VP 5 software (Shimadzu, Corporation, Kyoto, Japan). Neurotransmitters and their precursors/metabolites were identified by their characteristic retention times as determined by standard injections which were run at regular intervals during the sample analysis.

Data analysis: The chromatograms were processed using Class 5-VP software (Shimadzu Corporation, Kyoto, Japan). Analyte: Internal standard peak height ratios were measured and compared with standard injections and results were expressed as ng of analyte per g tissue weight.

4.2.10 RNA extraction and real-time polymerase chain reaction (RT-PCR)

RNA was isolated from the spinal cord samples using a Nucleospin RNAII kit (Macherey-Nagel GmbH, Germany). RNA quantity and purity was assessed by spectrophotometry with a Nanospec (Nanodrop Lite, Thermo Scientific, USA). RNA was reverse transcribed into complimentary DNA (cDNA) using a Transcriptor First Strand cDNA Synthesis Kit (Roche Products Ireland Ltd) as per manufacturer's instructions. Equal concentrations of cDNA were prepared for reverse transcription polymerase chain reaction (PCR) amplification. cDNA was amplified using Realtime ready Catalog or Custom Assays (Roche Diagnostics Ltd) or "Taqman Gene Expression Assays" containing forward and reverse primers and a FAM-labelled MGB Taqman probe for each gene (Applied Biosystems; Table 4.1) and SensiFAST™ Probe Hi-ROX Kit (Bioline). Real-time PCR was completed using an ABI Prism 7300 instrument (Applied Biosystems). Assay IDs are shown in Table 4.1. Relative mRNA expression was normalised to β -actin used as the endogenous control. Relative gene expression was calculated using the $\Delta\Delta$ CT method with Applied Biosystems RQ software (Applied Biosystems).

Gene title	Gene symbol	Assay ID	Configuration number
Dystrophin	Dmd	317524	1001317524
B-actin	Actb	307903	Mm00607939_s1
NF- κ B	Nfkb1	300085	1001300085
TNF α	Tnf	314800	1001314800
GFAP	Gfap	311752	Mm01253033_m1
CD11b	Itgam	26G09	Mm00434455_m1
IL-6	Il6	300699	1001300699
HIF-1 α	Hif1a	300617	1001300617
HIF-2 α	Epas1	314102	1001314102
iNOS	Nos2	300665	1001300665

Table 4.1 Real-time ready catalog and custom assays used for cDNA amplification.

4.2.11 Statistical analysis

Values are expressed as mean \pm SD or as box and whisker plots (median, 25-75 percentile, and scatter plot). Data were statistically compared using Prism 6.0 (Graphpad Software, San Diego, CA, USA). Data were tested for normal distribution and equal variances. Data sets which were normally distributed and of equal variance were statistically compared using unpaired two-tailed Student's *t* test. Welch's correction was applied in the case of unequal variance. Data which were not normally distributed were compared using Mann Whitney non-parametric tests. Data for diaphragm muscle force-frequency relationship and ventilatory responsiveness to chemostimulation were statistically compared by repeated measures two-way ANOVA (frequency x gene) with Bonferroni *post hoc* test. *P* < 0.05 was considered statistically significant in all tests.

4.3 Results

4.3.1 Breathing variability

Figure 4.1 shows Poincaré plots of the breath-to-breath (BB_n) and subsequent interval (BB_{n+1}) of 200 consecutive breaths for expiratory duration (T_e ; A and B) and total breath duration (T_{tot} ; E and F) in wild-type (A and E; open) and *mdx* (E and F; grey) mice. Assessment of the short-term (SD1) and long-term (SD2) variability of breathing indicated no evidence of respiratory instability for T_e (Fig. 4.1C and D; SD1 and SD2, respectively) and T_{tot} (Fig. 4.1 G and H; SD1 and SD2, respectively) in *mdx* compared with wild-type mice.

Figure 4.1 shows representative respiratory flow traces illustrating a sigh and post-sigh apnoeas (I) and a spontaneous apnoea (J) in a wild-type mouse during normoxia. Analysis of sighs revealed no difference in the frequency of sighs ($P = 0.3106$; Mann Whitney test; Fig. 4.1K) between wild-type and *mdx* mice. Similarly, no difference was observed in the frequency of post-sigh apnoeas ($P = 0.8157$; unpaired Student's *t* test; Fig. 4.1M) and the duration of post-sigh apnoeas ($P = 0.9460$; unpaired Student's *t* test; Fig. 4.1N). Analysis of spontaneous apnoeas, which were infrequent, showed no difference in the frequency of spontaneous apnoeas ($P = 0.4881$; Mann Whitney test; Fig. 4.1O) and the duration of apnoeas ($P = 0.1333$; Mann Whitney test; Fig. 4.1P).

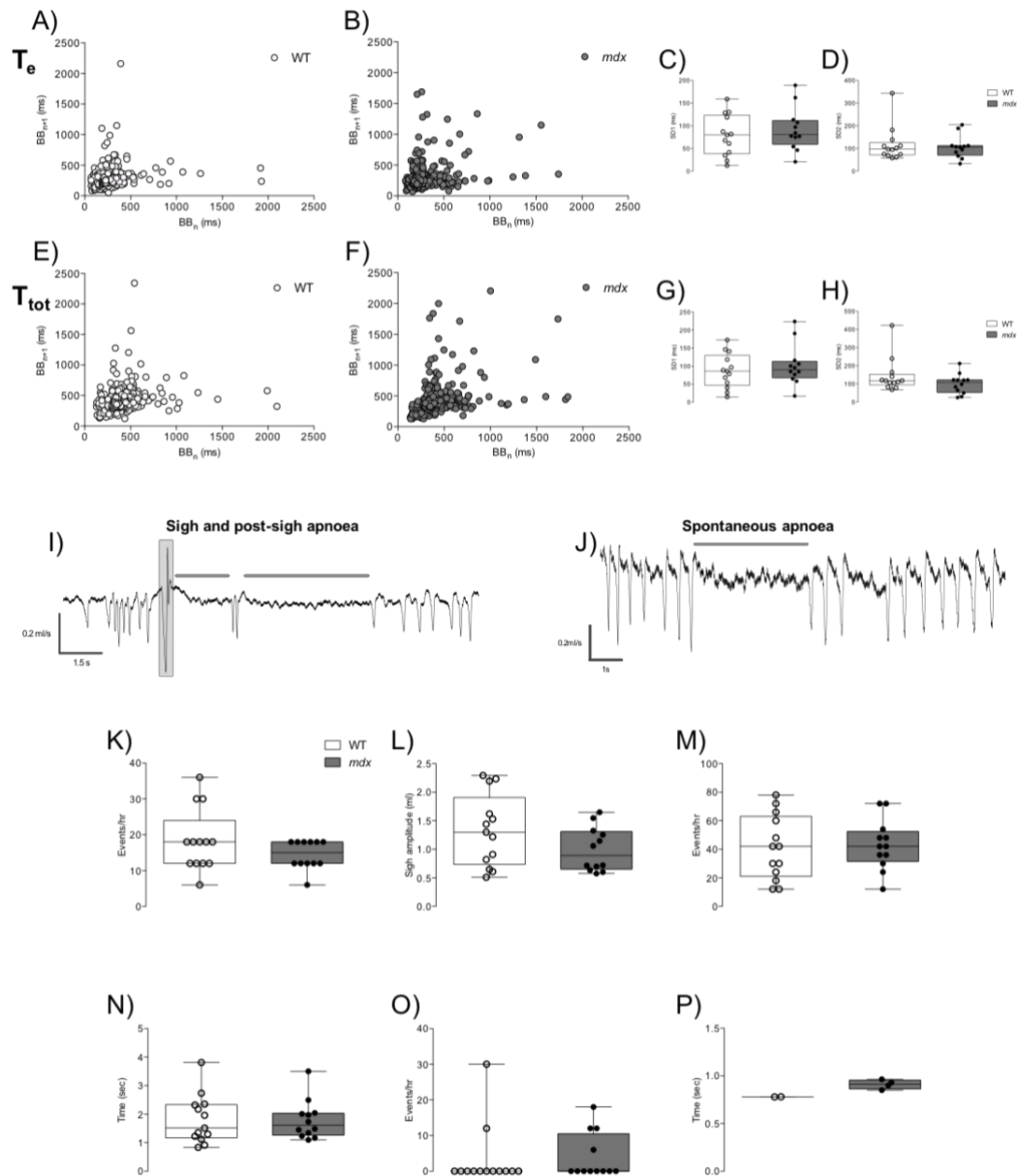
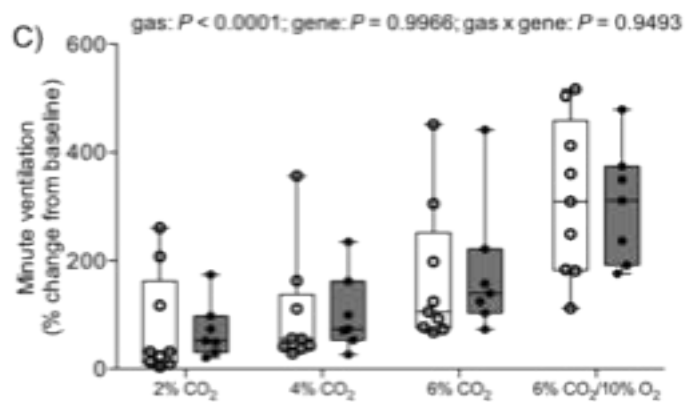
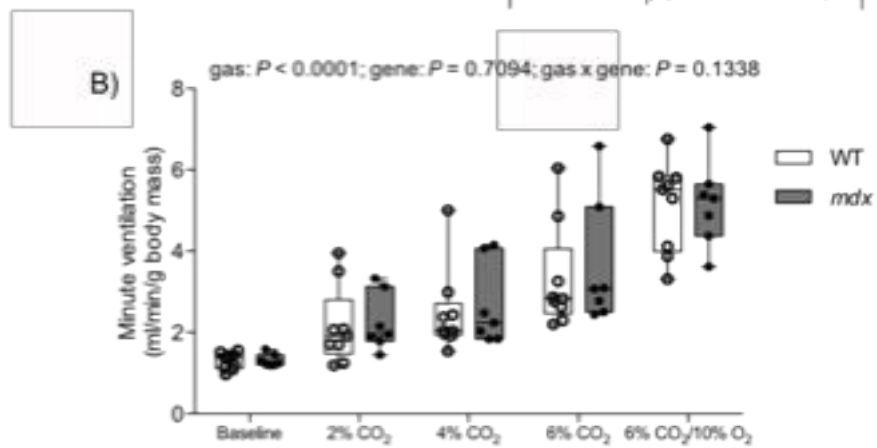
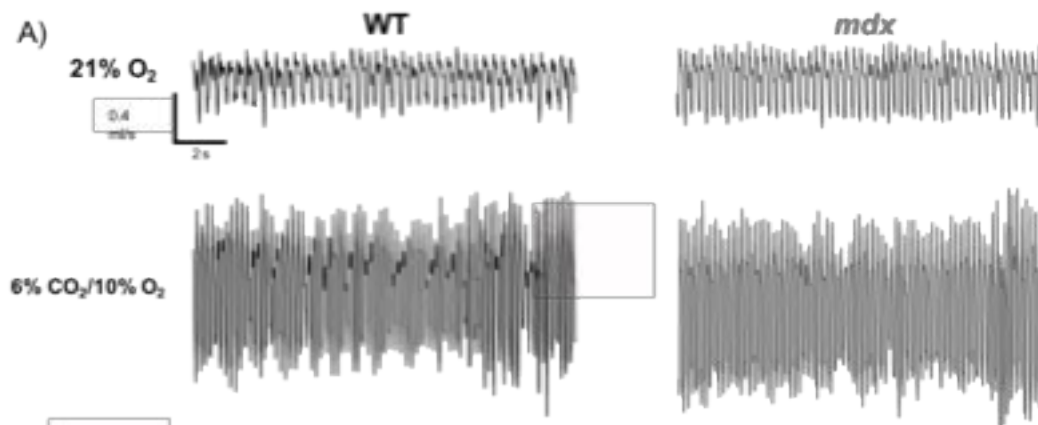


Figure 4.1 Respiratory measurements in conscious mice

A and B, Poincaré plot of breath-to-breath (BB_n) and subsequent breath-to-breath (BB_{n+1}) interval of expiratory duration (T_e) over 200 consecutive breaths for wild-type (A; WT) and *mdx* (B) mice. C and D, group data of short-term (C; SD1) and long-term (D; SD2) variability of breathing based on T_e for WT ($n = 13$) and *mdx* ($n = 12$) mice. E and F, Poincaré plot of BB_n and BB_{n+1} of total breath duration (T_{tot}) over 200 consecutive breaths for WT (E) and *mdx* (F) mice. G and H, group data of SD1 (G) and SD2 (H) based on T_{tot} for WT and *mdx* mice. For SD1 and SD2, values are expressed as scatter point box and whisker plots (median, 25-75 centile and scatter plot). Data were statistically compared by unpaired Student's *t* tests or Mann Whitney non-parametric test. I and J, representative respiratory flow traces showing a sigh (grey shading) and post-sigh apnoeas (grey line) in a WT mouse (I) and a spontaneous apnoea (grey line) in a WT mouse (J) during normoxia. K, L, M, N, O and P, group data for sigh frequency (K) and amplitude (L), post-sigh apnoea frequency (M) and duration (N) and spontaneous apnoea frequency (O) and duration (P) occurring during normoxia for WT and *mdx* mice. Values are expressed as scatter point box and whisker plots (median, 25-75 percentile and scatter plot). Data were statistically compared by unpaired Student's *t* tests or Mann Whitney non-parametric tests.

4.3.2 Ventilatory responsiveness to hypercapnic hypoxia

Figure 4.2 shows representative respiratory flow traces for wild-type and *mdx* mice during exposure to baseline air and hypercapnic-hypoxia (asphyxia). Chemostimulation with graded hypercapnia and asphyxia resulted in a significant increase in minute ventilation ($P < 0.0001$ (gas); repeated measures two-way ANOVA; Fig. 4.2B) for both wild-type and *mdx* mice, with no difference between groups. Ventilatory responsiveness to gas challenge expressed as % change from baseline was not different between wild-type and *mdx* mice (Fig. 4.2C).



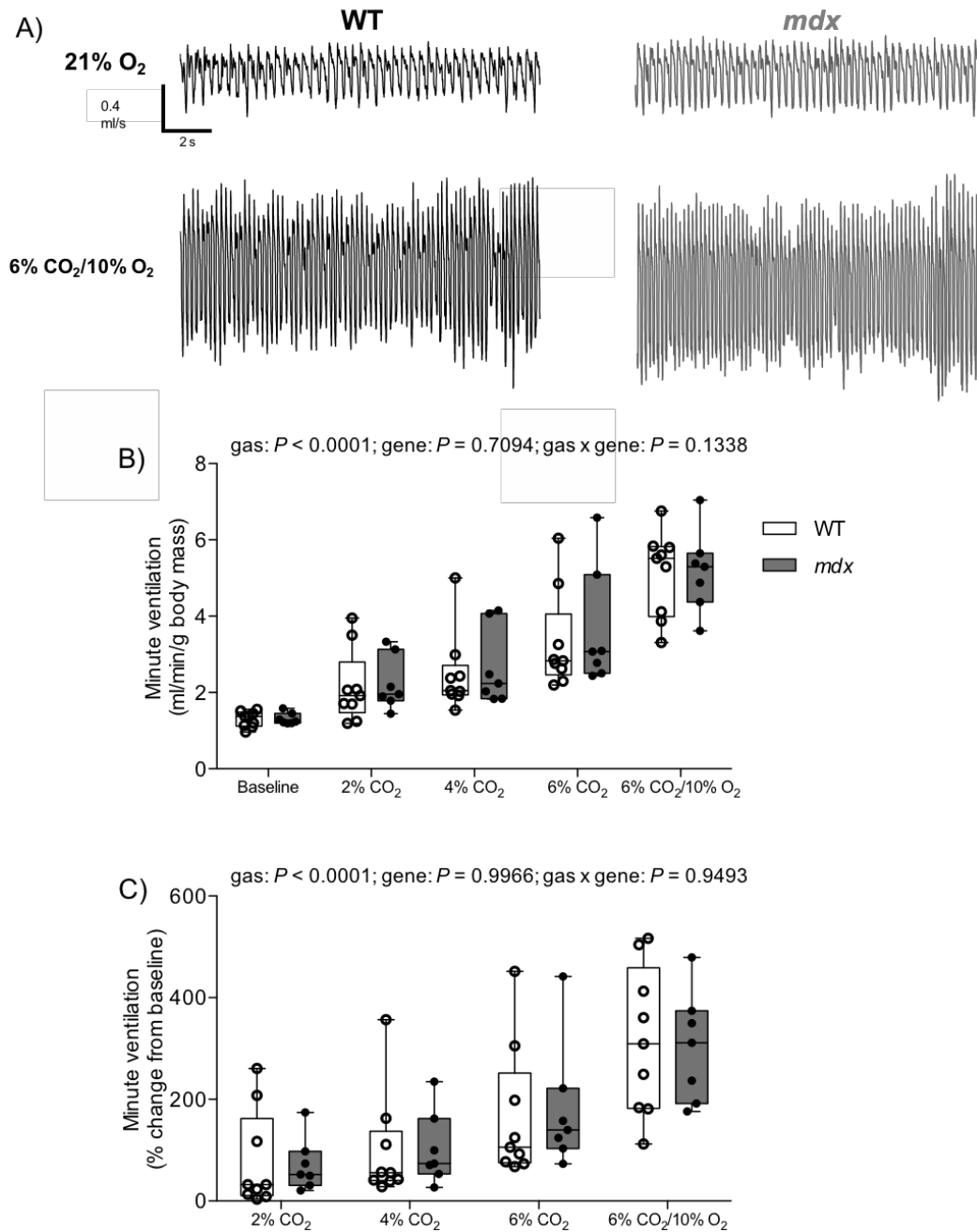


Figure 4.2 Ventilation in response to chemostimulation in conscious mice

A, representative respiratory flow traces during normoxia (21% O₂) and hypercapnic-hypoxia (6% CO₂/10% O₂) in a wild-type (black; WT) and *mdx* mouse (grey); inspiration downwards. B, group data for peak minute ventilation during graded hypercapnia (2, 4 and 6% CO₂) and hypercapnic-hypoxia. C, group data for ventilatory responsiveness to chemostimulation (expressed as % change from baseline). Values are expressed as scatter point box and whisker plots (median, 25-75 percentile and scatter plot). Data were statistically compared by repeated measures two-way ANOVA.

4.3.3 Oesophageal pressure and diaphragm EMG activity in vivo

Representative original recordings of oesophageal pressure and diaphragm EMG during baseline conditions (60% O₂) and during an augmented breath are shown in figure 4.3A. Table 4.2 shows baseline respiratory measurements in wild-type and *mdx* mice. Respiratory frequency was significantly higher in *mdx* mice compared with wild-type ($P < 0.0001$; unpaired Student's *t* test; Table 4.2). There was no significant difference in SpO₂ and ETCO₂ between wild-type and *mdx* mice (Table 4.2).

Peak inspiratory oesophageal pressure during baseline was equivalent between wild-type and *mdx* mice ($P = 0.2887$; unpaired Student's *t* test; Fig. 4.3B). Baseline diaphragm EMG activity was significantly lower in *mdx* ($P = 0.025$; unpaired Student's *t* test with Welch's correction; Fig. 4.3C) compared with wild-type. The peak inspiratory oesophageal pressure response (Δ amplitude) to asphyxia revealed a trend towards a significant increase in responsiveness in *mdx* mice compared with wild-type ($P = 0.08$; unpaired Student's *t* test with Welch's correction; Fig. 4.3D); diaphragm EMG response to asphyxia (Δ amplitude) was not different between wild-type and *mdx* ($P = 0.27$; unpaired Student's *t* test with Welch's correction; Fig. 4.3E). The magnitude of the change in peak inspiratory oesophageal pressure during an augmented breath was significantly greater in *mdx* ($P = 0.0006$; unpaired Student's *t* test; Fig. 4.3F) compared with wild-type mice; the magnitude of the change in diaphragm EMG during an augmented breath was equivalent between wild-type and *mdx* mice ($P = 0.4341$; unpaired Student's *t* test; Fig. 4.3G).

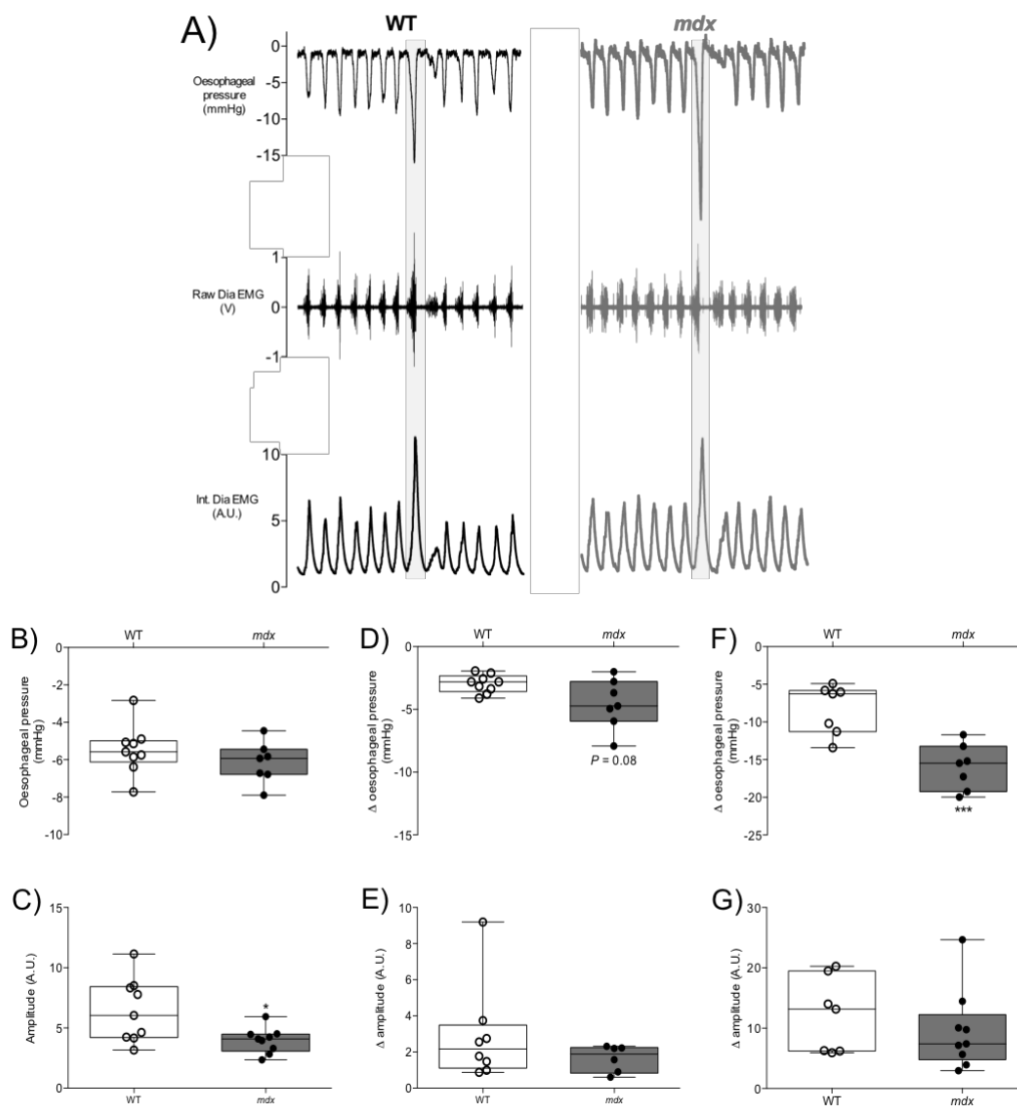


Figure 4.3 Oesophageal pressure and diaphragm muscle EMG activity in anaesthetised mice

A, representative traces of oesophageal pressure and diaphragm (Dia) muscle raw and integrated (Int.) EMG activity for a wild-type (WT) mouse (black) and *mdx* mouse (grey) during baseline (60% inspired O_2) and an augmented breath (shaded). B and C, group data for oesophageal pressure (B) and diaphragm muscle integrated EMG activity (C) during baseline conditions (both expressed as amplitude) for WT ($n = 7-9$) and *mdx* ($n = 7-9$) mice. D and E, group data for oesophageal pressure (D) and diaphragm muscle integrated EMG activity (E) in response to an asphyxiant gas challenge for WT and *mdx* mice. Both expressed as delta values. F and G, group data for oesophageal pressure (F) and diaphragm muscle integrated EMG activity (G) during an augmented breath for WT and *mdx* mice. Values are expressed as scatter point box and whisker plots (median, 25-75 percentile and scatter plot). Data were statistically compared by unpaired Student's t tests or Mann Whitney non-parametric test. * $P = 0.025$ (Fig. 4.3C), *** $P = 0.0006$ (Fig. 4.3F) compared with corresponding WT values.

	WT	<i>mdx</i>	<i>P</i> (Student's <i>t</i> test)
	(n = 9)	(n = 9)	
f_R (bpm)	195.1 ± 10.8	229.6 ± 10.6	< 0.0001
SpO ₂ (%)	97.2 ± 1.9	96.5 ± 2.0	0.4069
ETCO ₂ (%)	4.4 ± 0.4	4.0 ± 0.4	0.0966
Body mass (g)	24.9 ± 1.8	25.0 ± 2.3	0.911

Table 4.2 Baseline respiratory parameters in anaesthetised mice

Definition of abbreviations: f_R , respiratory frequency; SpO₂, peripheral capillary oxygen saturation; ETCO₂, end-tidal carbon dioxide; WT, wild-type. Data are shown as mean ± SD and were statistically compared using unpaired Student's *t* tests.

4.3.4 Diaphragm muscle contractile function ex vivo

Figure 4.4 shows representative original traces for wild-type (black) and *mdx* (grey) diaphragm twitch (A) and tetanic (B) contractions, force-frequency relationship (C) and maximal unloaded shortening (D). Twitch kinetics (CT and $\frac{1}{2}$ RT) and isotonic contractile parameters (S_{max} and V_{max}) are shown in Table 4.3. Twitch contraction time was significantly increased in *mdx* compared with wild-type diaphragm ($P = 0.027$; unpaired Student's *t* test). Twitch half-relaxation time and isotonic contractile parameters were not significantly different between wild-type and *mdx* diaphragm preparations. Diaphragm twitch ($P = 0.0241$; unpaired Student's *t* test; Fig. 4.4E, P_t) and tetanic force ($P < 0.0001$; unpaired Student's *t* test with Welch's correction; Fig. 4.4E, P_o) were both significantly depressed in *mdx* compared with wild-type. For the force-frequency relationship, diaphragm specific force was significantly lower in *mdx* compared with wild-type preparations ($P = 0.0003$ (genotype); repeated measures two-way ANOVA; Fig. 4.4F). *Post hoc* analysis revealed significant force depression in *mdx* across a broad range of stimulation frequencies (60-160 Hz).

	WT (n = 8)	<i>mdx</i> (n = 9)	<i>P</i> (Student's <i>t</i> test)
CT (ms)	17.3 ± 2.3	20.3 ± 2.6	0.027
$\frac{1}{2}$ RT (ms)	19.6 ± 6.9	23.2 ± 4.3	0.2177
S_{max} (L/ L_o)	0.36 ± 0.07	0.30 ± 0.13	0.3252
V_{max} (L_o /s)	4.1 ± 1.1	3.3 ± 1.9	0.3373

Table 4.3 Ex vivo diaphragm muscle contractile kinetics

Definition of abbreviations: CT, contraction time; $\frac{1}{2}$ RT, half-relaxation time; S_{max} , peak shortening; V_{max} , peak shortening velocity; L_o , optimum length. Data are shown as mean ± SD and were statistically compared using unpaired Student's *t* tests.

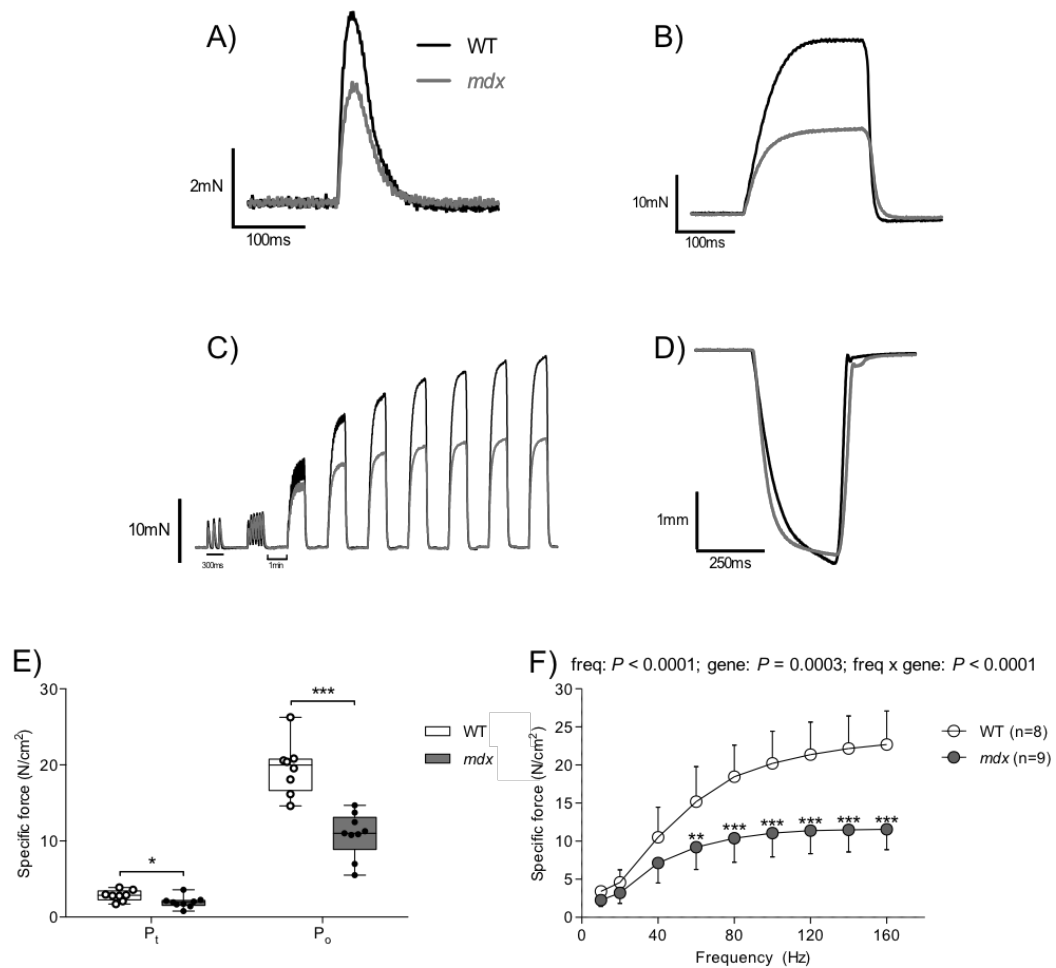


Figure 4.4 Ex vivo diaphragm muscle contractile function

A, B, C, and D, original traces of *ex vivo* diaphragm muscle twitch contraction (A), tetanic contraction (B), force-frequency relationship (C) and maximum unloaded shortening (D) for wild-type (WT; black) and *mdx* (grey) preparations. E, group data for diaphragm muscle twitch (P_t) and tetanic (P_o) force in WT (n = 8) and *mdx* (n = 9) mice. Tetanic force was measured following stimulation at 100 Hz *ex vivo*. Values are expressed as scatter point box and whisker plots (median, 25-75 percentile and scatter plot). Data were statistically compared by unpaired Student's *t* tests. * $P < 0.05$, *** $P < 0.001$ compared with corresponding WT value. F, group data (mean \pm SD) for diaphragm muscle force-frequency relationship *ex vivo* in WT (open) and *mdx* (grey) preparations. Data were statistically compared by repeated measures two-way ANOVA (frequency x gene) followed by Bonferroni *post hoc* test. ** $P < 0.01$ *** $P < 0.001$ compared with corresponding WT value.

4.3.5 Cervical spinal cord immune cell density

Figure 4.5 shows representative images for wild-type and *mdx* C3-C5 spinal cords immuno-fluorescently labelled with GFAP (a pan reactive astrocytic marker; Fig. 4.5A) and Iba-1 (a microglia-specific calcium binding protein; Fig. 4.5B). Circles identify the putative phrenic motor nucleus. There was no significant difference in GFAP positive cell counts (numerical density %) ($P = 0.1497$; unpaired Student's *t* test; Fig. 4.5C) between wild-type and *mdx* spinal cords. Similarly, there was no significant difference in IBA-1 positive cell counts ($P = 0.0823$; unpaired Student's *t* test; Fig. 4.5D), between wild-type and *mdx* spinal cords. Figure 4.6A shows spinal cord sections examined for cellular apoptosis using TUNEL assay. The ventral horn of the C3-C5 spinal cord, which contains the phrenic motor nucleus was devoid of brown apoptotic bodies in wild-type and *mdx* sections ($0.16 \pm 0.2\%$ versus $0.09 \pm 0.2\%$ TUNEL positive cell counts, unpaired Student's *t* test, $P = 0.6499$ for wild-type versus *mdx* (n=3 each) mice).

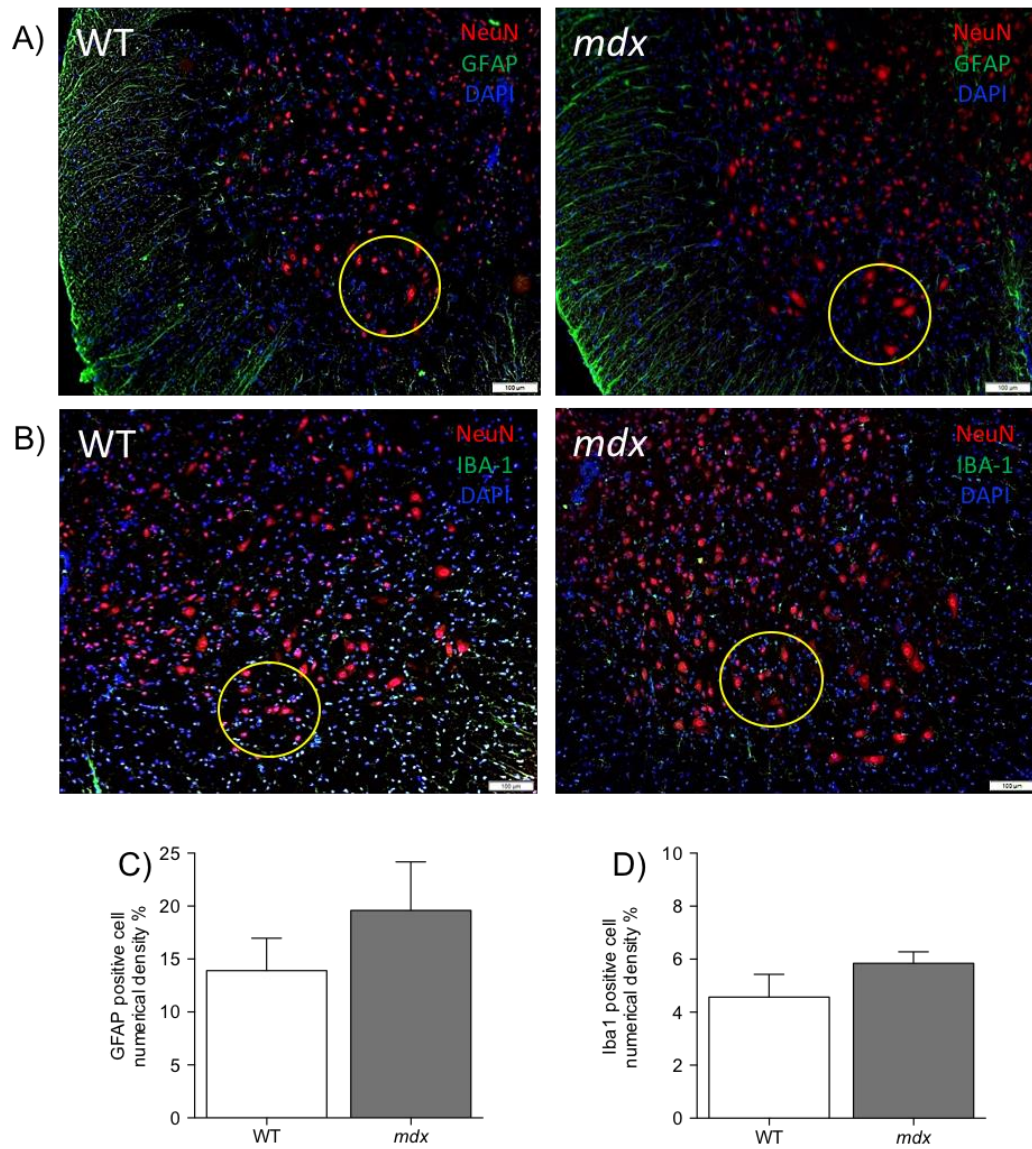


Figure 4.5 Cervical spinal cord immunohistochemistry

A and B, representative images of the ventral horn of the spinal cord (C3-C5 region) of wild-type (WT) and *mdx* mice immuno-fluorescently labelled for glial fibrillary acidic protein (A; GFAP, green) or ionizing calcium-binding adaptor molecule (B; Iba-1, green), NeuN (neuronal marker, red) and DAPI (nuclear stain, blue). Circles identify the putative phrenic motor nucleus. C and D, group data (mean \pm SD) for GFAP (C) and IBA-1 (D) positive cells in the putative phrenic motor nucleus of WT and *mdx* mice. Data were statistically compared by unpaired Student's *t* tests.

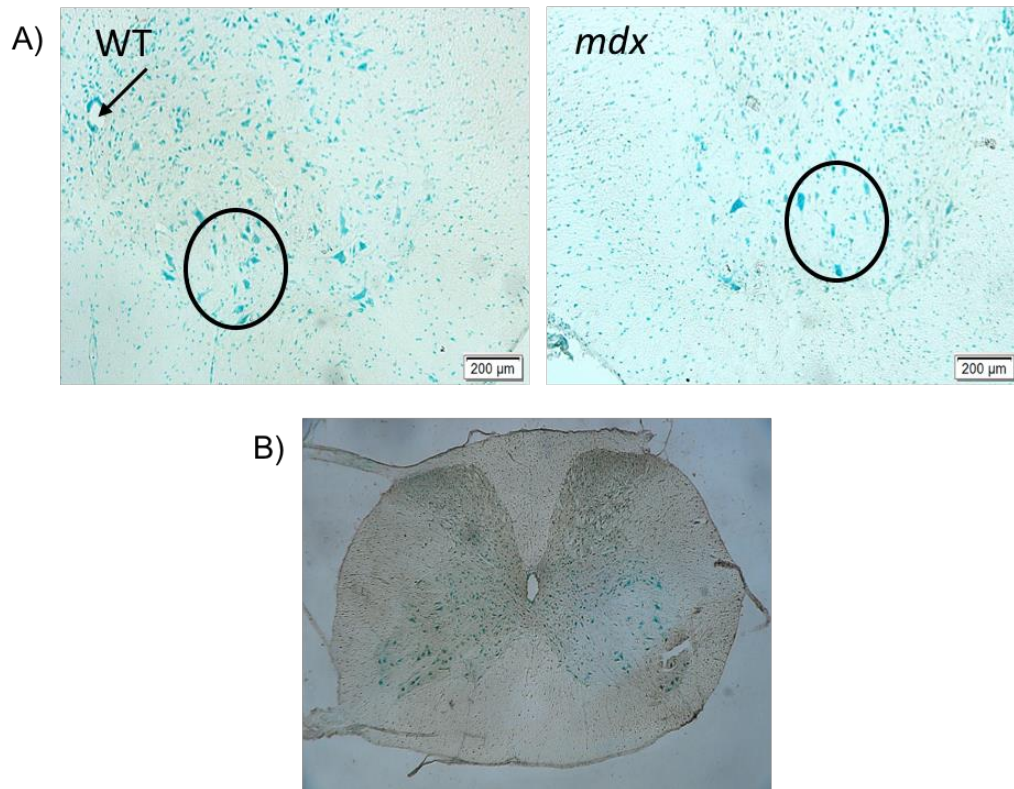


Figure 4.6 Cervical spinal cord TUNEL assay

A, representative images of terminal deoxynucleotidyl transferase dUTP nick end labelling (TUNEL) in the ventral horn of C3-5 region of the spinal cord for wild-type (WT) and *mdx* mice. Images from WT and *mdx* are devoid of brown apoptotic bodies. Circles identify the putative phrenic motor nucleus. B, shows positive control, DNAase-treated spinal cord displaying brown apoptotic bodies. Arrow indicates the central canal.

4.3.6 Cervical spinal cord monoamine concentration

Monoamine concentrations were determined in the C3-C5 spinal cord of wild-type and *mdx* mice (Fig. 4.7). Levels of NA and 5-HT and its metabolite 5-HIAA were quantified using HPLC. The concentration of NA ($P < 0.0001$; unpaired Student's *t* test; Fig. 4.7A) and 5-HT ($P = 0.0006$; unpaired Student's *t* test; Fig. 4.7B) were significantly increased in the C3-C5 spinal cord in *mdx* compared with wild-type. There was no significant difference in 5-HIAA concentration ($P = 0.1769$; Mann Whitney non-parametric test; Fig. 4.7C) between wild-type and *mdx* spinal cords.

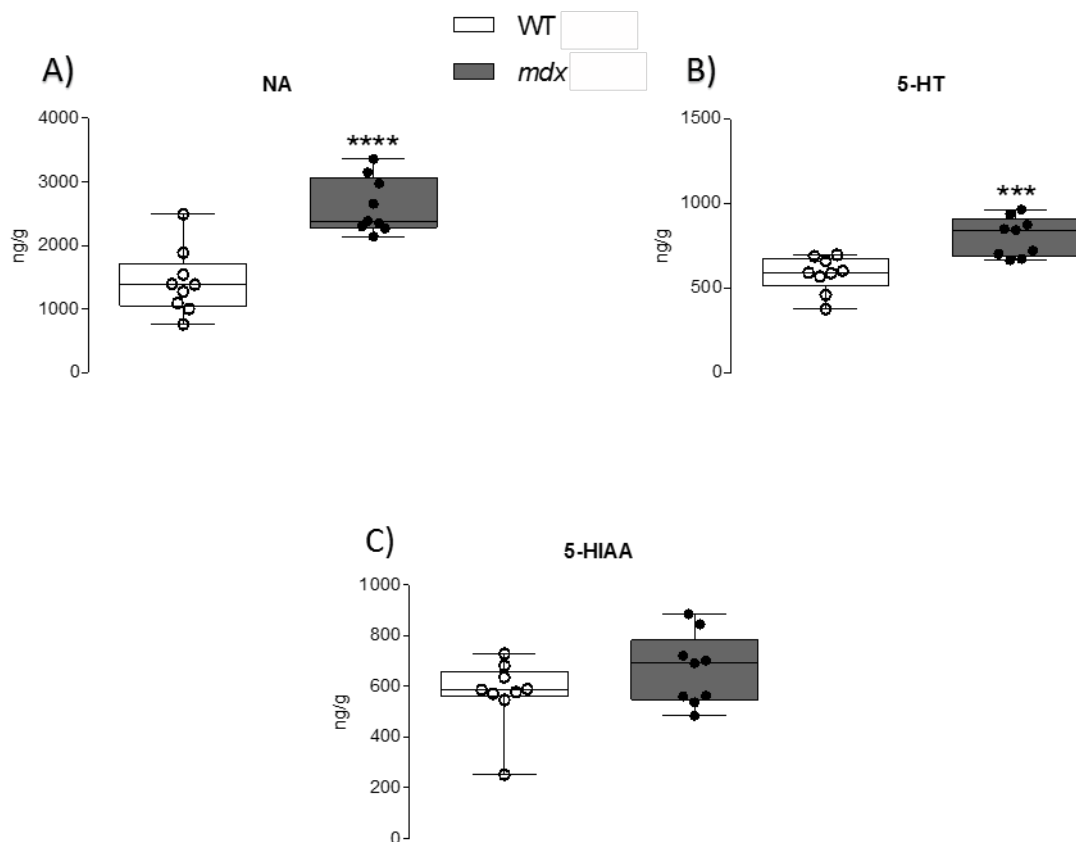


Figure 4.7 Cervical spinal cord monoamine concentration

A, B, and C, group data for the concentrations of noradrenaline (A; NA), 5-hydroxytryptamine (B; 5-HT) and 5-hydroxyindoleacetic acid (C; 5-HIAA) in the spinal cord (C3-C5 region) of wild-type (WT) and *mdx* mice. Values are expressed as scatter point box and whisker plots (median, 25-75 percentile and scatter plot). Data were statistically compared by unpaired Student's *t* tests or Mann Whitney non-parametric test. **** $P < 0.0001$ (Fig. 4.7A), *** $P = 0.0006$ (Fig. 4.7B), compared with corresponding WT value.

4.3.7 Cervical spinal cord gene expression

Messenger RNA (mRNA) levels were assessed in the C3-C5 spinal cord of wild-type and *mdx* mice (Fig. 4.8). Dystrophin mRNA was expressed in the cervical spinal cord of wild-type mice; dystrophin mRNA was significantly lower in *mdx* mice compared with wild-type ($P = 0.004$; unpaired Student's *t* test). GFAP mRNA was significantly lower in the spinal cord of *mdx* mice compared to wild-type ($P = 0.0173$). There were no significant differences in the expression of NF κ B, TNF- α , CD11b, IL-6, HIF-1 α , HIF-2 α and iNOS between wild-type and *mdx* cervical spinal cords.

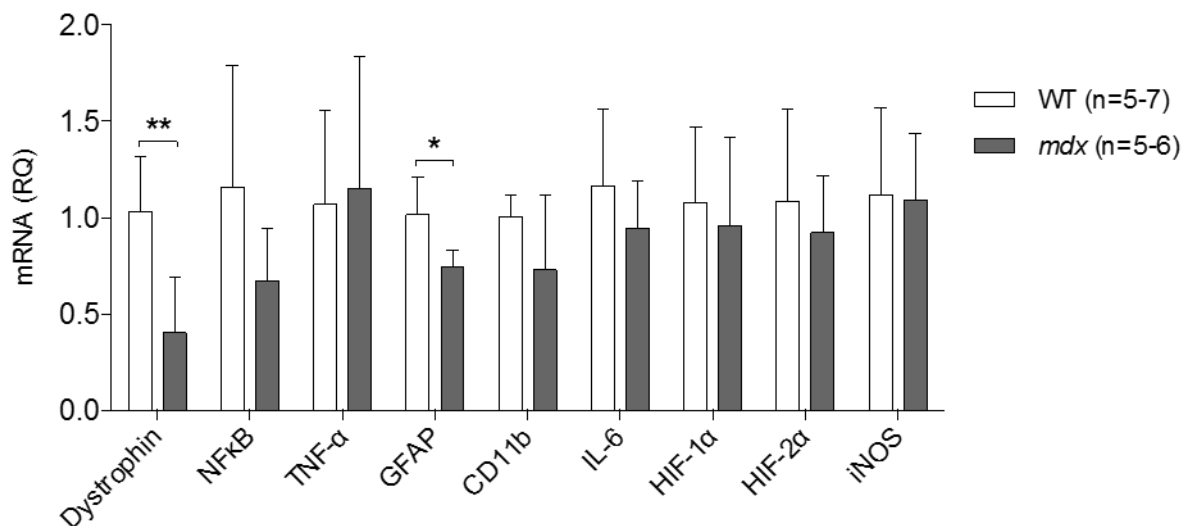


Figure 4.8 Cervical spinal cord gene expression analysis

Group data (mean \pm SD) for messenger RNA (mRNA) expression in spinal cord (C3-C5 region) of wild-type (WT) and *mdx* mice. Data were statistically compared by unpaired Student's *t* tests. * $P = 0.0173$, ** $P = 0.004$ compared with corresponding WT value. *Definition of abbreviations:* NF κ B, nuclear factor kappa-light-chain-enhancer of activated B cells; TNF- α , tumour necrosis factor alpha; GFAP, glial fibrillary acidic protein; CD11b, cluster of differentiation molecule 11B; IL-6, interleukin-6; HIF, hypoxia-inducible factor; iNOS, inducible nitric oxide synthase.

4.4 Discussion

The main findings of this study are: (i) there is no evidence of respiratory instability in young *mdx* mice; (ii) ventilatory capacity in response to maximum chemostimulation is equivalent between *mdx* and wild-type mice; (iii) despite substantial diaphragm muscle weakness, inspiratory oesophageal pressure generation is equivalent during basal and chemoactivated breathing and is greater during augmented breaths in *mdx* mice compared with wild-type; (iv) monoamine concentrations are elevated in the cervical spinal cord of *mdx* mice; (v) the density of activated astrocytes and microglia is equivalent in *mdx* and wild-type cervical spinal cords; (vi) dystrophin mRNA is expressed in the cervical spinal cord of wild-type mice, and expression is significantly lower in *mdx*; (vii) there is no increase in pro-inflammatory gene expression in *mdx* cervical spinal cords. Despite profound diaphragm dysfunction, ventilatory capacity is well preserved in *mdx* mice, probably through increased drive in accessory motor pathways of breathing.

Dystrophin is expressed in the CNS (Lidov, 1996), but the effect of dystrophin deficiency on respiratory rhythm and stability is not well described. Increased respiratory instability has the potential to contribute to disordered breathing during sleep, which is a feature of DMD (LoMauro *et al.*, 2017). Dysregulated control of respiratory timing could exacerbate ventilatory insufficiency in DMD due to recognised mechanical deficits. Our study demonstrated that respiratory timing variability in young *mdx* mice is equivalent to age-matched wild-type mice. Moreover, we observed no increase in the propensity for post-sigh or spontaneous apnoea during normoxia in *mdx* mice. Similarly, the frequency of augmented breaths (sighs) examined during normoxia was not different in *mdx* mice compared with wild-type. Our study cannot rule out a potential emergence of unstable respiratory timing in later stages of the progressive disease, but suggests that dystrophin deficiency does not manifest an overt respiratory control phenotype at a disease stage characterised by respiratory muscle pathology.

Our study confirmed substantial diaphragm muscle weakness in young *mdx* mice, consistent with our recent reports (Burns *et al.*, 2017a; Burns *et al.*, 2017c).

Diaphragm deficits in *mdx* mice were evidenced by significantly reduced twitch and tetanic isometric force compared with wild-type. The force-frequency relationship revealed considerable force loss in the frequency range of 60-160 Hz, corresponding to a broad range of ventilatory behaviours (Sieck *et al.*, 2013; Mantilla *et al.*, 2014). We have previously documented considerable muscle fibre damage and remodelling in dystrophic diaphragm at this age, with increased variability of muscle fibre size and centralised myonuclei (Burns *et al.*, 2017c).

We assessed ventilation in response to hypercapnic, and hypercapnic hypoxic (asphyxic) challenges, which revealed a remarkable capacity for *mdx* mice to enhance ventilation, despite substantial intrinsic diaphragm muscle weakness. Peak ventilation during graded hypercapnia was equivalent in *mdx* and wild-type mice, revealing that CO₂ chemosensitivity is intact in *mdx* mice, which retain considerable ventilatory reserve and, notwithstanding diaphragm dysfunction, maintain a capacity to elevate minute ventilation (through rate and volume changes) to wild-type levels. This impressive preserved capacity to elevate pulmonary ventilation was revealed during exposure to hypercapnic hypoxia with peak ventilation increasing more than 3-fold in *mdx* mice, equivalent to wild-type values. We acknowledge that compensatory mechanisms supporting ventilatory capacity early in disease progression may not prevail at later stages. Indeed, in older animals, blunted ventilatory responses to hypercapnic challenge have been observed in 7- and 16-month-old *mdx* mice (Gosselin *et al.*, 2003; Gayraud *et al.*, 2007). In DMD, there is a progressive decline in pulmonary function and respiratory muscle strength culminating in reduced ventilation (Smith *et al.*, 1989; De Bruin *et al.*, 1997; Hukins & Hillman, 2000; Khirani *et al.*, 2014). There is a paucity of data within the literature examining ventilatory responsiveness to hypercapnia in DMD patients.

In anaesthetised mice, we demonstrated that peak inspiratory oesophageal pressure generation was equivalent during basal breathing ($F_{iO_2} = 0.6$) in *mdx* and wild-type mice. Acute chemoactivation ($F_{iO_2} = 0.15$ and $F_{iCO_2} = 0.05$) increased ventilatory drive and the magnitude of the enhanced peak inspiratory oesophageal

pressure was equivalent in *mdx* and wild-type mice. This revealed that there is no apparent mechanical deficit limiting sub-atmospheric pressure generating capacity in young adult *mdx* mice. Considering the substantial diaphragm weakness and the force-frequency relationship of *mdx* diaphragm compared with wild-type, a rightward shift associated with increased chemoactivation produces only a small increment in force-generating capacity in the severely weakened *mdx* diaphragm. The increase in force above that required for basal breathing might suffice in generating the subatmospheric pressures required for chemoactivated breathing. Alternatively, potentiated neural recruitment of the diaphragm via the phrenic nerve (corresponding to a further right-shift in the force-frequency relationship) might facilitate inspiratory pressure generating capacity in *mdx* mice. Indeed, in support of this latter notion, we have recently reported apparent compensatory neuroplasticity in the motor drive to the diaphragm under some circumstances in *mdx* compared with wild-type mice (Burns *et al.*, 2017c). However, in the present study, the diaphragm EMG response to hypercapnic hypoxia was not potentiated in *mdx* mice compared with wild-type responses. This suggests that either the weakened diaphragm in *mdx* is sufficient to support ventilatory demand during chemoactivation (without neural compensation by way of added recruitment), which is unlikely, or ventilation is compensated in *mdx* by way of enhanced recruitment of accessory muscles of breathing.

We extended this line of enquiry by way of assessment of spontaneous augmented breaths (sighs), which result in elevated motor unit recruitment of the diaphragm beyond that observed during chemoactivation (Mantilla *et al.*, 2011; Seven *et al.*, 2014). In the light of our findings in respect of inspiratory pressure-generating capacity in anaesthetised mice, we also evaluated tidal volume during spontaneous augmented breaths in conscious mice during plethysmography studies. Surprisingly, during augmented breaths peak inspiratory oesophageal pressure generation was significantly greater in *mdx* mice compared with wild-type, once again demonstrating no mechanical constraint in 8-week-old *mdx* mice despite substantial diaphragm weakness (approaching 50% force loss compared with wild-type in the range 60-100Hz). Moreover, enhanced diaphragm EMG activity during

spontaneous augmented breaths was equivalent (not potentiated) in *mdx* compared with wild-type mice. Together, these observations strongly suggest that preservation of inspiratory pressure-generating capacity in *mdx* is independent of the motor drive to the diaphragm. Force-generating capacity of the diaphragm is severely curtailed in *mdx* such that even maximum activation of the muscle may not be sufficient to generate substantial subatmospheric pressures, unless one considers that the loss of force corresponds to loss of the considerable ventilatory reserve of the diaphragm affecting airway protective behaviours but allowing for 'normal' ventilation and activity capable of generating augmented breaths. Although this possibility remains, at least presumably until progressive further loss of diaphragm force with disease progression, we favour the likelihood that ventilatory capacity is maintained owing to enhanced accessory muscle activation in support of pulmonary ventilation.

We acknowledge that our assessment of ventilatory capacity is limited to peak ventilation during chemoactivation of breathing (albeit pronounced hypercapnic hypoxia), and spontaneous single augmented breaths. It may be that the preserved capacity in *mdx*, whatever the mechanism, is limited such that dysfunction would be revealed by maximal inspiratory efforts particularly over sustained periods. For example, it would be interesting to determine peak inspiratory pressure-generating capacity in *mdx* mice during progressive tracheal occlusion, which results in further motor recruitment beyond that of augmented breaths (Mantilla *et al.*, 2011; Greising *et al.*, 2013; Seven *et al.*, 2014). We further acknowledge that trans-diaphragmatic pressure is a clinically-relevant index of diaphragm strength *in situ* (Syabbalo, 1998). Trans-diaphragmatic pressure can be recorded in mice, but requires significant abdominal banding, which impacts on the potential contribution of abdominal musculature to ventilatory mechanics in spontaneously breathing mice. Nevertheless, we recognise that peak trans-diaphragmatic pressure recordings during maximum ventilatory behaviours, and bilateral phrenic nerve stimulation, would provide a useful index of diaphragm performance *in vivo* (Greising *et al.*, 2013).

Full length dystrophin (Dp427) is expressed in the central nervous system of healthy individuals. Similar to muscle, dystrophin has a structural role in neurons where it associates with membrane spanning proteins forming the dystrophin associated protein complex and connects the intracellular cytoskeleton to the extracellular matrix. The consequences of dystrophin lack in the brainstem and spinal cord are unclear. Studies indicate altered acetylcholine and GABA neurotransmission and receptor expression in the CNS of *mdx* mice, although much of this work has been limited to the hippocampus since cognitive deficits are apparent in DMD (Sekiguchi *et al.*, 2009; Kueh *et al.*, 2011; Ghedini *et al.*, 2012; Parames *et al.*, 2014; Cohen *et al.*, 2015; Xu *et al.*, 2015; Vaillend & Chaussonot, 2017). In the light of our previous observations of potentiated diaphragm EMG responsiveness in *mdx* mice in circumstances of high ventilatory demand (Burns *et al.*, 2017c), we examined the concentrations of monoamines in cervical spinal cord, with a focus on serotonin, which is implicated in experimental paradigms of phrenic motor facilitation (MacFarlane *et al.*, 2014; Fields *et al.*, 2015; Perim *et al.*, 2018). The concentrations of serotonin and noradrenaline were significantly elevated in *mdx* cervical spinal cords providing a substrate for potentiated neuro-modulatory tone, although diaphragm EMG activity was not elevated in *mdx* compared with wild-type mice under any condition in the present study.

Systemic inflammation is a hallmark feature of dystrophin deficiency (Cruz-Guzmán *et al.*, 2015), and prior research has pointed to blood brain barrier leakiness (Goodnough *et al.*, 2014). We explored the possibility of a neuroinflammatory signature in the cervical spinal cord of *mdx*, which would have potential implications for motor control of the diaphragm and capacity for motor facilitation, since it is established that neuroinflammatory mediators strongly suppress phrenic motor facilitation (Huxtable *et al.*, 2013; Hocker *et al.*, 2017; Hocker & Huxtable, 2018). In the current study, we examined the density of activated immune cells (GFAP-positive astrocytes and Iba-1-positive microglia) in putative phrenic motor nuclei (C3-C5, (Qiu *et al.*, 2010)) demonstrating no evidence of neuroinflammation within the ventral horn and putative phrenic motor nuclei of the cervical spinal cord of *mdx* mice. Moreover, gene expression of pro-inflammatory molecules (NFκB,

TNF α , interleukin-6) and inducible nitric oxide synthase was not elevated in *mdx* cervical spinal cord homogenates. To examine cellular apoptosis, TUNEL assay was performed on wild-type and *mdx* spinal cord sections revealing no evidence of apoptotic bodies within putative phrenic motor nuclei of *mdx* mice. These findings reveal that there is no apparent neuroinflammatory signature that might otherwise curtail the capacity for respiratory plasticity and phrenic motor facilitation. The absence of apoptosis in *mdx* suggests no loss of trophic input to dystrophic diaphragm.

Interestingly, our previous finding of enhanced neural drive to the diaphragm muscle during chemostimulation (15% O₂ and 5% CO₂), revealed in diaphragm EMG recordings in anaesthetised *mdx* mice, which we considered a compensatory mechanism supporting ventilation, was not replicated in the current study. One major difference between studies is that the vagus nerves were sectioned in our former study in the mid-cervical region (Burns *et al.*, 2017c), but remained intact in the present study. Vagotomy and subsequent chemoactivation of breathing produces greater activation of diaphragm EMG compared with vagi intact, particularly in mice which adopt a pronounced frequency response to chemoactivation. Thus, it may be that potentiation of neural drive to the diaphragm in *mdx* mice is only revealed during near maximum or maximum ventilatory drive, or requires an absence of vagal inhibition of breathing (and perhaps superimposed chemoactivation), which would have relevance to obstructive airway events. The latter are characteristic features of sleep-disordered breathing common in DMD.

In summary, young adult *mdx* mice retain a remarkable capacity to preserve inspiratory pressure-generating and ventilatory capacity despite substantial diaphragm pathology and weakness. We conclude that enhanced recruitment of accessory muscles facilitates breathing. An increased understanding of the neuromechanical control of breathing in DMD and animal models is important in the context of disease progression, and may offer novel therapeutic strategies in respect of pulmonary support and rehabilitation in DMD boys.

4.5 Additional information

Competing interests

The authors have no financial, professional or personal conflicts relating to this publication.

Author contributions

DPB: experimental design; acquisition of data; data and statistical analysis and interpretation of data; drafting of the original manuscript; EO'D: spinal cord immunohistochemistry, TUNEL assay and PCR studies: acquisition of data; data analysis; KHM: ventilation during chemostimulation: acquisition of data; data analysis; KMO'C: HPLC studies: acquisition of data; data analysis; EFL: *in vivo* studies: experimental design; PD: sigh and apnoea studies: data analysis; GC: HPLC studies: acquisition of data; data analysis; DE: immunohistochemical and PCR studies: experimental design; acquisition of data; data and statistical analysis and interpretation of data; drafting and critical revision of the manuscript for important intellectual content; KDO'H: experimental design; statistical analysis and interpretation of data; drafting and critical revision of the manuscript for important intellectual content.

Funding

DPB was supported by funding from the Department of Physiology, UCC. Work carried out in TCD was supported by funding from The Physiological Society.

Acknowledgements

We are grateful to staff of the Biological Services Unit, University College Cork for their support in the breeding and maintenance of the murine colonies.

4.6 References

- Barbé F, Quera-Salva MA, McCann C, Gajdos P, Raphael JC, de Lattre J & Agustí AG. (1994). Sleep-related respiratory disturbances in patients with Duchenne muscular dystrophy. *Eur Respir J* **7**, 1403-1408.
- Beck J, Weinberg J, Hamnegård CH, Spahija J, Olofson J, Grimby G & Sinderby C. (2006). Diaphragmatic function in advanced Duchenne muscular dystrophy. *Neuromuscul Disord* **16**, 161-167.
- Burns DP, Ali I, Rieux C, Healy J, Jasionek G & O'Halloran KD. (2017a). Tempol Supplementation Restores Diaphragm Force and Metabolic Enzyme Activities in mdx Mice. *Antioxidants (Basel)* **6**.
- Burns DP & O'Halloran KD. (2016). Evidence of hypoxic tolerance in weak upper airway muscle from young mdx mice. *Respir Physiol Neurobiol* **226**, 68-75.
- Burns DP, Rowland J, Canavan L, Murphy KH, Brannock M, O'Malley D, O'Halloran KD & Edge D. (2017b). Restoration of pharyngeal dilator muscle force in dystrophin-deficient (mdx) mice following co-treatment with neutralizing interleukin-6 receptor antibodies and urocortin 2. *Exp Physiol* **102**, 1177-1193.
- Burns DP, Roy A, Lucking EF, McDonald FB, Gray S, Wilson RJ, Edge D & O'Halloran KD. (2017c). Sensorimotor control of breathing in the mdx mouse model of Duchenne muscular dystrophy. *J Physiol*.
- Carretta D, Santarelli M, Vanni D, Carrai R, Sbriccoli A, Pinto F & Minciacchi D. (2001). The organisation of spinal projecting brainstem neurons in an animal model of muscular dystrophy. A retrograde tracing study on mdx mutant mice. *Brain Res* **895**, 213-222.
- Chaussonot R, Edeline JM, Le Bec B, El Massioui N, Laroche S & Vaillend C. (2015). Cognitive dysfunction in the dystrophin-deficient mouse model of Duchenne muscular dystrophy: A reappraisal from sensory to executive processes. *Neurobiol Learn Mem* **124**, 111-122.
- Cohen EJ, Quarta E, Fulgenzi G & Minciacchi D. (2015). Acetylcholine, GABA and neuronal networks: a working hypothesis for compensations in the dystrophic brain. *Brain Res Bull* **110**, 1-13.
- Cruz-Guzmán OeR, Rodríguez-Cruz M & Escobar Cedillo RE. (2015). Systemic Inflammation in Duchenne Muscular Dystrophy: Association with Muscle Function and Nutritional Status. *Biomed Res Int* **2015**, 891972.
- De Bruin PF, Ueki J, Bush A, Khan Y, Watson A & Pride NB. (1997). Diaphragm thickness and inspiratory strength in patients with Duchenne muscular dystrophy. *Thorax* **52**, 472-475.

- Ervasti JM. (2007). Dystrophin, its interactions with other proteins, and implications for muscular dystrophy. *Biochim Biophys Acta* **1772**, 108-117.
- Fields DP, Springborn SR & Mitchell GS. (2015). Spinal 5-HT₇ receptors induce phrenic motor facilitation via EPAC-mTORC1 signaling. *J Neurophysiol* **114**, 2015-2022.
- Gayraud J, Matecki S, Hnia K, Mornet D, Prefaut C, Mercier J, Michel A & Ramonatxo M. (2007). Ventilation during air breathing and in response to hypercapnia in 5 and 16 month-old mdx and C57 mice. *J Muscle Res Cell Motil* **28**, 29-37.
- Ghedini PC, Avellar MC, De Lima TC, Lima-Landman MT, Lapa AJ & Souccar C. (2012). Quantitative changes of nicotinic receptors in the hippocampus of dystrophin-deficient mice. *Brain Res* **1483**, 96-104.
- Goodnough CL, Gao Y, Li X, Qutaish MQ, Goodnough LH, Molter J, Wilson D, Flask CA & Yu X. (2014). Lack of dystrophin results in abnormal cerebral diffusion and perfusion in vivo. *Neuroimage* **102 Pt 2**, 809-816.
- Gosselin LE, Barkley JE, Spencer MJ, McCormick KM & Farkas GA. (2003). Ventilatory dysfunction in mdx mice: impact of tumor necrosis factor- α deletion. *Muscle Nerve* **28**, 336-343.
- Greising SM, Sieck DC, Sieck GC & Mantilla CB. (2013). Novel method for transdiaphragmatic pressure measurements in mice. *Respir Physiol Neurobiol* **188**, 56-59.
- Hocker AD & Huxtable AG. (2018). IL-1 receptor activation undermines respiratory motor plasticity after systemic inflammation. *J Appl Physiol* (1985).
- Hocker AD, Stokes JA, Powell FL & Huxtable AG. (2017). The impact of inflammation on respiratory plasticity. *Exp Neurol* **287**, 243-253.
- Hoffman EP, Brown RH & Kunkel LM. (1987). Dystrophin: the protein product of the Duchenne muscular dystrophy locus. *Cell* **51**, 919-928.
- Hukins CA & Hillman DR. (2000). Daytime predictors of sleep hypoventilation in Duchenne muscular dystrophy. *Am J Respir Crit Care Med* **161**, 166-170.
- Huxtable AG, Smith SM, Peterson TJ, Watters JJ & Mitchell GS. (2015). Intermittent Hypoxia-Induced Spinal Inflammation Impairs Respiratory Motor Plasticity by a Spinal p38 MAP Kinase-Dependent Mechanism. *J Neurosci* **35**, 6871-6880.

- Huxtable AG, Smith SM, Vinit S, Watters JJ & Mitchell GS. (2013). Systemic LPS induces spinal inflammatory gene expression and impairs phrenic long-term facilitation following acute intermittent hypoxia. *J Appl Physiol* (1985) **114**, 879-887.
- Huxtable AG, Vinit S, Windelborn JA, Crader SM, Guenther CH, Watters JJ & Mitchell GS. (2011). Systemic inflammation impairs respiratory chemoreflexes and plasticity. *Respir Physiol Neurobiol* **178**, 482-489.
- Khirani S, Ramirez A, Aubertin G, Boulé M, Chemouny C, Forin V & Fauroux B. (2014). Respiratory muscle decline in Duchenne muscular dystrophy. *Pediatr Pulmonol* **49**, 473-481.
- Kueh SL, Dempster J, Head SI & Morley JW. (2011). Reduced postsynaptic GABAA receptor number and enhanced gaboxadol induced change in holding currents in Purkinje cells of the dystrophin-deficient mdx mouse. *Neurobiol Dis* **43**, 558-564.
- Lewis P, Sheehan D, Soares R, Varela Coelho A & O'Halloran KD. (2015). Chronic sustained hypoxia-induced redox remodeling causes contractile dysfunction in mouse sternohyoid muscle. *Front Physiol* **6**, 122.
- Lidov HG. (1996). Dystrophin in the nervous system. *Brain Pathol* **6**, 63-77.
- LoMauro A, D'Angelo MG & Aliverti A. (2017). Sleep Disordered Breathing in Duchenne Muscular Dystrophy. *Curr Neurol Neurosci Rep* **17**, 44.
- MacFarlane PM, Mayer CA & Litvin DG. (2016). Microglia modulate brainstem serotonergic expression following neonatal sustained hypoxia exposure: implications for sudden infant death syndrome. *J Physiol* **594**, 3079-3094.
- MacFarlane PM, Vinit S & Mitchell GS. (2014). Spinal nNOS regulates phrenic motor facilitation by a 5-HT_{2B} receptor- and NADPH oxidase-dependent mechanism. *Neuroscience* **269**, 67-78.
- Mantilla CB, Seven YB, Hurtado-Palomino JN, Zhan WZ & Sieck GC. (2011). Chronic assessment of diaphragm muscle EMG activity across motor behaviors. *Respir Physiol Neurobiol* **177**, 176-182.
- Mantilla CB, Seven YB & Sieck GC. (2014). Convergence of pattern generator outputs on a common mechanism of diaphragm motor unit recruitment. *Prog Brain Res* **209**, 309-329.
- Mayer OH, Finkel RS, Rummey C, Benton MJ, Glanzman AM, Flickinger J, Lindström BM & Meier T. (2015). Characterization of pulmonary function in Duchenne Muscular Dystrophy. *Pediatr Pulmonol* **50**, 487-494.

- Messina S, Vita GL, Aguenouz M, Sframeli M, Romeo S, Rodolico C & Vita G. (2011). Activation of NF-kappaB pathway in Duchenne muscular dystrophy: relation to age. *Acta Myol* **30**, 16-23.
- Muntoni F, Torelli S & Ferlini A. (2003). Dystrophin and mutations: one gene, several proteins, multiple phenotypes. *Lancet Neurol* **2**, 731-740.
- Parames SF, Coletta-Yudice ED, Nogueira FM, Nering de Sousa MB, Hayashi MA, Lima-Landman MT, Lapa AJ & Souccar C. (2014). Altered acetylcholine release in the hippocampus of dystrophin-deficient mice. *Neuroscience* **269**, 173-183.
- Peng YJ, Nanduri J, Khan SA, Yuan G, Wang N, Kinsman B, Vaddi DR, Kumar GK, Garcia JA, Semenza GL & Prabhakar NR. (2011). Hypoxia-inducible factor 2 α (HIF-2 α) heterozygous-null mice exhibit exaggerated carotid body sensitivity to hypoxia, breathing instability, and hypertension. *Proc Natl Acad Sci U S A* **108**, 3065-3070.
- Perim RR, Fields DP & Mitchell GS. (2018). Cross-talk inhibition between 5-HT. *Am J Physiol Regul Integr Comp Physiol*.
- Pinto ML, Tokunaga HH, Souccar C, Schoorlemmer GH & da Silva Lapa ReC. (2008). Loss of neuronal projections in the dystrophin-deficient mdx mouse is not progressive. *Brain Res* **1224**, 127-132.
- Popa D, Fu Z, Go A & Powell FL. (2011). Ibuprofen blocks time-dependent increases in hypoxic ventilation in rats. *Respir Physiol Neurobiol* **178**, 381-386.
- Qiu K, Lane MA, Lee KZ, Reier PJ & Fuller DD. (2010). The phrenic motor nucleus in the adult mouse. *Exp Neurol* **226**, 254-258.
- Rufo A, Del Fattore A, Capulli M, Carvello F, De Pasquale L, Ferrari S, Pierroz D, Morandi L, De Simone M, Rucci N, Bertini E, Bianchi ML, De Benedetti F & Teti A. (2011). Mechanisms inducing low bone density in Duchenne muscular dystrophy in mice and humans. *J Bone Miner Res* **26**, 1891-1903.
- Sawnani H, Thampratankul L, Szczesniak RD, Fenchel MC & Simakajornboon N. (2015). Sleep disordered breathing in young boys with Duchenne muscular dystrophy. *J Pediatr* **166**, 640-645.e641.
- Sbriccoli A, Santarelli M, Carretta D, Pinto F, Granato A & Minciacchi D. (1995). Architectural changes of the cortico-spinal system in the dystrophin defective mdx mouse. *Neurosci Lett* **200**, 53-56.

- Sekiguchi M, Zushida K, Yoshida M, Maekawa M, Kamichi S, Sahara Y, Yuasa S, Takeda S & Wada K. (2009). A deficit of brain dystrophin impairs specific amygdala GABAergic transmission and enhances defensive behaviour in mice. *Brain* **132**, 124-135.
- Seven YB, Mantilla CB & Sieck GC. (2014). Recruitment of rat diaphragm motor units across motor behaviors with different levels of diaphragm activation. *J Appl Physiol (1985)* **117**, 1308-1316.
- Sheikhabaehi S, Turovsky EA, Hosford PS, Hadjihambi A, Theparambil SM, Liu B, Marina N, Teschemacher AG, Kasparov S, Smith JC & Gourine AV. (2018). Astrocytes modulate brainstem respiratory rhythm-generating circuits and determine exercise capacity. *Nat Commun* **9**, 370.
- Sieck GC, Ferreira LF, Reid MB & Mantilla CB. (2013). Mechanical properties of respiratory muscles. *Compr Physiol* **3**, 1553-1567.
- Smith PE, Edwards RH & Calverley PM. (1989). Ventilation and breathing pattern during sleep in Duchenne muscular dystrophy. *Chest* **96**, 1346-1351.
- Souza GM, Bonagamba LG, Amorim MR, Moraes DJ & Machado BH. (2015). Cardiovascular and respiratory responses to chronic intermittent hypoxia in adult female rats. *Exp Physiol* **100**, 249-258.
- Stedman HH, Sweeney HL, Shrager JB, Maguire HC, Panettieri RA, Petrof B, Narusawa M, Leferovich JM, Sladky JT & Kelly AM. (1991). The mdx mouse diaphragm reproduces the degenerative changes of Duchenne muscular dystrophy. *Nature* **352**, 536-539.
- Stokes JA, Arbogast TE, Moya EA, Fu Z & Powell FL. (2017). Minocycline blocks glial cell activation and ventilatory acclimatization to hypoxia. *J Neurophysiol* **117**, 1625-1635.
- Suresh S, Wales P, Dakin C, Harris MA & Cooper DG. (2005). Sleep-related breathing disorder in Duchenne muscular dystrophy: disease spectrum in the paediatric population. *J Paediatr Child Health* **41**, 500-503.
- Syabbalo N. (1998). Assessment of respiratory muscle function and strength. *Postgrad Med J* **74**, 208-215.
- Vaillend C & Chaussonnet R. (2017). Relationships linking emotional, motor, cognitive and GABAergic dysfunctions in dystrophin-deficient mdx mice. *Hum Mol Genet* **26**, 1041-1055.
- Xu S, Shi D, Pratt SJ, Zhu W, Marshall A & Lovering RM. (2015). Abnormalities in brain structure and biochemistry associated with mdx mice measured by in

vivo MRI and high resolution localized (1)H MRS. *Neuromuscul Disord* **25**, 764-772.

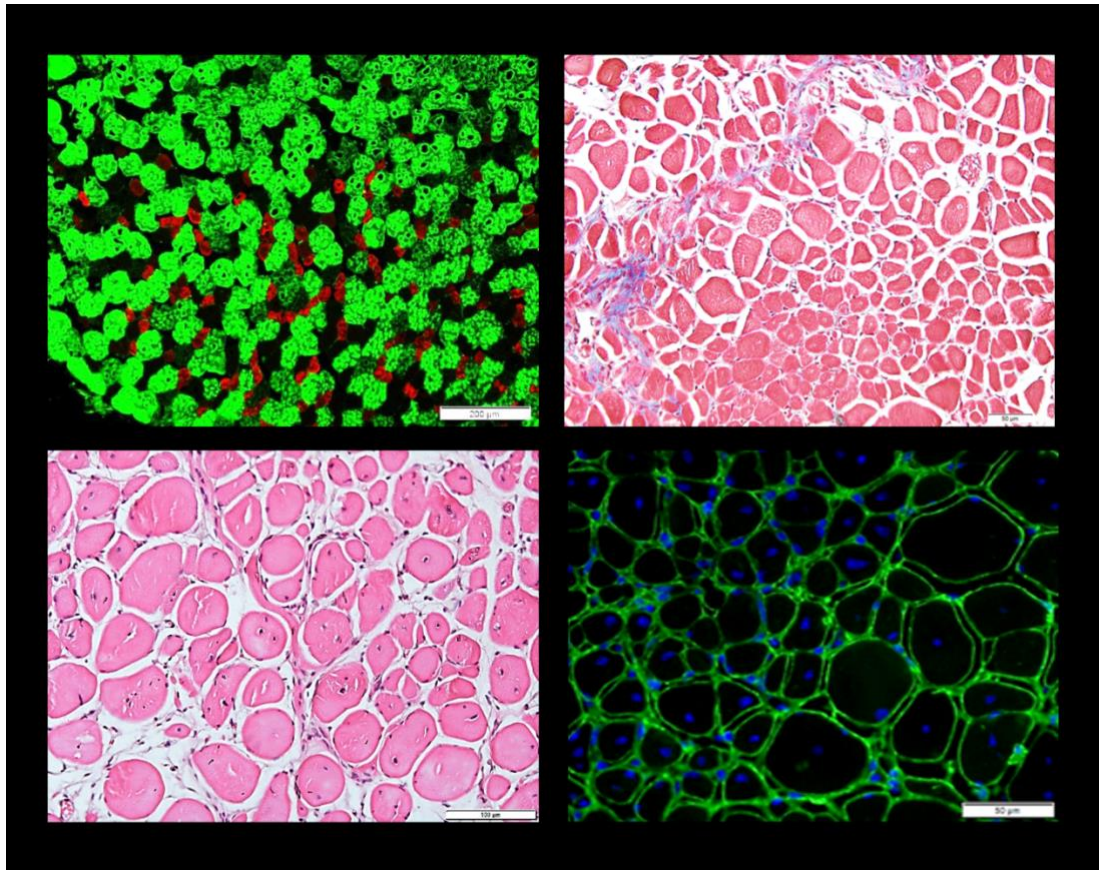
Yiu EM & Kornberg AJ. (2008). Duchenne muscular dystrophy. *Neurol India* **56**, 236-247.

Chapter 5. Restoration of pharyngeal dilator muscle force in dystrophin-deficient (*mdx*) mice following co-treatment with neutralising interleukin-6 receptor antibodies and urocortin 2

David P. Burns¹, Jane Rowland², Leonie Canavan², Kevin H. Murphy¹, Molly Brannock², Dervla O'Malley¹, Ken D. O'Halloran¹ and Deirdre Edge²

¹*Department of Physiology, School of Medicine, University College Cork, Cork, Ireland*

²*Department of Physiology, Trinity Biomedical Sciences Institute, Trinity College Dublin, the University of Dublin, Dublin, Ireland*



Cover image panel shows a collection of immunofluorescent and histological images of mouse respiratory muscle. Top left shows sternohyoid muscle fluorescently labelled for type IIa (red), type IIx (untagged, appearing black) and type IIb (green) fibres. Top right shows sternohyoid muscle stained with Masson's trichrome to examine collagen content. Bottom left shows sternohyoid muscle stained with Haematoxylin and Eosin to examine muscle fibre nucleation and cellular infiltrates. Bottom right shows diaphragm muscle immunofluorescently labelled for laminin (green) and myonuclei (blue).

Key points

What is the central question of this study?

We previously reported impaired upper airway dilator muscle function in the *mdx* mouse model of Duchenne muscular dystrophy (DMD). Our aim was to assess the effect of blocking interleukin-6 receptor signalling and stimulating corticotrophin-releasing factor receptor 2 signalling on *mdx* sternohyoid muscle structure and function.

What is the main finding and its importance?

The interventional treatment had a positive inotropic effect on sternohyoid muscle force, restoring mechanical work and power to wild type values, reduced myofibre central nucleation and preserved the myosin heavy chain type IIb fibre complement of *mdx* sternohyoid muscle. These data might have implications for the development of pharmacotherapies for DMD with relevance to respiratory muscle performance.

Abbreviations: SDB, sleep disordered breathing; CRF, corticotrophin releasing factor; CRFR, CRF receptor; TNF, tumor necrosis factor; IL, interleukin; IL-6R, interleukin-6 receptor; Ucn2, urocortin2; MyHC, myosin heavy chain; WT, wild-type; xIL-6R, anti-IL-6R; CSA, cross-sectional area; L_o , optimum length; CT, contraction time; $\frac{1}{2}$ RT, half relaxation time; S_{max} , total shortening; V_{max} , shortening velocity.

Abstract

The *mdx* mouse model of Duchenne muscular dystrophy (DMD) shows evidence of impaired pharyngeal dilator muscle function. We hypothesised that inflammatory and stress-related factors are implicated in airway dilator muscle dysfunction. Six-week-old *mdx* (n = 26) and wild-type (WT; n = 26) mice received either saline (0.9% w/v) or a co-administration of neutralising interleukin-6 receptor antibodies (0.2 mg/kg) and corticotrophin releasing factor receptor 2 agonist (urocortin 2; 30µg/kg) over 2 weeks. Sternohyoid muscle isometric and isotonic contractile function was examined *ex vivo*. Muscle fibre centronucleation, and muscle cellular infiltration, collagen content, fibre type distribution and fibre cross-sectional area were determined by histology and immunofluorescence. Muscle chemokine content was examined by use of a multiplex assay. Sternohyoid peak specific force at 100Hz was significantly reduced in *mdx* compared with WT. Drug treatment completely restored force in *mdx* sternohyoid to WT levels. The percentage of centrally-nucleated muscle fibres was significantly increased in *mdx* and this was partially ameliorated following drug treatment. The areal density of infiltrates and collagen content were significantly increased in *mdx* sternohyoid; both indices were unaffected by drug treatment. The abundance of myosin heavy chain type IIb fibres was significantly decreased in *mdx* sternohyoid; drug treatment preserved myosin heavy chain type IIb complement in *mdx* muscle. The chemokines macrophage inflammatory protein 2, interferon- γ -induced protein 10 and macrophage inflammatory protein 3 α were significantly increased in *mdx* sternohyoid compared with WT. Drug treatment significantly increased chemokine expression in *mdx* but not WT sternohyoid. Recovery of contractile function was impressive in our study, with implications for DMD. The precise molecular mechanisms by which the drug treatment exerts an inotropic effect on *mdx* sternohyoid muscle remains to be elucidated.

Keywords: Duchenne muscular dystrophy, *mdx*, interleukin-6, stress, corticotrophin releasing factor, sternohyoid muscle.

5.1 Introduction

Duchenne muscular dystrophy (DMD) is a fatal neuromuscular disease that occurs in 1:3,500 male births (Emery, 1991). Patients have defects in the dystrophin gene, which results in a lack of the structural protein dystrophin (427 kDa). Dystrophin is a rod-shaped protein expressed in skeletal, cardiac and smooth muscle, where it links cytoskeleton actin to the sarcolemma and has a physiological role in preventing damage during muscle contraction (Nowak & Davies, 2004). The absence of dystrophin in DMD induces severe damage to muscle fibres, with resultant inflammation (Deconinck & Dan, 2007). As the disease progresses there is a loss of functional muscle fibres due to necrosis and the deposition of fibrotic and adipose tissue prevails, resulting in muscle weakness.

The respiratory system is severely impaired in DMD due to respiratory and abdominal muscle weakness, as well as scoliosis (De Bruin *et al.*, 1997; Beck *et al.*, 2006). DMD is a progressive disease and thus respiratory function deteriorates with age, with patients often presenting with reduced vital capacity and breathing disturbances such as hypoventilation and sleep-disordered breathing (SDB) (Smith *et al.*, 1989; Hill *et al.*, 1992; Barbé *et al.*, 1994). While the diaphragm has been the focus of many studies in this field, there is a paucity of information pertaining to the upper airway muscles controlling airway calibre and collapsibility, thereby facilitating breathing (White & Younes, 2012). The prevalence of obstructive sleep apnoea (OSA) in DMD (Suresh *et al.*, 2005), suggests that upper airway muscle dysfunction, and poor control of airway patency during sleep, potentially contributes to breathing disturbances in DMD.

The *mdx* mouse is the most widely studied animal model of DMD. We have previously reported respiratory dysfunction, which presents at an early age in the *mdx* mouse (8 weeks), consisting of hypoventilation and upper airway (sternohyoid) muscle weakness (Burns *et al.*, 2015; Burns & O'Halloran, 2016). In human patients and *mdx* mice, functional impairments are driven by pathological changes in skeletal muscles due to dystrophin deficiency, including fibre degeneration and

necrosis, with inflammation thought to play an integral part in DMD muscle pathology (Deconinck & Dan, 2007).

In patients and *mdx* mice, sarcolemmal damage is accompanied by the infiltration of immune cells, primarily macrophages and T cells, a key source of inflammatory cytokines (Moran & Mastaglia, 2014). These molecules mount an inflammatory response through activation of additional cytokines and recruitment of further immune cells to the damaged muscle (Villalta *et al.*, 2015). Immune cells are not the only source of cytokines, with damaged muscle fibres also serving as a contributory factor (Whitham & Febbraio, 2016). In DMD, the heightened expression of pro-inflammatory cytokines such as tumour necrosis factor alpha (TNF- α) and interleukins (IL)-1 and -6, are early disease indicators and are associated with exacerbation of the inflammatory response in dystrophic muscle (Evans *et al.*, 2009b, a). IL-6 is released from a variety of tissues including immune cells and adipocytes and is commonly referred to as a myokine as it can be secreted from muscle in response to physical activity (Jonsdottir *et al.*, 2000; Pedersen & Febbraio, 2008). This inflammatory cytokine is of particular interest in DMD pathology since it is elevated in muscle and plasma samples from DMD patients (Messina *et al.*, 2011; Rufo *et al.*, 2011; Pelosi *et al.*, 2015a) and *mdx* mice (Pelosi *et al.*, 2015a). IL-6 is pleiotropic, however it mediates its pro-inflammatory effects via its trans-signalling pathway by use of the soluble IL-6 receptor (IL-6R) (Pedersen & Febbraio, 2008). Its importance in *mdx* skeletal muscle pathology was recently highlighted (Pelosi *et al.*, 2015a), showing that blockade of IL-6 signalling in *mdx* mice has beneficial functional outcomes in dystrophic skeletal muscle.

Muscle wasting is a common feature of DMD due to muscle proteolysis, thus pharmacological interventions aimed at rescuing muscle are attractive. Corticotrophin releasing factor receptor 2 (CRFR2) agonists have been shown to modulate muscle mass through the activation of anabolic signalling pathways and a capacity to alter the rate of proteolysis during atrophying conditions (Hall *et al.*, 2007). In addition, CRFR2 can reduce nerve damage, corticosteroid-induced atrophy and loss of muscle mass due to immobilisation (Hinkle *et al.*, 2003). The CRFR2

agonist, urocortin 2 (Ucn2), has been shown to improve diaphragm function and reduce fibrosis and immune cell infiltration in *mdx* mice (Reutenauer-Patte *et al.*, 2012). Recent work demonstrated that neutralisation of IL-6 receptor (xIL-6R) or stimulation of CRFR2 both had positive inotropic effects on the major pump muscle of breathing – the diaphragm (Manning *et al.*, 2017). Furthermore, Manning *et al.* (2017) reported that co-treatment of xIL-6R and Ucn2 had an additive inotropic effect on diaphragm muscle force. We hypothesised that co-administration of xIL-6R antibodies and Ucn2 alleviates upper airway muscle weakness in dystrophin deficient *mdx* mice. We sought to examine structure and function of sternohyoid muscle (pharyngeal dilator) from age-matched wild type (WT) and *mdx* mice following saline or combined xIL-6R and Ucn2 drug treatment.

5.2 Methods

5.2.1 Ethical approval

All procedures were performed under licence in accordance with National and European guidelines following local research ethics committee approval.

5.2.2 Animals

Male and female wild type (WT; C57BL/10ScSnJ) and *mdx* (C57BL/10ScSn-Dmd^{mdx}/J) mice were purchased from the Jackson Laboratory (Jackson Laboratory, Bar Harbor, ME) and were bred in our institution's animal housing facility. Animals were housed conventionally in a temperature- and humidity-controlled facility, operating on a 12 h light: 12 h dark cycle with food and water available *ad libitum*. 6 week old male WT and *mdx* mice received a treatment consisting of a co-administration of xIL-6R (IL-6R neutralising antibody; MR1-61 (Okazaki *et al.*, 2002); 0.2 mg/kg) and Ucn2 (CRFR2 agonist; 30 µg/kg; U9507, Sigma Aldrich, Wicklow, Ireland) or saline (vehicle control; 0.9% w/v). MR1-61 stock was kept at -80°C and Ucn2 stock at -20°C. A working solution containing both MR1-61 (26.7µg/ml) and Ucn2 (4µg/ml) was made in sterile saline, aliquoted and stored at -20°C until day of injection. Doses and treatment protocol were chosen based on previous studies (Manning *et al.*, 2016, 2017). Treatment consisted of six sub-cutaneous injections to the scruff of the neck on alternate days over the course of two weeks beginning at 6 weeks of age. A 20g mouse received an injection bolus of 150µl. WT and *mdx* animals were assigned at random to saline or drug treatment, establishing 4 groups: WT saline (21.4 ± 1.6g; n = 13), WT treatment (22.0 ± 1.2g; n = 13), *mdx* saline (24.4 ± 1.6g; n = 13) and *mdx* treatment (24.5 ± 1.7g; n = 13). Animals were anaesthetised with 5% isoflurane by inhalation in oxygen and euthanised by cervical dislocation.

5.2.3 Muscle physiology

5.2.3.1 Ex vivo muscle preparation

The sternohyoid muscles were immediately excised and placed in a tissue bath at room temperature containing continuously gassed hyperoxic (95% O₂/ 5% CO₂) Krebs solution (NaCl 120 mM, KCl 5mM, Ca²⁺ gluconate 2.5 mM, MgSO₄ 1.2 mM, NaH₂PO₄ 1.2 mM, NaHCO₃ 25mM, glucose11.5mM) and D-tubocurarine (25µM).

The paired sternohyoid muscles were carefully separated along a natural division in the midline. One half was used immediately for functional analysis and the other half was snap frozen in liquid nitrogen for subsequent molecular analysis (section 2.5). A single longitudinal muscle strip (2mm in diameter) for each animal was studied in a water-jacketed muscle bath, containing Krebs solution, maintained at 35°C gassed with 95% O₂/ 5% CO₂. Each muscle strip was placed between a pair of platinum plate electrodes, with the caudal end fixed to an immobile hook and the rostral end attached to a dual-mode lever transducer system by non-elastic string. Muscle preparations were allowed a 5-min equilibration period.

5.2.3.2 Isometric protocol

Following equilibration, the optimum length (L_0) was determined by adjusting the position of the force transducer by use of a micro-positioner between intermittent twitch contractions. The L_0 was taken as the muscle length associated with maximal isometric twitch force in response to single isometric twitch stimulation (supramaximal stimulation, 1ms duration). Once L_0 was determined, the muscle stayed at this length for the duration of the protocol. A single isometric twitch was measured. Peak isometric twitch force, contraction time (CT; time to peak force) and half relaxation time ($\frac{1}{2}$ RT; time for peak force to decay by 50%) were determined. Next, an isometric tetanic contraction was elicited by stimulating muscle strips with supramaximal voltage at 100 Hz for 300 ms duration. Peak isometric tetanic force was determined at 100Hz (O'Halloran, 2006; Burns & O'Halloran, 2016).

5.2.3.3 Isotonic protocol

Following the isometric protocol, concentric contractions were elicited in incremental steps with varying load (0%, 5%, 10%, 15%, 20%, 25%, 30%, 35%, 40%, 60%; % of force at 100Hz) with 30 s rest between each contraction. Muscle length returned to L_0 following each contraction. Total shortening was determined as the maximum distance shortened during contraction. Shortening velocity was determined as the distance shortened during the initial 30 ms of shortening (Lewis *et al.*, 2015; Lewis *et al.*, 2016). Mechanical work (force x total shortening) and

power (force x shortening velocity) were determined at each step of the incremental load step test (Lewis *et al.*, 2015; Williams *et al.*, 2015; Burns & O'Halloran, 2016; O'Leary & O'Halloran, 2016).

5.2.4 Muscle immunohistochemistry and histology

5.2.4.1 Tissue preparation

The sternohyoid muscles were excised and divided down the midline; one half was embedded in optimum cutting temperature (OCT) embedding medium and frozen in isopentane cooled in liquid nitrogen and stored at -80°C for subsequent structural analysis (n = 4-5 per group). The other half of the muscle was placed in 4% paraformaldehyde overnight at 4°C before being transferred to 70% ethanol prior to tissue processing and paraffin embedding for histological analysis (n = 4-5 per group).

5.2.4.2 Myosin heavy chain fluorescence immunohistochemistry

Serial transverse muscle sections (10 µm) were cryo-sectioned (Model CM30505; Leica Microsystems, Nussloch, Germany) at -22°C and mounted on polylysine-coated glass slides (VWR International, Dublin, Ireland). Sections were captured from the middle belly and distal regions of the muscle. Slides were immersed in PBS (0.01 M) containing 1% bovine serum albumin (BSA) for 15 minutes. After 3x5 minute PBS washes, slides were immersed in PBS containing 5% goat serum for 30 minutes. Following a further 3x5 minute PBS rinses, slides were incubated with an unconjugated AffiniPure Fab Fragment Goat Anti-Mouse IgG (H+L) diluted in PBS (1:13, Jackson ImmunoResearch Labs) for 1 hour at room temperature, to enable the use of mouse monoclonal primary antibody staining on mouse tissue. After 3x2 minute washes in PBS, primary antibodies were applied. Primary monoclonal myosin antibodies were obtained from the Developmental Studies Hybridoma Bank (DSHB), University of Iowa, Iowa City, IA, USA and a rabbit anti-laminin antibody was obtained from Sigma-Aldrich (L9393). A triple-labelling approach was applied to tag MyHC types I (BAD5, 1:100), IIa (sc71 1:100) and IIb (BFF3 1:100) on a single section. On a serial section, a double-labelling approach consisted of a rabbit anti-laminin antibody (1:500) and a pan-MyHC antibody for the indirect determination

of pure MyHC I α fibres, BF35 (1:50), labelling all MyHC isoforms but I α , enabling visualisation of I α fibres by absence of staining; all antibodies were diluted in PBS and 1% BSA solution. Triple and double labelling solutions were applied on alternate sections on each slide. Individual sections were encircled with a hydrophobic pen (ImmEdge™ Vector Labs) to prevent contamination from neighbouring sections on the same slide. Slides were incubated with the primary antibodies overnight at 4°C in a humidity chamber.

After the incubation period, slides were washed with PBS for 3x5 minutes before the appropriate secondary antibodies were applied. All secondary antibodies were diluted in PBS and 1% BSA. For the triple-labelled slides, a cocktail of secondary antibodies was prepared containing AlexaFluor350-conjugated goat anti-mouse IgG2b (1:500, Invitrogen, Biosciences Ltd, Dun Laoghaire, Ireland), Dylight594-conjugated goat anti-mouse IgG1 (1:500, Jackson ImmunoResearch Europe Ltd, Suffolk, UK) and AlexaFluor488-conjugated goat anti-mouse IgM (1:250, Invitrogen), targeting MyHC I, I α and I β , respectively. Secondary antibodies for double-labelled sections were Dylight594-conjugated goat anti-mouse IgG1 (1:500, Jackson) and FITC-conjugated anti-rabbit secondary antibody (1:250, Sigma-Aldrich). Secondary antibodies were applied and slides were incubated for 1 hour in the dark at room temperature. Slides were rinsed with PBS for 3x5 minutes, cover slipped with polyvinyl alcohol mounting medium with DABCO® anti-fade (Sigma) before observation with a fluorescent microscope (Olympus BX51). Negative controls were also performed in which primary antibodies were omitted and sections were instead incubated in diluent. Images were merged using ImageJ software (W. S. Rasband, ImageJ; US National Institutes of Health, Bethesda, MD, USA).

5.2.4.3 Histological analysis

Muscle samples were dehydrated (70% ethanol, 80% ethanol, 95% ethanol, 60 minutes each) and then placed in 100% ethanol (60 minutes x2). Samples were then cleared in xylene (60 minutes x2), before being transferred to two changes of paraffin (one hour each) (Leica TP1020, Histokinet). Tissue samples were then embedded in paraffin (Sakura Tissue-Tek TEC, Histolab Histowax embedding

medium), and serial cross-sections (5 μ m thick) were sectioned using a microtome (Leica RM2135). Serial sections were collected throughout the muscle (mid-belly and distal regions) onto glass slides and oven-dried (overnight at 37°C).

To examine putative inflammatory cell infiltration, and central nucleation of muscle fibres, tissue sections were stained with haematoxylin and eosin (H&E). Tissue sections were deparaffinised in xylene (2 x 5 minutes each), rehydrated through a graded series of alcohols (100% ethanol, 95% ethanol, 70% ethanol, one minute each). Sections were stained with haematoxylin (DeLafield's Haematoxylin) (5 min) and subsequently rinsed in distilled H₂O (5 min), stained in eosin (alcoholic Eosin-Y, Sigma Aldrich; 1 min), rinsed in distilled H₂O, and dehydrated (70% ethanol, 95% ethanol, 1 min each, 100% ethanol, 2 x 1 minute) and xylene (5 min). For collagen staining, a Masson's trichrome protocol was followed (Sigma Aldrich). Slides were mounted using DPX mounting medium (Sigma Aldrich, USA), air-dried and visualised on a bright field microscope (Olympus BX51) x 20 magnification.

5.2.5 Molecular studies

5.2.5.1 Tissue preparation

Sternohyoid samples stored at -80°C were removed and allowed to defrost at 4°C for 5 minutes. All procedures were performed at 4°C to prevent protein degradation. Samples were homogenized in a lysis buffer (RIPA) made up from 10X RIPA, deionized water, 200mM sodium fluoride (NAF), 100mM phenylmethylsulfonylfluoride (PMSF), protease cocktail inhibitor 1 and phosphatase cocktail inhibitor 2. Following the homogenization process, the reactant mixtures were centrifuged (14,000 x rpm) at 4°C for 20 min and the supernatants were harvested. Total amount of protein for each tissue sample was determined using Pierce[®] Bicinchoninic Acid Assay (BCA assay, Thermo Scientific, Fisher, Dublin, Ireland). Supernatants were stored at -80°C for future use.

5.2.5.2 Chemokines

A chemokine assay (U-PLEX Chemokine Combo; K15099K-1, Meso Scale Discovery, Rockville, MD) was used to examine chemokines in sternohyoid muscle from all

four groups: WT saline (n = 7-8), WT treatment (n = 7-8), *mdx* saline (n = 8) and *mdx* treatment (n = 7). The assay was performed according to the manufacturer's instructions using an extended incubation time to improve detection (the plate was incubated overnight at 4°C). Following incubation, the plate was read on QuickPlex SQ 120 imager (Meso Scale Discovery, Rockville, MD). Signals within the detectable range were achieved with reliability for the following 3 chemokines: macrophage inflammatory protein 2 (MIP-2), interferon- γ -induced protein 10 (IP-10) and macrophage inflammatory protein-3 α (MIP-3 α).

5.2.6 Data and image analysis

Specific force was calculated in N/cm² of estimated muscle cross-sectional area (CSA). The CSA of each strip was determined by dividing the muscle mass (weight in grams) by the product of muscle L₀ (cm) and muscle density (assumed to be 1.06 g/cm³). The CT and ½ RT were measured as indices of isometric twitch kinetics. For isotonic load relationships, data were plotted as the measured variable versus % load. Total muscle shortening was normalised to L₀ and expressed in L/L₀. Similarly, shortening velocity was normalised to L₀ and expressed in L₀/s. Maximum total shortening (S_{max}) and maximum shortening velocity (V_{max}) were measured when both were maximal at 0% load. Mechanical work was measured in J/cm². Mechanical power was expressed in W/cm². Maximum mechanical work (W_{max}) and power (P_{max}) were also measured and typically occurred between 30% and 40% load.

For MyHC fibre type analysis, muscle sections were viewed at x10 magnification and images captured using an Olympus BX51 microscope and an Olympus DP71 camera. Cell Sens™ (Olympus) was used to digitally capture the images. Analysis was carried out using image J software, where fibre type CSA and fibre type distribution for each MyHC fibre type were determined. CSA measurements were made by fibre "circling" based on MyHC labelling. A square test frame (640,000 μm^2) with inclusion and exclusion boundaries was employed to calculate these parameters in a given randomly chosen field. For each animal, multiple sections throughout the length of the muscle were viewed and 3-4 images analysed per fibre

type. H&E stained sections were visualised x20 magnification. Six sections were examined across the muscle from the rostral, middle and caudal regions. Two randomly selected areas were captured per muscle section from non-overlapping areas for analysis. Muscle pathology was scored using ImageJ software. The number of myofibres displaying central nucleation was expressed as a percentage of the total number of myofibres per image. Putative inflammatory cell infiltration (the presence of cells in the extracellular matrix), was also scored and expressed as a percentage of the total area of muscle. For Masson's trichrome staining, the microscope lighting exposure was maintained throughout. Three sections, with two images captured per section, from the mid-portion of the muscle, were analysed per animal. Images were analysed using a colour balance threshold (ImageJ software), and the area of collagen was expressed as a percentage of the total area of muscle. For chemokine analysis, chemokine signals within the detectable range were expressed as relative fluorescence units per μg protein (RFU/ μg protein), with equal protein loading in all wells.

5.2.7 Statistical analysis

Values are expressed as mean \pm SD. Muscle functional data were statistically compared using two-way ANOVA (genotype x treatment) with Bonferroni *post hoc* test. For muscle histology, group means were generated from multiple images averaged per animal and then compared by two-way ANOVA (genotype x treatment) with Bonferroni *post hoc* test. $P < 0.05$ was deemed to be statistically significant.

5.3 Results

5.3.1 Body mass

There was a significant difference in body mass ($P < 0.0001$; two-way ANOVA) between age-matched WT and *mdx* mice; the latter were slightly heavier. Drug treatment had no effect on body mass.

5.3.2 Isometric force and twitch contractile kinetics

Table 5.1 shows data for sternohyoid muscle twitch force and contractile kinetics (CT and $\frac{1}{2}$ RT) from animals following drug or saline treatment. *Mdx* sternohyoid twitch force was significantly lower ($P = 0.01$ (genotype); two-way ANOVA) compared with WT. *Post hoc* analysis revealed that drug treatment significantly increased twitch force in *mdx* sternohyoid ($P < 0.01$; two-way ANOVA with Bonferroni), but not in WT ($P > 0.05$). There was no significant difference between WT and *mdx* in values for CT and $\frac{1}{2}$ RT; both were unaffected by drug treatment. Although statistical differences were not observed for CT and $\frac{1}{2}$ RT across groups, sizeable effects were noticed which could have physiological relevance. CT was increased by $\sim 45\%$ and $\frac{1}{2}$ RT by $\sim 28\%$ for *mdx* sternohyoid compared with WT. Treatment reduced CT by $\sim 18\%$ and $\frac{1}{2}$ RT by $\sim 19\%$ in *mdx* mice. Peak force at 100Hz was significantly lower in *mdx* sternohyoid ($P = 0.0003$) compared with WT (Fig. 5.1). *Post hoc* analysis showed that drug treatment significantly increased force for WT ($P < 0.01$) and *mdx* ($P < 0.01$) sternohyoid.

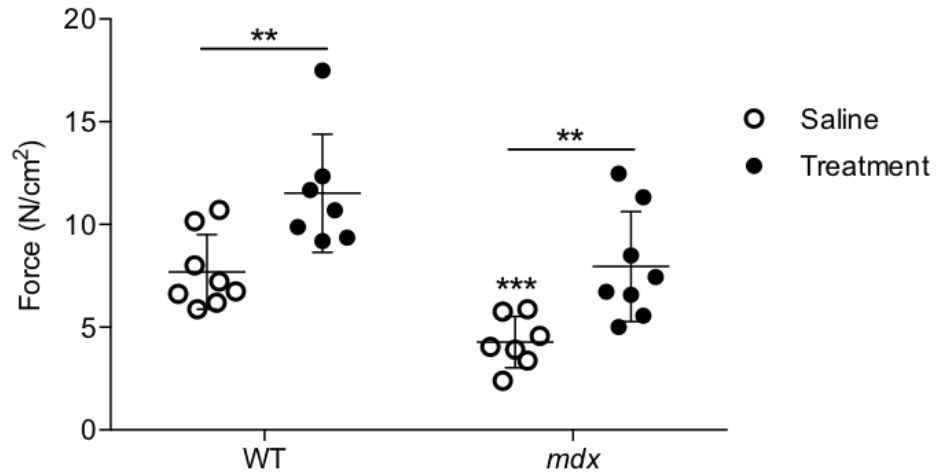


Figure 5.1 Peak isometric tetanic force

Group data (mean \pm SD) for tetanic force in wild-type WT (n = 7-8) and *mdx* (n = 7-8) sternohyoid muscle following 6 sub-cutaneous injections with saline (0.9% w/v) or treatment (xIL-6R (0.2 mg/kg) and Ucn2 (30 μ g/kg); co-administered) over two weeks. Peak tetanic force was measured following stimulation at 100Hz *ex vivo*. Data were statistically compared by two-way ANOVA followed by Bonferroni *post hoc* test. ** $P < 0.01$. Genotype: *** $P = 0.0003$; treatment $P = 0.0001$; interaction $P = 0.9$.

5.3.3 Isotonic contractile parameters and kinetics

Table 5.1 shows data for sternohyoid muscle isotonic contractile parameters: W_{max} , P_{max} , S_{max} and V_{max} . W_{max} was significantly reduced in *mdx* sternohyoid ($P = 0.004$; two-way ANOVA) compared with WT. Drug treatment significantly increased W_{max} for WT ($P < 0.05$; two-way ANOVA with Bonferroni), but not *mdx* muscle ($P > 0.05$). P_{max} was significantly reduced in *mdx* sternohyoid ($P = 0.0003$) compared with WT, and drug treatment significantly increased P_{max} in *mdx* ($P = 0.01$). V_{max} was significantly reduced in *mdx* sternohyoid ($P = 0.008$) compared with WT, and this was unaffected by drug treatment. There was no significant difference in S_{max} between WT and *mdx*. Drug treatment had no effect on S_{max} in both groups.

	WT		<i>mdx</i>		Two-way ANOVA		
	Saline (n = 8)	Treatment (n = 7)	Saline (n = 7)	Treatment (n = 8)	Genotype	Treatment	Interaction
CT (ms)	11.7 ± 2.0	12.6 ± 3.4	17.0 ± 8.8	13.9 ± 4.3	<i>P</i> = 0.1	<i>P</i> = 0.6	<i>P</i> = 0.3
½ RT (ms)	18.2 ± 6.4	18.0 ± 5.8	23.4 ± 0.8	18.8 ± 5.7	<i>P</i> = 0.1	<i>P</i> = 0.2	<i>P</i> = 0.3
Twitch Force (N/cm ²)	1.2 ± 0.4	1.8 ± 0.6	0.5 ± 0.3 £	1.5 ± 0.8 #	<i>P</i> = 0.01	<i>P</i> = 0.0004	<i>P</i> = 0.5
Wmax (J/cm ²)	0.4 ± 0.1	0.6 ± 0.4 \$	0.2 ± 0.08	0.3 ± 0.09	<i>P</i> = 0.004	<i>P</i> = 0.01	<i>P</i> = 0.2
Pmax (W/cm ²)	4.7 ± 1.7	7.4 ± 3.9	2.1 ± 1.5 £	3.6 ± 0.6	<i>P</i> = 0.0003	<i>P</i> = 0.01	<i>P</i> = 0.5
Smax (L/L ₀)	0.3 ± 0.07	0.3 ± 0.06	0.3 ± 0.07	0.3 ± 0.08	<i>P</i> = 0.3	<i>P</i> = 0.7	<i>P</i> = 0.3
Vmax (L ₀ /s)	4.6 ± 1.8	4.1 ± 1.5	2.4 ± 1.1 £	3.3 ± 1.2	<i>P</i> = 0.008	<i>P</i> = 0.8	<i>P</i> = 0.2

Table 5.1 Sternohyoid muscle contractile properties

Values (mean ± SD) for twitch contraction time (CT), twitch half-relaxation time (½ RT), peak twitch force, maximum mechanical work (Wmax), maximum mechanical power (Pmax), peak shortening (Smax) and peak shortening velocity (Vmax) of sternohyoid muscle from wild-type (WT), n = 7-8) and *mdx* (n = 7-8) mice injected sub-cutaneously with saline (0.9% w/v) or drug treatment (xIL-6R (0.2mg/kg) and Ucn2 (30µg/kg); co-administered) for two weeks. Data were statistically compared by two-way ANOVA followed by Bonferroni *post hoc* test. £ *mdx* saline significantly different from corresponding WT saline value; *P* < 0.05. \$ WT treatment significantly different from corresponding WT saline value, *P* < 0.05. # *mdx* treatment significantly different from corresponding *mdx* saline value, *P* < 0.05.

5.3.4 Isotonic load relationships

Fig. 5.2 (A-D) shows data for sternohyoid muscle isotonic load relationships. Loading had a significant effect on work ($P < 0.0001$; two-way ANOVA; Fig. 5.2A), power ($P < 0.0001$; Fig. 5.2B), shortening ($P < 0.0001$; Fig. 5.2C) and shortening velocity ($P < 0.0001$; Fig. 5.2D) for both WT and *mdx* sternohyoid. *Mdx* muscle had significantly reduced work ($P < 0.0001$), power ($P < 0.0001$) and shortening velocity ($P < 0.0001$) compared with WT. Drug treatment significantly increased work production for WT ($P < 0.0001$; two-way ANOVA with Bonferroni) and *mdx* muscle ($P < 0.0001$). Power production was also significantly increased for WT ($P < 0.0001$) and *mdx* ($P < 0.0001$) sternohyoid following drug treatment. Shortening velocity was significantly increased for *mdx* muscle ($P = 0.02$) following drug treatment.

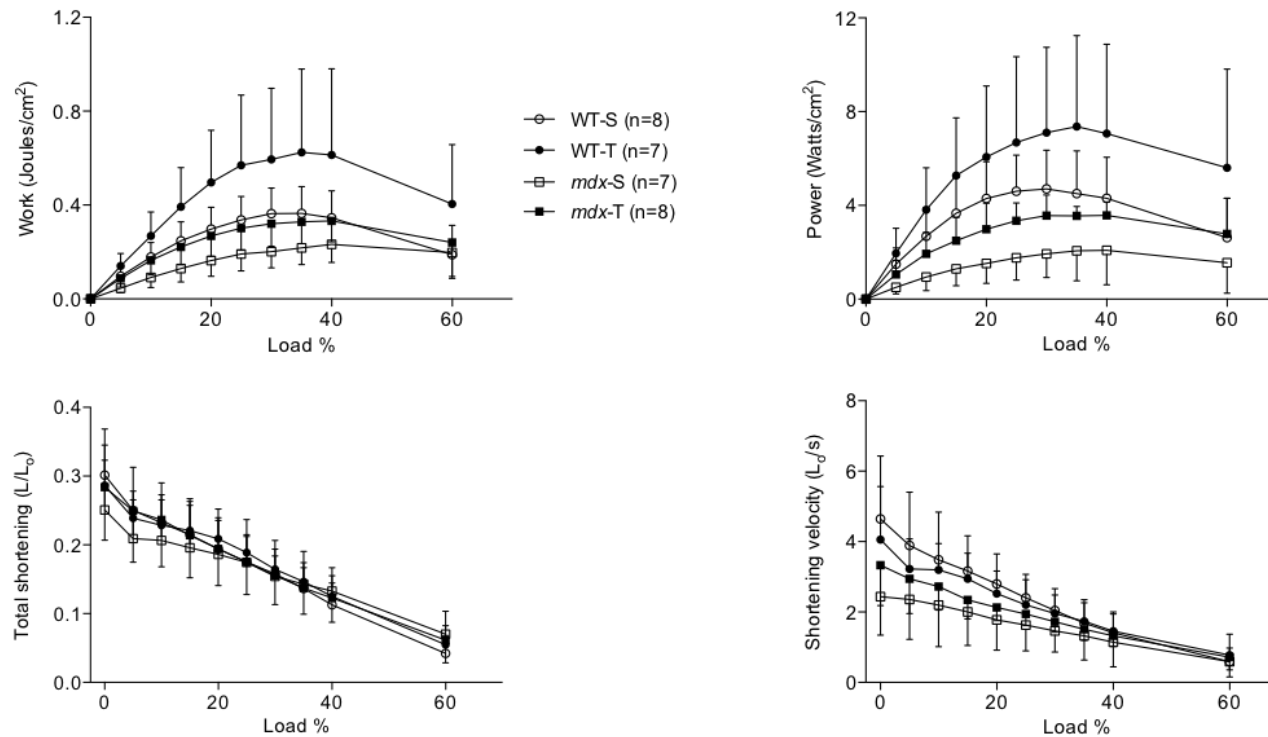


Figure 5.2 Sternohyoid muscle isotonic contractile properties

Group data (mean \pm SD) for work-load (A), power-load (B), shortening-load (C) and shortening velocity-load (D) relationships in wild-type (WT, n = 7-8) and *mdx* (n = 7-8) sternohyoid muscle following 6 sub-cutaneous injections of saline (0.9% w/v) or treatment (xIL-6R (0.2 mg/kg) and Ucn2 (30 μ g/kg); co-administered) over two weeks. Data were statistically compared by two-way ANOVA. Work: load $P < 0.0001$; genotype $P < 0.0001$; WT treatment $P < 0.0001$; *mdx* treatment $P < 0.0001$. Power: load $P < 0.0001$; genotype $P < 0.0001$; WT treatment $P < 0.0001$; *mdx* treatment $P < 0.0001$. Shortening: load $P < 0.0001$; genotype $P = 0.2$; WT treatment $P = 0.5$; *mdx* treatment $P = 0.2$. Velocity: load $P < 0.0001$; genotype $P < 0.0001$; WT treatment $P = 0.2$; *mdx* treatment $P = 0.002$.

5.3.5 Myosin heavy chain fibre type distribution

Type I fibres were absent from sternohyoid muscle in all groups. A positive control image for type I fibre staining in WT mouse diaphragm muscle is shown in Fig. 5.3A. The fibre type distribution of type IIa fibres did not vary significantly between the four groups (Fig. 5.3B). For *mdx* saline, the distribution of type IIx fibres was significantly increased compared with WT saline (Fig. 5.3C; $P < 0.0001$; two-way ANOVA), whereas the distribution of type IIb fibres was significantly reduced in *mdx* saline compared with WT saline (Fig. 5.3D; $P < 0.01$). Sternohyoid fibre type changes were prevented/reversed by drug treatment in *mdx* with significant changes in type IIx (Fig. 5.3C; $P < 0.01$; two-way ANOVA with Bonferroni) and type IIb fibres (Fig. 5.3D; $P < 0.05$) compared with *mdx* saline.

5.3.6 Fibre cross-sectional area

Figure 5.3E shows data for the CSA for all fibre types. There was a significant increase in the CSA of type IIa ($P < 0.05$; two-way ANOVA) and type IIx fibres ($P < 0.05$) in *mdx* sternohyoid compared with WT. Drug treatment had no significant effect on type IIa ($P = 0.08$) or type IIx ($P = 0.628$) CSA for both WT and *mdx*. The CSA of type IIb fibres were not significantly different between WT and *mdx*. With treatment, type IIb CSA was significantly increased in WT only ($P < 0.05$; two-way ANOVA with Bonferroni).

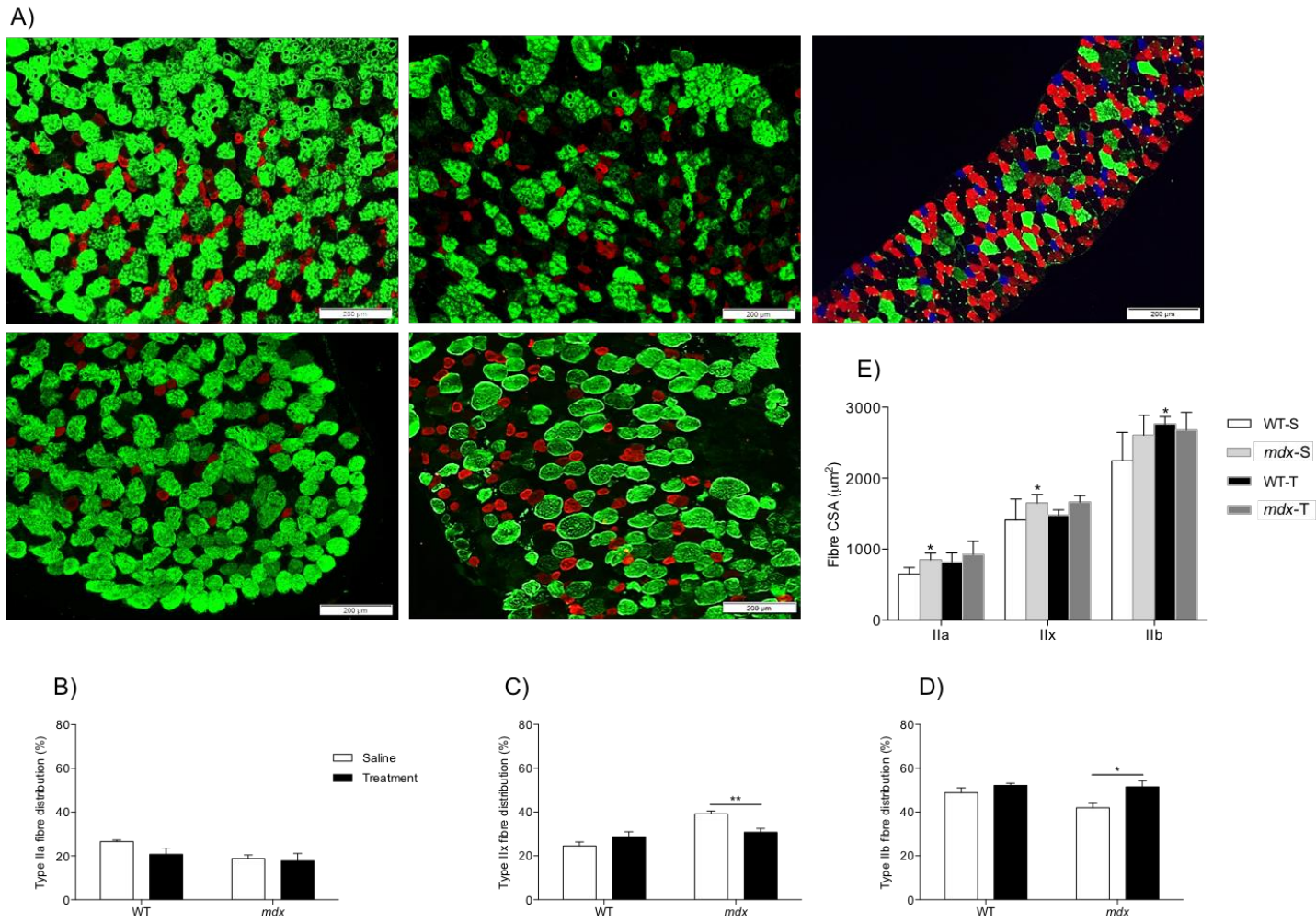


Figure 5.3 Sternohyoid muscle fibre distribution and cross-sectional area

Representative immunofluorescence images of Sternohyoid (SH) muscle fibre type distribution (A), showing type IIa fibres (red), type IIx (untagged, appearing black) and type IIb (green) for WT saline (top left), *mdx* saline (top middle), WT drug-treated (bottom left) and *mdx* drug-treated (bottom middle). Note: the mouse sternohyoid muscle is devoid of type I – slow fibres, a positive control from type I fibre staining is shown in a section of WT mouse diaphragm (top right). Scale bars = 200 μ m. Group data (mean \pm SD) showing fibre distribution of type IIa fibres (B), type IIx (C) and type IIb (D) in WT (n = 4) and *mdx* saline treated mice (n = 5), and WT drug-treated (n = 4) and *mdx* drug-treated mice (n = 4). Mice received 6 sub-cutaneous injections of saline (0.9% w/v) or treatment (xlL-6R (0.2 mg/kg) and Ucn2 (30 μ g/kg); co-administered) over two weeks. Data were statistically compared by two-way ANOVA followed by Bonferroni *post hoc* test. In *mdx* mice, type IIx areal density was significantly increased (C), whereas type IIb fibre distribution was decreased (D). With drug treatment, type IIx fibre distribution was significantly decreased in *mdx* mice compared with *mdx* saline (C), while type IIb fibre distribution (D) was increased compared with *mdx* saline. * $P < 0.05$; ** $P < 0.01$. B) Genotype $P = 0.3$; treatment $P = 0.3$; interaction $P = 0.4$. C) Genotype $P = 0.0001$; treatment $P = 0.007$; interaction $P = 0.03$. D) Genotype $P = 0.006$; treatment $P = 0.04$; interaction $P = 0.1$. E, Group data (mean \pm SD) showing mean CSAs of sternohyoid muscle fibre type IIa, type IIx and type IIb (E). The CSA of type IIa and type IIx fibres was significantly increased in *mdx* mice. Drug treatment increased the CSA of type IIb fibres in WT mice only. Type IIa: Genotype * $P = 0.03$; treatment $P = 0.08$; interaction $P = 0.5$. Type IIx: Genotype * $P = 0.02$; treatment $P = 0.6$; interaction $P = 0.8$. Type IIb: Genotype $P = 0.3$; treatment: * $P = 0.049$; interaction $P = 0.1$.

5.3.7 Central nucleation and putative inflammatory cell infiltration

The percentage of sternohyoid muscle fibres with centrally located nuclei was significantly increased in *mdx* (Fig 5.4A-B; $P < 0.0001$; two-way ANOVA) compared with WT sternohyoid. Central nucleation was reduced slightly in *mdx* mice following drug treatment compared with *mdx* saline (Fig 5.4A-B; $P < 0.05$; two-way ANOVA with Bonferroni). The areal density of inflammatory cell infiltration was significantly increased in *mdx* sternohyoid muscle (Fig 5.4A+C; $P < 0.001$; two-way ANOVA) compared with WT. Drug treatment had no significant effect on the relative area of putative immune cell infiltration (Fig 5.4 A+C).

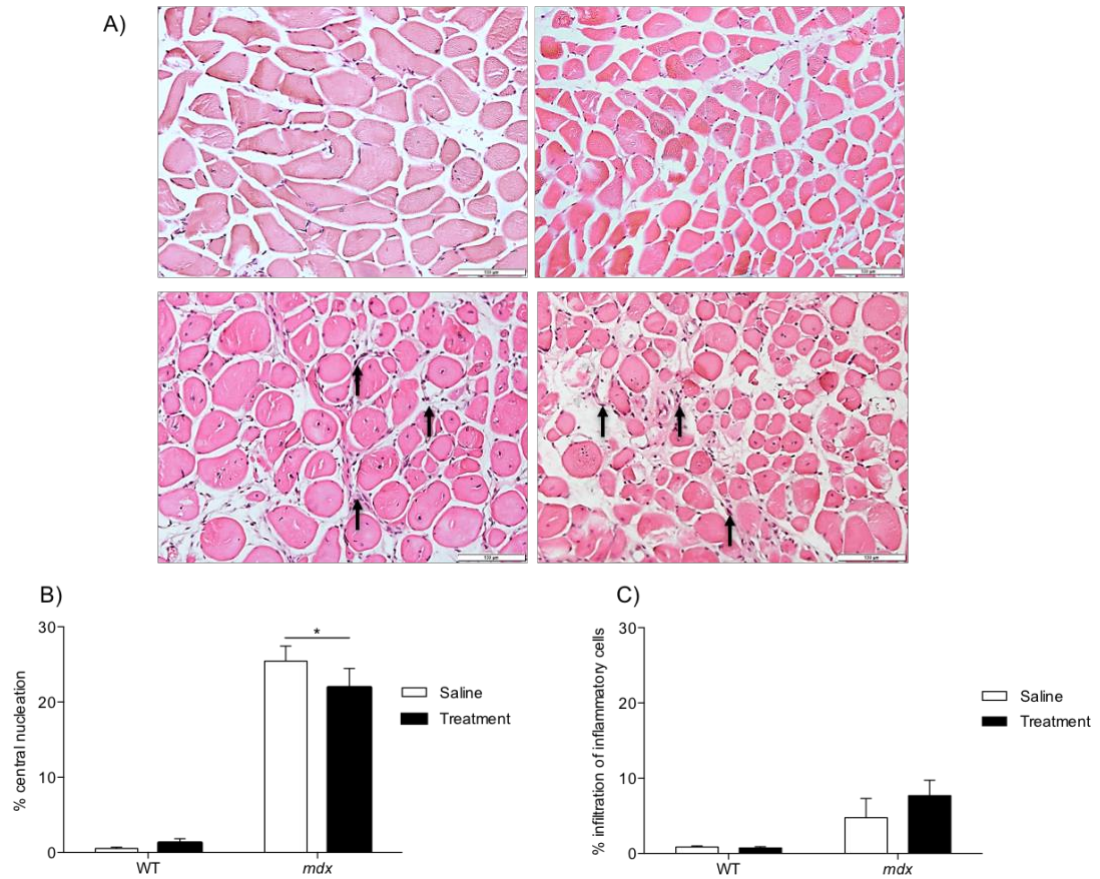


Figure 5.4 Central nucleation and inflammatory cell infiltration of sternohyoid muscle

Representative histological images (A) of sternohyoid muscle transverse sections stained with H&E in WT saline (top left), *mdx* saline (bottom left), WT drug-treated (top right) and *mdx* drug-treated (bottom right) scale bars 100 μ m. Peripherally located nuclei are apparent in WT saline and WT drug-treated images. In comparison, *mdx* mice (saline and drug-treated) displayed an increased incidence of centrally located nuclei. Inflammatory cell infiltration is not apparent in WT saline and WT drug-treated groups. *Mdx* muscle (saline and treatment) displayed inflammatory cell infiltration, highlighted with black arrows. Group data (mean \pm SD) showing percentage of central nucleation (B) and percentage of infiltration of inflammatory cells (C) in sternohyoid muscle from saline-treated WT (n = 4-5) and saline-treated *mdx* mice (n = 5), and WT (n = 4-5) and *mdx* (n = 4-5) mice treated with xIL-6R (0.2 mg/kg) and Ucn2 (30 μ g/kg) given as 6 sub-cutaneous injections over 2 weeks. Data were statistically compared by two-way ANOVA followed by Bonferroni *post hoc* test. The percentage of centrally nucleated fibres was significantly increased in *mdx* mice. Drug treatment slightly ameliorated central nucleation in *mdx* mice only. The percentage of inflammatory cell infiltrates was significantly increased in *mdx* mice. Drug treatment did not affect this response; $P = 0.2284$ compared with *mdx*. * $P < 0.05$. Central nucleation: Genotype $P < 0.0001$; treatment $P = 0.1$; interaction $P = 0.02$. Infiltration: Genotype: *** $P = 0.0002$, treatment $P = 0.2$; interaction $P = 0.2$.

5.3.8 Collagen content

Masson's trichrome staining was applied to investigate muscle collagen content between groups. The percentage area of collagen was significantly increased in *mdx* sternohyoid compared with WT (Fig. 5.5A+B; $P = 0.0103$; two-way ANOVA). Drug treatment had no significant effect on collagen content for both WT ($P > 0.05$) and *mdx* ($P > 0.05$) sternohyoid.

5.3.9 Chemokines

Figure 5.6 shows data for chemokine content in sternohyoid muscle from WT and *mdx* mice following drug or saline treatment. MIP-2, IP-10 and MIP-3 α were significantly increased in the *mdx* sternohyoid ($P < 0.0002$, MIP-2 and IP-10; $P = 0.004$, MIP-3 α ; two-way ANOVA) compared with WT controls. *Post hoc* analysis revealed that drug treatment significantly increased MIP-2, IP-10 and MIP-3 α in *mdx* sternohyoid ($P < 0.0001$, MIP-2 and IP-10; $P < 0.01$ MIP-3 α ; two-way ANOVA with Bonferroni), but not in WT mice ($P > 0.05$, Fig. 5.6A-C).

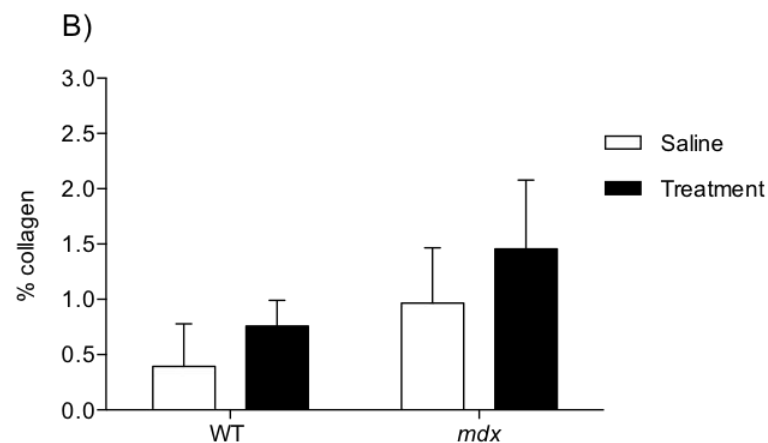
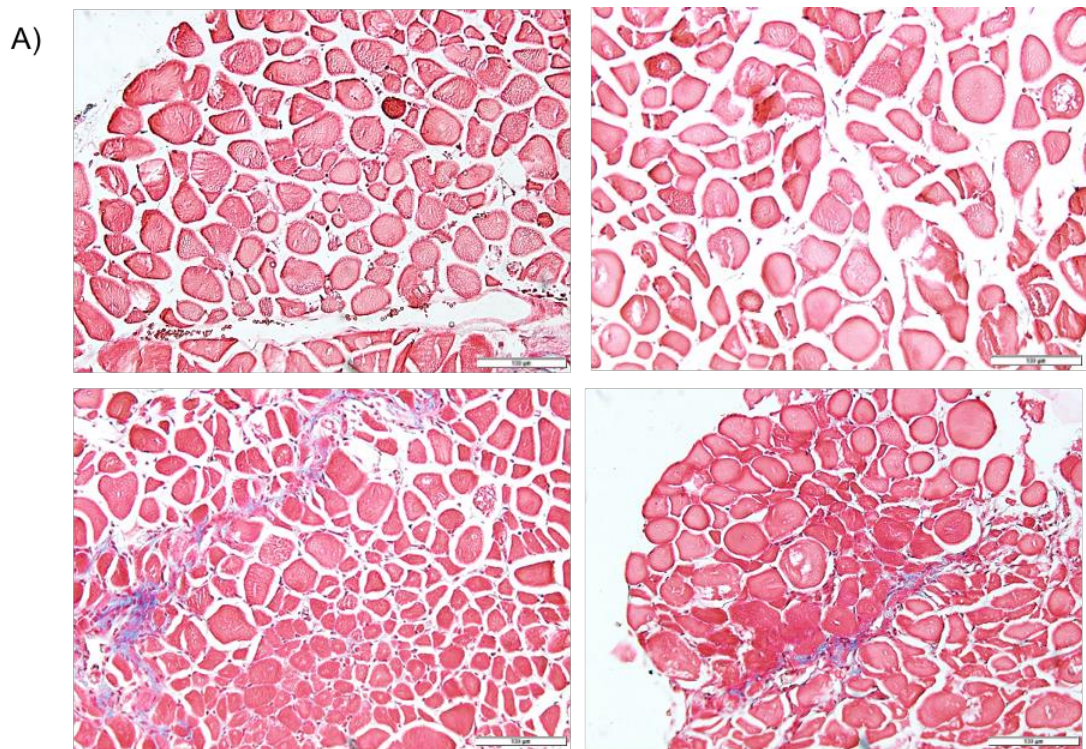


Figure 5.5 Collagen deposition in sternohyoid muscle

Representative histological images (A) of sternohyoid muscle transverse sections stained with mason's trichrome in WT saline (top left), *mdx* saline (bottom left), WT drug-treated (top right) and *mdx* drug-treated (bottom right) scale bars 100 μ m. Group data (mean \pm SD) showing percentage of collagen content (B) in sternohyoid muscle from saline-treated WT ($n = 5$) and saline-treated *mdx* mice ($n = 4$), and WT ($n = 4$) and *mdx* ($n = 5$) mice treated with xIL-6R (0.2 mg/kg) and Ucn2 (30 μ g/kg) given as 6 sub-cutaneous injections over 2 weeks. Data were statistically compared by two-way ANOVA followed by Bonferroni *post hoc* test. The percentage of collagen content was significantly increased in *mdx* mice. Drug treatment had no significant effect on collagen content for both WT and *mdx*. Genotype: $P = 0.0103$, treatment: $P = 0.0673$; interaction $P = 0.7779$.

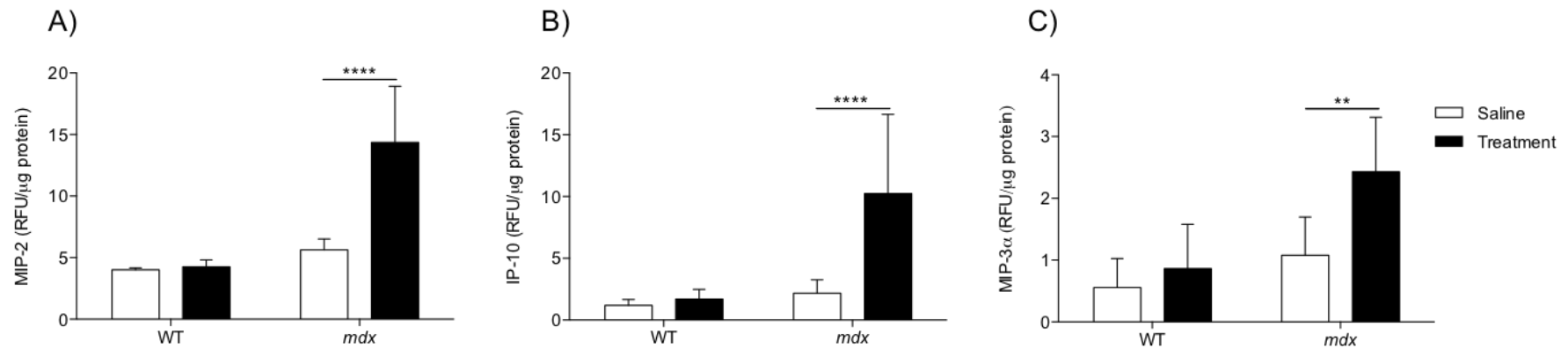


Figure 5.6 Chemokine expression in sternohyoid muscle

Values (mean \pm SD) for macrophage inflammatory protein 2 (MIP-2; A), interferon- γ induced protein (IP-10; B) and macrophage inflammatory protein-3 (MIP-3 α ; C) chemokine expression in sternohyoid muscle from WT (n = 7-8) and *mdx* (n = 7-8) mice injected sub-cutaneously with saline (0.9% w/v) or drug treatment (xIL-6R (0.2mg/kg) and Ucn2 (30 μ g/kg); co-administered) for two weeks. Data were statistically compared by two-way ANOVA followed by Bonferroni *post hoc* test. ** $P < 0.01$; **** $P < 0.0001$. MIP-2: genotype: $P < 0.0001$; treatment $P < 0.0001$; interaction: $P < 0.0001$. IP-10: genotype: $P = 0.0002$; treatment: $P = 0.0007$; interaction: $P = 0.0022$. MIP-3 α : genotype: $P = 0.0004$; treatment: $P = 0.0033$; interaction: $P = 0.0510$.

5.4 Discussion

The key findings of the present study are: (1) Sternohyoid muscle weakness in *mdx* mice is evidenced by reduced specific force and power output; (2) Sternohyoid weakness is associated with changes in myosin heavy chain isoform expression, with an increase in the abundance of type IIx and a concomitant decrease in type IIb fibres; (3) The incidence of centrally-nucleated muscle fibres, percentage and areal density of inflammatory cell infiltrates, and deposition of collagen was significantly increased in *mdx* sternohyoid; (4) Chemokines were significantly increased in *mdx* sternohyoid; (5) Co-treatment with the α IL-6R antibody and Ucn2 restored mechanical force and power production in *mdx* sternohyoid muscle; (6) Drug treatment significantly prevented or reversed fibre transitions in *mdx* sternohyoid, reduced the proportion of centrally nucleated fibres, but did not affect the total area of putative inflammatory cell infiltration, or collagen content within *mdx* muscle; (7) Drug treatment significantly increased chemokines in *mdx* sternohyoid muscle.

Chronic respiratory insufficiency is a cardinal feature of DMD. The diaphragm is severely affected, with muscle fibre degeneration and fibrosis central characteristics of the disease (De Bruin et al., 1997). DMD patients often suffer from SDB, with episodes of hypoventilation during sleep, associated with aberrant blood gas disturbances, necessitating ventilator use at later stages to maintain respiratory function, (Hukins & Hillman, 2000).

The *mdx* mouse, a dystrophin deficient model (Bulfield *et al.*, 1984), has been studied extensively to understand the pathophysiology of DMD and has also served as a pre-clinical model for the study of pharmacological treatment strategies (Manning & O'Malley, 2015). As DMD progresses, cardiopulmonary failure is the leading cause of death (Hukins & Hillman, 2000). The dystrophin deficient *mdx* mouse has a milder phenotype than DMD patients in the context of cardiac and limb muscle. In contrast, the respiratory muscles, including the sternohyoid muscle, show severe mechanical weakness at a young age in the *mdx* mouse (Burns & O'Halloran, 2016). Dystrophic diaphragm muscle undergoes repetitive cycles of

degeneration and regeneration, with additional activation of inflammatory cascades that further exacerbate muscle weakness. Whilst diaphragm muscle function has been well characterised in DMD (De Bruin *et al.*, 1997), and the *mdx* mouse (Coirault *et al.*, 1999; Coirault *et al.*, 2003; Bates *et al.*, 2013), little is known about the complementary muscles of breathing, especially the airway dilator muscles of the pharynx that are critical in the control of airway calibre, which is surprising given the prevalence of SDB in DMD boys (Bersanini *et al.*, 2012).

In the present study, we demonstrate that *mdx* sternohyoid muscle shows impaired performance at 8 weeks of age, consistent with our recent report (Burns & O'Halloran, 2016). This functional impairment is characterised by reduced specific force (twitch and tetanic contractions), reduced maximum mechanical work and power production, and reduced Vmax. Work and power production as a function of load bearing was significantly reduced for *mdx* saline compared with WT saline. We observed a ~44% decrease in sternohyoid muscle peak tetanic force for *mdx* saline versus WT saline, which is consistent with previous findings (Attal *et al.*, 2000; Burns & O'Halloran, 2016). These studies reveal severe mechanical dysfunction in sternohyoid muscle from young and aged *mdx* mice suggesting that upper airway obstruction in DMD may be a result of increased collapsibility of the pharyngeal airway arising from dysfunction of upper airway dilator muscles.

Sternohyoid muscle weakness in *mdx* was associated with a shift in the myosin heavy chain isoform distribution. Contractile performance in muscle correlates with fibre type distribution (Schiaffino & Reggiani, 2011). The sternohyoid muscle is phasically active during respiration (Van de Graaff *et al.*, 1984; O'Halloran *et al.*, 2002) and is composed solely of fast fibres (type II). Type II fibres display progressively increasing force production from type IIa to IIx fibres, with type IIb fibres producing the greatest forces but least resistance to fatigue (Polla *et al.*, 2004; Schiaffino & Reggiani, 2011). We observed a significant decrease in the relative proportion of type IIb fibres with a concomitant increase in the type IIx fibre count in *mdx* muscle. Since the type IIb fibres are the maximum force

producing units with the fastest kinetics, this finding is consistent with the functional data demonstrating decreased force-generating capacity and reduced shortening velocity in *mdx* compared with WT. Our findings are consistent with the observations of others (Attal *et al.*, 2000), who likewise reported reduced force-generating capacity and an increased proportion of type IIx and reduced type IIb in sternohyoid muscle from aged (6 month) *mdx* mice. We reason that this shift in the fibre type composition of the sternohyoid relates to muscle fibre degeneration and regeneration such that the muscle is in a relatively immature state. Muscle fibre remodelling will also alter motor neuronal input to the muscle. Since muscle fibre types are determined by the motor unit they are innervated by (Mantilla & Sieck, 2003), it is plausible to speculate that dystrophic muscle may have an altered motor unit innervation pattern which warrants investigation. There is a paucity of information pertaining to the accessory muscles of breathing in *mdx* mice. Unlike the well-characterised *mdx* diaphragm, the temporal profile of *mdx* sternohyoid muscle structure-function relationship throughout life is unknown, but published works suggest that the sternohyoid most likely undergoes a similar pathology to *mdx* diaphragm muscle (Attal *et al.* 2000; Burns *et al.* 2016).

The CSA of a muscle fibre is a determinant of force production. CSA varies between fibres increasing from type I fibres to type IIa and IIx, and type IIb (figure 5.3E). In DMD, the cycles of degeneration and regeneration within muscles leads to alterations in fibre size. As such, dystrophic muscle has myofibres of varying size compared to the uniformity of diameter found in a normal muscle (Pastoret & Sebille, 1995). Investigation of the CSA of individual muscle fibre types revealed that *mdx* sternohyoid shows evidence of hypertrophied type IIa and type IIx fibres. Increasing CSA can be viewed as an adaptive mechanism in the context of force production, often observed with resistance training increasing muscle strength. However, alterations in fibre size secondary to degeneration and regeneration are characteristic of *mdx* muscle with regeneration producing hypertrophied fibres, which are often functionally weaker (Lynch *et al.*, 2001).

Dystrophic skeletal muscle undergoes progressive cycles of fibre degeneration and regeneration following damage, a process that continues until the regenerative capacity is exhausted. Skeletal muscle fibre central nucleation is a histological indicator of muscle fibre repair and regeneration. We observed a significant increase in the percentage of centrally nucleated myofibres in *mdx* sternohyoid compared with WT, with ~25% of *mdx* sternohyoid fibres presenting with central nuclei. This reveals that sternohyoid muscle from *mdx* mice is undergoing significant muscle damage and repair as early as 8 weeks of age, consistent with evidence of severe muscle weakness.

Inflammation is recognised to be a contributing factor to DMD pathology, which is characterised by a persistent inflammatory response in skeletal muscle due to chronic damage and stress to functional muscle fibres due to the absence of dystrophin (Deconinck & Dan, 2007). Inflammatory cell infiltration of damaged and degenerating dystrophic muscle fibres is a hallmark feature of skeletal muscle pathology in DMD. Inflammatory cell infiltration has been shown to exacerbate myofibre damage in *mdx* mice (Evans *et al.*, 2009a), with loss of muscle fibres, subsequent fibrosis, and adipose tissue deposition culminating in impaired muscle function (Deconinck & Dan, 2007). We observed a significant increase in putative inflammatory cell infiltration in young *mdx* sternohyoid muscle, typically thought to be associated with muscle damage and subsequent regeneration. Enhanced inflammatory cell infiltrate drives a fibrotic environment (Pelosi *et al.*, 2015b). Indeed, we observed a significant increase in the collagen content of the *mdx* sternohyoid. Fibrosis is well characterised in the diaphragm of *mdx* mice (Stedman *et al.*, 1991), but to our knowledge this is the first report of enhanced collagen deposition in a complementary muscle of breathing, the sternohyoid. Enhanced collagen deposition within the muscle impairs muscle functional performance, which given the role of the sternohyoid as an airway dilator has implications for adequate control of airway calibre in DMD.

DMD patients and the *mdx* mouse have elevated levels of circulating pro-inflammatory cytokines, namely IL-1, IL-6 and TNF α (Gosselin & Williams, 2006),

promoting an inflammatory response associated with dystrophic changes (Kumar & Boriek, 2003). Anti-inflammatory treatment with glucocorticoids is the main treatment strategy in delaying loss of ambulation in DMD but treatment is unfortunately associated with deleterious side effects (Pichavant *et al.*, 2011). Therefore, there is a need for new therapeutic strategies that can rescue or at least halt muscle impairments in DMD.

IL-6 is a pleiotropic cytokine, exhibiting both pro and anti-inflammatory properties, hence mediating diverse biological functions (Pedersen & Febbraio, 2008). Several studies have targeted pro-inflammatory cytokine signalling in *mdx* and examined their respective roles in the dystrophic process. TNF- α inhibition has been shown to have beneficial effects in *mdx* mice (Messina *et al.*, 2006; Messina *et al.*, 2009). IL-6 has been shown to promote muscle atrophy in rats (Haddad *et al.*, 2005) and mice (Tsujiyama *et al.*, 1996), which is amenable to blockade. Additionally, *mdx* mice crossed with mice overexpressing IL-6, present with a significant reduction in limb muscle force and a decline in performance during treadmill exercise, indicative of impaired muscle function (Pelosi *et al.*, 2015b). Treatment with an xIL-6R antibody, blocking IL-6 signalling, has been shown to decrease pro-inflammatory cytokine expression in the diaphragm, improving treadmill performance in *mdx* mice (Pelosi *et al.*, 2015b).

In the present study, co-administration of an IL-6 neutralising antibody (xIL-6R) and a CRFR2 agonist (Ucn2) in *mdx* mice resulted in significantly increased force-generating capacity compared with *mdx* mice treated with saline (~86% increase). Specific force in *mdx* sternohyoid following treatment was increased to values equivalent to WT saline. Drug treatment increased *mdx* sternohyoid work, power and shortening velocity over the load continuum (0-60% max tension). Increased work production following treatment in *mdx* is due to a positive inotropic effect on force-generating capacity since we observed no significant difference in peak shortening between *mdx* treatment and *mdx* saline. In contrast, increased *mdx* sternohyoid power production is due to both an increase in force-generating capacity and shortening velocity. Drug treatment in WT also had a positive inotropic

effect on force generation (~49% increase) compared with WT saline. For WT, drug treatment increased sternohyoid work and power as a function of load bearing, both of which are due to an inotropic effect on muscle force. Significant increases in WT sternohyoid specific force suggest direct inotropic effects of drug co-treatment on sternohyoid muscle fibres. However, it should be noted that we determined tissue, and not fibre, CSA for our calculation of specific force. Therefore, whilst our measurement accounts for force normalised to tissue CSA, it does not account for alterations in myofibre CSA, which contribute to force-generation in muscle. This is an important distinction since drug co-treatment caused fibre hypertrophy in WT (but not *mdx*) muscle. Ucn2 elevates cAMP, protein kinase A and the cAMP-binding protein Epac (Reutenauer-Patte et al., 2012), and improves calcium homeostasis in calcium over-loaded *mdx* striated muscle with beneficial protective effects reducing muscle necrosis (Reutenauer-Patte et al., 2012). CRFR2 agonists increase muscle fibre mass, with evidence of increased muscle fibre CSA and absolute muscle force (Hinkle et al. 2004), in addition to actions that prevent atrophying of muscle in various experimental models (Hinkle et al., 2003, 2004). As such, we posit that fibre hypertrophy likely contributed to enhanced force generation in WT sternohyoid. It remains unclear however, if drug co-treatment exerted direct inotropic effects on myofibres contributing to muscle force. Of interest, direct positive inotropic effects of Ucn2 have been noted in the treatment of heart failure (Bale et al, 2004) and Ucn2 has been shown to exert a positive inotropic effect in the isolated rat heart through cAMP-dependent mechanisms (Calderon-Sanchez et al., 2009), a major regulator of skeletal muscle contractility (Berdeaux et al., 2012).

Drug treatment in *mdx* mice significantly reduced type IIx and increased type IIb fibre distribution compared with untreated *mdx* saline. As such, drug treatment restored/ prevented fibre type transitions that are evident in the *mdx* saline group compared with WT saline. The preservation of type IIb fibres is likely contributing to the restoration of muscle force in *mdx* sternohyoid. Conversely, there was no difference in the distribution of any fibre type in the WT drug treatment group compared with WT saline. Ucn2 has been shown to induce anabolism in skeletal muscle (Reutenauer-Patte *et al.*, 2012). Anabolism in fibres supports increased

force production, which could be beneficial to the dystrophic muscles of *mdx* mice. Interestingly, we observed hypertrophy of type IIb fibres in WT sternohyoid, but not *mdx* sternohyoid following drug treatment, revealing a different structural basis for improved force comparing WT (hypertrophy) to *mdx* (fibre preservation).

Drug treatment in *mdx* slightly ameliorated sternohyoid muscle fibre central nucleation compared with *mdx* saline; conversely, percentage central nucleation was unaffected by treatment in WT sternohyoid. This suggests that drug treatment suppressed muscle fibre damage, resulting in fewer necrotic fibres, which should be beneficial for muscle performance. This observation highlights that muscle fibre preservation (and maturation to type IIb) is likely an important contributor to force generation in *mdx*-treated muscles in our study. However, of interest, drug treatment had no effect on collagen content or putative immune cell infiltration in *mdx* sternohyoid. As such, drug treatment was ineffective in reducing muscle fibrosis, perhaps resulting from muscle inflammation. As we did not characterise the nature of the infiltrate area (which we concede will also include non-immune cell types), we are unable to determine if drug treatment altered the cellular milieu in the interstitial spaces between myofibres. Chemokines were significantly increased in *mdx* sternohyoid muscle which is consistent with previous reports of elevated chemokines in muscle from *mdx* mice (Porter *et al.*, 2003; Demoule *et al.*, 2005). Interestingly, drug treatment in *mdx* significantly increased the content of chemo-attractant agents, suggesting that there may follow a heightened immune response in *mdx* muscle following drug treatment. Such a response could act to recruit immune cells to repair damaged muscle fibres, and thus lead to functional improvements in sternohyoid muscle, perhaps contributing to the impressive force recovery observed in our study.

From the present work we cannot ascertain which of the two drug treatments is responsible for the inotropic and structural effects observed in WT and *mdx* mice. Recent work investigated the individual roles of xIL-6R and Ucn2 in improving *mdx* diaphragm force (Manning *et al.*, 2017). Of relevance to the current study, Manning *et al.* (2017) revealed an additive effect of xIL-6R and Ucn2 co-treatment on

diaphragm muscle force providing the rationale for our combined drug approach. Additional studies describing the cellular mechanisms whereby xIL-6R and Ucn2 improve sternohyoid muscle function are warranted.

Our relatively short (2 week) intervention has yielded impressive findings, preserving sternohyoid muscle force-generating capacity in *mdx* mice. Although there are no temporal studies of the *mdx* sternohyoid during development to adulthood, the drug treatment began at a time when significant muscle remodelling is likely to be under way (based on work in *mdx* diaphragm (Coirault *et al.*, 2003). Intervention at a younger age and for a longer treatment duration would be an interesting study to explore the efficacy of the drug treatment before onset of muscle necrosis. It would also be of interest to determine if performance is preserved in older animals following treatment and if there are any adverse side effects due to prolonged drug treatment. Although drug treatment fully restored sternohyoid muscle force, there was no difference in the relative area of infiltration in the *mdx* sternohyoid drug-treatment group compared with *mdx* saline. Our data suggest that the beneficial effect of drug treatment on sternohyoid muscle fibre form and function is achieved without any apparent influence on local muscle inflammation and fibrosis, linked to on-going muscle fibre damage and repair. This suggests that the beneficial effect of the drug therapy relates to a retardation in muscle fibre damage allowing maturation of functional fibres, but without overt changes in muscle infiltrate. However, it is important to note that the nature of the inflammatory infiltrate may be favourably altered by drug treatment. Macrophages can exist in one of two states, M1 or M2. While M2 macrophages contribute to muscle repair, M1 macrophages can increase muscle fibre lysis (Villalta *et al.*, 2015). Therefore, depending on the state of the infiltrating macrophage, inflammation can result in adaptive or maladaptive processes promoting regeneration or driving muscle wasting. We did not characterise the nature of the infiltrate in *mdx* muscle and therefore we cannot comment on the effect of drug treatment on the immune cell signature in *mdx* muscle. This requires further investigation, especially in the light of our observation that chemokines were increased in *mdx* and further increased by drug treatment, which may have established a beneficial immune

response that favoured muscle performance. We also acknowledge that IL-6 blockade may have arrested beneficial actions of the myokine in muscle such as promoting myoblast proliferation and myotube formation.

In summary, *mdx* sternohyoid shows evidence of severe mechanical dysfunction and fibre type immaturity at an early age. Co-treatment with an anti-IL-6 receptor antibody and CRF-2 receptor agonist (Ucn2) had a positive inotropic effect, restoring mechanical force and power in dystrophic sternohyoid muscle. Drug treatment preserved fibre complement in *mdx* sternohyoid and slightly ameliorated the proportion of fibres with evidence of central nucleation indicative of damage. Preservation of MyHC type IIb fibres as well as a partial reduction in centronucleation suggesting a preservation of functional fibres may underpin, at least in part, recovery of force production in the *mdx* drug-treated mice. Following a relatively short drug intervention period, recovery of contractile function was impressive in our study highlighting the potential utility of this combination therapy in DMD.

5.5 Additional information

Disclosures

The authors have no financial, professional or personal conflicts relating to this publication.

Author contributions

DPB: experimental design; acquisition of data; analysis and interpretation of data; drafting of the original manuscript; JR: immunohistochemistry studies: acquisition of data; analysis; LC: histology studies: acquisition of data; analysis; KM: muscle function studies: acquisition of data; analysis; MB: collagen studies: acquisition of data; analysis; DOM: experimental design; critical revision of the manuscript for important intellectual content; KOH: experimental design; interpretation of data; drafting and critical revision of the manuscript for important intellectual content; DE: immunohistochemistry and histological studies: experimental design; data acquisition; interpretation of data; drafting and critical revision of the manuscript for important intellectual content.

Acknowledgements

DPB was supported by funding from the Department of Physiology, UCC. The monoclonal anti-IL-6 receptor antibody was gifted by Chugai Pharmaceuticals, Tokyo, Japan. We are grateful to staff of the Biological Services Unit, UCC for support with animal care and welfare. We are grateful to Dr. G. Jasionek, Department of Physiology, UCC for technical support.

5.6 References

- Attal P, Lambert F, Marchand-Adam S, Bobin S, Pourny JC, Chemla D, Lecarpentier Y & Coirault C. (2000). Severe mechanical dysfunction in pharyngeal muscle from adult mdx mice. *Am J Respir Crit Care Med* **162**, 278-281.
- Barbé F, Quera-Salva MA, McCann C, Gajdos P, Raphael JC, de Lattre J & Agustí AG. (1994). Sleep-related respiratory disturbances in patients with Duchenne muscular dystrophy. *Eur Respir J* **7**, 1403-1408.
- Bates G, Sigurdardottir S, Kachmar L, Zitouni NB, Benedetti A, Petrof BJ, Rassier D & Lauzon AM. (2013). Molecular, cellular, and muscle strip mechanics of the mdx mouse diaphragm. *Am J Physiol Cell Physiol* **304**, C873-880.
- Beck J, Weinberg J, Hamnegård CH, Spahija J, Olofson J, Grimby G & Sinderby C. (2006). Diaphragmatic function in advanced Duchenne muscular dystrophy. *Neuromuscul Disord* **16**, 161-167.
- Bersanini C, Khirani S, Ramirez A, Lofaso F, Aubertin G, Beydon N, Mayer M, Maincent K, Boulé M & Fauroux B. (2012). Nocturnal hypoxaemia and hypercapnia in children with neuromuscular disorders. *Eur Respir J* **39**, 1206-1212.
- Bulfield G, Siller WG, Wight PA & Moore KJ. (1984). X chromosome-linked muscular dystrophy (mdx) in the mouse. *Proc Natl Acad Sci U S A* **81**, 1189-1192.
- Burns DP, Edge D, O'Malley D & O'Halloran KD. (2015). Respiratory Control in the mdx Mouse Model of Duchenne Muscular Dystrophy. *Adv Exp Med Biol* **860**, 239-244.
- Burns DP & O'Halloran KD. (2016). Evidence of hypoxic tolerance in weak upper airway muscle from young mdx mice. *Respir Physiol Neurobiol* **226**, 68-75.
- Coirault C, Lambert F, Marchand-Adam S, Attal P, Chemla D & Lecarpentier Y. (1999). Myosin molecular motor dysfunction in dystrophic mouse diaphragm. *Am J Physiol* **277**, C1170-1176.
- Coirault C, Pignol B, Cooper RN, Butler-Browne G, Chabrier PE & Lecarpentier Y. (2003). Severe muscle dysfunction precedes collagen tissue proliferation in mdx mouse diaphragm. *J Appl Physiol (1985)* **94**, 1744-1750.
- De Bruin PF, Ueki J, Bush A, Khan Y, Watson A & Pride NB. (1997). Diaphragm thickness and inspiratory strength in patients with Duchenne muscular dystrophy. *Thorax* **52**, 472-475.
- Deconinck N & Dan B. (2007). Pathophysiology of duchenne muscular dystrophy: current hypotheses. *Pediatr Neurol* **36**, 1-7.

- Demoule A, Divangahi M, Danialou G, Gvozdic D, Larkin G, Bao W & Petrof BJ. (2005). Expression and regulation of CC class chemokines in the dystrophic (mdx) diaphragm. *Am J Respir Cell Mol Biol* **33**, 178-185.
- Emery AE. (1991). Population frequencies of inherited neuromuscular diseases--a world survey. *Neuromuscul Disord* **1**, 19-29.
- Evans NP, Misyak SA, Robertson JL, Bassaganya-Riera J & Grange RW. (2009a). Dysregulated intracellular signaling and inflammatory gene expression during initial disease onset in Duchenne muscular dystrophy. *Am J Phys Med Rehabil* **88**, 502-522.
- Evans NP, Misyak SA, Robertson JL, Bassaganya-Riera J & Grange RW. (2009b). Immune-mediated mechanisms potentially regulate the disease time-course of duchenne muscular dystrophy and provide targets for therapeutic intervention. *PM R* **1**, 755-768.
- Gosselin LE & Williams JE. (2006). Pentoxifylline fails to attenuate fibrosis in dystrophic (mdx) diaphragm muscle. *Muscle Nerve* **33**, 820-823.
- Haddad F, Zaldivar F, Cooper DM & Adams GR. (2005). IL-6-induced skeletal muscle atrophy. *J Appl Physiol (1985)* **98**, 911-917.
- Hall JE, Kaczor JJ, Hettinga BP, Isfort RJ & Tarnopolsky MA. (2007). Effects of a CRF2R agonist and exercise on mdx and wildtype skeletal muscle. *Muscle Nerve* **36**, 336-341.
- Hill NS, Redline S, Carskadon MA, Curran FJ & Millman RP. (1992). Sleep-disordered breathing in patients with Duchenne muscular dystrophy using negative pressure ventilators. *Chest* **102**, 1656-1662.
- Hinkle RT, Donnelly E, Cody DB, Bauer MB & Isfort RJ. (2003). Urocortin II treatment reduces skeletal muscle mass and function loss during atrophy and increases nonatrophying skeletal muscle mass and function. *Endocrinology* **144**, 4939-4946.
- Hukins CA & Hillman DR. (2000). Daytime predictors of sleep hypoventilation in Duchenne muscular dystrophy. *Am J Respir Crit Care Med* **161**, 166-170.
- Jonsdottir IH, Schjerling P, Ostrowski K, Asp S, Richter EA & Pedersen BK. (2000). Muscle contractions induce interleukin-6 mRNA production in rat skeletal muscles. *J Physiol* **528 Pt 1**, 157-163.
- Kumar A & Boriek AM. (2003). Mechanical stress activates the nuclear factor-kappaB pathway in skeletal muscle fibers: a possible role in Duchenne muscular dystrophy. *FASEB J* **17**, 386-396.

- Lewis P, Sheehan D, Soares R, Coelho AV & O'Halloran KD. (2016). Redox Remodeling Is Pivotal in Murine Diaphragm Muscle Adaptation to Chronic Sustained Hypoxia. *Am J Respir Cell Mol Biol* **55**, 12-23.
- Lewis P, Sheehan D, Soares R, Varela Coelho A & O'Halloran KD. (2015). Chronic sustained hypoxia-induced redox remodeling causes contractile dysfunction in mouse sternohyoid muscle. *Front Physiol* **6**, 122.
- Lynch GS, Hinkle RT, Chamberlain JS, Brooks SV & Faulkner JA. (2001). Force and power output of fast and slow skeletal muscles from mdx mice 6-28 months old. *J Physiol* **535**, 591-600.
- Manning J, Buckley MM, O'Halloran KD & O'Malley D. (2016). In vivo neutralization of IL-6 receptors ameliorates gastrointestinal dysfunction in dystrophin-deficient mdx mice. *Neurogastroenterol Motil* **28**, 1016-1026.
- Manning J, Buckley MM, O'Halloran KD & O'Malley D. (2017). Combined xIL-6R and urocortin-2 treatment restores mdx diaphragm muscle force. *Muscle Nerve*.
- Manning J & O'Malley D. (2015). What has the mdx mouse model of duchenne muscular dystrophy contributed to our understanding of this disease? *J Muscle Res Cell Motil*.
- Mantilla CB & Sieck GC. (2003). Invited review: Mechanisms underlying motor unit plasticity in the respiratory system. *J Appl Physiol (1985)* **94**, 1230-1241.
- Messina S, Bitto A, Aguenouz M, Mazzeo A, Migliorato A, Polito F, Irrera N, Altavilla D, Vita GL, Russo M, Naro A, De Pasquale MG, Rizzuto E, Musarò A, Squadrito F & Vita G. (2009). Flavocoxid counteracts muscle necrosis and improves functional properties in mdx mice: a comparison study with methylprednisolone. *Exp Neurol* **220**, 349-358.
- Messina S, Bitto A, Aguenouz M, Minutoli L, Monici MC, Altavilla D, Squadrito F & Vita G. (2006). Nuclear factor kappa-B blockade reduces skeletal muscle degeneration and enhances muscle function in Mdx mice. *Exp Neurol* **198**, 234-241.
- Messina S, Vita GL, Aguenouz M, Sframeli M, Romeo S, Rodolico C & Vita G. (2011). Activation of NF-kappaB pathway in Duchenne muscular dystrophy: relation to age. *Acta Myol* **30**, 16-23.
- Moran EM & Mastaglia FL. (2014). Cytokines in immune-mediated inflammatory myopathies: cellular sources, multiple actions and therapeutic implications. *Clin Exp Immunol* **178**, 405-415.
- Nowak KJ & Davies KE. (2004). Duchenne muscular dystrophy and dystrophin: pathogenesis and opportunities for treatment. *EMBO Rep* **5**, 872-876.

- O'Halloran KD. (2006). Effects of nicotine on rat sternohyoid muscle contractile properties. *Respir Physiol Neurobiol* **150**, 200-210.
- O'Halloran KD, McGuire M, O'Hare T & Bradford A. (2002). Chronic intermittent asphyxia impairs rat upper airway muscle responses to acute hypoxia and asphyxia. *Chest* **122**, 269-275.
- O'Leary AJ & O'Halloran KD. (2016). Diaphragm muscle weakness and increased UCP-3 gene expression following acute hypoxic stress in the mouse. *Respir Physiol Neurobiol* **226**, 76-80.
- Okazaki M, Yamada Y, Nishimoto N, Yoshizaki K & Mihara M. (2002). Characterization of anti-mouse interleukin-6 receptor antibody. *Immunol Lett* **84**, 231-240.
- Pastoret C & Sebillé A. (1995). Age-related differences in regeneration of dystrophic (mdx) and normal muscle in the mouse. *Muscle Nerve* **18**, 1147-1154.
- Pedersen BK & Febbraio MA. (2008). Muscle as an endocrine organ: focus on muscle-derived interleukin-6. *Physiol Rev* **88**, 1379-1406.
- Pelosi L, Berardinelli MG, De Pasquale L, Nicoletti C, D'Amico A, Carvello F, Moneta GM, Catizone A, Bertini E, De Benedetti F & Musarò A. (2015a). Functional and Morphological Improvement of Dystrophic Muscle by Interleukin 6 Receptor Blockade. *EBioMedicine* **2**, 285-293.
- Pelosi L, Berardinelli MG, Forcina L, Spelta E, Rizzuto E, Nicoletti C, Camilli C, Testa E, Catizone A, De Benedetti F & Musarò A. (2015b). Increased levels of interleukin-6 exacerbate the dystrophic phenotype in mdx mice. *Hum Mol Genet* **24**, 6041-6053.
- Pichavant C, Aartsma-Rus A, Clemens PR, Davies KE, Dickson G, Takeda S, Wilton SD, Wolff JA, Wooddell CI, Xiao X & Tremblay JP. (2011). Current status of pharmaceutical and genetic therapeutic approaches to treat DMD. *Mol Ther* **19**, 830-840.
- Polla B, D'Antona G, Bottinelli R & Reggiani C. (2004). Respiratory muscle fibres: specialisation and plasticity. *Thorax* **59**, 808-817.
- Porter JD, Guo W, Merriam AP, Khanna S, Cheng G, Zhou X, Andrade FH, Richmonds C & Kaminski HJ. (2003). Persistent over-expression of specific CC class chemokines correlates with macrophage and T-cell recruitment in mdx skeletal muscle. *Neuromuscul Disord* **13**, 223-235.
- Reutenauer-Patte J, Boittin FX, Patthey-Vuadens O, Ruegg UT & Dorchies OM. (2012). Urocortins improve dystrophic skeletal muscle structure and

function through both PKA- and Epac-dependent pathways. *Am J Pathol* **180**, 749-762.

Rufo A, Del Fattore A, Capulli M, Carvello F, De Pasquale L, Ferrari S, Pierroz D, Morandi L, De Simone M, Rucci N, Bertini E, Bianchi ML, De Benedetti F & Teti A. (2011). Mechanisms inducing low bone density in Duchenne muscular dystrophy in mice and humans. *J Bone Miner Res* **26**, 1891-1903.

Schiaffino S & Reggiani C. (2011). Fiber types in mammalian skeletal muscles. *Physiol Rev* **91**, 1447-1531.

Smith PE, Edwards RH & Calverley PM. (1989). Ventilation and breathing pattern during sleep in Duchenne muscular dystrophy. *Chest* **96**, 1346-1351.

Stedman HH, Sweeney HL, Shrager JB, Maguire HC, Panettieri RA, Petrof B, Narusawa M, Leferovich JM, Sladky JT & Kelly AM. (1991). The mdx mouse diaphragm reproduces the degenerative changes of Duchenne muscular dystrophy. *Nature* **352**, 536-539.

Suresh S, Wales P, Dakin C, Harris MA & Cooper DG. (2005). Sleep-related breathing disorder in Duchenne muscular dystrophy: disease spectrum in the paediatric population. *J Paediatr Child Health* **41**, 500-503.

Tsujinaka T, Fujita J, Ebisui C, Yano M, Kominami E, Suzuki K, Tanaka K, Katsume A, Ohsugi Y, Shiozaki H & Monden M. (1996). Interleukin 6 receptor antibody inhibits muscle atrophy and modulates proteolytic systems in interleukin 6 transgenic mice. *J Clin Invest* **97**, 244-249.

Van de Graaff WB, Gottfried SB, Mitra J, van Lunteren E, Cherniack NS & Strohl KP. (1984). Respiratory function of hyoid muscles and hyoid arch. *J Appl Physiol* **57**, 197-204.

Villalta SA, Rosenberg AS & Bluestone JA. (2015). The immune system in Duchenne muscular dystrophy: Friend or foe. *Rare Dis* **3**, e1010966.

White DP & Younes MK. (2012). Obstructive sleep apnea. *Compr Physiol* **2**, 2541-2594.

Whitham M & Febbraio MA. (2016). The ever-expanding myokinome: discovery challenges and therapeutic implications. *Nat Rev Drug Discov*.

Williams R, Lemaire P, Lewis P, McDonald FB, Lucking E, Hogan S, Sheehan D, Healy V & O'Halloran KD. (2015). Chronic intermittent hypoxia increases rat sternohyoid muscle NADPH oxidase expression with attendant modest oxidative stress. *Front Physiol* **6**, 15.

Chapter 6. Recovery of respiratory function in *mdx* mice co-treated with neutralizing interleukin-6 receptor antibodies and urocortin 2

David P. Burns¹, Leonie Canavan², Jane Rowland², Robin O'Flaherty¹, Molly Brannock², Sarah E. Drummond¹, Dervla O'Malley¹, Deirdre Edge² and Ken D. O'Halloran¹

¹*Department of Physiology, School of Medicine, College of Medicine and Health, University College Cork, Cork, Ireland*

²*Department of Physiology, School of Medicine, Trinity Biomedical Sciences Institute, Trinity College Dublin, the University of Dublin, Dublin, Ireland*

Paper published in *The Journal of Physiology*.

Key points

- Impaired ventilatory capacity and diaphragm muscle weakness are prominent features of Duchenne muscular dystrophy (DMD), with strong evidence of attendant systemic and muscle inflammation.
- We performed a two-week intervention in young wild-type and *mdx* mice, consisting of either injection of saline or co-administration of a neutralizing interleukin-6 receptor antibody (xIL-6R) and urocortin-2 (Ucn2), a corticotrophin releasing factor receptor 2 agonist. We examined breathing and diaphragm muscle form and function.
- Breathing and diaphragm muscle functional deficits are improved following xIL-6R and Ucn2 co-treatment in *mdx* mice. The functional improvements were associated with a preservation of *mdx* diaphragm muscle myosin heavy chain IIx fibre complement.
- The concentration of the pro-inflammatory cytokine interleukin-1 β was reduced and the concentration of the anti-inflammatory cytokine interleukin-10 was increased in *mdx* diaphragm following drug co-treatment.
- Our novel findings may have implications for the development of pharmacotherapies for the dystrophinopathies with relevance for breathing and respiratory muscle performance.

Abbreviations: ANOVA, analysis of variance; BB_n , breath-to-breath; BB_{n+1} , breath-to-breath interval; CRFR, corticotrophin releasing factor receptor; CSA, cross-sectional area; CT, contraction time; DMD, Duchenne muscular dystrophy; F_iO_2 , fractional inspired oxygen concentration; f_R , respiratory frequency; IL, interleukin; IL-6R, IL-6 receptor; L_o , optimum length; MyHC, myosin heavy chain; OCT, optimum cutting temperature; P_{max} , maximum mechanical power; SD1, short-term variability; SD2, long-term variability; S_{max} , maximum total shortening; T_e , expiratory duration; T_i , inspiratory duration; TNF- α , tumor necrosis factor alpha; Ucn2, Urocortin-2; V_{max} , maximum shortening velocity; V_E , minute ventilation; V_E/VCO_2 , ventilatory equivalent for carbon dioxide; V_E/VO_2 , ventilatory equivalent for oxygen; VCO_2 , carbon dioxide production; VO_2 , oxygen consumption; V_T , tidal volume; W_{max} , maximum mechanical work; WT, wild-type; xIL-6R, anti-IL-6R; $\frac{1}{2}$ RT, half relaxation time.

Abstract

The *mdx* mouse model of Duchenne muscular dystrophy shows evidence of hypoventilation and pronounced diaphragm dysfunction. Six-week-old male *mdx* (n = 32) and wild-type (WT; n = 32) mice received either saline (0.9% w/v) or a co-administration of neutralizing interleukin-6 receptor antibodies (xIL-6R; 0.2 mg/kg) and corticotrophin-releasing factor receptor 2 agonist (urocortin-2; 30 µg/kg), subcutaneously over 2 weeks. Breathing and diaphragm muscle contractile function (*ex vivo*) were examined. Diaphragm structure was assessed using histology and immunofluorescence. Muscle cytokine concentration was determined using a multiplex assay. Minute ventilation and diaphragm muscle peak specific force at 100 Hz were significantly depressed in *mdx* compared with WT. Drug treatment completely restored ventilation in *mdx* mice during normoxia and significantly increased *mdx* diaphragm force- and power-generating capacity. The number of centrally nucleated muscle fibres and the areal density of infiltrates and collagen content were significantly increased in *mdx* diaphragm; all indices were unaffected by drug co-treatment. The abundance of myosin heavy chain (MyHC) type IIx fibres was significantly decreased in *mdx* diaphragm; drug treatment preserved MyHC type IIx complement in *mdx* muscle. Drug co-treatment increased the cross-sectional area of MyHC type I and IIx fibres in *mdx* diaphragm. The cytokines IL-1 β , IL-6, KC/GRO and tumor necrosis factor- α were significantly increased in *mdx* diaphragm compared with WT. Drug co-treatment significantly decreased IL-1 β and increased IL-10 in *mdx* diaphragm. Drug co-treatment had no significant effect on WT diaphragm muscle structure or cytokine concentrations. Recovery of breathing and diaphragm force was impressive in our studies, with implication for human dystrophinopathies.

Keywords: Duchenne muscular dystrophy; *mdx*; interleukin-6; Urocortin-2; corticotrophin releasing factor; diaphragm muscle; breathing.

6.1 Introduction

Duchenne muscular dystrophy (DMD) is a fatal neuromuscular disease wherein patients lack the structural protein dystrophin. In the absence of dystrophin, extensive skeletal muscle weakness, damage and fibre remodelling occurs (Blake *et al.*, 2002). Weakness extends to the striated muscles of breathing, with patients displaying diaphragm muscle dysfunction (De Bruin *et al.*, 1997; Khirani *et al.*, 2014) with consequential respiratory disturbance (Smith *et al.*, 1989; Khan & Heckmatt, 1994) and disrupted blood gas homeostasis (Smith *et al.*, 1988).

Similar to DMD, the *mdx* mouse model of DMD shows evidence of diaphragmatic dysfunction and impaired ventilation (Stedman *et al.*, 1991; Coirault *et al.*, 1999; Mosqueira *et al.*, 2013; Burns *et al.*, 2015; Burns *et al.*, 2017c). Skeletal muscle weakness due to dystrophin deficiency is further driven by pathological changes due to extensive muscle damage, including muscle fibre degeneration and necrosis, fibrosis, inflammation and adipose tissue deposition. Inflammation is a secondary feature of DMD due to muscle damage caused by the absence of dystrophin (Deconinck & Dan, 2007). Inflammatory cells infiltrate damaged muscles mounting an inflammatory response through activation of cytokines and recruitment of additional immune cells to the damaged muscle (De Paepe & De Bleecker, 2013).

The expression of inflammatory cytokines is elevated in muscle biopsies and plasma samples from DMD patients and the *mdx* mouse model of DMD, some of which include tumor necrosis factor (TNF α), interleukin-1 (IL-1) and interleukin-6 (IL-6) (Chahbouni *et al.*, 2010; Messina *et al.*, 2011; Pelosi *et al.*, 2015a). IL-6 is considered a myokine that can be released from damaged muscle in response to muscle injury and is pleiotropic in nature. IL-6 exerts its pro-inflammatory actions via its trans-signalling pathway, mediated by the soluble IL-6 receptor (IL-6R). Recent studies examining blockade of IL-6 signalling in *mdx* mice have shown functional improvements in skeletal and smooth muscle (Pelosi *et al.*, 2015a; Manning *et al.*, 2016, 2017).

Muscle fibre loss occurs in DMD, with necrotic muscle fibres replaced by connective and adipose tissue. Signalling through the corticotrophin releasing factor receptor (CRFR) has been shown to modulate muscle mass. Activation of CRFR2 (expressed in skeletal muscle) in mice has been shown to increase muscle mass and prevent muscle mass and function loss in atrophying muscle (Hinkle *et al.*, 2003a; Hinkle *et al.*, 2003b; Hinkle *et al.*, 2004). Similarly, the CRFR2 agonist urocortin-2 (Ucn2) has been demonstrated to increase muscle mass and force in *mdx* mice (Reutenauer-Patte *et al.*, 2012; Manning *et al.*, 2017). Moreover, Ucn2 has been shown to exert beneficial effects on cardiac function in healthy subjects and heart failure patients (Stirrat *et al.*, 2016).

Recent studies have demonstrated that neutralization of the IL-6R (xIL-6R) and stimulation of CRFR2 (Ucn2) via a combined drug strategy in young *mdx* mice leads to beneficial improvements in diaphragm muscle functional capacity (Manning *et al.*, 2017), with a combinational strategy more effective than either drug administered independently. Similarly, a co-treatment of xIL-6R and Ucn2 completely recovered pharyngeal dilator muscle force loss in *mdx* mice (Burns *et al.*, 2017b).

We hypothesized that co-administration of xIL-6R antibodies and Ucn2 would improve ventilatory capacity in *mdx* by improvements in diaphragm muscle force-generating capacity. We further hypothesized that drug co-treatment would reduce inflammation and improve the quality of diaphragm muscle, preserving muscle fibre type distribution. We sought to examine ventilation and the form and function of diaphragm muscle from age-matched wild-type (WT) and *mdx* mice following saline or combined xIL-6R and Ucn2 drug treatment.

6.2 Methods

6.2.1 Ethical approval

Procedures on live animals were performed under licence in accordance with Irish and European directive 2010/63/EU following approval by University College Cork animal research ethics committee.

6.2.2 Animals

Male and female WT (C57BL/10ScSnJ) and *mdx* (C57BL/10ScSn-Dmd^{mdx}/J) mice were purchased from the Jackson Laboratory (Jackson Laboratory, Bar Harbor, ME, USA) and were bred in our institution's animal housing facility. Animals were housed conventionally in a temperature- and humidity-controlled facility, operating on a 12 h light:12 h dark cycle with food and water available *ad libitum*. Six-week-old male WT and *mdx* mice received an interventional drug treatment consisting of a co-administration of xIL-6R (IL-6R neutralizing antibody; MR16-1 (Okazaki *et al.*, 2002); 0.2 mg/kg; Chugai Pharmaceuticals, Chuo, Tokyo, Japan) and Ucn2 (CRFR2 agonist; 30 µg/kg; U9507; Sigma Aldrich, Wicklow, Ireland) or saline (vehicle control; 0.9% w/v). MR1-61 stock was stored at -80°C and Ucn2 stock was stored at -20°C. A working solution containing both MR16-1 (26.7µg/ml) and Ucn2 (4µg/ml) was made in sterile saline, distributed in aliquots and stored at -20°C until day of injection. The doses and treatment protocol were chosen based on previous studies by our research group (Manning *et al.*, 2016; Manning *et al.*, 2017). Drug treatment consisted of a total of six consecutive subcutaneous injections to the scruff of the neck, each on alternate days over the course of two weeks beginning at 6 weeks of age. Animals were injected with a 7.5 µl bolus per gram body mass. Male WT and *mdx* mice were assigned at random to saline or drug treatment, establishing the following four groups: WT + saline, WT + treatment, *mdx* + saline and *mdx* + treatment. Animals were anaesthetised with 5% isoflurane by inhalation in air and euthanized by cervical dislocation. A study of sternohyoid muscle form and function from these mice was published previously (Burns *et al.*, 2017b).

6.2.3 Respiratory measurements

Whole body plethysmography was used to examine ventilation in unrestrained and unanaesthetised mice during quiet rest. Mice from all four groups were studied: WT + saline (n = 14), WT + treatment (n = 10), *mdx* + saline (n = 10) and *mdx* + treatment (n = 12). Mice were introduced into plethysmograph chambers (Model PLY4211; volume=0.6L, Buxco Research Systems, Wilmington, NC, USA) and allowed a 60-90 minute acclimation period until sufficiently settled, with room air passing through each chamber (1 L/min).

Experimental protocol: Following acclimation, a 20-30 minute baseline recording was performed in normoxia. This was followed by a 20 minute hypoxic challenge ($F_{iO_2} = 0.1$; balance N_2). Following a 60 minute recovery in normoxia, a 20-30 minute normoxic baseline was recorded. Following this period, ventilatory responses to hypercapnic challenge (5% CO_2 ; balance O_2) were assessed in mice from all four groups. Unfortunately, technical issues encountered in two groups (WT + treatment and *mdx* + treatment) relating to inaccurate pre-calibrated gases necessitated exclusion of the complete data set, limiting comparisons to WT + saline versus *mdx* + saline during hypercapnic ventilation. Respiratory parameters including respiratory frequency (f_R), tidal volume (V_T), minute ventilation (V_E), inspiratory duration (T_i) and expiratory duration (T_e) were recorded on a breath-by-breath basis for analysis offline.

Data analysis: For the assessment of ventilatory parameters in normoxia, both normoxia bouts were pooled to generate one set of baseline (normoxia) data. For the hypoxic gas challenge, data are compared to the preceding baseline period and data are presented on a minute-by-minute basis thereafter. V_T and V_E were normalised for body mass (g). To assess respiratory stability during normoxia, the breath-to-breath (BB_n) and subsequent interval (BB_{n+1}) of 200 consecutive breaths were analysed. Short-term variability (SD1) and long-term variability (SD2) were calculated for all four groups (Peng *et al.*, 2011; Souza *et al.*, 2015).

6.2.4 Metabolism measurements

O₂ consumption (VO₂) and CO₂ production (VCO₂) were measured in mice undergoing the whole-body plethysmography protocol during normoxic baseline periods and during exposure to hypoxia. Airflow through the chamber was maintained at 1 L/min. Fractional concentrations of O₂ and CO₂ were measured in air entering and exiting the plethysmograph (O₂ and CO₂ analyser; ADInstruments, Colorado Springs, CO, USA) as previously described (Burns *et al.*, 2017c).

Data analysis: Calculation of VO₂ and VCO₂ was performed as previously described (Haouzi *et al.*, 2009; Burns *et al.*, 2017c). For the 20 min hypoxic challenge, data are shown after 5 min of exposure and are presented on a minute-by-minute basis thereafter. Data during hypoxia exposure were compared with the preceding baseline (F_iO₂ = 0.21). VO₂ and VCO₂ were normalised for body mass (g).

6.2.5 Tissue collection

The distance from nose-to-anus and nose-to-tail was examined postmortem as an index of somatic growth. The diaphragm muscle was excised with rib and central tendon intact and placed in a tissue bath at room temperature containing continuously gassed hyperoxic (95% O₂/ 5% CO₂) Krebs solution (in mM: NaCl, 120; KCl, 5; Ca²⁺ gluconate, 2.5; MgSO₄, 1.2; NaH₂PO₄, 1.2; NaHCO₃, 25; and glucose, 11.5) and *d*-tubocurarine (25µM) prior to functional analysis. The following organs and muscles were weighed (wet weight): spleen, lung, whole heart, right heart ventricle, left heart ventricle, tibialis anterior, extensor digitorum longus and soleus.

6.2.6 Muscle physiology

6.2.6.1 Ex vivo muscle preparation

One costal portion of the diaphragm was used immediately for functional analysis and the other portion was snap frozen in liquid nitrogen and stored at -80°C for subsequent molecular analysis. Longitudinally arranged bundles were prepared for assessment of contractile function. A single longitudinal strip (2 mm in diameter) for each animal was suspended vertically between two platinum plate electrodes.

Rib was attached to a fixed hook at one end and the central tendon was attached to a dual-mode lever transducer system (Aurora Scientific Inc.; Aurora, ON, Canada) by non-elastic string. Muscle preparations were studied in a water-jacketed muscle bath, containing Krebs solution, maintained at 35°C gassed with 95% O₂/ 5% CO₂. Preparations were allowed a 5 min equilibration period.

6.2.6.2 Isometric protocol

Following equilibration, the optimum length (L_o) was determined by adjusting the position of the force transducer by use of a micro-positioner between intermittent twitch contractions. The L_o was taken as the muscle length associated with maximal isometric twitch force in response to single isometric twitch stimulation (supramaximal stimulation, 1ms duration). Once L_o was determined, the muscle stayed at this length for the duration of the protocol. A single isometric twitch was measured. Peak isometric twitch force, contraction time (CT; time to peak force) and half relaxation time ($\frac{1}{2}$ RT; time for peak force to decay by 50%) were determined. Next, an isometric tetanic contraction was elicited by stimulating muscle strips with supramaximal voltage at 100 Hz for 300 ms duration. Peak isometric tetanic force was determined at 100Hz (O'Halloran, 2006; Burns & O'Halloran, 2016).

Data analysis: Specific force was calculated in N/cm² of muscle cross-sectional area (CSA). The CSA of each muscle strip was determined by dividing the muscle mass (weight in grams) by the product of muscle L_o (cm) and muscle density (assumed to be 1.06 g/cm³). The CT and $\frac{1}{2}$ RT were measured as indices of isometric twitch kinetics.

6.2.6.3 Isotonic protocol

Following the isometric protocol, concentric contractions were elicited in incremental steps with varying load (0%, 5%, 10%, 15%, 20%, 25%, 30%, 35%, 40%, 60%, 80, 100; % of force at 100Hz), with 30 s rest between each contraction. Muscle length returned to L_o following each contraction. Total shortening was determined as the maximum distance shortened during contraction. Shortening velocity was

determined as the distance shortened during the initial 30 ms of shortening (Lewis *et al.*, 2015; Lewis *et al.*, 2016). Mechanical work (force x total shortening) and power (force x shortening velocity) were determined at each step of the incremental load step test (Lewis *et al.*, 2015; Williams *et al.*, 2015; Burns & O'Halloran, 2016; O'Leary & O'Halloran, 2016).

Data analysis: Data were plotted as the measured variable versus % load. Total muscle shortening was normalised to L_0 and expressed in L/L_0 . Similarly, shortening velocity was normalised to L_0 and expressed in L_0/s . Maximum total shortening (S_{max}) and maximum shortening velocity (V_{max}) were measured when both were maximal at 0% load. Mechanical work was measured in J/cm^2 . Mechanical power was expressed in W/cm^2 . Maximum mechanical work (W_{max}) and power (P_{max}) were also measured and typically occurred between 30% and 40% load.

6.2.7 Muscle immunohistochemistry and histology

6.2.7.1 Tissue preparation

A section of the diaphragm muscle was excised and mounted on a cube of liver, allowing for a transverse orientation of muscle fibres. The tissue was covered in optimum cutting temperature (OCT; VWR International, Dublin, Ireland) embedding medium and frozen in isopentane cooled in liquid nitrogen and stored at $-80^{\circ}C$ for subsequent structural analysis ($n = 4-5$ per group). A separate section of the muscle was placed in 4% paraformaldehyde overnight at $4^{\circ}C$ before being transferred to 70% ethanol prior to tissue processing (Leica TP1020, Histokinetic; Leica Biosystems, Dublin, Ireland) and paraffin embedding (Sakura Tissue-Tek TEC, Histolab Histowax embedding medium), for histological analysis ($n = 4-5$ per group).

6.2.7.2 Myosin heavy chain fluorescence immunohistochemistry

Serial transverse sections ($10\mu m$) were cryosectioned (Model CM30505; Leica Microsystems, Nussloch, Germany) at $-22^{\circ}C$ and mounted on polylysine-coated glass slides (VWR International). Two slides per animal from 2 distinct regions containing a minimum of 4 sections per slide were processed for myosin heavy chain (MyHC) immunofluorescence. A hydrophobic pen (ImmEdgeTM; Vector

Laboratories Ltd., Peterborough, UK) was used to circumscribe each section on the slide, creating a well allowing for the containment of antibodies and to stop cross-reactivity of antibodies between muscle sections. Slides were immersed in phosphate-buffered saline (0.01M PBS; Sigma-Aldrich, Wicklow, Ireland) containing 1% bovine serum albumin (BSA; Sigma-Aldrich) for 15 mins, followed by three 5 min PBS rinses. This was followed by a 30 min wash in PBS containing 5% goat serum (Sigma-Aldrich). Before application of the primary mouse monoclonal antibodies (developed by S. Schiaffino and obtained from the Developmental Studies Hybridoma Bank (DSHB) at the University of Iowa, IA, USA), slides were subject to a further blocking step to enable the use of mouse monoclonal primary antibody staining on mouse tissue. Slides were incubated for 1 hour at room temperature with an unconjugated AffiniPure Fab Fragment Goat Anti-Mouse IgG (1:13; Jackson ImmunoResearch Labs, West Grove, PA, USA) diluted in PBS, followed by three 2 min washes in PBS. A triple-labelled approach was used to tag the 3 principal myosin isoforms using a cocktail of antibodies that targeted MyHC types I (BAD5, 1:100), IIa (sc71 1:100) and IIb (BFF3 1:100) on a single section. On a serial section a double-labelled approach was employed using a cocktail which consisted of a rabbit anti-laminin antibody (1:500, Sigma-Aldrich) and a pan-MyHC antibody for the indirect determination of pure MyHC IIx fibres, BF35 (1:50), labelling all MyHC isoforms but IIx, enabling visualization of IIx fibres by the absence of staining. The antibodies were diluted in PBS and 1% BSA and were incubated overnight at 4°C in a humidity chamber. Following this, slides were rinsed for three 5 min washes in PBS before application of the relevant secondary antibodies, diluted in PBS and 1% BSA. A cocktail of secondary antibodies was prepared containing AlexaFluor350-conjugated goat anti-mouse IgG2b (1:500, Invitrogen, Biosciences Ltd, Dun Laoghaire, Ireland), Dylight594-conjugated goat anti-mouse IgG1 (1:500; Jackson ImmunoResearch) and AlexaFluor488-conjugated goat anti-mouse IgM (1:250; Invitrogen), targeting MyHC I, IIa and IIb, respectively. For the double-labelled sections a Dylight594-conjugated goat anti-mouse IgG₁ (1:500; Jackson) and FITC-conjugated anti-rabbit secondary antibody (1:250; Sigma-Aldrich) were applied for 1 hour in the dark at room temperature. Slides were rinsed with PBS for three 5 min washes, cover slipped with polyvinyl alcohol (PVA) mounting medium with DABCO®

anti-fade (Sigma-Aldrich) before observation with a fluorescent microscope (Olympus BX51). Negative control experiments were run in parallel where the primary antibodies were omitted and the secondary antibodies were applied to ensure that tagging was specific.

Data analysis: For MyHC fibre type analysis, muscle sections were viewed at x10 magnification and images captured using an Olympus BX51 microscope and an Olympus DP71 camera. Cell Sens™ (Olympus) was used to digitally capture the images. Analysis was carried out using image J software, where fibre type CSA and fibre type distribution (areal density) for each MyHC fibre type were determined (Burns *et al.*, 2017b). For each animal, multiple sections throughout the muscle were viewed and 3-4 images analysed per fibre type.

6.2.7.3 Histological analysis

Paraffin embedded diaphragm muscle samples were sectioned using a microtome (Leica RM2135). Serial cross-sections (5 μm thick) were collected throughout the muscle (mid-belly and distal regions) onto polylysine coated glass slides (VWR) and oven-dried (overnight at 37°C) for histological analysis. To examine putative inflammatory cell infiltration, and central nucleation of muscle fibres, tissue sections were stained with Haematoxylin and Eosin (H&E). For collagen staining, a Masson's trichrome protocol was followed (Sigma-Aldrich). Slides were mounted using DPX mounting medium (Sigma-Aldrich, USA), air-dried and visualized on a bright field microscope (Olympus BX51) at x20 magnification.

Data analysis: H&E stained sections were visualized at x20 magnification. Six sections were examined across the muscle from the rostral, middle and caudal regions. Two randomly selected areas were captured per muscle section from non-overlapping areas for analysis. Muscle pathology was scored using ImageJ software. The number of myofibres displaying central nucleation was expressed as a percentage of the total number of myofibres per image. Putative inflammatory cell infiltration (the presence of cells in the extracellular matrix) was also scored and expressed as a percentage of the total area of muscle. For Masson's trichrome

staining, the microscope lighting exposure was maintained throughout. Three sections, with two images captured per section, from the mid-portion of the muscle, were analysed per animal. Images were analysed using a colour balance threshold (ImageJ software), and the area of collagen was expressed as a percentage of the total area of muscle.

6.2.7.4 Fluorescently labelled collagen binding protein

Additional collagen staining of the diaphragm muscle was carried out using a fluorescent collagen marker (CNA35-OG488), developed by (Krahn *et al.*, 2006) and kindly gifted by the Department of Zoology, Trinity College Dublin. The CNA-35 probe is specific for type I and III collagen, found abundantly in skeletal muscle tissue. Following deparaffinisation, slides were prepared for a citrate buffer (pH 6) antigen retrieval step and subsequently stored in PBS (0.01M) prior to fluorescent staining. Slides were incubated over night at 4°C with CNA35-OG488 (1:100 dilution in PBS). Following staining, slides were washed with PBS, incubated with Hoescht stain (Sigma-Aldrich) to visualize cell nuclei and finally cover slipped with PVA-DABCO mounting medium before observation with a confocal microscope (Leica SP8).

Data analysis: For CNA35-OG488 analysis, non-overlapping serial images (x20 magnification) were taken across a whole diaphragm muscle section. Images were analysed using a colour balance threshold (ImageJ software), and the area of collagen was expressed as a percentage of the total area of muscle.

6.2.8 Molecular studies

6.2.8.1 Tissue preparation

Diaphragm samples stored at -80°C were removed and allowed to defrost at 4°C for 5 minutes. All procedures were performed at 4°C to prevent protein degradation. Samples were homogenized in a lysis buffer (RIPA) made up from 10X RIPA, deionized water, 200mM sodium fluoride (NAF), 100mM phenylmethylsulfonyl fluoride (PMSF), protease cocktail inhibitor 1 and phosphatase cocktail inhibitor 2. Following the homogenization process, the reactant mixtures

were centrifuged (15,339 x *g*) at 4°C for 20 min and the supernatants were harvested. The total amount of protein for each tissue sample was determined using the Pierce Bicinchoninic Acid Assay (BCA assay; Thermo Fisher Scientific, Dublin, Ireland). Supernatants were stored at -80°C for subsequent use.

6.2.8.2 Cytokines

A multiplex cytokine assay (K15048G-1; Meso Scale Discovery, Rockville, MD) was used to examine cytokine concentrations in diaphragm muscle from all four groups (n = 8 per group). The assay was performed according to the manufacturer's instructions using an extended incubation time to improve detection (the plate was incubated overnight at 4°C). Following incubation, the plate was read on a Quickplex SQ 120 imager (Meso Scale Discovery).

6.2.9 Statistical analysis

Data are expressed as scatter point box and whisker plots (median, 25-75 centile, and scatter plot) or as mean ± SD. Data were statistically compared using Prism 6.0 (Graphpad Software, San Diego, CA, USA). For muscle immunohistochemistry and histology, group means were generated from multiple images averaged per animal. All data were statistically compared by two-way ANOVA (genotype x treatment) with Bonferroni *post hoc* test. *P* < 0.05 was deemed to be statistically significant.

6.3 Results

6.3.1 Body mass and organ measurements

Table 6.1 compares body mass, body length, organ and muscle mass in WT and *mdx* mice treated with saline or xIL-6R and Ucn2 (treatment). Spleen mass was significantly increased in *mdx* + saline ($P < 0.0001$; two-way ANOVA with Bonferroni) compared with WT + saline. Muscle mass was significantly increased for *mdx* + saline tibialis anterior ($P < 0.0001$) and soleus ($P < 0.01$) compared with WT + saline. Extensor digitorum longus from *mdx* mice was significantly heavier than WT ($P = 0.001$ (genotype); two-way ANOVA). There was a significant difference in body mass ($P < 0.0001$ (genotype); two-way ANOVA) between age-matched WT and *mdx* mice; *mdx* mice were heavier. Drug co-treatment had no effect on body mass ($P = 0.411$ (treatment); two-way ANOVA). Spleen and muscle mass were also unaffected by drug treatment.

	WT		<i>mdx</i>		Two-way ANOVA
	Saline (n = 10)	Treatment (n = 7)	Saline (n = 10)	Treatment (n = 6)	
Body mass (g)	21.0 ± 1.3	21.6 ± 0.8	24.4 ± 1.7*	24.7 ± 1.6	Genotype: <i>P</i> < 0.0001; Treatment: <i>P</i> = 0.411; Interaction: <i>P</i> = 0.7638
N-A (cm)	9.1 ± 0.2	9.2 ± 0.3	9.4 ± 0.2	9.1 ± 0.3	Genotype: <i>P</i> = 0.2576; Treatment: <i>P</i> = 0.2576; Interaction: <i>P</i> = 0.0121
N-T (cm)	16.5 ± 0.3	16.8 ± 0.4	16.6 ± 0.3	16.8 ± 0.4	Genotype: <i>P</i> = 0.4746; Treatment: <i>P</i> = 0.038; Interaction: <i>P</i> = 0.549
Spleen (mg)	55.8 ± 8.9	60.6 ± 6.2	119.4 ± 13.5*	118.8 ± 23.3	Genotype: <i>P</i> < 0.0001; Treatment: <i>P</i> = 0.6693; Interaction: <i>P</i> = 0.5816
Wet lung (mg)	124.5 ± 10.2	113.7 ± 7.5	121.8 ± 9.0	124.0 ± 9.4	Genotype: <i>P</i> = 0.2576; Treatment: <i>P</i> = 0.1966; Interaction: <i>P</i> = 0.0556
Heart (mg)	103.1 ± 8.1	96.7 ± 7.6	106.0 ± 10.1	110.1 ± 11.0	Genotype: <i>P</i> = 0.0167; Treatment: <i>P</i> = 0.7295; Interaction: <i>P</i> = 0.1112
RV (mg)	25.8 ± 5.3	30.9 ± 3.5	31.5 ± 5.3	31.7 ± 6.8	Genotype: <i>P</i> = 0.1073; Treatment: <i>P</i> = 0.1821; Interaction: <i>P</i> = 0.2172
LV (mg)	77.4 ± 7.6	68.5 ± 7.1	74.5 ± 7.1	78.5 ± 8.4	Genotype: <i>P</i> = 0.2028; Treatment: <i>P</i> = 0.3757; Interaction: <i>P</i> = 0.027
RV:LV	0.34 ± 0.09	0.46 ± 0.09	0.42 ± 0.07	0.41 ± 0.09	Genotype: <i>P</i> = 0.5691; Treatment: <i>P</i> = 0.105; Interaction: <i>P</i> = 0.0354
TA (mg)	34.7 ± 2.5	35.7 ± 1.5	58.4 ± 3.4*	70.0 ± 4.8	Genotype: <i>P</i> < 0.0001; Treatment: <i>P</i> = 0.1363; Interaction: <i>P</i> = 0.5224
EDL (mg)	7.6 ± 2.2	6.2 ± 1.5	9.1 ± 1.8	9.2 ± 0.6	Genotype: <i>P</i> = 0.001; Treatment: <i>P</i> = 0.2852; Interaction: <i>P</i> = 0.266
Sol (mg)	5.9 ± 1.3	6.0 ± 1.2	8.5 ± 1.7*	8.7 ± 1.9	Genotype: <i>P</i> < 0.0001; Treatment: <i>P</i> = 0.7927; Interaction: <i>P</i> = 0.9906

Table 6.1 Body mass, somatic growth, organ and muscle mass

Definition of abbreviations: N-A, distance from nose to anus; N-T, distance from nose to tip of tail; RV, right heart ventricle; LV, left heart ventricle; TA, tibialis anterior; EDL, extensor digitorum longus; sol, soleus; WT, wild-type. WT (n = 7-10) and *mdx* (n = 6-10) mice were injected subcutaneously with saline (0.9% w/v) or treatment [neutralizing interleukin-6 receptor antibodies (0.2 mg/kg) and urocortin 2 (30 µg/kg); co-administered] over 2 weeks. Data are shown as mean ± SD and were statistically compared using two-way ANOVA with Bonferroni *post hoc* test. **mdx* saline significantly different from corresponding WT saline values, *P* < 0.05.

6.3.2 Baseline ventilation and metabolism

Respiratory flow traces for WT and *mdx* mice following saline or drug co-treatment are shown in Fig. 6.1A. Minute ventilation during normoxia was significantly lower in *mdx* + saline compared with WT + saline (Fig. 6.1B; $P < 0.01$; two-way ANOVA with Bonferroni). The reduction in normoxic ventilation was due to a significantly lower tidal volume in *mdx* + saline compared with WT + saline (Table 6.2; $P < 0.05$). Respiratory frequency was significantly higher in *mdx* mice (Table 6.2; $P = 0.0047$ (genotype); two-way ANOVA). Drug co-treatment in *mdx* mice significantly increased minute ventilation (Fig. 6.1B; $P < 0.001$; two-way ANOVA with Bonferroni), due to a significant increase in tidal volume (Table 6.2. $P < 0.05$; two-way ANOVA with Bonferroni) and respiratory frequency (Table 6.2; $P = 0.0018$ (treatment); two-way ANOVA). There was no evidence of altered respiratory stability in *mdx* mice compared with WT, based on measures of breathing variability (SD1 and SD2; Table 6.2). Moreover, drug co-treatment had no effect on SD1 or SD2 for both WT and *mdx* mice.

When normalised for body mass, there was no difference in VO_2 (Table 6.2; $P = 0.4439$ (genotype); two-way ANOVA) and VCO_2 (Figure 6.1C.; $P = 0.8405$). When expressed in absolute terms, there was a slight increase in VO_2 in *mdx* mice compared with WT (Table 6.2; $P = 0.0432$); no difference was observed for VCO_2 (Table 6.2. $P = 0.117$). Drug co-treatment significantly decreased VO_2 (Table 6.2.) and VCO_2 (Fig. 6.1C) in WT ($P < 0.05$ and $P < 0.01$; two-way ANOVA with Bonferroni; VO_2 and VCO_2 , respectively) and *mdx* mice ($P < 0.05$ and $P < 0.05$). The ventilatory equivalent for O_2 (V_E/VO_2) was significantly increased in WT (Table 6.2.; $P < 0.05$) and *mdx* mice ($P < 0.05$) following drug co-treatment. Similarly, the ventilatory equivalent for CO_2 (V_E/VCO_2) was significantly increased by drug co-treatment for both WT (Fig. 6.1D; $P < 0.001$) and *mdx* mice (Fig. 6.1D; $P < 0.001$). Drug co-treatment had a significant effect on the ratio of VCO_2 to VO_2 (Table 6.2; $P = 0.0344$ (treatment); two-way ANOVA).

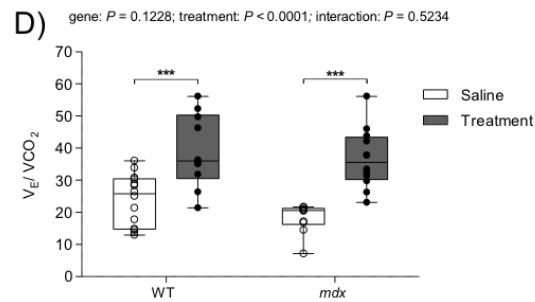
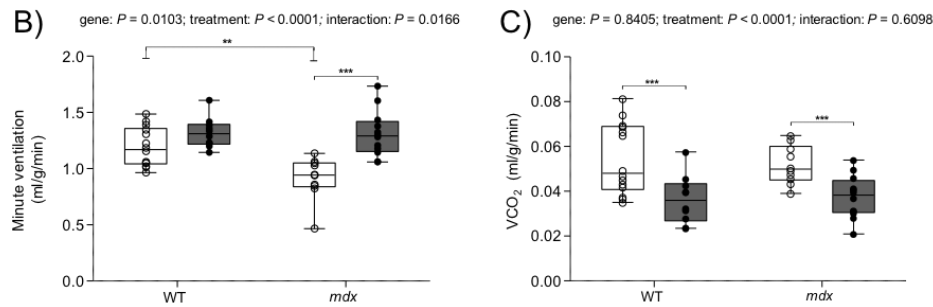
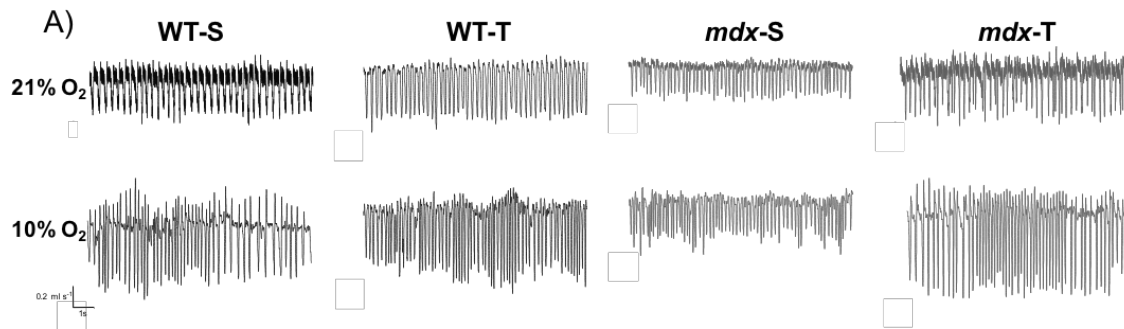


Figure 6.1 Ventilation in conscious mice

A, representative respiratory flow traces during normoxia (21% O₂) and hypoxia (10% O₂) in wild-type (WT) and *mdx* mice following six subcutaneous injections with saline (S; 0.9% w/v) or treatment [T; neutralizing interleukin-6 receptor antibodies (0.2 mg/kg) and urocortin 2 (30 µg/kg; co-administered)] over 2 weeks. Inspiration downwards. B-D, minute ventilation (B), carbon dioxide production (C; VCO₂) and ventilatory equivalent for carbon dioxide (D; V_E/V_{CO_2}) for WT and *mdx* mice following saline or drug treatment. Values (B-D) are expressed as scatter point box and whisker plots (median, 25-75 centile and scatter plot). Data were statistically compared by two-way ANOVA with Bonferroni *post hoc* test. ** $P < 0.01$; *** $P < 0.001$.

	WT		mdx		Two-way ANOVA
	Saline (n = 14)	Treatment (n = 10)	Saline (n = 10)	Treatment (n = 12)	
f_R (bpm)	165.0 ± 11.2	177.7 ± 11.9 [‡]	176.4 ± 15.7	189.0 ± 12.7	Genotype: <i>P</i> = 0.0047; Treatment: <i>P</i> = 0.0018; Interaction: <i>P</i> = 0.977
V_T (ml/g)	0.0074 ± 0.001	0.0076 ± 0.001	0.0053 ± 0.001*	0.0071 ± 0.001 [#]	Genotype: <i>P</i> < 0.0001; Treatment: <i>P</i> = 0.0016; Interaction: <i>P</i> = 0.017
VO₂ (ml/min)	1.38 ± 0.5	0.77 ± 0.2 [‡]	1.66 ± 0.4	1.04 ± 0.5 [#]	Genotype: <i>P</i> = 0.0432; Treatment: <i>P</i> < 0.0001; Interaction: <i>P</i> = 0.979
VO₂ (ml/g/min)	0.065 ± 0.02	0.037 ± 0.01 [‡]	0.068 ± 0.02	0.043 ± 0.02 [#]	Genotype: <i>P</i> = 0.4439; Treatment: <i>P</i> < 0.0001; Interaction: <i>P</i> = 0.7139
VCO₂ (ml/min)	1.16 ± 0.3	0.77 ± 0.2 [‡]	1.12 ± 0.2	0.90 ± 0.2 [#]	Genotype: <i>P</i> = 0.117; Treatment: <i>P</i> < 0.0001; Interaction: <i>P</i> = 0.8778
V_E/VO₂	21.9 ± 11.7	38.3 ± 10.6 [‡]	14.6 ± 5.1	35.5 ± 14.3 [#]	Genotype: <i>P</i> = 0.1344; Treatment: <i>P</i> < 0.0001; Interaction: <i>P</i> = 0.5089
VCO₂/VO₂	0.85 ± 0.2	1.03 ± 0.3	0.80 ± 0.2	0.97 ± 0.3	Genotype: <i>P</i> = 0.4647; Treatment: <i>P</i> = 0.0344; Interaction: <i>P</i> = 0.9504
Ti: SD1	18.9 ± 18.2	22.0 ± 8.6	16.3 ± 8.7	14.0 ± 5.0	Genotype: <i>P</i> = 0.128; Treatment: <i>P</i> = 0.9128; Interaction: <i>P</i> = 0.432
Ti: SD2	27.2 ± 14.0	28.1 ± 9.9	26.2 ± 21.1	21.0 ± 5.8	Genotype: <i>P</i> = 0.3048; Treatment: <i>P</i> = 0.579; Interaction: <i>P</i> = 0.4387
Te: SD1	59.8 ± 34.7	59.1 ± 26.0	63.7 ± 36.7	45.5 ± 17.6	Genotype: <i>P</i> = 0.5739; Treatment: <i>P</i> = 0.2777; Interaction: <i>P</i> = 0.3155
Te: SD2	93.1 ± 41.0	79.5 ± 19.6	75.6 ± 49.9	60.9 ± 19.5	Genotype: <i>P</i> = 0.0888; Treatment: <i>P</i> = 0.1827; Interaction: <i>P</i> = 0.9323

Table 6.2 Baseline ventilation and metabolic measurements

Definition of abbreviations: f_R, breathing frequency; V_T, tidal volume; VO₂, oxygen consumption; VCO₂, carbon dioxide production; V_E/VO₂, ventilatory equivalent for oxygen; VCO₂/VO₂, respiratory exchange ratio; Ti, inspiratory duration; Te, expiratory duration; SD1, short-term variability; SD2, long-term variability; WT, wild-type. WT (n = 10-14) and mdx (n = 10-12) mice were injected subcutaneously with saline (0.9% w/v) or treatment [neutralizing interleukin-6 receptor antibodies (0.2 mg/kg) and urocortin 2 (30 µg/kg); co-administered] over 2 weeks. Data are shown as mean ± SD and were statistically compared using two-way ANOVA with Bonferroni *post hoc* test. [‡]WT treatment significantly different from corresponding WT saline values, *P* < 0.05; *mdx saline significantly different from corresponding WT saline values, *P* < 0.05; [#]mdx treatment significantly different from corresponding mdx saline values, *P* < 0.05.

6.3.3 Ventilatory responsiveness to hypoxia

Figure 6.2A shows the time course of changes in minute ventilation in response to a 20 min hypoxic challenge ($F_{iO_2} = 0.1$; balance N_2). Ventilation increased rapidly in all four groups at the onset of hypoxia ($P < 0.0001$; two-way ANOVA) and then declined thereafter. Ventilation was significantly lower in *mdx* + saline compared with WT + saline when examined either over the time course of the hypoxic ventilatory response (Fig. 6.2A; $P = 0.0004$) or as maximum ventilation during challenge (Fig. 6.2B; $P < 0.0001$). The peak ventilatory response to hypoxia (ΔV_E) was lower in *mdx* + saline compared with WT + saline (Fig. 6.2C; $P < 0.001$; two-way ANOVA with Bonferroni). Drug co-treatment significantly increased minute ventilation for *mdx* + treatment compared with *mdx* + saline (Fig. 6.2A; $P = 0.02$; two-way ANOVA) during the 20 min exposure to hypoxia; peak ventilation was also higher (Fig. 6.2B; $P = 0.0006$). However, the peak ventilatory response to hypoxia (ΔV_E) was unchanged in *mdx* + treatment compared with *mdx* + saline (Fig. 6.2C; $P > 0.05$). By comparison, in WT mice, drug co-treatment had no significant effect on ventilation during exposure to hypoxia (Fig. 6.2A; $P = 0.9$) or peak ventilation in response to hypoxia (Fig. 6.2B; $P = 0.716$). V_E/VCO_2 increased in response to hypoxia (Fig. 6.2D; $P < 0.0001$). Drug co-treatment significantly increased V_E/VCO_2 during hypoxia in WT ($P = 0.024$) but not *mdx* mice ($P = 0.268$). Ventilation was significantly lower in *mdx* + saline compared with WT + saline during hypercapnic challenge (V_E during hypercapnia was 4.0 ± 1.4 versus 2.4 ± 0.8 ml/min/g, two-way ANOVA with Bonferroni *post hoc* test, $P < 0.001$ for WT + saline ($n = 8$) versus *mdx* + saline ($n = 8$)). The peak ventilatory response to hypercapnia (ΔV_E) was lower in *mdx* + saline compared with WT + saline (delta V_E was 2.9 ± 1.5 versus 1.4 ± 0.7 ml/min/g, unpaired Student's *t* test, $P = 0.21$ for WT + saline ($n = 8$) versus *mdx* + saline ($n = 8$)). We were unable to compare the effect of drug co-treatment on hypercapnic ventilation in WT and *mdx* mice.

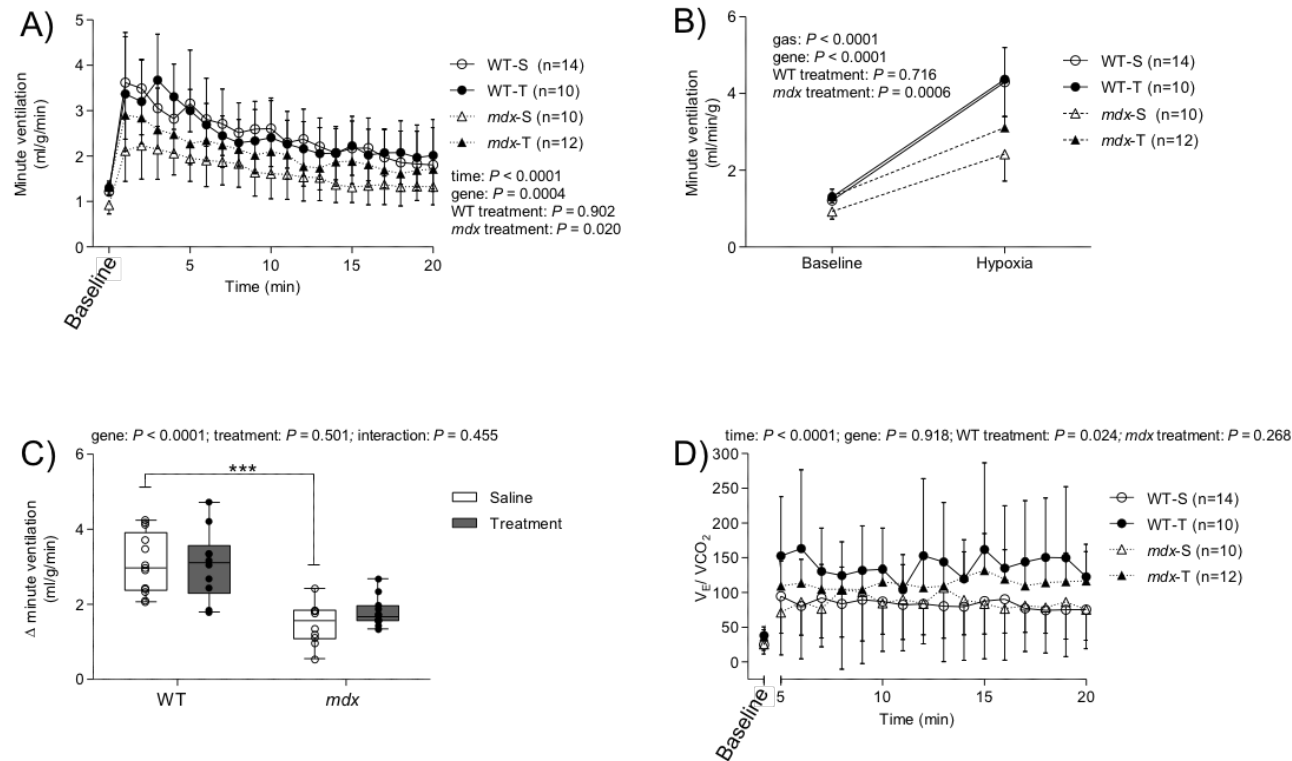


Figure 6.2 Ventilatory responsiveness to hypoxia

A, Group data (mean \pm SD) for minute ventilation during baseline and 20 min of exposure to hypoxia (A; 10% inspired oxygen; balance N_2) for wild-type (WT) and *mdx* mice following six subcutaneous injections with saline (0.9% w/v) or treatment [neutralizing interleukin-6 receptor antibodies (0.2 mg/kg) and urocortin 2 (30 μ g/kg); co-administered] over 2 weeks. Data were statistically compared by repeated measures two-way ANOVA. B, Group data (mean \pm SD) for minute ventilation during

baseline and peak ventilation during hypoxia for WT and *mdx* mice following saline or drug treatment. Data were statistically compared by repeated measures two-way ANOVA. C, Group data for peak ventilatory responsiveness (ΔV_E) to hypoxia for WT and *mdx* mice following saline or drug treatment. Values are expressed as scatter point box and whisker plots (median, 25-75 centile and scatter plot). Data were statistically compared by two-way ANOVA with Bonferroni *post hoc* test. * $P < 0.05$; *** $P < 0.001$. D, group data (mean \pm SD) for ventilatory equivalent for carbon dioxide (V_E/V_{CO_2}) during baseline and after 5-20 min of exposure to hypoxia for WT and *mdx* mice following saline or drug treatment. Data were statistically compared by repeated measures two-way ANOVA.

6.3.4 Isometric force and twitch contractile kinetics

Table 6.3 shows data for diaphragm muscle contractile kinetics (CT and $\frac{1}{2}$ RT) from WT and *mdx* mice following saline or drug co-treatment. Diaphragm CT was significantly higher for *mdx* + saline ($P < 0.05$; two-way ANOVA with Bonferroni) compared with WT + saline. Drug co-treatment had no significant effect on CT. There was no significant difference between WT and *mdx* for $\frac{1}{2}$ RT. Representative original traces for diaphragm muscle twitch and tetanic contractions, and maximum unloaded shortening are shown in Fig. 6.3A-C. Diaphragm twitch force was significantly lower in *mdx* + saline (Fig. 6.3D; $P < 0.05$) compared with WT + saline. Drug co-treatment had no significant effect on diaphragm twitch force (Fig. 6.3D; $P = 0.1766$ (treatment); two-way ANOVA). Diaphragm peak tetanic force at 100 Hz was significantly lower in *mdx* + saline (Fig. 6.3E; $P < 0.001$; two-way ANOVA with Bonferroni) compared with WT + saline. *Post hoc* analysis showed that drug treatment significantly increased tetanic force in *mdx*, but not WT diaphragm (Fig. 6.3E; $P < 0.05$).

6.3.5 Isotonic contractile parameters and kinetics

Table 6.3 shows data for diaphragm muscle isotonic contractile parameters: W_{max} , P_{max} , S_{max} and V_{max} . Diaphragm W_{max} was significantly reduced in *mdx* + saline compared with WT + saline ($P < 0.05$; two-way ANOVA with Bonferroni). There was no significant effect of drug co-treatment on W_{max} ($P = 0.0857$ (treatment); two-way ANOVA). P_{max} was significantly reduced in *mdx* + saline compared with WT + saline ($P < 0.05$; two-way ANOVA with Bonferroni). Drug treatment significantly increased P_{max} ($P = 0.0276$ (treatment); two-way ANOVA); P_{max} was increased by $\sim 130\%$ in *mdx* diaphragm following drug treatment. There was no significant difference in S_{max} or V_{max} between WT and *mdx* diaphragms. Although statistical significance was not achieved for the effect of drug co-treatment on W_{max} and V_{max} in *mdx* diaphragm, sizeable effects were noted, which may have physiological relevance. Drug co-treatment increased *mdx* diaphragm W_{max} by $\sim 100\%$ and V_{max} by $\sim 58\%$ compared with *mdx* + saline.

	WT		<i>mdx</i>		Two-way ANOVA
	Saline (n = 10)	Treatment (n = 7)	Saline (n = 8)	Treatment (n = 8)	
CT (ms)	18.4 ± 2.8	19.4 ± 2.1	21.8 ± 2.5*	21.6 ± 2.5	Genotype <i>P</i> = 0.0038; Treatment <i>P</i> = 0.6824; Interaction <i>P</i> = 0.5097
½ RT (ms)	23.5 ± 2.2	22.3 ± 2.6	23.9 ± 1.2	21.2 ± 6.4	Genotype <i>P</i> = 0.8129; Treatment <i>P</i> = 0.1353; Interaction <i>P</i> = 0.5761
Wmax (J/cm²)	1.5 ± 0.7	1.7 ± 1.0	0.5 ± 0.3*	1.0 ± 0.1	Genotype <i>P</i> = 0.0008; Treatment <i>P</i> = 0.0857; Interaction <i>P</i> = 0.6102
Pmax (W/cm²)	9.6 ± 3.9	11.9 ± 7.2	3.7 ± 2.9*	8.5 ± 2.5	Genotype <i>P</i> = 0.0047; Treatment <i>P</i> = 0.0276; Interaction <i>P</i> = 0.4137
Smax (L/L₀)	0.37 ± 0.11	0.42 ± 0.07	0.33 ± 0.11	0.39 ± 0.02	Genotype <i>P</i> = 0.2412; Treatment <i>P</i> = 0.0998; Interaction <i>P</i> = 0.7863
Vmax (L₀/s)	4.5 ± 1.3	4.3 ± 1.7	3.1 ± 1.9	4.9 ± 0.9	Genotype <i>P</i> = 0.4947; Treatment <i>P</i> = 0.1557; Interaction <i>P</i> = 0.0564

Table 6.3 Diaphragm muscle contractile properties

Group data (mean ± SD) for twitch contraction time (CT), twitch half-relaxation time (1/2 RT), maximum mechanical work (Wmax), maximum mechanical power (Pmax), peak shortening (Smax) and peak shortening velocity (Vmax) of diaphragm muscle from wild-type (WT; n = 7-10) and *mdx* (n = 8) mice injected subcutaneously with saline (0.9% w/v) or treatment [neutralizing interleukin-6 receptor antibodies (0.2 mg/kg) and urocortin 2 (30 µg/kg); co-administered] over 2 weeks. Data were statistically compared by two-way ANOVA followed by Bonferroni *post hoc* test. **mdx* saline significantly different from corresponding WT saline value, *P* < 0.05.

6.3.6 Isotonic load relationships

Figure 6.3 (F-I) shows data for diaphragm muscle isotonic load relationships. Loading had a significant effect on work (Fig. 6.3F; $P < 0.0001$; two-way ANOVA), power (Fig. 6.3G; $P < 0.0001$), shortening (Fig. 6.3H; $P < 0.0001$) and shortening velocity (Fig. 6.3I; $P < 0.0001$). Diaphragm from *mdx* + saline had significantly reduced work ($P < 0.0001$), power ($P < 0.0001$), shortening ($P < 0.0001$) and shortening velocity ($P = 0.0003$) compared with WT + saline. Drug treatment increased *mdx* diaphragm work ($P < 0.0001$) and WT diaphragm work ($P = 0.059$). Following drug co-treatment, power production was significantly increased in WT ($P = 0.009$) and *mdx* diaphragm ($P < 0.0001$). Shortening ($P = 0.0001$) and shortening velocity ($P < 0.0001$) were also significantly increased for *mdx* diaphragm after drug co-treatment.

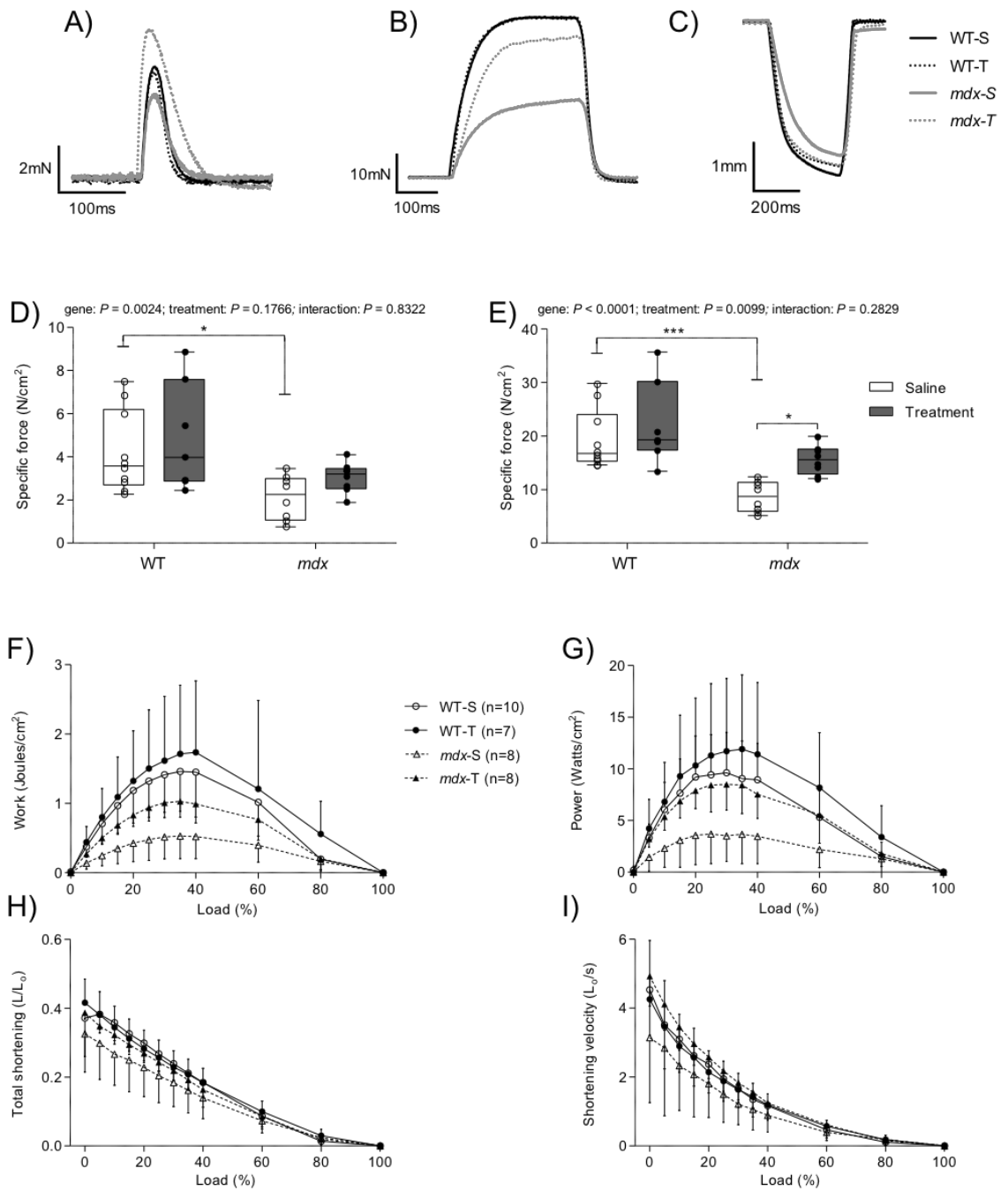


Figure 6.3 Diaphragm muscle function

A-C, original traces of muscle twitch (A) and tetanic (B) contractions and maximum unloaded shortening (C) for diaphragm muscle from wild-type (WT) and *mdx* mice following six subcutaneous injections with saline (S; 0.9% w/v) or treatment [T; neutralizing interleukin-6 receptor antibodies (0.2 mg/kg) and urocortin 2 (30 μ g/kg); co-administered] over 2 weeks. D and E, group data for twitch (D) and tetanic (E) force in WT ($n = 7-10$) and *mdx* ($n = 8$) diaphragm muscle following saline or treatment. Peak tetanic force was measured following stimulation at 100Hz *ex vivo*. Values are expressed as scatter point box and whisker plots (median, 25-75 centile and scatter plot). Data were statistically compared by two-way ANOVA followed by Bonferroni *post hoc* test. * $P < 0.05$; *** $P < 0.001$. F-I, group data (mean \pm SD) for work-load (F), power-load (G), shortening-load (H) and velocity-load (I) relationships in WT ($n = 7-10$) and *mdx* ($n = 8$) diaphragm muscle following saline or drug treatment. Data were statistically compared by two-way ANOVA. Work: load, $P < 0.0001$; genotype, $P < 0.0001$; WT treatment, $P = 0.059$; and *mdx* treatment, $P < 0.0001$. Power: load, $P <$

0.0001; genotype, $P < 0.0001$; WT treatment, $P = 0.009$; and *mdx* treatment, $P < 0.0001$. Shortening: load, $P < 0.0001$; genotype, $P < 0.0001$; WT treatment, $P = 0.968$; and *mdx* treatment, $P = 0.0001$. Velocity: load, $P < 0.0001$; genotype, $P = 0.0003$; WT treatment, $P = 0.642$; and *mdx* treatment, $P < 0.0001$.

6.3.7 Myosin heavy chain fibre-type distribution

Figure 6.4 shows data for MyHC fibre distribution of diaphragm muscles. The fibre type distribution of MyHC type I fibres did not vary significantly between the four groups (Fig. 6.4B). For *mdx* + saline, the abundance of MyHC type IIa fibres was significantly increased compared with WT + saline (Fig. 6.4C; $P < 0.001$; two-way ANOVA with Bonferroni), whereas the abundance of MyHC type IIx fibres was significantly reduced in *mdx* + saline compared with WT + saline (Fig. 6.4D; $P < 0.001$). The abundance of MyHC type IIb fibres was significantly reduced in *mdx* compared with WT diaphragm (Fig. 6.4E; $P = 0.0079$ (genotype); two-way ANOVA). Diaphragm fibre type changes were prevented or reversed by drug co-treatment in *mdx* with a significant decrease in type IIa fibres ($P < 0.001$; two-way ANOVA with Bonferroni) and a significant increase in type IIx fibres ($P < 0.001$) observed compared with *mdx* + saline.

6.3.8 Fibre cross-sectional area

Figure 6.4F shows data for CSA for all fibre types in all 4 groups. There was no significant difference in the CSA of MyHC type I, type IIa, type IIx or type IIb fibres in *mdx* diaphragm compared with WT. Drug co-treatment significantly increased MyHC type I fibre CSA ($P < 0.05$; two-way ANOVA with Bonferroni) and MyHC type IIx fibre CSA ($P < 0.05$) in *mdx* mice only. Drug co-treatment had no effect on the CSA of MyHC type IIa or type IIb fibres in WT and *mdx* diaphragms.

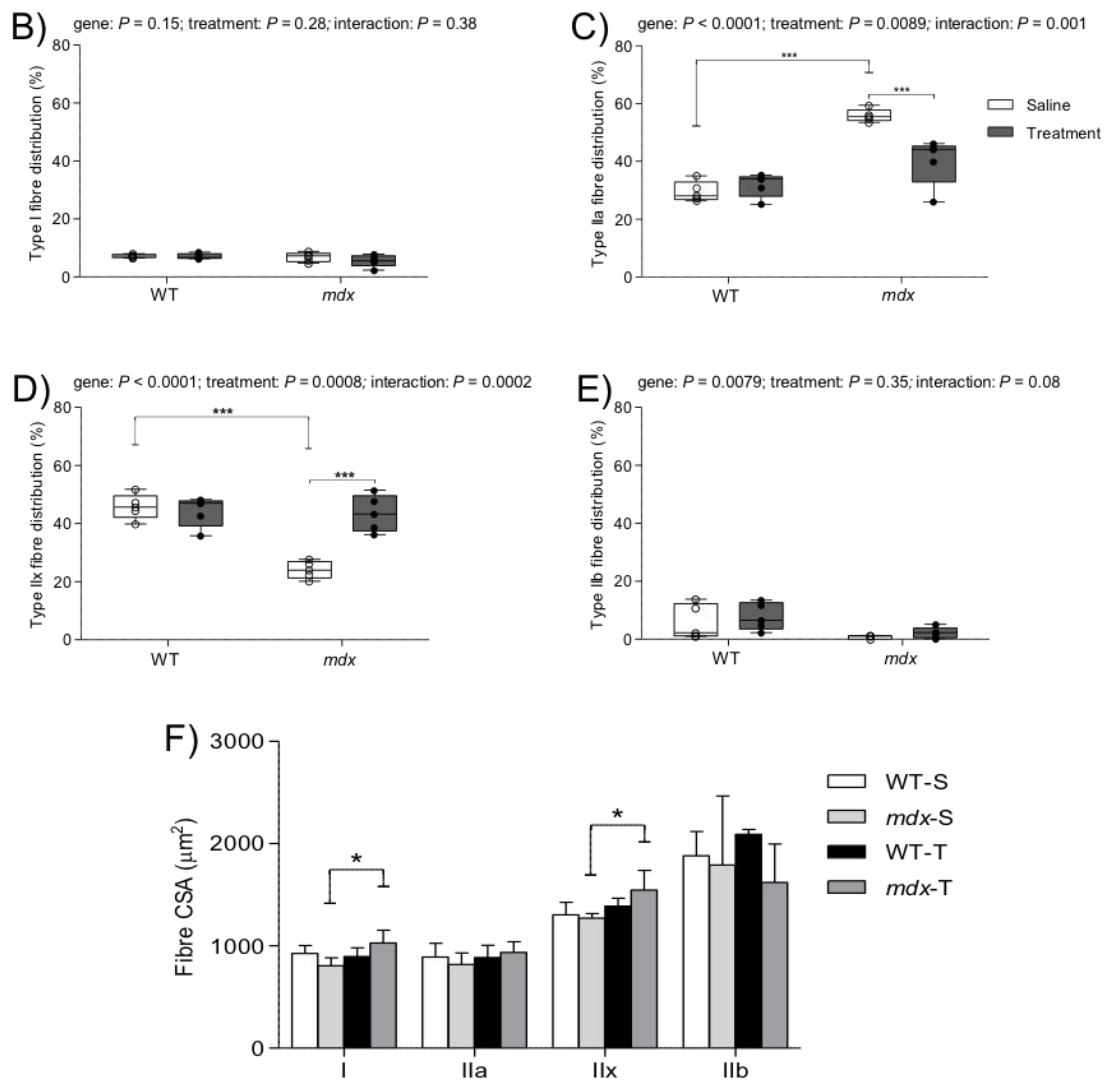
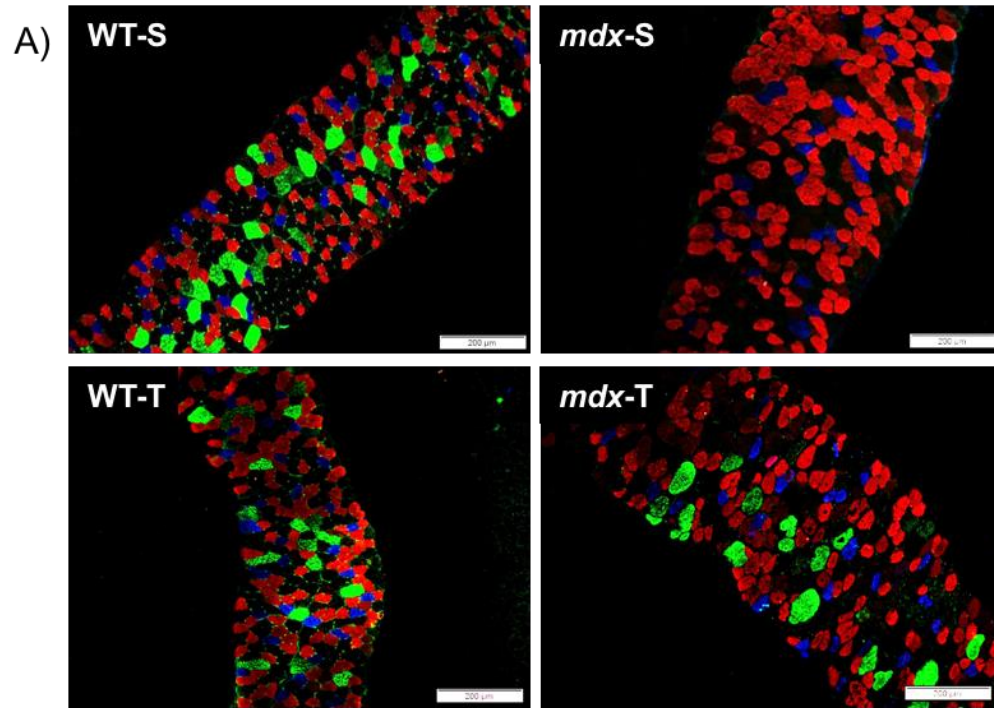


Figure 6.4 Diaphragm muscle fibre distribution and cross-sectional area

A, Representative immunofluorescence images of diaphragm muscle fibre-type distribution (A), showing type I (blue), type IIa (red), type IIx (untagged, appearing black) and type IIb fibres (green) for WT + saline (WT-S; top left), *mdx* + saline (*mdx*-S; top right), WT + treatment (WT-T; bottom left) and *mdx* + treatment (*mdx*-T; bottom right). Scale bars = 200 μ m. B-E, group data showing fibre distribution of type I (B), type IIa (C), type IIx (D) and type IIb fibres (E) in WT and *mdx* saline treated mice, and WT drug-treated and *mdx* drug-treated mice (n = 5) per group. Mice received six sub-cutaneous injections of saline (0.9% w/v) or treatment [neutralizing interleukin-6 receptor antibodies (0.2 mg/kg) and urocortin 2 (30 μ g/kg); co-administered] over two weeks. Values are expressed as scatter point box and whisker plots (median, 25-75 centile and scatter plot). Data were statistically compared by two-way ANOVA followed by Bonferroni *post hoc* test. *** $P < 0.001$. F, Group data (mean \pm SD) showing mean CSAs of diaphragm muscle fibre type I, type IIa, type IIx and type IIb. Data were statistically analysed by two-way ANOVA with Bonferroni *post hoc* test. * $P < 0.01$. Type I: Genotype, $P = 0.908$; treatment, $P = 0.036$; interaction, $P = 0.009$. Type IIa: Genotype, $P = 0.839$; treatment, $P = 0.291$; interaction, $P = 0.27$. Type IIx: Genotype, $P = 0.276$; treatment, $P = 0.005$; interaction, $P = 0.106$. Type IIb: Genotype, $P = 0.12$; treatment, $P = 0.905$; interaction, $P = 0.281$.

6.3.9 Central nucleation and putative inflammatory cell infiltration

Figure 6.5 shows data for diaphragm muscle histology. The proportion of diaphragm muscle fibres with centrally located nuclei was significantly increased in *mdx* + saline (Fig 6.5D; $P < 0.001$; two-way ANOVA with Bonferroni) compared with WT + saline. Drug co-treatment had no significant effect on central nucleation ($P = 0.414$ (treatment); two-way ANOVA). The areal density of inflammatory cell infiltration was significantly increased in *mdx* + saline diaphragm compared with WT + saline (Fig. 6.5E; $P < 0.001$; two-way ANOVA with Bonferroni). Drug co-treatment had no significant effect on the relative area of putative immune cell infiltration ($P = 0.3114$ (treatment); two-way ANOVA).

6.3.10 Collagen content

The areal density of collagen labelled using Masson's trichrome (type I collagen) staining was significantly increased in *mdx* + saline compared with WT + saline (Fig. 6.5F; $P < 0.0001$; two-way ANOVA with Bonferroni). Drug co-treatment had no significant effect on type I collagen content ($P = 0.278$ (treatment); two-way ANOVA). Type I and type III collagen co-expression, labelled with the fluorescent CNA35-OG488 probe, was significantly increased in *mdx* diaphragm compared with WT (Fig. 6.5G; $P = 0.0449$ (genotype); two-way ANOVA). Drug co-treatment did not affect the expression of diaphragm type I and III collagen ($P = 0.99$ (treatment); two-way ANOVA).

6.3.11 Inflammatory mediators

Figure 6.6 shows data for selective cytokine concentrations in diaphragm muscle from WT and *mdx* mice after saline administration or drug co-treatment. There was a significantly increased concentration of IL-2 (Fig. 6.6B; $P = 0.021$ (genotype); two-way ANOVA) and IL-5 (Fig. 6.6D; $P = 0.002$) in *mdx* diaphragm compared with WT. Diaphragms from *mdx* + saline showed significantly increased expression of IL-1 β (Fig. 6.6A; $P < 0.001$; two-way ANOVA with Bonferroni), IL-6 (Fig. 6.6E; $P < 0.001$), KC/GRO (Fig. 6.6H; $P < 0.001$) and TNF- α (Fig. 6.6J; $P < 0.001$) compared with WT + saline. *Post hoc* analysis revealed that drug co-treatment significantly decreased the pro-inflammatory cytokine IL-1 β ($P < 0.01$; two-way ANOVA with Bonferroni) and

significantly increased the anti-inflammatory cytokine IL-10 (Fig. 6.6F; $P < 0.05$) in *mdx* diaphragm compared with *mdx + saline*. The expression of IL-4 (Fig. 6.6C), IL-12p70 (Fig. 6.6G) and IFN- γ (Fig. 6.6I) were unchanged in *mdx* diaphragm compared with WT, and the concentrations of each of these were unaffected by drug co-treatment.

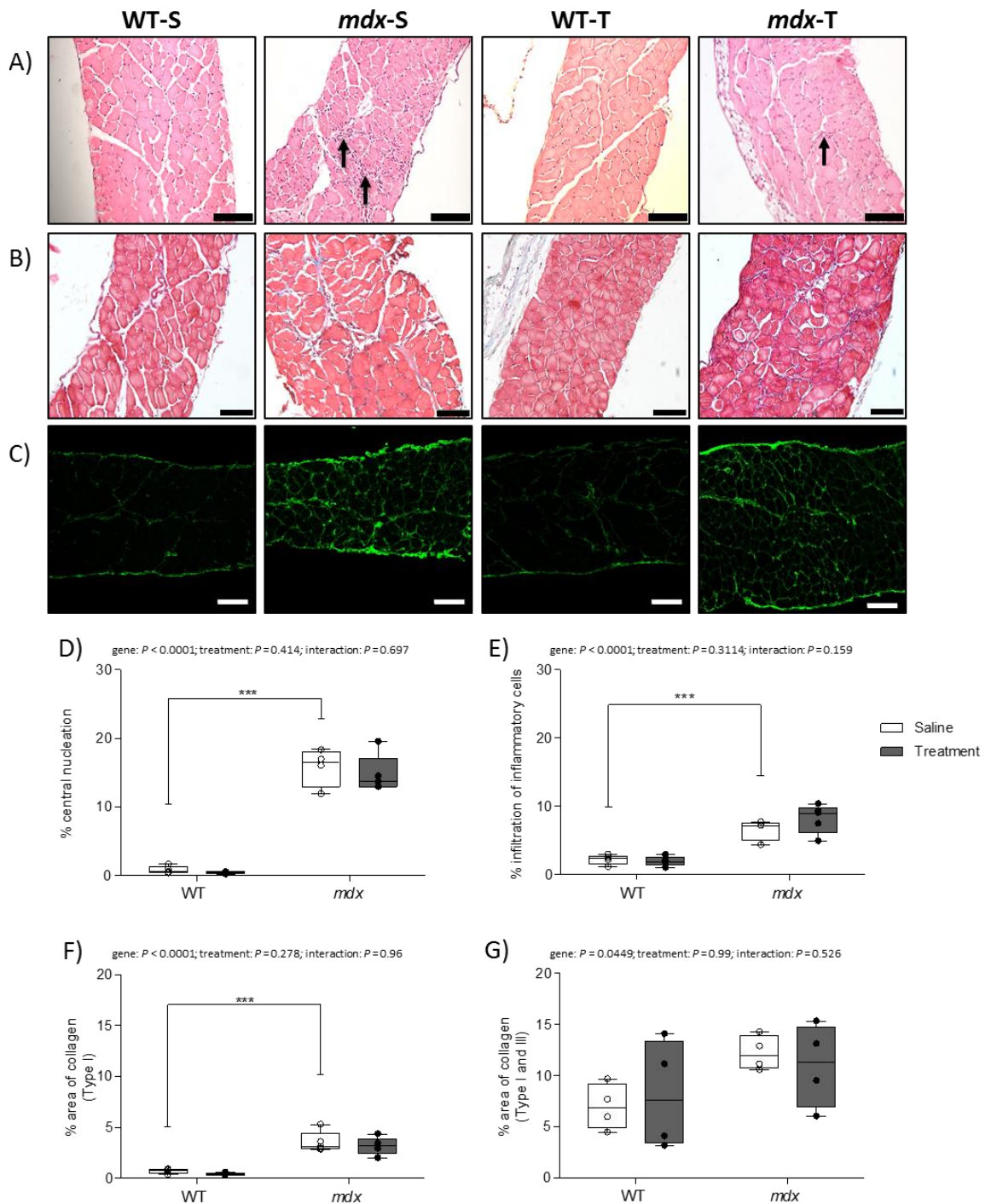


Figure 6.5 Diaphragm muscle histology

A-C, Representative histological images of diaphragm muscle transverse sections stained with Haematoxylin and Eosin (A), Masson's trichrome (B; type I collagen) and CNA35-OG488 (C; type I and III collagen) in WT + saline (WT-S; first column), *mdx* + saline (*mdx*-S; second column), WT + treatment (WT-T; third column) and *mdx* + treatment (*mdx*-T; fourth column) groups. Scale bars represent 100 μm . Peripherally located nuclei are apparent in WT saline and WT drug-treated images. In comparison, *mdx* mice (saline and drug-treated) displayed an increased incidence of centrally located nuclei. Inflammatory cell infiltration is not apparent in WT saline and WT drug-treated groups. The *mdx* muscle (saline and treatment) displayed inflammatory cell infiltration, highlighted with black arrows. D and E,

group data showing the percentage of central nucleation (D) and percentage of infiltration of inflammatory cells (E) in diaphragm muscle from saline-treated WT (n = 5) and saline-treated *mdx* mice (n = 4), and WT (n = 5) and *mdx* (n = 5) mice treated with neutralizing interleukin-6 receptor antibodies (0.2 mg/kg) and urocortin 2 (30 µg/kg), co-administered as six sub-cutaneous injections over 2 weeks. F and G, group data showing percentage of type I collagen content (C) and type I and III collagen content (D) in diaphragm muscle from saline-treated WT and saline-treated *mdx* mice, and WT and *mdx* mice (n = 4-5 per group) treated with neutralizing interleukin-6 receptor antibodies (0.2 mg/kg) and urocortin 2 (30 µg/kg) co-administered as six sub-cutaneous injections over 2 weeks. Values are expressed as scatter point box and whisker plots (median, 25-75 centile and scatter plot). Data were statistically compared by two-way ANOVA followed by Bonferroni *post hoc* test. ****P* < 0.001.

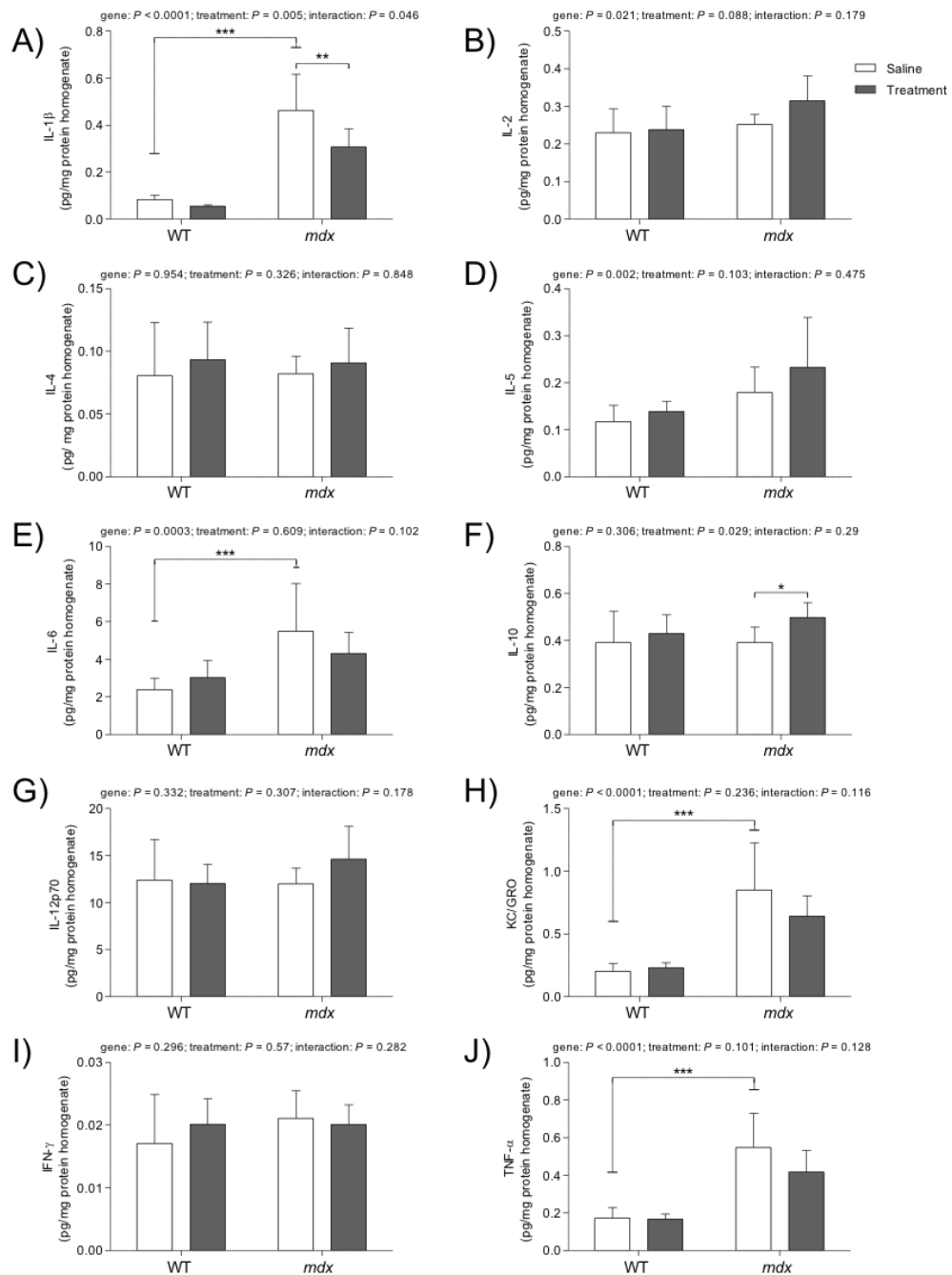


Figure 6.6 Cytokine concentrations in diaphragm muscle

A-J, Group data (mean \pm SD) for selective cytokine concentrations in diaphragm muscle. Cytokines include interleukin-1 β (A; IL-1 β), interleukin-2 (B; IL-2), interleukin-4 (C; IL-4), interleukin-5 (D; IL-5), interleukin-6 (E; IL-6), interleukin-10 (F; IL-10); interleukin-12 (F; IL-12p70), (G; KC/GRO), interferon- γ (F; IFN- γ) and tumour necrosis factor- α (TNF- α) in diaphragm muscle from wild-type (WT) and *mdx* mice (n = 8 per group) injected subcutaneously with saline (S; 0.9% w/v) or drug treatment [T; neutralizing interleukin-6 receptor antibodies (0.2 mg/kg) and urocortin 2 (30 μ g/kg); co-administered] over 2 weeks. Red represents an increase in concentration. Data were statistically compared by two-way ANOVA followed by Bonferroni *post hoc* test. * $P < 0.05$; ** $P < 0.01$; *** $P < 0.001$.

6.4 Discussion

The key findings of the present study are: (i) drug co-treatment with xIL-6R and Ucn2 restored muscle fibre complement equivalent to WT; (ii) drug co-treatment improved diaphragm force-generating capacity at 100Hz and restored normoxic ventilation in *mdx* mice; (iii) drug co-treatment had no significant effect on central nucleation, inflammatory cell infiltration and collagen deposition in *mdx* diaphragm; and (iv) drug co-treatment decreased IL-1 β concentration and increased IL-10 concentration in *mdx* diaphragm.

Striated muscle weakness is a devastating result of dystrophin deficiency in DMD. Respiratory muscle function is compromised and boys with DMD have reduced ventilatory capacity, which declines with age (De Bruin *et al.*, 1997; Khirani *et al.*, 2014). Diaphragm muscle weakness and likely impaired performance of the upper airway musculature translates to sleep disordered breathing including obstructive sleep apnoea and hypoventilation in many boys with DMD (Smith *et al.*, 1989; Barbé *et al.*, 1994). Cardiorespiratory failure is the leading cause of death in DMD, thus treatment strategies aimed at improving and prolonging adequate cardio-respiratory function are necessary.

Diaphragm muscle weakness is well described in *mdx* mice from a young age (Coirault *et al.*, 2003). In the current study, diaphragm muscle from *mdx* + saline mice showed significantly reduced twitch force and increased contraction time compared with WT + saline. Similarly, peak tetanic force at 100Hz and maximum work- and power-generating capacity were significantly reduced for *mdx* + saline diaphragm compared with WT + saline. These data confirm previous findings illustrating mechanical dysfunction in the *mdx* diaphragm due to the absence of dystrophin (Stedman *et al.*, 1991). We have previously reported depressed diaphragm force-generating capacity in *mdx* diaphragm at stimulation frequencies relevant to eupnoeic (basal) breathing, which has the capacity to limit tidal volume generation (Burns *et al.*, 2017c). Although the principal inspiratory muscle is compromised in DMD and *mdx* mice, few studies have comprehensively examined respiratory function and ventilatory capacity in *mdx* mice, both important measures

to consider when examining the effects of novel therapeutic strategies in animal models of myopathic disease.

In the current study, we assessed breathing in conscious unrestrained mice using whole-body plethysmography. Minute ventilation during normoxia was significantly reduced in *mdx* + saline compared with WT + saline mice, consistent with our recent reports (Burns *et al.*, 2015; Burns *et al.*, 2017c). The observed reductions in ventilation were the result of significant reductions in tidal volume in *mdx* mice, likely due to mechanical dysfunction and reduced force-generating capacity of the diaphragm muscle compared with WT. Although minute ventilation was lower in *mdx* mice, there was no difference in whole-body metabolism (as measured by VCO_2) between age-matched saline-treated WT and *mdx* mice, consistent with recent data (Burns *et al.*, 2017c). Consequentially, V_E/VCO_2 was lower in *mdx* compared with WT (24 versus 18; WT versus *mdx*), although this was not statistically significant by *post hoc* analysis. Despite evidence of impaired normoxic ventilation in the *mdx* model, there is no apparent evidence of inherent respiratory instability based on the analysis of variability of inspiratory and expiratory durations in young *mdx* mice.

Ventilatory capacity was significantly blunted in *mdx* mice evidenced by decreased minute ventilation during hypoxic gas exposure. Drug co-treatment significantly increased hypoxic ventilation, consistent with recovery of the mechanical deficits in *mdx* mice. Of note, the acute ventilatory response to hypoxia, measured as the absolute change in ventilation from baseline was blunted in *mdx* mice, a finding consistent with *mdx* carotid body hypoactivity (Burns *et al.*, 2017c). Drug co-treatment did not reverse this effect suggesting that the sensory deficit is unrelated to IL-6-dependent and/or CRFR2-dependent signalling in the hypoxic chemoafferent pathway of *mdx* mice. V_E/VCO_2 was elevated during hypoxic exposure revealing a hypoxic hyperventilation in WT and *mdx* mice. Drug co-treatment significantly increased V_E/VCO_2 during hypoxia in WT, but not in *mdx* mice.

Murine diaphragm muscle expresses MyHC type I, IIa, IIx and IIb fibres (Sieck *et al.*, 2012). Diaphragm muscle weakness in *mdx* + saline diaphragm was associated with an alteration in the distribution of MyHC isoform composition, with *mdx* + saline diaphragm expressing fewer MyHC IIx fibres and more MyHC IIa fibres compared with WT + saline. MyHC type II fibres display an incremental increase in force production from IIa to IIx to IIb, respectively. Thus, a shift in MyHC composition from IIx to IIa in *mdx* diaphragm muscle fibres likely has functional implications, consistent with *mdx* diaphragm exhibiting lower force- and power-generating capacity *ex vivo*. Similar alterations in MyHC distribution have been reported in pharyngeal dilator muscles from *mdx* mice (Burns *et al.*, 2017b) and are likely due to ongoing muscle fibre damage and repair processes preventing muscle fibre MyHC isoform maturation during muscle development.

Mechanical dysfunction of striated muscle is coupled with extensive inflammation of the respiratory and non-respiratory musculature in DMD (Messina *et al.*, 2011) and *mdx* mice (Barros Maranhão *et al.*, 2015). Inflammation occurs due to muscle fibre damage as a result of dystrophin deficiency. Inflammatory cells are recruited to the damaged muscle to repair injured fibres. There is heightened expression of inflammatory cytokines in plasma and muscle biopsies from DMD boys (De Pasquale *et al.*, 2012; Cruz-Guzmán *et al.*, 2015) and *mdx* mice (Rufo *et al.*, 2011). Chronic immune activation and attendant inflammation, observed in DMD, can have detrimental effects on normal physiological function. During the years of ambulation, plasma cytokine levels appear to be near maximal in DMD boys and begin to decline thereafter when patients become non-ambulatory (Cruz-Guzmán *et al.*, 2015), perhaps due to the disuse of the lower limb musculature. IL-6 is one of many cytokines reported to be elevated in DMD (Rufo *et al.*, 2011; Cruz-Guzmán *et al.*, 2015; Pelosi *et al.*, 2015a) and is of particular relevance due to its role as a myokine and muscle signalling molecule. Plasma IL-6 is known to increase in response to intense exercise and in pathological diseases such as Crohn's disease and rheumatoid arthritis (Maggio *et al.*, 2006). IL-6 binds to the IL-6R which signals via the Janus kinase/signal transducer activator of transcription (JAK/STAT) pathway. IL-6 can have divergent actions on skeletal muscle signalling such as

promoting both muscle growth and wasting. These opposing effects are consistent with the pro- and anti-inflammatory actions of IL-6. In some cases, IL-6 has been linked with hypertrophic muscle growth and paradoxically linked to muscle atrophy and wasting (Muñoz-Cánoves *et al.*, 2013). These conflicting actions may relate to different concentration levels of IL-6 and acute *versus* persistent activation of IL-6 signalling pathways.

The pro-inflammatory cytokines IL-1 β , IL-6, KC/GRO and TNF- α were significantly increased in *mdx* + saline diaphragm muscle compared with WT + saline, indicating a pro-inflammatory signature, consistent with previous reports in *mdx* muscle (Porter *et al.*, 2002). This elevated expression of inflammatory cytokines was associated with a significant increase in the percent infiltration of putative inflammatory cells in *mdx* + saline diaphragm compared with WT + saline. The number of muscle fibres expressing central nuclei in *mdx* + saline diaphragm was also elevated compared with WT + saline, indicating muscle fibre repair and regeneration. Blockade of IL-6 signalling in *mdx* mice has been shown to improve the capacity for treadmill exercise (Pelosi *et al.*, 2015a), to normalise function of gastrointestinal smooth muscle (Manning *et al.*, 2016), and exert modest effects on improving diaphragm force (Manning *et al.*, 2017). Conversely, overexpression of IL-6 in *mdx* mice promotes muscle necrosis and satellite cell exhaustion (Pelosi *et al.*, 2015b). Blockade of IL-6 signalling in dystrophin-/utrophin-deficient mice ameliorated skeletal muscle damage and promoted muscle regeneration in the limb, but no beneficial effects were observed for cardiac and respiratory muscle (Wada *et al.*, 2017).

Muscle wasting and proteolysis are pathophysiological features of myopathies such as DMD. Corticosteroids have been the treatment of choice for many years in DMD, notwithstanding their unwanted side effects (Ricotti *et al.*, 2013). Therapies aimed at activating anabolic signalling in functional muscle fibres may act to improve muscle force in DMD and *mdx* mice. The urocortins which bind to the CRFRs are known to modulate muscle mass and anabolic signalling pathways in skeletal muscle (Hinkle *et al.*, 2003a). Upon activation of CRFR2, there is an increase in

adenylyl cyclase and cAMP formation (Reutenauer-Patte *et al.*, 2012). Skeletal muscle is known to express CRFR2, and activation of CRFR2 decreased nerve damage and corticosteroid- and disuse-induced skeletal muscle mass and function loss in mice, and increased muscle mass in non-atrophying muscle (Hinkle *et al.*, 2003b). The CRFR2 agonist, Ucn2, has been shown to improve diaphragm muscle force (Hinkle *et al.*, 2007; Manning *et al.*, 2017), increase muscle mass (Hall *et al.*, 2007) and decrease muscle damage (Reutenauer-Patte *et al.*, 2012) in *mdx* mice.

In the current study, we investigated the effects of IL-6R blockade (xIL-6R) and CRFR2 agonism (Ucn2) on ventilation and metabolism and diaphragm muscle structure, function and cytokine concentration. Blocking the action of IL-6 was performed using a neutralizing IL-6R monoclonal antibody (Okazaki *et al.*, 2002). Recent findings from our group have shown this treatment strategy to improve diaphragm force-generating capacity (Manning *et al.*, 2017) and to restore pharyngeal dilator muscle force in *mdx* mice (Burns *et al.*, 2017b). In the latter study, the observed improvements in *mdx* pharyngeal dilator muscle function was associated with significantly reduced central nucleation of sternohyoid muscle from *mdx* mice following drug co-treatment (Burns *et al.*, 2017a).

Co-treatment of xIL-6R and Ucn2 significantly increased diaphragm specific force in *mdx* + treatment compared with saline-treated *mdx* (9 versus 16 N/cm²; *mdx* + saline versus *mdx* + treatment). For isotonic load relationships, drug co-treatment significantly increased diaphragm work, power, shortening and shortening velocity for *mdx* diaphragm. These findings confirm previous data describing improved muscle force following administration of xIL-6R and Ucn2 in *mdx* diaphragm (Manning *et al.*, 2017) and upper airway muscle (Burns *et al.*, 2017b). Of interest, enhanced force-generating capacity in WT diaphragm was not observed following co-treatment with xIL-6R and Ucn2.

Diaphragm muscle MyHC composition was significantly altered following xIL-6R and Ucn2 co-treatment in *mdx* mice. Drug co-treatment significantly reduced MyHC type IIa and increased MyHC type IIx fibre distribution in *mdx* diaphragm compared

with saline treated *mdx* mice. Improved *mdx* diaphragm force-generating capacity following drug co-treatment may be due to preservation of MyHC type IIx fibres. Drug co-treatment in WT mice had no effect on diaphragm fibre type distribution compared with saline-treated WT, consistent with no change in force-generating capacity in WT diaphragm. Progression of *mdx* diaphragm muscle fibres from MyHC IIa to IIx may be due, at least in part, to a suppression of muscle fibre damage and thus maturation of muscle fibres. The findings are consistent with previous observations in sternohyoid muscle from *mdx* mice following the same therapeutic intervention (Burns *et al.*, 2017b). In addition to preservation of MyHC fibre type distribution, drug co-treatment promoted hypertrophy (increased CSA) of MyHC type I and IIx fibres in *mdx* diaphragm which likely translates to functional improvements, since muscle force-generating capacity is proportional to fibre cross-sectional area. The observed hypertrophy of MyHC type I and IIx fibres may be a result of altered anabolic signaling mediated by Ucn2 in *mdx* mice. Drug co-treatment had no effect on muscle fibre central nucleation indicating there were no apparent improvements in muscle fibre damage and repair processes. Moreover, collagen content was also unaffected by drug co-treatment. These data suggest that functional improvements observed in the *mdx* diaphragm are not as a result of improvements in muscle damage and fibrosis.

Enhanced diaphragm functional capacity and altered MyHC isoform composition following drug co-treatment in *mdx* mice, was associated with significantly increased tidal volume and minute ventilation during normoxia compared with saline-treated *mdx*. Both tidal volume and minute ventilation, which were decreased in *mdx* + saline compared to WT + saline, were restored to WT + saline values in *mdx* mice following co-treatment. Indices of metabolism, VO_2 and VCO_2 were significantly reduced by drug co-treatment in WT and *mdx* compared with saline controls. The ventilatory equivalents for O_2 and CO_2 were both significantly increased by drug treatment in WT and *mdx* compared with saline-treated controls. Drug co-treatment had no effect on the variability of breathing in WT and *mdx* mice showing no overt effects of xIL-6R and Ucn2 on respiratory stability. The

mechanism of the hypometabolic effect of drug co-treatment is unclear and warrants attention in future studies.

Interestingly, drug co-treatment significantly decreased IL-1 β concentration in *mdx* diaphragm, with a concomitant increase in the concentration of the anti-inflammatory cytokine, IL-10. These data suggest modest improvements in the pro/anti-inflammatory cytokine balance in *mdx* diaphragm. There was no significant effect of drug co-treatment on the relative area of the putative inflammatory cell infiltration. Blockade of IL-6 signalling with α IL-6R did not significantly affect IL-6 concentration in *mdx* diaphragm muscle. Drug co-treatment in WT and *mdx* mice had no effect on body mass, indices of somatic growth and muscle and organ mass, demonstrating no apparent adverse effects of the drug co-treatment at their respective doses for the two-week duration of the current intervention.

In summary, *mdx* mice have impaired ventilation, diaphragm muscle weakness and MyHC fibre-type immaturity at an early age. Co-treatment with α IL-6R antibodies and Ucn2 recovered *mdx* diaphragm force-generating capacity. Drug co-treatment preserved the MyHC fibre complement in *mdx* diaphragm and also promoted hypertrophy of MyHC type I and IIx fibres in *mdx* but not WT diaphragm. Preservation and hypertrophy of *mdx* diaphragm muscle MyHC type IIx fibres may be adequate for functional improvements, especially since drug co-treatment did not influence measures of necrosis, fibrosis and immune cell infiltration. Normoxic ventilation was recovered in *mdx* drug-treated mice, mediated by restored tidal volume. It appears that improvements in diaphragm force-generating capacity and MyHC composition has the capacity to improve ventilation in young *mdx* mice.

Limitations

Peak diaphragm force-generating capacity was determined in *ex vivo* preparations in this study, and ventilatory capacity in *mdx* mice was assessed by whole-body plethysmography in conscious animals, which provides an estimate of tidal volume with known limitations (Mortola & Frappell, 1998; Burns *et al.*, 2017c). We employed hypoxic gas challenges to increase ventilation, but this provides only a

modest ventilatory challenge, especially in mice, which adopt a hypometabolic strategy in response to hypoxia, such that the increase in minute ventilation is relatively small. We assessed hypercapnic breathing, which revealed a clear deficit in *mdx* compared with WT, but again the activation of the diaphragm required to increase ventilation in response to chemostimulation is modest. As such, we did not assess the full range of ventilatory capacity (and deficit) in *mdx* mice and the efficacy of drug co-treatment in restoring physiological function associated with high levels of diaphragm and accessory muscle activation. Assessment of respiratory muscle function *in situ*, such as measurements of transdiaphragmatic pressure in mice across a range of ventilatory and non-ventilatory behaviours (Greising *et al.*, 2013) would be useful in characterizing the magnitude of the mechanical deficit in *mdx* mice at 8 weeks of age, and the efficacy of drug co-treatment in the preservation of ventilatory capacity.

We acknowledge that our intervention strategy was relatively short-lived and drug co-treatment for longer durations are necessary to fully explore the capacity for this novel intervention to influence muscle quality and strength, including the potential for deleterious outcomes or side effects with long-term drug treatment. Moreover, whereas the restoration of diaphragm strength and ventilation was impressive in our study, we concede that drug intervention did not affect muscle necrosis and fibrosis, and did not reduce the area of immune cell infiltrate in muscle tissue, although the explicit cellular nature of the infiltrate was not explored in this study. As such, the improvements in muscle function appear to relate to actions on healthy fibres, which has implications in the context of translation of this interventional strategy to DMD patients.

6.5 Additional information

Disclosures

The authors have no financial, professional or personal conflicts relating to this publication.

Author contributions

DPB: experimental design; acquisition of data; analysis and interpretation of data; drafting of the original manuscript; LC: histology studies: acquisition of data; analysis; JR: immunohistochemistry studies: acquisition of data; analysis; RO'F: muscle function studies: acquisition of data; analysis; MB: histology studies: acquisition of data; analysis; SED: gross measures: acquisition of data; DO'M: experimental design; critical revision of the manuscript for important intellectual content; DE: histology and immunohistochemistry studies: experimental design; data acquisition; interpretation of data; drafting and critical revision of the manuscript for important intellectual content; KDO'H: experimental design; interpretation of data; drafting and critical revision of the manuscript for important intellectual content.

Acknowledgements

DPB was supported by funding from the Department of Physiology, UCC. Work carried out in TCD was supported by funding from the Department of Physiology, TCD. The monoclonal anti-IL-6 receptor antibody was gifted by Chugai Pharmaceuticals, Tokyo, Japan. We are grateful to staff of the Biological Services Unit, UCC for support with animal care and welfare. We are grateful to Dr. G. Jasionek, Department of Physiology, UCC for technical support.

6.6 References

- Barbé F, Quera-Salva MA, McCann C, Gajdos P, Raphael JC, de Lattre J & Agustí AG (1994). Sleep-related respiratory disturbances in patients with Duchenne muscular dystrophy. *Eur Respir J* **7**, 1403-1408.
- Barros Maranhão J, de Oliveira Moreira D, Maurício AF, de Carvalho SC, Ferretti R, Pereira JA, Santo Neto H & Marques MJ (2015). Changes in caldesmon, TNF- α , TGF- β and MyoD levels during the progression of skeletal muscle dystrophy in mdx mice: a comparative analysis of the quadriceps, diaphragm and intrinsic laryngeal muscles. *Int J Exp Pathol* **96**, 285-293.
- Blake DJ, Weir A, Newey SE & Davies KE (2002). Function and genetics of dystrophin and dystrophin-related proteins in muscle. *Physiol Rev* **82**, 291-329.
- Burns DP, Ali I, Rieux C, Healy J, Jasione G & O'Halloran KD (2017a). Tempol Supplementation Restores Diaphragm Force and Metabolic Enzyme Activities in mdx Mice. *Antioxidants (Basel)* **6**.
- Burns DP, Edge D, O'Malley D & O'Halloran KD (2015). Respiratory Control in the mdx Mouse Model of Duchenne Muscular Dystrophy. *Adv Exp Med Biol* **860**, 239-244.
- Burns DP & O'Halloran KD (2016). Evidence of hypoxic tolerance in weak upper airway muscle from young mdx mice. *Respir Physiol Neurobiol* **226**, 68-75.
- Burns DP, Rowland J, Canavan L, Murphy KH, Brannock M, O'Malley D, O'Halloran KD & Edge D (2017b). Restoration of pharyngeal dilator muscle force in dystrophin-deficient (mdx) mice following co-treatment with neutralizing interleukin-6 receptor antibodies and urocortin 2. *Exp Physiol* **102**, 1177-1193.
- Burns DP, Roy A, Lucking EF, McDonald FB, Gray S, Wilson RJ, Edge D & O'Halloran KD (2017c). Sensorimotor control of breathing in the mdx mouse model of Duchenne muscular dystrophy. *J Physiol* **595**, 6653-6672.
- Chahbouni M, Escames G, Venegas C, Sevilla B, García JA, López LC, Muñoz-Hoyos A, Molina-Carballo A & Acuña-Castroviejo D (2010). Melatonin treatment normalizes plasma pro-inflammatory cytokines and nitrosative/oxidative stress in patients suffering from Duchenne muscular dystrophy. *J Pineal Res* **48**, 282-289.
- Coirault C, Lambert F, Marchand-Adam S, Attal P, Chemla D & Lecarpentier Y (1999). Myosin molecular motor dysfunction in dystrophic mouse diaphragm. *Am J Physiol* **277**, C1170-1176.

- Coirault C, Pignol B, Cooper RN, Butler-Browne G, Chabrier PE & Lecarpentier Y (2003). Severe muscle dysfunction precedes collagen tissue proliferation in mdx mouse diaphragm. *J Appl Physiol (1985)* **94**, 1744-1750.
- Cruz-Guzmán OeR, Rodríguez-Cruz M & Escobar Cedillo RE (2015). Systemic Inflammation in Duchenne Muscular Dystrophy: Association with Muscle Function and Nutritional Status. *Biomed Res Int* **2015**, 891972.
- De Bruin PF, Ueki J, Bush A, Khan Y, Watson A & Pride NB (1997). Diaphragm thickness and inspiratory strength in patients with Duchenne muscular dystrophy. *Thorax* **52**, 472-475.
- De Paepe B & De Bleecker JL (2013). Cytokines and chemokines as regulators of skeletal muscle inflammation: presenting the case of Duchenne muscular dystrophy. *Mediators Inflamm* **2013**, 540370.
- De Pasquale L, D'Amico A, Verardo M, Petrini S, Bertini E & De Benedetti F (2012). Increased muscle expression of interleukin-17 in Duchenne muscular dystrophy. *Neurology* **78**, 1309-1314.
- Deconinck N & Dan B (2007). Pathophysiology of duchenne muscular dystrophy: current hypotheses. *Pediatr Neurol* **36**, 1-7.
- Greising SM, Sieck DC, Sieck GC & Mantilla CB (2013). Novel method for transdiaphragmatic pressure measurements in mice. *Respir Physiol Neurobiol* **188**, 56-59.
- Hall JE, Kaczor JJ, Hettinga BP, Isfort RJ & Tarnopolsky MA (2007). Effects of a CRF2R agonist and exercise on mdx and wildtype skeletal muscle. *Muscle Nerve* **36**, 336-341.
- Haouzi P, Bell HJ, Notet V & Bihain B (2009). Comparison of the metabolic and ventilatory response to hypoxia and H2S in unsedated mice and rats. *Respir Physiol Neurobiol* **167**, 316-322.
- Hinkle RT, Donnelly E, Cody DB, Bauer MB & Isfort RJ (2003a). Urocortin II treatment reduces skeletal muscle mass and function loss during atrophy and increases nonatrophying skeletal muscle mass and function. *Endocrinology* **144**, 4939-4946.
- Hinkle RT, Donnelly E, Cody DB, Bauer MB, Sheldon RJ & Isfort RJ (2004). Corticotropin releasing factor 2 receptor agonists reduce the denervation-induced loss of rat skeletal muscle mass and force and increase non-atrophying skeletal muscle mass and force. *J Muscle Res Cell Motil* **25**, 539-547.

- Hinkle RT, Donnelly E, Cody DB, Samuelsson S, Lange JS, Bauer MB, Tarnopolsky M, Sheldon RJ, Coste SC, Tobar E, Stenzel-Poore MP & Isfort RJ (2003b). Activation of the CRF 2 receptor modulates skeletal muscle mass under physiological and pathological conditions. *Am J Physiol Endocrinol Metab* **285**, E889-898.
- Hinkle RT, Lefever FR, Dolan ET, Reichart DL, Dietrich JA, Gropp KE, Thacker RI, Demuth JP, Stevens PJ, Qu XA, Varbanov AR, Wang F & Isfort RJ (2007). Corticotrophin releasing factor 2 receptor agonist treatment significantly slows disease progression in mdx mice. *BMC Med* **5**, 18.
- Khan Y & Heckmatt JZ (1994). Obstructive apnoeas in Duchenne muscular dystrophy. *Thorax* **49**, 157-161.
- Khirani S, Ramirez A, Aubertin G, Boulé M, Chemouny C, Forin V & Fauroux B (2014). Respiratory muscle decline in Duchenne muscular dystrophy. *Pediatr Pulmonol* **49**, 473-481.
- Krahn KN, Bouten CV, van Tuijl S, van Zandvoort MA & Merckx M (2006). Fluorescently labeled collagen binding proteins allow specific visualization of collagen in tissues and live cell culture. *Anal Biochem* **350**, 177-185.
- Lewis P, Sheehan D, Soares R, Coelho AV & O'Halloran KD (2016). Redox Remodeling Is Pivotal in Murine Diaphragm Muscle Adaptation to Chronic Sustained Hypoxia. *Am J Respir Cell Mol Biol* **55**, 12-23.
- Lewis P, Sheehan D, Soares R, Varella Coelho A & O'Halloran KD (2015). Chronic sustained hypoxia-induced redox remodeling causes contractile dysfunction in mouse sternohyoid muscle. *Front Physiol* **6**, 122.
- Maggio M, Guralnik JM, Longo DL & Ferrucci L (2006). Interleukin-6 in aging and chronic disease: a magnificent pathway. *J Gerontol A Biol Sci Med Sci* **61**, 575-584.
- Manning J, Buckley MM, O'Halloran KD & O'Malley D (2016). In vivo neutralization of IL-6 receptors ameliorates gastrointestinal dysfunction in dystrophin-deficient mdx mice. *Neurogastroenterol Motil* **28**, 1016-1026.
- Manning J, Buckley MM, O'Halloran KD & O'Malley D (2017). Combined xIL-6R and urocortin-2 treatment restores mdx diaphragm muscle force. *Muscle Nerve*.
- Messina S, Vita GL, Aguenouz M, Sframeli M, Romeo S, Rodolico C & Vita G (2011). Activation of NF-kappaB pathway in Duchenne muscular dystrophy: relation to age. *Acta Myol* **30**, 16-23.

- Mortola JP & Frappell PB (1998). On the barometric method for measurements of ventilation, and its use in small animals. *Can J Physiol Pharmacol* **76**, 937-944.
- Mosqueira M, Baby SM, Lahiri S & Khurana TS (2013). Ventilatory chemosensory drive is blunted in the mdx mouse model of Duchenne Muscular Dystrophy (DMD). *PLoS One* **8**, e69567.
- Muñoz-Cánoves P, Scheele C, Pedersen BK & Serrano AL (2013). Interleukin-6 myokine signaling in skeletal muscle: a double-edged sword? *FEBS J* **280**, 4131-4148.
- O'Halloran KD (2006). Effects of nicotine on rat sternohyoid muscle contractile properties. *Respir Physiol Neurobiol* **150**, 200-210.
- O'Leary AJ & O'Halloran KD (2016). Diaphragm muscle weakness and increased UCP-3 gene expression following acute hypoxic stress in the mouse. *Respir Physiol Neurobiol* **226**, 76-80.
- Okazaki M, Yamada Y, Nishimoto N, Yoshizaki K & Mihara M (2002). Characterization of anti-mouse interleukin-6 receptor antibody. *Immunol Lett* **84**, 231-240.
- Pelosi L, Berardinelli MG, De Pasquale L, Nicoletti C, D'Amico A, Carvello F, Moneta GM, Catizone A, Bertini E, De Benedetti F & Musarò A (2015a). Functional and Morphological Improvement of Dystrophic Muscle by Interleukin 6 Receptor Blockade. *EBioMedicine* **2**, 285-293.
- Pelosi L, Berardinelli MG, Forcina L, Spelta E, Rizzuto E, Nicoletti C, Camilli C, Testa E, Catizone A, De Benedetti F & Musarò A (2015b). Increased levels of interleukin-6 exacerbate the dystrophic phenotype in mdx mice. *Hum Mol Genet* **24**, 6041-6053.
- Peng YJ, Nanduri J, Khan SA, Yuan G, Wang N, Kinsman B, Vaddi DR, Kumar GK, Garcia JA, Semenza GL & Prabhakar NR (2011). Hypoxia-inducible factor 2 α (HIF-2 α) heterozygous-null mice exhibit exaggerated carotid body sensitivity to hypoxia, breathing instability, and hypertension. *Proc Natl Acad Sci U S A* **108**, 3065-3070.
- Porter JD, Khanna S, Kaminski HJ, Rao JS, Merriam AP, Richmonds CR, Leahy P, Li J, Guo W & Andrade FH (2002). A chronic inflammatory response dominates the skeletal muscle molecular signature in dystrophin-deficient mdx mice. *Hum Mol Genet* **11**, 263-272.
- Reutenauer-Patte J, Boittin FX, Patthey-Vuadens O, Ruegg UT & Dorchies OM (2012). Urocortins improve dystrophic skeletal muscle structure and

function through both PKA- and Epac-dependent pathways. *Am J Pathol* **180**, 749-762.

Ricotti V, Ridout DA, Scott E, Quinlivan R, Robb SA, Manzur AY, Muntoni F & Network NC (2013). Long-term benefits and adverse effects of intermittent versus daily glucocorticoids in boys with Duchenne muscular dystrophy. *J Neurol Neurosurg Psychiatry* **84**, 698-705.

Rufo A, Del Fattore A, Capulli M, Carvello F, De Pasquale L, Ferrari S, Pierroz D, Morandi L, De Simone M, Rucci N, Bertini E, Bianchi ML, De Benedetti F & Teti A (2011). Mechanisms inducing low bone density in Duchenne muscular dystrophy in mice and humans. *J Bone Miner Res* **26**, 1891-1903.

Sieck DC, Zhan WZ, Fang YH, Ermilov LG, Sieck GC & Mantilla CB (2012). Structure-activity relationships in rodent diaphragm muscle fibers vs. neuromuscular junctions. *Respir Physiol Neurobiol* **180**, 88-96.

Smith PE, Calverley PM & Edwards RH (1988). Hypoxemia during sleep in Duchenne muscular dystrophy. *Am Rev Respir Dis* **137**, 884-888.

Smith PE, Edwards RH & Calverley PM (1989). Ventilation and breathing pattern during sleep in Duchenne muscular dystrophy. *Chest* **96**, 1346-1351.

Souza GM, Bonagamba LG, Amorim MR, Moraes DJ & Machado BH (2015). Cardiovascular and respiratory responses to chronic intermittent hypoxia in adult female rats. *Exp Physiol* **100**, 249-258.

Stedman HH, Sweeney HL, Shrager JB, Maguire HC, Panettieri RA, Petrof B, Narusawa M, Leferovich JM, Sladky JT & Kelly AM (1991). The mdx mouse diaphragm reproduces the degenerative changes of Duchenne muscular dystrophy. *Nature* **352**, 536-539.

Stirrat CG, Venkatasubramanian S, Pawade T, Mitchell AJ, Shah AS, Lang NN & Newby DE (2016). Cardiovascular effects of urocortin 2 and urocortin 3 in patients with chronic heart failure. *Br J Clin Pharmacol* **82**, 974-982.

Wada E, Tanihata J, Iwamura A, Takeda S, Hayashi YK & Matsuda R (2017). Treatment with the anti-IL-6 receptor antibody attenuates muscular dystrophy via promoting skeletal muscle regeneration in dystrophin-/utrophin-deficient mice. *Skelet Muscle* **7**, 23.

Williams R, Lemaire P, Lewis P, McDonald FB, Lucking E, Hogan S, Sheehan D, Healy V & O'Halloran KD (2015). Chronic intermittent hypoxia increases rat sternohyoid muscle NADPH oxidase expression with attendant modest oxidative stress. *Front Physiol* **6**, 15.

Chapter 7. Combinational pharmacotherapy in the treatment of respiratory deficits in dystrophin-deficient *mdx* mice

David P. Burns¹, Deirdre Edge² and Ken D. O'Halloran¹

¹*Department of Physiology, School of Medicine, College of Medicine & Health,
University College Cork, Cork, Ireland.*

²*Department of Physiology, School of Medicine, Trinity Biosciences Institute, Trinity
College Dublin, the University of Dublin, Dublin, Ireland.*

Abstract

Duchenne muscular dystrophy (DMD) is a genetic disease characterised by a deficiency in the structural protein dystrophin. Skeletal muscle weakness is a major pathological feature of the disease, which extends to the striated muscles of breathing with adverse consequences for respiratory function. Disordered breathing is observed in DMD boys, particularly during sleep. We have previously described deficits within the respiratory control network of a murine model of DMD, the *mdx* mouse. Extensive muscle weakness and remodelling occurs in the diaphragm (respiratory pump) and the sternohyoid muscle (representative pharyngeal dilator) in young (8 week old) *mdx* mice. Herein, we review recent work by our group exploring a combined anti-inflammatory and anti-stress interventional strategy aimed at alleviating respiratory deficits in the *mdx* mouse. Treatment consisted of a combination of a neutralizing interleukin-6-receptor antibody and urocortin-2, a corticotrophin releasing factor receptor 2 agonist. We describe encouraging findings from our studies showing impressive restoration of muscle function and breathing capacity in *mdx* mice, of potential translational value for human dystrophinopathies. Our work highlights the potential use of combinational treatment strategies in the continued search for interventional treatments in DMD.

Keywords: Breathing; Duchenne muscular dystrophy; diaphragm; upper airway; interleukin-6; *mdx*; corticotrophin releasing factor; urocortin.

Abbreviations: CCR2, C-C chemokine receptor type 2; CRF, corticotrophin releasing factor; CRFR, CRF receptor; IP-10, interferon γ -induced protein; MIP-2, macrophage inflammatory protein 2; MIP-3 α , macrophage inflammatory protein 3 α MyHC, myosin heavy chain; IL, interleukin; TNF- α , tumour necrosis factor- α ; Ucn2, urocortin 2; $V\text{CO}_2$, carbon dioxide production; $V_E/V\text{CO}_2$, ventilatory equivalent for carbon dioxide;

7.1 Respiratory dysfunction in Duchenne muscular dystrophy (DMD)

Respiratory failure is a leading cause of death in Duchenne muscular dystrophy (DMD), a neuromuscular disease that occurs in males (Bye *et al.*, 1990; Yiu & Kornberg, 2008). DMD is caused by defects in the dystrophin gene and subsequent absence of dystrophin protein. Dystrophin is found in muscle, where it anchors the actin cytoskeleton to the sarcolemma and forms part of the dystrophin associated protein complex (Ervasti, 2007). Dystrophin deficiency has major consequences for the physiological function of muscle. Clinically, patients present with delayed motor milestones in the early years of life. As patients grow, they begin to experience weakness of the skeletal muscles of the upper and lower limbs, which eventually results in reduced ambulation and the requirement for wheelchair assistance (Yiu & Kornberg, 2008). Muscle weakness extends to the striated muscles of breathing, including the diaphragm muscle, which has major consequences for respiratory function (Baydur *et al.*, 1990). Lung volume assessments in DMD boys indicate a progressive decline in forced vital capacity with increasing age (Phillips *et al.*, 2001; Mayer *et al.*, 2015). Examination of the diaphragm muscle in patients using trans-diaphragmatic pressure measurements, revealed values lower than predicted in DMD for maximal inspiration during sniffing behaviours (Khirani *et al.*, 2014).

Sleep disordered breathing is commonly reported in DMD (Cerveri *et al.*, 1993; LoMauro *et al.*, 2017). Sleep studies indicate obstructive sleep apnoea is a prominent feature of DMD during the teenage years (Khan & Heckmatt, 1994), which suggests inadequate upper airway muscle function during sleep. Muscle weakness in DMD extends to the skeletal muscles comprising the upper airway, with implications for the control of airway calibre. Diaphragm muscle weakness translates to hypoventilation during sleep in patients (Smith *et al.*, 1989). Both apnoea and hypoventilation have implications for the maintenance of blood oxygenation and the retention of carbon dioxide in patients, both factors which can impact on muscle health, compounding the inherent muscle deficits at play in DMD.

Muscle fibre remodelling occurs in dystrophic muscle, wherein fibres display central nucleation due to ongoing damage and repair processes; immune cell infiltration is

widespread. There is an increased expression of chemokines in DMD myofibres (De Paepe *et al.*, 2012), which recruit immune cells to repair damaged myofibres (De Paepe & De Bleecker, 2013). Cytokine concentrations are elevated in muscle biopsies and plasma samples from DMD patients (Porreca *et al.*, 1999; Saito *et al.*, 2000; Messina *et al.*, 2011; De Pasquale *et al.*, 2012; Cruz-Guzmán *et al.*, 2015). Of interest to our research, interleukin-6 is significantly elevated in serum and muscle samples from DMD patients (Messina *et al.*, 2011; Rufo *et al.*, 2011; Cruz-Guzmán *et al.*, 2015; Pelosi *et al.*, 2015a). In addition to inflammation, attendant oxidative stress presents in DMD, with an elevated redox signature in dystrophic muscle (Haycock *et al.*, 1996; Rodriguez & Tarnopolsky, 2003; Nakae *et al.*, 2004; Abdel *et al.*, 2007; Petrillo *et al.*, 2017). There is no cure for DMD. The current treatment strategy in DMD involves the use of glucocorticoids, notwithstanding their undesirable side effects.

7.2 Respiratory muscle remodelling in the dystrophin-deficient *mdx* mouse

The *mdx* mouse is a dystrophin-deficient model of DMD (Bulfield *et al.*, 1984). Dystrophin is absent from skeletal, cardiac and smooth muscle in the *mdx* mouse and functional deficits present from a young age (Coirault *et al.*, 2003; Quinlan *et al.*, 2004; Manning *et al.*, 2016). Compared to the human condition, the *mdx* mouse presents with modest limb muscle pathology, owing to considerable compensation and recovery of force. In comparison, the diaphragm muscle exhibits loss of contractile force from a young age, which persists throughout life (Stedman *et al.*, 1991; Petrof *et al.*, 1993; Coirault *et al.*, 1999; Coirault *et al.*, 2003; Burns *et al.*, 2017a; Burns *et al.*, 2017c). Moreover, extensive muscle fibre remodelling and inflammation is apparent in the diaphragm of *mdx* mice (Stedman *et al.*, 1991; Petrof *et al.*, 1993; Coirault *et al.*, 1999; Coirault *et al.*, 2002; Coirault *et al.*, 2003; Burns *et al.*, 2017c).

Diaphragm muscle comprises a mixed myosin heavy chain (MyHC) isoform composition in mice, with the expression of type I, IIa, IIx and IIb fibres (Sieck *et al.*, 2012). Muscle fibres show an incremental increase in force from MyHC type I to IIa to IIx to IIb, sequentially, and a concomitant decrease in fatigue resistance (Polla *et*

al., 2004; Schiaffino & Reggiani, 2011). There is altered expression of MyHC isoform composition in the dystrophic diaphragm, characterised by a significant reduction in the number of fibres expressing MyHC type IIx and an increase in type IIa (Petrof *et al.*, 1993; Coirault *et al.*, 1999; Coirault *et al.*, 2002), highlighting MyHC fibre immaturity. We have reported central nucleation in 16-20% of muscle fibres in *mdx* diaphragm, compared with <1% in wild-type (Burns *et al.*, 2017c). Muscle fibre central nucleation is a common hallmark of muscle fibre damage. Repeated cycles of muscle fibre degeneration and regeneration in dystrophic muscle, ultimately culminates in muscle fibre necrosis. Necrotic muscle fibres are replaced by connective tissue and adipocytes, resulting in a further decline in muscle force. Collagen (type I) accumulation in dystrophic muscle begins at a young age and is consistent with muscle fibre damage and resultant necrosis; of note, diaphragm contractile dysfunction precedes collagen deposition (Coirault *et al.*, 2003). The frequency distribution of muscle fibres is left-shifted for *mdx* diaphragm, with *mdx* expressing smaller fibres compared with wild-type diaphragm, and an increased number of fibres (Burns *et al.*, 2017c). Dystrophic muscle is further characterised by an increase in the variability of muscle fibre size. Such remodelling is indicative of new regenerating muscle fibres and most likely branched fibres.

An inflammatory signature similar to DMD is revealed in *mdx* mice, evidenced by enhanced muscle and serum cytokines and chemokines (Porter *et al.*, 2002; Nelson *et al.*, 2011; Rufo *et al.*, 2011; Pelosi *et al.*, 2015a). Diaphragm from *mdx* mice displays a pro-inflammatory signature, with elevated concentrations of interleukin-1 β (IL-1 β), IL-6, TNF α and KC/GRO (Kumar & Boriek, 2003; Pelosi *et al.*, 2015a). Moreover, the C-C chemokine receptor type 2 (CCR2) and its ligands are elevated in *mdx* diaphragm (Demoule *et al.*, 2005; Mojumdar *et al.*, 2014).

In conjunction with the diaphragm, other accessory muscles are important for the homeostatic regulation of breathing, the maintenance of arterial blood gases and pH. The upper airway comprises up to 20 skeletal muscles which strive cooperatively to maintain airway patency. Despite the occurrence of sleep disordered breathing and obstructive apnoeas in DMD, there is a dearth of information

pertaining to airway physiology in the dystrophinopathies and pre-clinical models of disease. The sternohyoid muscle is a representative pharyngeal dilator involved in the maintenance of airway calibre. The sternohyoid muscles attach the hyoid bone to the sternum and are principally composed of MyHC type II muscle fibres in rodents (Skelly *et al.*, 2011; Skelly *et al.*, 2012; Burns *et al.*, 2017b). Similar to diaphragm, sternohyoid muscle from *mdx* mice express fibres containing centralised myonuclei (~25% of fibres) (Burns *et al.*, 2017b). Examination of the MyHC isoform composition indicates a significant reduction in type IIb fibres with an accompanying increase in type IIa (Attal *et al.*, 2000; Burns *et al.*, 2017b).

Chemoattractant agents including, macrophage inflammatory protein (MIP-2), interferon- γ induced protein (IP-10) and macrophage inflammatory protein-3 (MIP-3 α), are increased in *mdx* sternohyoid (Burns *et al.*, 2017b). These molecules have a cellular role in the initiation of inflammatory cascades in muscle. We have observed a modest increase in collagen expression in *mdx* sternohyoid compared with wild-type and an increase in the relative area of putative cell infiltrates. Activation of inflammatory cascades in muscle, have implications for normal physiological function. In addition to the recruitment of inflammatory mediators to muscle, muscle itself is considered an endocrine organ and has been documented to release cytokines under physiological stress (Welc & Clanton, 2013).

7.3 Respiratory muscle weakness in the *mdx* mouse

Studies of sternohyoid muscle function *ex vivo* reveal contractile deficits for *mdx* mice at eight weeks (Burns & O'Halloran, 2016; Burns *et al.*, 2017c) and six months (Attal *et al.*, 2000) of age. Deficits include reduced twitch and tetanic contractile force (Burns & O'Halloran, 2016; Burns *et al.*, 2017b). Twitch contractile kinetics were altered for *mdx* sternohyoid muscle, evidenced by a prolonged contraction time and half-relaxation time compared with wild-type, suggesting altered calcium release and re-uptake (Burns & O'Halloran, 2016; Burns *et al.*, 2017b). Work and power as a function of load bearing were significantly reduced for *mdx* sternohyoid compared with wild-type (Attal *et al.*, 2000; Burns & O'Halloran, 2016; Burns *et al.*, 2017b). Shortening velocity was reduced over the load continuum, indicating the

poor mechanical efficiency of dystrophic muscle (Attal *et al.*, 2000; Burns *et al.*, 2017b). Such pronounced upper airway muscle dysfunction in *mdx*, has the potential to create a perfect storm for ventilatory control and airway defence mechanisms.

The functional consequences of dystrophin deficiency on *mdx* diaphragm include dramatic force loss (Petrof *et al.*, 1993; Coirault *et al.*, 1999; Coirault *et al.*, 2003; Burns *et al.*, 2017a; Burns *et al.*, 2017c). Twitch contraction time was elevated suggesting slowed calcium release from the sarcoplasmic reticulum for *mdx* muscle preparations; half-relaxation time remained unchanged. Work, power, shortening and velocity of shortening were significantly reduced across the load continuum for *mdx* diaphragm compared with wild-type. Diaphragm force-frequency relationships show profound muscle weakness in the frequency range of 40-160 Hz for *mdx* diaphragm (Burns *et al.*, 2017c), indicating deficits in the range implicated in ventilatory and non-ventilatory (airway protection) behaviours.

7.4 Ventilatory deficits in *mdx* mice

Mechanical dysfunction in *mdx* diaphragm places limits on ventilation (Mosqueira *et al.*, 2013; Burns *et al.*, 2015; Burns *et al.*, 2017c). We have recently reported reduced minute ventilation in 8-week-old *mdx* mice, owing to substantial reductions in tidal volume during normoxia as measured by whole-body plethysmography in conscious unanaesthetised mice (Burns *et al.*, 2017c). It is likely that compromised diaphragm muscle performance in *mdx* mice contributes to observed reductions in tidal volume, since diaphragm muscle weakness is present in the eupnoeic range of breathing (20-50Hz). Of note, V_E/V_{CO_2} (ventilation as a function of CO_2 production) was significantly reduced in *mdx* mice confirming hypoventilation (Burns *et al.*, 2017c) during basal breathing.

In subsequent studies (chapter 6), we confirmed that *mdx* mice had significantly reduced tidal volume compared with wild-type, contributing to a pronounced reduction in minute ventilation for *mdx* mice, consistent with our prior report (Burns *et al.*, 2017c). Ventilatory challenge with hypoxia, indicated decreased

minute ventilation across all levels of inspired oxygen (Burns *et al.*, 2017c). Ventilation in response to hypercapnic challenge revealed a capacity for *mdx* mice to further increase ventilation despite hypoventilation during normoxia (Burns *et al.*, 2017c). Curiously, as revealed in chapter 4, *mdx* mice retain a remarkable capacity to increase ventilation during maximum chemoactivation during hypercapnic hypoxia challenge, and during augmented breaths, despite profound diaphragm muscle dysfunction. The observations strongly suggest that accessory muscle recruitment supports the preservation of ventilatory capacity in *mdx* mice, at least in early adult life. This in turn suggests that the observation of resting hypoventilation in *mdx* mice is at least partly determined by sensory deficit in *mdx* mice (hypoactivity of the carotid body).

7.5 Combinational pharmacotherapy in DMD

Inflammation

Evidence is mounting in support of the role of inflammation in promoting muscle damage in dystrophic muscle (Deconinck & Dan, 2007; De Paepe *et al.*, 2012; De Paepe & De Bleecker, 2013). Blockade of global regulators of inflammation such as NF κ B and TNF α in *mdx* mice has alleviated muscle functional deficits and improved muscle structural integrity (Pan *et al.*, 2008; Enwere *et al.*, 2013; Ermolova *et al.*, 2014). In addition to elevated cytokine expression in DMD, *mdx* mice also have elevated levels in plasma and muscle, indicating a pro-inflammatory state. Monocyte chemoattractant protein-1 (MCP-1) is increased in the plasma of *mdx* mice (Nelson *et al.*, 2011). Characterisation of cytokines and chemokines in DMD has led to interventional studies aimed at reducing chemokine and cytokine signalling in *mdx* mice to test the efficacy of interventions in improving muscle physiology.

Blockade of IL-6 signalling *in vivo* with a neutralizing interleukin-receptor (xIL-6R) antibody normalised gastrointestinal morphology and function in *mdx* mice (Manning *et al.*, 2016). Furthermore, xIL-6R reduced NF κ B and TNF α in *mdx* diaphragm and improved treadmill exercise (Pelosi *et al.*, 2015a). Conversely, an overexpression of IL-6 in *mdx* had detrimental effects on diaphragm muscle quality

and exacerbated the dystrophic muscle phenotype (Pelosi *et al.*, 2015b; Pelosi *et al.*, 2017). Inhibition of the cytokine transforming growth factor beta (TGF β) in *mdx* mice by use of a neutralising antibody to all three isoforms of TGF β , led to improvements in respiratory function (increased minute ventilation) (Nelson *et al.*, 2011). Ablation of the anti-inflammatory cytokine IL-10 in *mdx* mice, led to increased muscle damage (Villalta *et al.*, 2011) and promoted cardiovascular (reduced % fractional shortening and % ejection fraction) and respiratory (reduced tidal volume) dysfunction (Nitahara-Kasahara *et al.*, 2014). These studies suggest a role for pro-inflammatory cytokines in mediating muscle and respiratory dysfunction in *mdx* mice.

Stress and anabolic signalling

The urocortins are a group of proteins belonging to the corticotrophin releasing factor (CRF) family. Urocortin-2 (Ucn2) is an endogenous peptide highly selective for the CRF 2 receptor. Skeletal muscle is known to express CRF receptors and Ucn2 has been shown to promote anabolic signalling in muscle, modulating muscle mass (Hinkle *et al.*, 2003; Hinkle *et al.*, 2004; Hall *et al.*, 2007). Urocortin treatment in *mdx* mice has been shown to improve diaphragm muscle force, decreasing fibrosis and immune cell infiltration (Hinkle *et al.*, 2007; Reutenauer-Patte *et al.*, 2012; Manning *et al.*, 2017).

To date, little work has examined a combinational approach to anti-inflammatory interventions in *mdx* mice. We hypothesised that inflammatory and stress related factors are implicated in respiratory system deficits in *mdx* mice. Previous work by our research group reported that blockade of IL-6 signalling and Ucn2 treatment in *mdx* mice improved diaphragm muscle force (Manning *et al.*, 2017). In the current studies, wild-type and *mdx* mice received a sub-cutaneous injection of a combination of xIL-6R (MR16-1 (Okazaki *et al.*, 2002)) and Ucn2 or saline (0.9% w/v). The treatment intervention began at six weeks of age and studies were performed following a two week treatment period (Burns *et al.*, 2017b). We extended studies by Manning *et al.* (2007) to breathing and metabolism

measurements, diaphragm structure and cytokine concentrations and upper airway muscle structure and function.

7.6 Combinational pharmacotherapy in *mdx* mice: Ventilation

Ventilation and metabolism was assessed in conscious wild-type and *mdx* mice following xIL-6R and Ucn2 co-treatment, or saline, using whole-body plethysmography. Drug co-treatment alleviated tidal volume deficits in *mdx* mice, restoring minute ventilation to wild-type levels. Tidal volume changes were restricted to the *mdx* + vehicle group. Carbon dioxide production (VCO_2) was significantly reduced following treatment for both wild-type and *mdx* mice. The net effect of changes in V_E and VCO_2 , was a significant recovery of V_E/VCO_2 for *mdx*. A similar increase in V_E/VCO_2 was observed for wild-type mice, due to an increase in respiratory frequency and VCO_2 . These data illustrate a restoration of ventilation during normoxia in *mdx* mice following treatment. Challenging ventilation with hypoxia highlighted enhanced ventilation in *mdx* mice following treatment compared with *mdx* + vehicle, indicating an improved capacity for ventilation. Improvements in respiratory function and ventilatory capacity have physiological implications for the control of breathing, blood-gas homeostasis and the maintenance of pH.

7.7 Combinational pharmacotherapy in *mdx* mice: Respiratory muscle function

Therapeutic intervention of combined xIL-6R and Ucn2 for two weeks in *mdx* mice remarkably restored sternohyoid muscle functional deficits (Burns *et al.*, 2017b). Isometric force restoration was achieved for twitch and tetanic contractions. Mechanical work and power and shortening velocity were considerably potentiated for *mdx* sternohyoid muscle as a function of load bearing. In addition to restoring sternohyoid muscle force in *mdx*, co-treatment had a positive inotropic effect on wild-type sternohyoid muscle with significantly enhanced isometric tetanic force and mechanical work and power. Such improvements would have benefit for the control of upper airway patency and airway behaviours in *mdx* mice.

Neutralisation of IL-6R in *mdx* mice provided modest improvements in diaphragm muscle functional capacity (Manning *et al.*, 2017). Stimulation of CRF-R2 provided a further increase in diaphragm force, with a combined treatment of xIL-6R and Ucn2 revealing the greatest improvement in force and mechanical work (Manning *et al.*, 2017). In our subsequent study we revealed that drug co-treatment improved maximum force, work and power generation in *mdx* mice. Moreover, work, power, shortening and velocity of shortening were all significantly increased for *mdx* diaphragm following a combined treatment of xIL-6R and Ucn2. Unlike observations in sternohyoid muscle, no potentiation in diaphragm muscle force-generating capacity was observed following drug co-treatment in wild-type mice. Conversely, modest increases in wild-type diaphragm work and power production against varied load were noted. Such improvements in diaphragm functional capacity are likely contributing to tidal volume restoration and enhanced ventilatory capacity in *mdx* mice following treatment. These findings are of clinical relevance and are of translational value in DMD, where respiratory deficits are prominent.

7.8 Combinational pharmacotherapy in *mdx* mice: Respiratory muscle form

Sternohyoid muscle fibre central nucleation was slightly ameliorated following combinational treatment of xIL-6R and Ucn2. Force restoration in *mdx* sternohyoid muscle was associated with complete restoration of the MyHC isoform complement. The proportion of MyHC IIx was significantly reduced and MyHC IIb significantly increased in *mdx* sternohyoid following treatment. MyHC isoform composition in wild-type muscle was unaltered following treatment. Combinational therapy had no effect on collagen content and areal density of putative cell infiltrates in *mdx* sternohyoid. Surprisingly, treatment increased the relative concentrations of the chemokines MIP-2, IP-10 and MIP-3a. For wild-type sternohyoid muscle, no histological differences were evidenced following treatment. We observed hypertrophy (increased cross-sectional area) of MyHC IIb fibres for wild-type muscle following treatment, which may be responsible for the force potentiation in this group.

Preservation of MyHC isoform composition also occurred in *mdx* diaphragm following combinational therapy. There was a significant reduction in the distribution of type IIa fibres and a remarkable increase in the distribution of type IIx fibres. Hypertrophy of MyHC I and IIx fibres occurred in *mdx* diaphragm following treatment. These adjustments in MyHC composition and cross-sectional area likely mediate the improvements in diaphragm force-generating capacity in *mdx* following co-treatment. Wild-type MyHC fibre complement was unchanged following treatment. Histologically, there were no improvements in muscle fibre central nucleation, relative area of putative cell infiltrates and collagen deposition. The pro-inflammatory cytokine IL-1 β was reduced and the anti-inflammatory cytokine IL-10 was elevated in *mdx* diaphragm following co-treatment, indicating an improvement in the balance of pro- and anti-inflammatory cytokines.

Collectively, these data indicate that restoration of MyHC fibre complement in dystrophic sternohyoid and diaphragm muscle is of major benefit to muscle functional capacity. Similarly, hypertrophy of functional fibres may also be contributing to increased force generation. Therapies which support MyHC fibre maturation in dystrophic muscle may have therapeutic value in *mdx* mice and potentially DMD.

7.9 Combinational pharmacotherapy in *mdx* mice: Knowledge gaps

We acknowledge that our intervention was of short duration (two weeks) and at a young age in a progressive disease. Future studies should examine the safety and efficacy of combined xIL-6R and Ucn2 over prolonged treatment periods. Early intervention may be key in protecting dystrophic muscle from functional deficits, which in turn have implications for respiratory control. Potential side effects or adverse outcomes as a result of treatment over prolonged periods should be considered. In the current studies, we measured somatic growth, organ and muscle mass and did not observe any adverse effects following this two week intervention.

To fully elucidate the benefits of the current therapy in *mdx* mice, studies should be conducted to further examine ventilatory capacity during maximal respiratory

activity to determine if breathing is restored across the ventilatory range. Recordings of diaphragm EMG and trans-diaphragmatic pressure *in vivo* would be useful in assessing if ventilatory drive and diaphragm mechanics are altered across ventilatory and non-ventilatory behaviours following xIL-6R and Ucn2 treatment. Similarly, assessment of the force-frequency relationship of sternohyoid and diaphragm muscle *ex vivo* following drug intervention would be useful to determine the frequency range in which force generating capacity is improved. Upper airway collapsibility should be determined in *mdx* mice following co-treatment. Further examining the benefits of combinational therapy on upper airway physiology will be useful in assessing if this therapy promotes improved control of the upper airway in *mdx* mice.

Additional work should be undertaken to examine the precise signalling mechanisms of xIL-6R and Ucn2 intervention on *mdx* sternohyoid and diaphragm muscle, underpinning alleviation of respiratory muscle deficits and ventilatory dysfunction in *mdx* mice. Such pathways should be further interrogated in the search of therapies for DMD. Studies examining IL-6R signalling blockade and Ucn2 should be examined in more severe models of dystrophic mice, such as the *mdx*/utrophin double knockout mouse.

7.10 Towards combinational pharmacotherapy for the treatment of respiratory dysfunction in DMD

In summary, studies of dystrophic respiratory muscles from *mdx* mice indicate functional deficits with implications for the maintenance of upper airway calibre and ventilation. Our interventional studies in *mdx* mice provide a rational basis for consideration of combinational pharmacotherapy for DMD, with a combined treatment intervention in the current studies yielding the most promising results, compared to either treatment alone. Our studies support the use of anti-inflammatory and anti-stress interventions as adjunctive therapies in the treatment of respiratory system deficits arising from dystrophin deficiency and associated pathology. These studies have relevance for the development of pharmacotherapies in DMD, which aim to improve respiratory performance.

Acknowledgements

We are grateful to our co-authors on the original research articles reviewed herein (Burns *et al.*, 2017b; Manning *et al.*, 2017) for their important contributions to the original studies. DPB is supported by the Department of Physiology, University College Cork, Ireland.

7.11 References

- Abdel SE, Abdel-Meguid I & Korraa S (2007). Markers of oxidative stress and aging in Duchene muscular dystrophy patients and the possible ameliorating effect of He:Ne laser. *Acta Myol* **26**, 14-21.
- Attal P, Lambert F, Marchand-Adam S, Bobin S, Pourny JC, Chemla D, Lecarpentier Y & Coirault C (2000). Severe mechanical dysfunction in pharyngeal muscle from adult mdx mice. *Am J Respir Crit Care Med* **162**, 278-281.
- Baydur A, Gilgoff I, Prentice W, Carlson M & Fischer DA (1990). Decline in respiratory function and experience with long-term assisted ventilation in advanced Duchenne's muscular dystrophy. *Chest* **97**, 884-889.
- Bulfield G, Siller WG, Wight PA & Moore KJ (1984). X chromosome-linked muscular dystrophy (mdx) in the mouse. *Proc Natl Acad Sci U S A* **81**, 1189-1192.
- Burns DP, Ali I, Rieux C, Healy J, Jasione G & O'Halloran KD (2017a). Tempol Supplementation Restores Diaphragm Force and Metabolic Enzyme Activities in mdx Mice. *Antioxidants (Basel)* **6**.
- Burns DP, Edge D, O'Malley D & O'Halloran KD (2015). Respiratory Control in the mdx Mouse Model of Duchenne Muscular Dystrophy. *Adv Exp Med Biol* **860**, 239-244.
- Burns DP & O'Halloran KD (2016). Evidence of hypoxic tolerance in weak upper airway muscle from young mdx mice. *Respir Physiol Neurobiol* **226**, 68-75.
- Burns DP, Rowland J, Canavan L, Murphy KH, Brannock M, O'Malley D, O'Halloran KD & Edge D (2017b). Restoration of pharyngeal dilator muscle force in dystrophin-deficient (mdx) mice following co-treatment with neutralizing interleukin-6 receptor antibodies and urocortin 2. *Exp Physiol* **102**, 1177-1193.
- Burns DP, Roy A, Lucking EF, McDonald FB, Gray S, Wilson RJ, Edge D & O'Halloran KD (2017c). Sensorimotor control of breathing in the mdx mouse model of Duchenne muscular dystrophy. *J Physiol* **595**, 6653-6672.
- Bye PT, Ellis ER, Issa FG, Donnelly PM & Sullivan CE (1990). Respiratory failure and sleep in neuromuscular disease. *Thorax* **45**, 241-247.
- Cerveri I, Fanfulla F, Zoia MC, Manni R & Tartara A (1993). Sleep disorders in neuromuscular diseases. *Monaldi Arch Chest Dis* **48**, 318-321.
- Coirault C, Lambert F, Marchand-Adam S, Attal P, Chemla D & Lecarpentier Y (1999). Myosin molecular motor dysfunction in dystrophic mouse diaphragm. *Am J Physiol* **277**, C1170-1176.

- Coirault C, Lambert F, Pourny JC & Lecarpentier Y (2002). Velocity of actomyosin sliding in vitro is reduced in dystrophic mouse diaphragm. *Am J Respir Crit Care Med* **165**, 250-253.
- Coirault C, Pignol B, Cooper RN, Butler-Browne G, Chabrier PE & Lecarpentier Y (2003). Severe muscle dysfunction precedes collagen tissue proliferation in mdx mouse diaphragm. *J Appl Physiol (1985)* **94**, 1744-1750.
- Cruz-Guzmán OeR, Rodríguez-Cruz M & Escobar Cedillo RE (2015). Systemic Inflammation in Duchenne Muscular Dystrophy: Association with Muscle Function and Nutritional Status. *Biomed Res Int* **2015**, 891972.
- De Paepe B, Creus KK, Martin JJ & De Bleecker JL (2012). Upregulation of chemokines and their receptors in Duchenne muscular dystrophy: potential for attenuation of myofiber necrosis. *Muscle Nerve* **46**, 917-925.
- De Paepe B & De Bleecker JL (2013). Cytokines and chemokines as regulators of skeletal muscle inflammation: presenting the case of Duchenne muscular dystrophy. *Mediators Inflamm* **2013**, 540370.
- De Pasquale L, D'Amico A, Verardo M, Petrini S, Bertini E & De Benedetti F (2012). Increased muscle expression of interleukin-17 in Duchenne muscular dystrophy. *Neurology* **78**, 1309-1314.
- Deconinck N & Dan B (2007). Pathophysiology of duchenne muscular dystrophy: current hypotheses. *Pediatr Neurol* **36**, 1-7.
- Demoule A, Divangahi M, Danialou G, Gvozdic D, Larkin G, Bao W & Petrof BJ (2005). Expression and regulation of CC class chemokines in the dystrophic (mdx) diaphragm. *Am J Respir Cell Mol Biol* **33**, 178-185.
- Enwere EK, Boudreault L, Holbrook J, Timusk K, Earl N, LaCasse E, Renaud JM & Korneluk RG (2013). Loss of cIAP1 attenuates soleus muscle pathology and improves diaphragm function in mdx mice. *Hum Mol Genet* **22**, 867-878.
- Ermolova NV, Martinez L, Vetrone SA, Jordan MC, Roos KP, Sweeney HL & Spencer MJ (2014). Long-term administration of the TNF blocking drug Remicade (cV1q) to mdx mice reduces skeletal and cardiac muscle fibrosis, but negatively impacts cardiac function. *Neuromuscul Disord* **24**, 583-595.
- Ervasti JM (2007). Dystrophin, its interactions with other proteins, and implications for muscular dystrophy. *Biochim Biophys Acta* **1772**, 108-117.
- Hall JE, Kaczor JJ, Hettinga BP, Isfort RJ & Tarnopolsky MA (2007). Effects of a CRF2R agonist and exercise on mdx and wildtype skeletal muscle. *Muscle Nerve* **36**, 336-341.

- Haycock JW, MacNeil S, Jones P, Harris JB & Mantle D (1996). Oxidative damage to muscle protein in Duchenne muscular dystrophy. *Neuroreport* **8**, 357-361.
- Hinkle RT, Donnelly E, Cody DB, Bauer MB & Isfort RJ (2003). Urocortin II treatment reduces skeletal muscle mass and function loss during atrophy and increases nonatrophying skeletal muscle mass and function. *Endocrinology* **144**, 4939-4946.
- Hinkle RT, Donnelly E, Cody DB, Bauer MB, Sheldon RJ & Isfort RJ (2004). Corticotropin releasing factor 2 receptor agonists reduce the denervation-induced loss of rat skeletal muscle mass and force and increase non-atrophying skeletal muscle mass and force. *J Muscle Res Cell Motil* **25**, 539-547.
- Hinkle RT, Lefever FR, Dolan ET, Reichart DL, Dietrich JA, Gropp KE, Thacker RI, Demuth JP, Stevens PJ, Qu XA, Varbanov AR, Wang F & Isfort RJ (2007). Corticotrophin releasing factor 2 receptor agonist treatment significantly slows disease progression in mdx mice. *BMC Med* **5**, 18.
- Khan Y & Heckmatt JZ (1994). Obstructive apnoeas in Duchenne muscular dystrophy. *Thorax* **49**, 157-161.
- Khirani S, Ramirez A, Aubertin G, Boulé M, Chemouny C, Forin V & Fauroux B (2014). Respiratory muscle decline in Duchenne muscular dystrophy. *Pediatr Pulmonol* **49**, 473-481.
- Kumar A & Boriek AM (2003). Mechanical stress activates the nuclear factor-kappaB pathway in skeletal muscle fibers: a possible role in Duchenne muscular dystrophy. *FASEB J* **17**, 386-396.
- LoMauro A, D'Angelo MG & Aliverti A (2017). Sleep Disordered Breathing in Duchenne Muscular Dystrophy. *Curr Neurol Neurosci Rep* **17**, 44.
- Manning J, Buckley MM, O'Halloran KD & O'Malley D (2016). In vivo neutralization of IL-6 receptors ameliorates gastrointestinal dysfunction in dystrophin-deficient mdx mice. *Neurogastroenterol Motil* **28**, 1016-1026.
- Manning J, Buckley MM, O'Halloran KD & O'Malley D (2017). Combined xIL-6R and urocortin-2 treatment restores mdx diaphragm muscle force. *Muscle Nerve*.
- Mayer OH, Finkel RS, Rummey C, Benton MJ, Glanzman AM, Flickinger J, Lindström BM & Meier T (2015). Characterization of pulmonary function in Duchenne Muscular Dystrophy. *Pediatr Pulmonol* **50**, 487-494.
- Messina S, Vita GL, Aguenouz M, Sframeli M, Romeo S, Rodolico C & Vita G (2011). Activation of NF-kappaB pathway in Duchenne muscular dystrophy: relation to age. *Acta Myol* **30**, 16-23.

- Mojumdar K, Liang F, Giordano C, Lemaire C, Danialou G, Okazaki T, Bourdon J, Rafei M, Galipeau J, Divangahi M & Petrof BJ (2014). Inflammatory monocytes promote progression of Duchenne muscular dystrophy and can be therapeutically targeted via CCR2. *EMBO Mol Med* **6**, 1476-1492.
- Mosqueira M, Baby SM, Lahiri S & Khurana TS (2013). Ventilatory chemosensory drive is blunted in the mdx mouse model of Duchenne Muscular Dystrophy (DMD). *PLoS One* **8**, e69567.
- Nakae Y, Stoward PJ, Kashiyama T, Shono M, Akagi A, Matsuzaki T & Nonaka I (2004). Early onset of lipofuscin accumulation in dystrophin-deficient skeletal muscles of DMD patients and mdx mice. *J Mol Histol* **35**, 489-499.
- Nelson CA, Hunter RB, Quigley LA, Girgenrath S, Weber WD, McCullough JA, Dinardo CJ, Keefe KA, Ceci L, Clayton NP, McVie-Wylie A, Cheng SH, Leonard JP & Wentworth BM (2011). Inhibiting TGF- β activity improves respiratory function in mdx mice. *Am J Pathol* **178**, 2611-2621.
- Nitahara-Kasahara Y, Hayashita-Kinoh H, Chiyo T, Nishiyama A, Okada H, Takeda S & Okada T (2014). Dystrophic mdx mice develop severe cardiac and respiratory dysfunction following genetic ablation of the anti-inflammatory cytokine IL-10. *Hum Mol Genet* **23**, 3990-4000.
- Okazaki M, Yamada Y, Nishimoto N, Yoshizaki K & Mihara M (2002). Characterization of anti-mouse interleukin-6 receptor antibody. *Immunol Lett* **84**, 231-240.
- Pan Y, Chen C, Shen Y, Zhu CH, Wang G, Wang XC, Chen HQ & Zhu MS (2008). Curcumin alleviates dystrophic muscle pathology in mdx mice. *Mol Cells* **25**, 531-537.
- Pelosi L, Berardinelli MG, De Pasquale L, Nicoletti C, D'Amico A, Carvello F, Moneta GM, Catizone A, Bertini E, De Benedetti F & Musarò A (2015a). Functional and Morphological Improvement of Dystrophic Muscle by Interleukin 6 Receptor Blockade. *EBioMedicine* **2**, 285-293.
- Pelosi L, Berardinelli MG, Forcina L, Spelta E, Rizzuto E, Nicoletti C, Camilli C, Testa E, Catizone A, De Benedetti F & Musarò A (2015b). Increased levels of interleukin-6 exacerbate the dystrophic phenotype in mdx mice. *Hum Mol Genet* **24**, 6041-6053.
- Pelosi L, Forcina L, Nicoletti C, Scicchitano BM & Musarò A (2017). Increased Circulating Levels of Interleukin-6 Induce Perturbation in Redox-Regulated Signaling Cascades in Muscle of Dystrophic Mice. *Oxid Med Cell Longev* **2017**, 1987218.

- Petrillo S, Pelosi L, Piemonte F, Travaglini L, Forcina L, Catteruccia M, Petrini S, Verardo M, D'Amico A, Musarò A & Bertini E (2017). Oxidative stress in Duchenne muscular dystrophy: focus on the NRF2 redox pathway. *Hum Mol Genet* **26**, 2781-2790.
- Petrof BJ, Stedman HH, Shrager JB, Eby J, Sweeney HL & Kelly AM (1993). Adaptations in myosin heavy chain expression and contractile function in dystrophic mouse diaphragm. *Am J Physiol* **265**, C834-841.
- Phillips MF, Quinlivan RC, Edwards RH & Calverley PM (2001). Changes in spirometry over time as a prognostic marker in patients with Duchenne muscular dystrophy. *Am J Respir Crit Care Med* **164**, 2191-2194.
- Polla B, D'Antona G, Bottinelli R & Reggiani C (2004). Respiratory muscle fibres: specialisation and plasticity. *Thorax* **59**, 808-817.
- Porreca E, Guglielmi MD, Uncini A, Di Gregorio P, Angelini A, Di Febbo C, Pierdomenico SD, Baccante G & Cuccurullo F (1999). Haemostatic abnormalities, cardiac involvement and serum tumor necrosis factor levels in X-linked dystrophic patients. *Thromb Haemost* **81**, 543-546.
- Porter JD, Khanna S, Kaminski HJ, Rao JS, Merriam AP, Richmonds CR, Leahy P, Li J, Guo W & Andrade FH (2002). A chronic inflammatory response dominates the skeletal muscle molecular signature in dystrophin-deficient mdx mice. *Hum Mol Genet* **11**, 263-272.
- Quinlan JG, Hahn HS, Wong BL, Lorenz JN, Wensch AS & Levin LS (2004). Evolution of the mdx mouse cardiomyopathy: physiological and morphological findings. *Neuromuscul Disord* **14**, 491-496.
- Reutenauer-Patte J, Boittin FX, Patthey-Vuadens O, Ruegg UT & Dorchies OM (2012). Urocortins improve dystrophic skeletal muscle structure and function through both PKA- and Epac-dependent pathways. *Am J Pathol* **180**, 749-762.
- Rodriguez MC & Tarnopolsky MA (2003). Patients with dystrophinopathy show evidence of increased oxidative stress. *Free Radic Biol Med* **34**, 1217-1220.
- Rufo A, Del Fattore A, Capulli M, Carvello F, De Pasquale L, Ferrari S, Pierroz D, Morandi L, De Simone M, Rucci N, Bertini E, Bianchi ML, De Benedetti F & Teti A (2011). Mechanisms inducing low bone density in Duchenne muscular dystrophy in mice and humans. *J Bone Miner Res* **26**, 1891-1903.
- Saito K, Kobayashi D, Komatsu M, Yajima T, Yagihashi A, Ishikawa Y, Minami R & Watanabe N (2000). A sensitive assay of tumor necrosis factor alpha in sera from Duchenne muscular dystrophy patients. *Clin Chem* **46**, 1703-1704.

- Schiaffino S & Reggiani C (2011). Fiber types in mammalian skeletal muscles. *Physiol Rev* **91**, 1447-1531.
- Sieck DC, Zhan WZ, Fang YH, Ermilov LG, Sieck GC & Mantilla CB (2012). Structure-activity relationships in rodent diaphragm muscle fibers vs. neuromuscular junctions. *Respir Physiol Neurobiol* **180**, 88-96.
- Skelly JR, Edge D, Shortt CM, Jones JF, Bradford A & O'Halloran KD (2012). Tempol ameliorates pharyngeal dilator muscle dysfunction in a rodent model of chronic intermittent hypoxia. *Am J Respir Cell Mol Biol* **46**, 139-148.
- Skelly JR, O'Connell RA, Jones JF & O'Halloran KD (2011). Structural and functional properties of an upper airway dilator muscle in aged obese male rats. *Respiration* **82**, 539-549.
- Smith PE, Edwards RH & Calverley PM (1989). Ventilation and breathing pattern during sleep in Duchenne muscular dystrophy. *Chest* **96**, 1346-1351.
- Stedman HH, Sweeney HL, Shrager JB, Maguire HC, Panettieri RA, Petrof B, Narusawa M, Leferovich JM, Sladky JT & Kelly AM (1991). The mdx mouse diaphragm reproduces the degenerative changes of Duchenne muscular dystrophy. *Nature* **352**, 536-539.
- Villalta SA, Rinaldi C, Deng B, Liu G, Fedor B & Tidball JG (2011). Interleukin-10 reduces the pathology of mdx muscular dystrophy by deactivating M1 macrophages and modulating macrophage phenotype. *Hum Mol Genet* **20**, 790-805.
- Welc SS & Clanton TL (2013). The regulation of interleukin-6 implicates skeletal muscle as an integrative stress sensor and endocrine organ. *Exp Physiol* **98**, 359-371.
- Yiu EM & Kornberg AJ (2008). Duchenne muscular dystrophy. *Neurol India* **56**, 236-247.

Chapter 8. Summary and conclusion

8.1 Summary of major findings

Respiratory muscle weakness and decreased ventilatory capacity occurs in Duchenne muscular dystrophy (DMD) patients with attendant systemic and muscle inflammation. Respiratory failure is a leading cause of death in DMD. This thesis addresses knowledge gaps relating to dystrophin deficiency and respiratory control in a murine model of DMD, the *mdx* mouse. Studies were performed to explore deficits and intrinsic compensatory mechanisms within the integrated respiratory control network of young (8 week old) *mdx* mice.

We reveal considerable deficits within this network, which have major implications for the control of breathing in young *mdx* mice. Profound diaphragm muscle weakness was confirmed in our studies and was associated with considerable muscle fibre remodelling, including increased co-efficient of variation of muscle fibre size, immune cell infiltration, muscle fibre central nucleation and altered distribution of myosin heavy chain isoform composition (increased type IIa and decreased IIx). Plethysmography studies in conscious mice indicate tidal volume deficits resulting in reduced minute ventilation; carbon dioxide production was unchanged. The ventilatory equivalent for carbon dioxide was reduced in *mdx*, indicating hypoventilation during normoxia, which likely related to sensory deficit in the peripheral control of breathing and/or mechanical disadvantage due to diaphragm muscle weakness (reduced force in 40-160Hz frequency range). Dystrophin is expressed in the carotid body (principal oxygen sensor), and carotid bodies from *mdx* mice have a blunted response to hyperoxia, indicating carotid body hypoactivity (sensory deficit). Decreased chemoafferent input to the cardiorespiratory integrative sites of the central nervous system, could indeed contribute to hypoventilation in *mdx* mice, given the physiological contribution of the peripheral oxygen sensors to eupnoeic (basal) ventilation. The carotid body, ventilation and metabolic response to hypoxia were equivalent in wild-type and *mdx* mice. Arterial blood gas analysis suggested a compensated respiratory acidosis in *mdx* mice.

Conversely, we highlight evidence of compensatory mechanisms, which may serve to limit respiratory deficits in *mdx* mice. Ventilatory capacity in response to maximal chemostimulation and peak inspiratory oesophageal pressure during baseline and chemoactivation are preserved in *mdx* mice, in the presence of a weakened diaphragm. Interestingly, peak sub-atmospheric pressure during an augmented breath (considered near maximal respiratory muscle activation) is greater in *mdx* mice compared with wild-type, while diaphragm EMG activity was equivalent in wild-type and *mdx* mice. In conscious mice, the volume of augmented breaths was equivalent between wild-type and *mdx*. Increased inspiratory pressure generation in *mdx* mice with a profoundly weak diaphragm muscle, suggests enhanced accessory respiratory motor drive. A phenomenon of enhanced motor output and recruitment of accessory respiratory muscles in *mdx* mice, could act to preserve or limit ventilatory deficits. The cervical spinal cord (C3-5 region), which contains the phrenic motor nucleus, was examined in wild-type and *mdx* mice and monoamine concentrations were determined. NA and 5-HT were increased in the cervical spinal cord of *mdx* mice, suggesting altered neuromodulatory tone. EMG recordings assessing neural drive to the diaphragm in anaesthetised vagotomised mice, revealed enhanced neural drive to the diaphragm in *mdx* mice during maximal chemoactivation compared with wild-type, suggesting compensatory neuroplasticity acting to increase motor output to the diaphragm muscle, in turn facilitating ventilation. Of note, however, potentiated diaphragm EMG was not observed under all experimental conditions.

Analysis of breathing variability indicated no perturbed respiratory rhythm generation in *mdx* mice. Investigations examining the density of activated astrocytes and microglia and pro-inflammatory gene expression in the cervical spinal cord of *mdx* mice highlight no evidence of neuroinflammation in the putative phrenic motor nucleus.

Collectively, these data describe deficits at multiple sites of the respiratory control network at a young age in *mdx* mice. In stark contrast, our data also reveal altered neuromechanical coupling in *mdx* mice revealing compensatory mechanisms, which

evidently protect ventilatory capacity despite diaphragm muscle dysfunction. Studies providing mechanistic insight into the intrinsic compensatory mechanisms in *mdx* mice are important for interventional strategies and adjunct therapies aimed at improving respiratory performance in *mdx* mice and human dystrophinopathies.

Inflammation is a major pathological feature of DMD due to dystrophin deficiency and resultant muscle damage. Inflammatory mediators such as cytokines and chemokines are elevated in plasma and muscle samples from DMD patients and the *mdx* mouse. Histological studies show there is considerable inflammatory cell invasion in dystrophic muscle fibres and a progressive accumulation of connective tissue and adipocytes following muscle fibre necrosis.

In additional studies, we examined a combinational treatment strategy aimed at alleviating respiratory muscle deficits and improving respiratory performance in *mdx* mice. This intervention consisted of neutralizing interleukin-6 receptor antibodies and urocortin 2, a corticotrophin releasing factor receptor 2 agonist. This combinational therapy had previously been shown by our research group to improve diaphragm muscle strength in *mdx* mice. We repeated this intervention and extended studies to breathing and metabolic measurements, diaphragm muscle structure and fibre type composition, and cytokine concentrations. In concert, we examined the skeletal musculature of the upper airway, which has relevance for the physiological control of upper airway patency and airway clearance. This involved examination of sternohyoid muscle (representative pharyngeal dilator) form and function.

Two weeks of blocking interleukin-6 receptor signalling with neutralizing antibodies and stimulating corticotrophin releasing factor receptor 2 with urocortin 2, resulted in considerable improvements in respiratory function and diaphragm muscle health. Breathing and diaphragm muscle deficits were alleviated following treatment, with minute ventilation restored in *mdx* mice following treatment. Diaphragm muscle fibre complement was restored, with a reduction in myosin

heavy chain type IIa and an accompanying increase in type IIx. Pro-inflammatory cytokines were increased in the diaphragm from *mdx* mice, and treatment decreased the pro-inflammatory cytokine interleukin-1 β and increased the anti-inflammatory cytokine IL-10 in *mdx* diaphragm. Type I and III collagen was increased in *mdx* diaphragm, along with muscle fibre central nucleation (indicator of muscle fibre damage), and immune cell infiltrates; all indices were unaffected by treatment.

In addition to the diaphragm, considerable mechanical dysfunction and motor deficits have been reported in the sternohyoid muscle of *mdx* mice. Force- and power-generating capacity is severely compromised in *mdx* sternohyoid. Alterations in myosin heavy chain isoform distribution is apparent, with a reduction in type IIb fibres and an increase in IIx in *mdx* muscle. Immune cell infiltrations, muscle fibre central nucleation, collagen content and chemokine concentrations are increased in *mdx* sternohyoid muscle compared to wild-type. Combinational pharmacotherapy restored sternohyoid muscle force-, work- and power-generating capacity to wild-type levels. Myosin heavy chain isoform composition was restored, with a reduction in type IIx and a concomitant increase in IIb. Treatment decreased central nucleation in *mdx* sternohyoid, indicating reduced fibre damage. Cell infiltrates and collagen content were not affected by treatment.

Collectively, these findings reveal the potential for a combinational approach of anti-inflammatory and anti-stress interventions in alleviating respiratory deficits and improving respiratory performance in *mdx* mice. Combinational therapy studies have relevance for the development of new pharmacotherapies in the treatment of DMD.

8.2 Future studies

Whilst we have examined many aspects of the control of breathing in *mdx* mice, there are still many questions that remain to be addressed. Longitudinal studies tracking ventilatory capacity as a function of age and disease progression in *mdx* mice would allow for a better understanding of ventilation over the entire time course of the disease. Contemporaneous recordings of breathing and respiratory muscle EMG activity in conscious mice across the sleep wake cycle would provide a comprehensive assessment.

Assessment of trans-diaphragmatic pressures are required in *mdx* mice to fully examine diaphragm contractile strength *in vivo* across ventilatory and airway protective behaviours, and during maximal activation with bilateral phrenic nerve stimulation. To fully examine the phrenic motor neuron pool, retrograde labelling should be performed and motor neuronal counts examined. Phrenic nerve recordings in reduced preparations would provide information on motor output to the diaphragm muscle. Since alterations in axonal counts have been observed in dystrophic nerves, it will be important to assess phrenic nerve morphometry in wild-type and *mdx* mice. It is clear from the current thesis that compensatory mechanisms are at play in the respiratory control network of *mdx* mice. Discerning the precise locus and exact mediators of this compensation will be pivotal in future work if these findings are to be of translational value.

Studies should further examine neuro-immune interactions and monoamine concentrations and receptor expression at sites of the respiratory control network, such as pattern generating sites, key integrative centres such as the nucleus tractus solitarius (NTS), and at the level of key respiratory motor nuclei in the brainstem and spinal cord. Recordings of fictive respiratory neuronal discharge in brainstem slice preparations would determine if central pattern generation was affected by dystrophin deficiency in developing *mdx* mice. Since we report a sensory deficit within dystrophic carotid bodies, it would be interesting to ascertain if sensory processing in the NTS is altered in *mdx* mice. Studies examining the motor pathways of accessory respiratory muscles in *mdx* mice are paramount to further

understand respiratory control and compensation in *mdx* mice. Of particular interest, the intercostal and abdominal muscles should be examined to determine the putative compensatory role that they play in preserving ventilatory capacity in *mdx*.

Given the prevalence of sleep disordered breathing and obstructive sleep apnoea in DMD, studies are required to determine if motor control of the upper airway is affected by dystrophin deficiency. EMG recordings of the genioglossus muscle (pharyngeal dilator) or hypoglossal nerve activity would help determine if neural drive to the upper airway is altered in *mdx* mice. Moreover, an examination of the hypoglossal motor nucleus for neuroinflammation and monoamine concentrations is required. It is necessary to reveal if there are deficits or compensation in the motor control of the upper airway in *mdx* mice, to fully reveal all consequences of dystrophin deficiency on the control of breathing. Furthermore, since sleep disordered breathing and hypoxaemic periods occur in patients, it would be interesting to examine the consequences of intermittent hypoxia (modelling sleep disordered breathing) on respiratory control and respiratory muscle form and function in *mdx* mice. Such studies would draw focus to the potential concern that sleep disordered breathing exacerbates respiratory morbidity in DMD. It is also important in future work to determine if low dose therapeutic intermittent hypoxia is efficacious in boosting respiratory motor outputs facilitating breathing in *mdx* mice with potential application to DMD.

Given that deficits are present at multiple sites within the respiratory control network, there is an argument in support of the pharmacological use of respiratory stimulants to enhance ventilation and potentially alleviate respiratory dysfunction in *mdx* mice. There is a remarkable capacity for plasticity within the respiratory control system. Studies exploring if there is a capacity for plasticity within the respiratory control network of *mdx* mice are necessary. Harnessing respiratory plasticity and motor facilitation in animal models of motor neuron disease and spinal cord injury have proved beneficial for improving ventilatory capacity. Motor

facilitation of the diaphragm and accessory respiratory muscles may have potential for enhancing ventilation in animal models of DMD.

Although the *mdx* mouse has had a fundamental role in understanding the pathophysiology of DMD and the assessment of therapeutic interventions, studies in models closer to human DMD are required, such as the golden retriever and porcine models. This is of particular importance for the clinical translation of therapeutic interventions.

8.3 Conclusion

We conclude that respiratory control is altered in *mdx* mice – a murine model of Duchenne muscular dystrophy. Dystrophin deficiency in *mdx* mice results in deficits in respiratory muscle, breathing and sensory control. Compensation within the respiratory control system includes altered neuromechanical control of breathing which facilitates greater inspiratory pressure generation in *mdx* mice during near maximal ventilatory behaviours, despite profound diaphragm muscle weakness. A combinational drug therapy targeting anti-inflammatory and anti-stress pathways improves respiratory performance in *mdx* mice. These data have relevance for the development of interventional strategies in DMD.

Publications

Published articles

1. Burns DP, Canavan L, Rowland J, O’Flaherty R, Brannock M, Drummond SE, O’Malley D, Edge D & O’Halloran KD “Recovery of respiratory function in *mdx* mice co-treated with neutralizing interleukin-6 receptor antibodies and Urocortin-2”. *The Journal of Physiology*, in press.
2. O’Halloran KD & Burns DP “Breathing with neuromuscular disease: Does compensatory plasticity in the motor drive to breathe offer a potential therapeutic target in muscular dystrophy?”. *Respiratory Physiology and Neurobiology*, in press.
3. O’Halloran KD, Murphy KM & Burns DP (2017) “Antioxidant therapy for muscular dystrophy: Caveat lector!”. *The Journal of Physiology*, 596 (4): 737-738.
4. Burns DP, Ali I, Rieux C, Healy J, Jasione G & O’Halloran KD (2017) “Tempol supplementation restores diaphragm force and metabolic enzyme activities in *mdx* mice”. *Antioxidants (Basel, Switzerland)*, 6(4):101.
5. Burns DP, Roy A, Lucking EF, McDonald FB, Gray S, Wilson RJ, Edge D & O’Halloran KD (2017) “Sensorimotor control of breathing in the *mdx* mouse model of Duchenne muscular dystrophy”. *The Journal of Physiology*, 1:595 (21):6653-6672.
6. Burns DP, Rowland J, Canavan L, Murphy K, Brannock M, O’Malley D, O’Halloran KD & Edge D (2017) “Restoration of pharyngeal dilator muscle force in dystrophin deficient (*mdx*) mice following co-treatment with neutralizing IL-6 receptor antibodies and Urocortin-2”. *Experimental Physiology*, 102(9):1177-1193.
7. Burns DP & O’Halloran KD (2016) “Evidence of hypoxic tolerance in weak upper airway muscle from young *mdx* mice”. *Respiratory Physiology and Neurobiology*, 226:68-75.
8. Burns DP, Edge D, O’Malley D & O’Halloran KD (2015) “Respiratory control in the *mdx* mouse model of Duchenne muscular dystrophy”. *Advances in Experimental Medicine and Biology*, 860:239-44.

Manuscripts in preparation

1. Burns DP, O’Driscoll E, Murphy KH, O’Connor KM, Lucking EF, Dhaliwal P, Clarke G, Edge D & O’Halloran KD “Neuromechanical control of breathing in the dystrophin-deficient *mdx* mouse”.
2. Burns DP, Edge D & O’Halloran KD “Combinational pharmacotherapy in the treatment of respiratory deficits in dystrophin-deficient *mdx* mice”
3. Burns DP, O’Driscoll E, Gray S, Edge D & O’Halloran KD “Genioglossus EMG activity in the *mdx* mouse model of Duchenne muscular dystrophy”.

4. Burns DP, Lefevre N & O'Halloran KD "Dystrophic diaphragm muscle from *mdx* mice displays a relative resistance to acute hypoxic stress".
5. Burns DP, Wollman LD, Fuller DD & O'Halloran KD "Respiratory motor output in the *mdx* mouse model of Duchenne muscular dystrophy".
6. Burns DP, Drummond SE, Bolger D, Murphy KH, Edge D & O'Halloran KD "N-Acetyl Cysteine improves *mdx* diaphragm muscle quality and strength".
7. Burns DP, Drummond SE, Sheeran L, D & O'Halloran KD "Effects of chronic intermittent hypoxia on respiratory control in the *mdx* mouse model of Duchenne muscular dystrophy".

Presentations

Invited

1. Research Seminar, Department of Physiology, University College Cork, Cork, Ireland (2018).
2. Therapeutic Intermittent Hypoxia Retreat 2018, University of Florida, Gainesville, FL, USA (2018).
3. Research Seminar, Sieck and Mantilla Lab, Department of Physiology and Biomedical Engineering, Mayo Clinic, Rochester, MN, USA (2017).
4. Respiratory Social and Science Seminar, Centre for Respiratory Research and Rehabilitation, University of Florida, Gainesville, FL, USA (2017).
5. Experimental Biology Meeting, Chicago, USA - Trainee Highlights Breakfast (2017).
6. Centre for Respiratory Research and Rehabilitation Data Blitz, University of Florida, FL, USA (2016).
7. Hypoxia Research Symposium, Cork, Ireland (2016).
8. Muscular Dystrophy Ireland AGM, Dublin, Ireland (2015).
9. Hypoxia Research Satellite Symposium, University of Calgary, Calgary, Canada (2015).

Selected

1. Europhysiology, a meeting of The Physiological Society, the Scandanavian Physiological Society, the Deutsche Physiologische Gesellschaft and the Federation of European Physiological Societies, London, UK (2018).
2. New Horizons in Medical Research, School of Medicine, University College Cork, Cork, Ireland (2017).
3. Royal Academy of Medicine in Ireland Biomedical Sciences Meeting, Cork, Ireland (2016).
4. Experimental Biology Meeting, San Diego, USA - Trainee Highlights Breakfast (2016).
5. Irish Thoracic Society Annual Meeting, Cork, Ireland (2015).
6. Experimental Biology Meeting, Boston, USA (2015).
7. Oxford Control of Breathing Meeting, Sydney, Australia (2014).
8. International Society for Arterial Chemoreception Meeting, Leeds, UK (2014).
9. Royal Academy of Medicine in Ireland Biomedical Sciences Meeting, Dublin, Ireland (2014).

Conference proceedings

1. Europhysiology 2018 (London, UK). The Physiological Society. Burns DP, O'Driscoll E, Rowland J, Canavan L, Murphy KH, O'Connor KM, O'Malley D, Clarke G, Edge D & O'Halloran KD (2018) "Breathing with neuromuscular disease: insights from pre-clinical studies" (Selected talk).
2. Europhysiology 2018 (London, UK). The Physiological Society. Burns DP, Drummond SE, Sheeran L, Coiscaud A, O'Hehir C, Edge D & O'Halloran KD (2018) "Chronic intermittent hypoxia enhances respiratory muscle weakness in dystrophin-deficient *mdx* mice" (Poster).
3. Therapeutic Intermittent Hypoxia Retreat (Florida, USA). The University of Florida. Burns DP & O'Halloran KD (2018) "Intermittent hypoxia in neuromuscular disease: pathological feature or potential therapy?" (Invited talk).
4. Experimental Biology 2018 (San Diego, USA). American Physiological Society. Murphy KH, Burns DP, Lucking EF & O'Halloran KD (2018) "Respiratory EMG responsiveness to hypercapnic hypoxia in *mdx* mice" (Poster).
5. Experimental Biology 2018 (San Diego, USA). American Physiological Society. Burns DP, Edge D, Murphy KH & O'Halloran KD (2018) "Chronic intermittent hypoxia enhances respiratory muscle weakness in dystrophin-deficient *mdx* mice" (Poster).
6. Experimental Biology 2018 (San Diego, USA). American Physiological Society. Burns DP, O'Driscoll E, Lucking EF, Edge D & O'Halloran KD (2018) "Aspects of respiratory control in the dystrophin-deficient *mdx* mouse" (Poster).
7. Experimental Biology 2018 (San Diego, USA). American Physiological Society. Wollman LB, Sunshine MD, Burns DP, O'Halloran KD & Fuller DD (2018) "Serotonergic immunoreactivity in the brainstem and spinal cord of *mdx* mice" (Poster).
8. New Horizons in Medical Research UCC (Cork, IRL). Burns DP, Roy A, Lucking EF, McDonald FB, Wilson RJ, Fuller DD, Edge D & O'Halloran KD (2018) "Respiratory control in the *mdx* mouse model of Duchenne muscular dystrophy" (Selected talk).
9. Oxford Control of Breathing Meeting (Oxford, UK). Burns DP, Lucking EF, Walter GA, Fuller DD & O'Halloran KD (2017) "Respiratory motor output in the *mdx* mouse model of Duchenne muscular dystrophy" (Poster).
10. Oxford Control of Breathing Meeting (Oxford, UK). O'Halloran KD & Burns DP (2017) "Respiratory control in the *mdx* mouse model of Duchenne muscular dystrophy" (Invited talk).
11. Royal Academy of Medicine in Ireland Biomedical Sciences Meeting 2017 (Dublin, IRL). O'Driscoll E, Gray S, Burns DP, O'Halloran KD & Edge D (2017) "Is there evidence of central pathology in the respiratory network of the *mdx* mouse model of Duchenne muscular dystrophy?" (Poster).

12. Royal Academy of Medicine in Ireland Biomedical Sciences Meeting 2017 (Dublin, IRL). Burns DP, Lucking EF, Gray S, Edge D & O'Halloran KD (2017) "Enhanced diaphragm muscle EMG activity in response to chemostimulation in dystrophin deficient *mdx* mice" (Poster).
13. Royal Academy of Medicine in Ireland Biomedical Sciences Meeting 2017 (Dublin, IRL). Heelan R, Golubeva A, Khochanskiy D, Burns DP, Cryan JF & O'Halloran KD (2017) "Colonic myenteric plexus morphology in the *mdx* mouse model of Duchenne muscular dystrophy" (Poster).
14. Experimental Biology 2017 (Chicago, USA). American Physiological Society. Burns DP, Canavan L, Rowland J, O'Flaherty R, O'Malley D, Edge D & O'Halloran KD (2017) "Targeting IL-6 and CRFR2 improves diaphragm muscle function and restores ventilation in *mdx* mice" (Poster).
15. Experimental Biology 2017 (Chicago, USA). American Physiological Society. Burns DP, Lucking EF, Roy A, McDonald FB, Wilson R, Edge D & O'Halloran KD (2017) "Aberrant respiratory control in the *mdx* mouse model of Duchenne muscular dystrophy" (Invited talk & poster).
16. New Horizons in Medical Research UCC (Cork, IRL). Murphy K, Burns DP, Rowland J, Canavan L, O'Malley D, O'Halloran KD & Edge D (2016) "Restoration of pharyngeal dilator muscle force in dystrophin-deficient (*mdx*) mice following co-treatment with neutralizing IL-6R antibody and Urocortin-2" (Poster).
17. Physiology 2016 (Dublin, IRL). Burns DP, Roy A, Rowland J, Lucking E, McDonald F, Edge D, Wilson R & O'Halloran KD (2016) "Carotid body dysfunction and hypoventilation in the dystrophin deficient *mdx* mouse" (Poster).
18. Physiology 2016 (Dublin, IRL). Burns DP, Rieux C, Ali I, Healy J, Edge D & O'Halloran KD (2016) "Chronic Tempol supplementation restores diaphragm muscle force-generating capacity in the dystrophin-deficient *mdx* mouse" (Poster).
19. Physiology 2016 (Dublin, IRL). Burns DP, Rowland J, Canavan L, Murphy K, O'Malley D, O'Halloran KD & Edge D (2016) "Restoration of pharyngeal dilator muscle force in dystrophin-deficient (*mdx*) mice following co-treatment with neutralizing IL-6R antibody and Urocortin-2" (Poster).
20. Royal Academy of Medicine in Ireland Biomedical Sciences Meeting 2016 (Cork, IRL). Murphy K, Burns DP, Rowland J, Canavan L, O'Malley D, O'Halloran KD & Edge D (2016) "Restoration of pharyngeal dilator muscle force in dystrophin deficient (*mdx*) mice following co-treatment with neutralizing IL-6R antibody and urocortin-2" (Selected talk).
21. Royal Academy of Medicine in Ireland Biomedical Sciences Meeting 2016 (Cork, IRL). Burns DP, Roy A, Rowland J, Lucking EF, McDonald FB, Edge D,

- Wilson R & O'Halloran KD (2016) "Carotid body dysfunction and hypoventilation in the dystrophin deficient *mdx* mouse" (Selected talk).
22. Royal Academy of Medicine in Ireland Biomedical Sciences Meeting 2016 (Cork, IRL). Burns DP, Rieux C, Ali I, Healy J, Edge D & O'Halloran KD (2016) "Chronic tempol supplementation restores diaphragm muscle force-generating capacity in the dystrophin deficient *mdx* mouse" (Poster).
 23. Experimental Biology 2016 (San Diego, USA). American Physiological Society. Burns DP, Roy A, McDonald F, Wilson RJ & O'Halloran KD (2016) "Hypoventilation in the *mdx* mouse model of Duchenne muscular dystrophy" (Selected talk & Poster).
 24. Advances in Skeletal Muscle Biology in Health and Disease (Florida, USA). Burns DP & O'Halloran KD (2016) "Evidence of hypoxic tolerance in respiratory muscle from young *mdx* mice" (Poster).
 25. Irish Thoracic Society Annual Scientific Meeting (Cork, IRL). Burns DP & O'Halloran KD (2015) "Respiratory function in the *mdx* mouse model of Duchenne muscular dystrophy: a role for hypoxia?" (Selected talk).
 26. Physiological Society Annual Meeting (Cardiff, UK). Burns DP, Manning J, O'Malley D & O'Halloran KD (2015) "Respiratory dysfunction in the *mdx* mouse model of Duchenne muscular dystrophy" (Poster).
 27. Royal Academy of Medicine in Ireland Biomedical Sciences Annual Meeting (Dublin, IRL). Ali I, Burns DP, Lewis P, O'Malley D & O'Halloran KD (2015) "The superoxide scavenger Tempol does not improve diaphragm muscle weakness in the *mdx* mouse model of Duchenne muscular dystrophy" (Poster).
 28. Experimental Biology 2015 (Boston, USA). American Physiological Society – Respiration Section featured topic. Burns DP, Manning J, O'Malley D & O'Halloran KD (2015) "Respiratory function in the *mdx* mouse model of Duchenne muscular dystrophy: Role of hypoxia, stress and inflammation" (Selected talk & poster).
 29. New Horizons in Medical Research Conference, UCC School of Medicine (Cork, IRL). Burns DP, O'Malley D & O'Halloran KD (2014) "Respiratory function in the *mdx* mouse model of Duchenne muscular dystrophy" (Poster).
 30. Oxford Control of Breathing Meeting (Sydney, Australia). Burns DP, O'Leary A, O'Malley D & O'Halloran KD (2014) "Effects of acute sustained hypoxic stress on sternohyoid and diaphragm muscle function in the *mdx* mouse model of Duchenne muscular dystrophy" (Selected talk).
 31. European Muscle Conference (Salzburg, Austria). Burns DP & O'Halloran KD (2014) "Dystrophin deficiency impairs upper airway dilator muscle function in the *mdx* mouse" (Poster).

32. European Muscle Conference (Salzburg, Austria). Burns DP & O'Halloran KD (2014) "Effects of acute sustained hypoxia on diaphragm muscle function in the *mdx* mouse" (Poster).
33. International Society for Arterial Chemoreception (Leeds, UK). Burns DP, Edge D & O'Halloran KD (2014) "Respiratory control in the *mdx* mouse model of Duchenne muscular dystrophy" (Selected talk).
34. Royal Academy of Medicine in Ireland Biomedical Sciences Annual Meeting (Dublin, IRL). Burns DP & O'Halloran KD (2014) "Respiratory control and diaphragm muscle function in the *mdx* mouse model of Duchenne muscular dystrophy" (Selected talk).